

DISSERTATION

Post Combustion CO₂ Capture based on Temperature Swing Adsorption – from Process Evaluation to Continuous Bench Scale Operation

ausgeführt zum Zwecke der Erlangung des akademischen Grades eines
Doktors der technischen Wissenschaften Verfahrenstechnik unter der Leitung von

Univ.Prof. Dipl.-Ing. Dr.techn. Tobias Pröll

Univ.Prof. Dipl.-Ing. Dr.techn. Hermann Hofbauer

E166

Institut für Verfahrenstechnik, Umwelttechnik und technische Biowissenschaften

eingereicht an der Technischen Universität Wien

Fakultät für Maschinenwesen und Betriebswissenschaften

von

Dipl.-Ing. Gerhard Schöny

Matrikelnummer: 0525572

Costagasse 5/16, 1150 Wien

ABSTRACT

Chemical absorption by means of aqueous amine solvents can be considered as the currently most mature post-combustion CO₂ capture process. However, amine scrubbing technologies exhibit several disadvantages that are intrinsic to the process and result in large process heat demands and CO₂ capture costs. Thus, in order to achieve breakthroughs in the reduction of CO₂ capture costs the development of alternative capture technologies is required. Adsorption based processes have been proposed as appropriate methods to achieve significant reduction of CO₂ capture costs compared to amine scrubbing technologies. Inspired by the excellent CO₂ absorption properties of amine-based solvents, researchers immobilized amines onto solid support materials and thereby developed a new class of highly selective CO₂ adsorbent materials. In the recent years, a great effort has been made to further develop amine functionalized adsorbents that are optimized for CO₂ capture from stack flue gas. However, not much work has been attributed to the development of suitable reactor designs. This thesis is concerned with the development of a novel reactor system that enables efficient CO₂ capture with solid amine functionalized adsorbent material by means of TSA.

Basic thermodynamic investigations of the TSA CO₂ capture process showed, that for economic process operation it is required to provide counter-current contact between gas and adsorbent streams in the adsorber and desorber. Furthermore, it has been concluded that the deployment of fluidized bed technology is crucial to allow for optimum heat transfer characteristics within the system. According to these findings, a novel TSA system consisting of interconnected multi-stage fluidized bed columns has been proposed as suitable reactor design and selected for further investigations. A thermodynamic equilibrium model has been used to quantitatively assess the process performance of the proposed TSA system and to compare it with MEA scrubbing technology performance data. Simulations clearly showed that the TSA system is at least competitive in terms of regeneration energy even if process improvements from heat integration are not considered. The fluid-dynamic characteristics of the proposed multi-stage fluidized bed system have been studied within a cold flow model (CFM) that has been designed, constructed and put into operation during the course of this thesis. Experiments conducted within the CFM showed that stable operation is possible within a broad range and proved that the proposed reactor system is feasible from a fluid-dynamic point of view. Basing on the results from the CFM campaign, a fully integrated TSA bench scale unit (BSU) for continuous capture of about 35 kg of CO₂ per day has been designed, constructed and put into operation during the course of this thesis. A proof of concept for the proposed TSA process has been delivered within one of the very first CO₂ capture experiments conducted. Steady-state operation with CO₂ capture efficiencies above 90 % and capture rates of around 35 kg_{CO2} per day have been achieved in several experiments. Furthermore, the influence of the main operating parameters on the process performance has been assessed through comprehensive parameter variations. Obtained BSU results indicated that adsorption/desorption kinetics are fast and that heat exchange was limiting the performance of the unit. Introduction of steam, either as stripping gas in the desorber or in form of humid adsorber feed gas had a significant impact on the system, which was most likely caused by co-adsorption of steam onto the adsorbent material.

KURZFASSUNG

Chemische Absorption von CO_2 mittels wässriger Aminlösungen wird derzeit als das am weitesten entwickelte CO_2 -Abscheideverfahren angesehen. Dennoch weisen Abscheideverfahren die auf dieser Technologie basieren mehrere prozessbedingte Nachteile auf, die einen großen Prozesswärmebedarf und hohe CO_2 -Abscheidekosten mit sich bringen. Um die derzeit erreichbaren CO_2 -Abscheidekosten wesentlich zu reduzieren ist es daher notwendig alternative Abscheideverfahren zu entwickeln. Prozesse basierend auf der kontinuierlichen Adsorption von CO_2 wurden kürzlich als potentielle Alternativen zur chemischen Absorption vorgeschlagen da diese die prozessinhärenten Nachteile der Absorption nicht aufweisen und somit geringer In den letzten Jahren wurden daher große Anstrengung unternommen um geeignete Adsorbentien zur Abtrennung von CO_2 aus Rauchgasen zu entwickeln. Derzeit gibt es jedoch nur wenige Arbeiten die sich mit der Entwicklung von geeigneten Adsorptions-Reaktorsystemen und damit mit der Umsetzung dieser Technologie befassen. Diese Doktorarbeit beschäftigt sich daher mit der Entwicklung eines neuartigen Reaktorsystems, welches eine effiziente CO_2 -Abtrennung mittels Temperaturwechseladsorption (TSA) ermöglichen soll.

Thermodynamische Untersuchungen am TSA Verfahrens wurden durchgeführt und zeigten, dass eine Gas und Adsorbentien innerhalb des Adsorbers und Desorbers im Gegenstrom geführt werden müssen um eine wirtschaftliche Arbeitsweise zu ermöglichen. Weiterhin wurde festgestellt, dass ein Gas-Feststoff-Kontakt im Wirbelbett zu optimale Wärmeübertragungseigenschaften führt. Basierend auf diesen Erkenntnissen wurde ein neuartiges TSA-System, bestehend aus zwei mehrstufigen Wirbelschichtkolonnen als geeignetes Reaktordesign entwickelt. Ein thermodynamisches Gleichgewichts-Modell wurde verwendet, um das Potential des vorgeschlagenen TSA-Systems zu erfassen und mit dem Stand der Technik zu vergleichen. Simulationsergebnisse zeigten deutlich, dass das TSA-System auch ohne Wärmeintegrationsmaßnahmen einen zumindest vergleichbaren Prozesswärmebedarf aufweist. Die fluid-dynamischen Eigenschaften des vorgeschlagenen mehrstufigen Wirbelschichtsystems wurden in einem Wirbelschicht-Kaltmodell (CFM) untersucht, welches im Verlauf dieser Arbeit entworfen, gebaut und in Betrieb genommen wurde. Versuche im CFM zeigten, dass ein stabiler Betrieb in einem weiten Bereich möglich ist, und bewiesen, dass eine Verwendung des vorgeschlagenen Reaktorsystems aus fluid-dynamischer Sicht möglich ist. Basierend auf den Ergebnissen aus der CFM-Kampagne, wurde ein TSA Laboranlage (BSU) für die kontinuierliche Abscheidung von bis zu 35 kg CO_2 pro Tag ausgelegt, gebaut und im Laufe dieser Arbeit in Betrieb genommen. Erste Versuche innerhalb der BSU lieferten einen „proof of concept“ für das vorgeschlagene TSA-Abscheidesystem. Ein stationärer Betrieb mit CO_2 -Trenngraden von über 90% und Abscheideraten von rund 35 kg $_{\text{CO}_2}$ pro Tag wurde in mehreren Experimenten erreicht. Darüber hinaus wurde durch umfangreiche Parametervariationen der Einfluss der wichtigsten Betriebsparameter auf die Abscheideleistung untersucht. Erhaltene BSU Ergebnisse zeigten schnelle Adsorptions-/Desorptions-Kinetik innerhalb der Wirbelschichtkolonnen und eine Limitierung der Abscheideleistung durch den erreichbaren Wärmeaustausch mit den Wirbelbetten. Die Einbringung von Wasserdampf, entweder als Strippgas im Desorber oder in Form von feuchten Abgas im Adsorber hatte eine signifikante Auswirkung auf den Wärmehaushalt im System. Dieser Einfluss wurde durch die Co-Adsorption von Wasserdampf auf dem Adsorbent begründet.

ACKNOWLEDGEMENT

I would like to take the opportunity to express my deepest gratitude to some of the people who supported me along the way of preparation of this thesis and contributed in one way or another in making it possible.

First of all, I like to thank **Tobias Pröll** for giving me the opportunity to work in his former research group, for initiating the TSA process development program and for providing space and equipment at his new laboratories. Furthermore, I like to thank him for encouraging my personal way of working and for his support during finalisation of this work.

I would also like to extend my sincerest gratitude to **Hermann Hofbauer** for giving me the opportunity to work at the Institute of Chemical Engineering, for his guidance and support whenever it was needed and for the trust he put in me.

Furthermore, I would like to express my deepest gratitude to **Gerald Sprachmann**. Without his confidence in the TSA technology and in our capabilities the development of the TSA process would not have been possible at all. Special thanks for sharing several very enjoyable and sometimes legendary times especially after the end of the official part of our meetings.

I would like to express a very warm thank you to **Rob Moene** for many interesting discussions, for his guidance and encouragement and for his positive and always friendly attitude.

Johannes Fuchs, to whom I owe a great debt of gratitude. The implementation of this work would just not have been possible without his great contributions. I would like to thank him for his friendship, the perfect teamwork and the uncountable enjoyable moments and discussions we had during the last years. I would also like to thank him and his family members for unforgettable and very enjoyable times in Schwarzenau.

Egon Zehetner, also for his friendship and his outstanding support during the last year. Without his expertise and photo equipment the cold flow model studies presented in this work would not have been as complete as they are.

I would also like to thank **Thomas Ringhofer** and **Florian Dietrich** for contributing with their Master Theses to the success of this work.

Very warm and great thanks to all members of the Zero Emission Technologies group, especially to **Stefan Penthor**, **Karl Mayer** and **Stephan Piesenberger** for numerous memorable and very enjoyable times, interesting discussions as well as for their support during the past years.

To my parents **Waltraud** and **Herbert** as well as to my brother **Michael**, for almost three decades of uncompromising love, support and encouragement. I owe you so much, all I can say is thank you.

Finally, my deepest and greatest gratitude to my love **Evelyn**, for being the most important person in my life. This thesis would simply not exist without you and your support. Thank you so much for making me smile and for lifting me up whenever I'm down and for teaching me every day what it means to be open minded, generous, polite and tolerant. Thank you for your faith in me and, above all, thank you for your love. I'm so much looking forward to spending a life-time together with you.

TABLE OF CONTENTS

ABSTRACT	I
KURZFASSUNG	II
ACKNOWLEDGEMENT	III
TABLE OF CONTENTS	IV
1. INTRODUCTION	1
1.1 CLIMATE CHANGE MITIGATION	1
1.1.1 <i>Climate change</i>	1
1.1.2 <i>Global energy demand and climate change mitigation strategies</i>	3
1.2 CARBON CAPTURE AND STORAGE	6
1.2.1 <i>General aspects and rationale of carbon capture and storage</i>	6
1.2.2 <i>Technological background</i>	7
1.2.3 <i>CO₂ capture processes</i>	8
1.2.4 <i>Post-combustion CO₂ capture via chemical absorption</i>	10
1.3 PROBLEM DEFINITION	12
1.3.1 <i>Aim of this work</i>	12
1.3.2 <i>Key objectives</i>	13
1.3.3 <i>Organization of this thesis</i>	13
2. THEORETICAL BACKGROUND	15
2.1 ADSORPTION TECHNOLOGY	15
2.1.1 <i>Definitions and historical background</i>	15
2.1.2 <i>Fundamental aspects of adsorption</i>	16
2.1.3 <i>Adsorption isotherms and calculation models</i>	20
2.1.4 <i>Adsorption processes for gas separation</i>	23
2.1.5 <i>Adsorbent materials</i>	28
2.2 FLUIDIZATION ENGINEERING	29
2.2.1 <i>General aspects of gas-solids contact</i>	29
2.2.2 <i>Fluidized bed existence range</i>	30
2.2.3 <i>Minimum fluidization velocity and single particle terminal velocity</i>	31
2.2.4 <i>Particle size definition</i>	33
2.2.5 <i>Particle classification according to Geldart</i>	35
2.2.6 <i>Fluidized bed regimes</i>	36
2.2.7 <i>Fluidized bed regime map</i>	38
2.2.8 <i>Bubbling fluidized beds</i>	39
2.2.9 <i>Bed-to-surface heat transfer in bubbling fluidized beds</i>	40
3. TEMPERATURE SWING ADSORPTION: REACTOR DESIGN	45
3.1 GENERAL ASPECTS	45
3.2 ADSORBENT MATERIAL	45

3.2.1	<i>General requirements on adsorbent materials for post-combustion CO₂ capture</i>	45
3.2.2	<i>Adsorbents for continuous TSA- chemisorbents vs. physisorbents</i>	46
3.2.3	<i>PEI impregnated solid sorbent materials</i>	50
3.3	HEAT MANAGEMENT AND PROCESS UP-SCALING	56
3.4	THERMODYNAMIC CONSIDERATIONS	58
3.5	MULTI-STAGE FLUIDIZED BED SYSTEMS	61
3.5.1	<i>General aspects of multi-stage fluidized bed systems</i>	61
3.5.2	<i>Design aspects of multi-stage fluidized bed systems with downcomers</i>	62
3.6	DOUBLE-LOOP MULTI-STAGE FLUIDIZED BED REACTOR DESIGN	66
3.7	CONCLUSIONS	69
4.	MODELLING AND PROCESS EVALUATION	70
4.1	MODEL DESCRIPTION	70
4.1.1	<i>General aspects</i>	70
4.1.2	<i>Adsorption thermodynamics</i>	71
4.1.3	<i>Model of a fluidized bed gas-solid contacting stage</i>	72
4.1.4	<i>Models used for thermodynamic evaluation of the TSA process</i>	73
4.2	RESULTS AND DISCUSSION	74
4.2.1	<i>Specification of the separation task</i>	74
4.2.2	<i>Performance evaluation of a single-stage TSA configuration</i>	75
4.2.3	<i>Performance of the multi-stage system with five stages in each contactor</i>	77
4.2.4	<i>Heat integration measures</i>	80
4.3	CONCLUSIONS	83
5.	FLUID DYNAMIC STUDY ON THE MULTI-STAGE FLUIDIZED BED REACTOR SYSTEM	84
5.1	COLD FLOW MODEL DESIGN	84
5.1.1	<i>General aspects</i>	84
5.1.2	<i>Cold flow model design</i>	84
5.2	EXPERIMENTAL	87
5.2.1	<i>CFM setup</i>	87
5.2.2	<i>CFM start-up and commissioning</i>	89
5.3	RESULTS FROM COLD FLOW MODEL TESTING	91
5.3.1	<i>Variation of solids circulation rate</i>	91
5.3.2	<i>Variation of column fluidization rate</i>	93
5.3.3	<i>Variation of total system solids inventory</i>	94
5.3.4	<i>Study of dense bed expansion using long-time exposure photography</i>	95
5.4	CONCLUSIONS FROM THE COLD FLOW MODEL STUDY	99
6.	TSA BENCH SCALE UNIT FOR CONTINUOUS CO₂ CAPTURE	100
6.1	BENCH SCALE UNIT DESIGN	100
6.1.1	<i>General description</i>	100
6.1.2	<i>BSU design and specifications</i>	100
6.2	EXPERIMENTAL	103
6.2.1	<i>Experimental setup</i>	103
6.2.2	<i>Measurement and instrumentation</i>	104

6.3	COMMISSIONING OF THE BSU	105
6.3.1	<i>Determination of screw conveying rates</i>	105
6.3.2	<i>BSU start-up procedure.....</i>	106
6.3.3	<i>Assessment of gas leakage between both columns.....</i>	107
6.4	RESULTS FROM CONTINUOUS CO₂ CAPTURE TESTS	110
6.4.1	<i>Experimental plan</i>	110
6.4.2	<i>First continuous CO₂ capture test</i>	112
6.4.3	<i>Results from performed dry gas parameter variations.....</i>	115
6.4.4	<i>Variation of stripping gas composition</i>	120
6.4.5	<i>Variation of flue gas humidity</i>	121
6.5	CONCLUSIONS FROM CONTINUOUS CO₂ CAPTURE TESTS.....	125
7.	SUMMARY	128
8.	CONCLUSIONS.....	133
9.	OUTLOOK	136
	NOTATION	139
	REFERENCES.....	144
	APPENDIX	152

1. INTRODUCTION

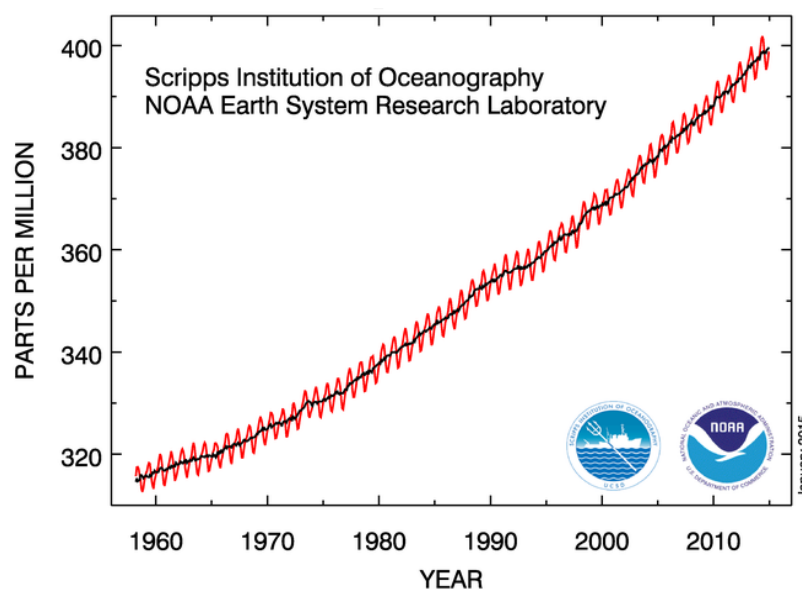
1.1 CLIMATE CHANGE MITIGATION

1.1.1 *Climate change*

Abnormal changes in the global climate system can be observed with progressing industrialisation since the late 19th century. An increase of the average temperature in the northern hemisphere of about 0.85 °C has taken place since 1880. In Austria the average temperature has increased by even 2.0 °C in the same period, whereby half of the warming occurred from 1980 on [APCC, 2014]. Globally, each of the last three decades has been warmer than any preceding decade since 1850 with the period from 1983-2012 being likely the warmest 30-year period since 1400 years [IPCC, 2014]. The circumstance of increasing global average temperature has been referred to as global warming and it represents the most important indicator for the observed climate change.

The Earth's climate is a highly complex system with many subsystems such as the atmosphere, the hydrosphere, the biosphere or the cryosphere. The subsystems are interconnected through the exchange of energy, carbon, or other chemical species, whereby these exchange processes are driven by the energy received from the sun. The equilibrium temperature in this system depends on the difference between the amount of energy received from the sun and the amount of energy that the Earth re-emits into space. This equilibrium can be influenced by different external and internal forcings such as fluctuations of the incoming solar radiation, variations of the Earth's orbit or surface albedo as well as changing concentrations of climate active gas species (i.e. greenhouse gases) within the atmosphere. In the past, variations of these forcings have led to changes of the global climate system. For example, the present geological climate period (Quaternary) had long periods of ice ages that were alternating with shorter and warmer periods which were caused by variations of the Earth's orbit. For the recently observed climate change, however, great concerns were raised by the global scientific community that human activities may represent the main driver for this change.

Figure 1.1: Atmospheric CO₂ concentrations measured at Mauna Loa Observatory (taken from [ESRL, 2015]).



Anthropogenic activities, especially since industrialisation have led to increasing CO₂ concentrations in the atmosphere. Figure 1.1 shows the average atmospheric CO₂ concentrations over the second half of the 19th century, recorded on Mt. Mauna Loa, Hawaii. As can be seen from this figure, the CO₂ concentration in the atmosphere has increased from around 300 ppm in 1950 to almost 400 ppm today. Since pre-industrial times (280 ppm), the CO₂ concentration even increased by 40 %. Furthermore, current CO₂ levels are higher than they have been for the last 800000 years in Earth's history [IPCC, 2014].

Since the 19th century it is known that the heat absorption capability of the atmosphere is strongly influenced by the concentration of so called greenhouse gases [Tyndall, 1861] and that CO₂ is such a gas [Arrhenius, 1886]. Thus, the key questions regarding the present climate change are

- 1. Is it caused by human activities**
- 2. How will the climate further evolve and**
- 3. What consequences would we have to face with further changes in the climate system**

In 2014, the Intergovernmental Panel on Climate Change (IPCC) published its 5th Assessment Report on global climate change that provides scientific answers to these questions [IPCC, 2014]. Similar to previous reports the assessment is structured into three different scientific topics that address the physical science basis of climate change, the associated risks for global society and ecosystems as well as strategies for climate change mitigation. To predict future climate trends and their consequences a new set of scenarios of future GHG emissions, aerosols and other anthropogenic drivers have been used (i.e. Representative Concentration Pathways (RCPs)). The key messages from the evaluations of past climate conditions and projections of potential future climate changes are clear and can be summarized as follows [IPCC, 2014]:

- 1. Warming of the Earth's climate is unequivocal.**
- 2. It is extremely likely that human activities have been the dominant cause of the observed global warming since the mid-20th century.**
- 3. Continued greenhouse gas emissions will cause further climate change that in turn causes potential risks for human health and infrastructure as well as for marine and land ecosystems and will set the need for substantial adaptations.**

There is further strong evidence that the present climate change already impacts natural systems. For example, annual precipitation has changed regionally, significant melting of glaciers and ice shells occurred and many terrestrial, freshwater and marine species have shifted their geographical ranges, seasonal activities or even worse became extinct. However, not only changes in ecosystems but also impacts on human systems have been observed and attributed to climate change. For example, it was shown that climate change had more commonly negative impacts on multi-regional crop yields than positive impacts. Furthermore, there is medium confidence that in some regions the heat-related mortality increased whereas the cold-related mortality decreased. In addition to that, changes in the occurrence of weather extremes with more common warm temperature extremes and less cold temperature extremes and increasing number of heavy precipitation and high sea level events are observable since about 1950. [IPCC, 2014]

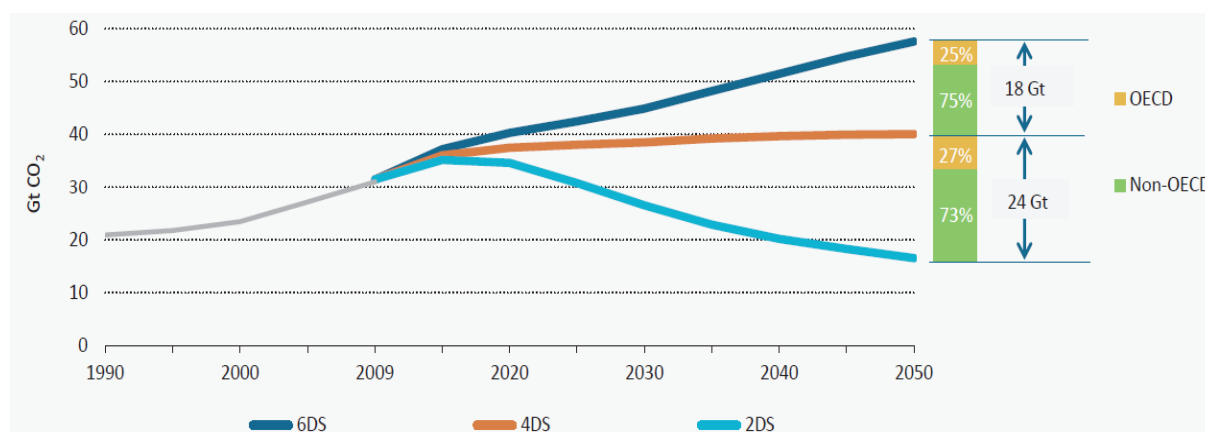
Damages or risks from climate change emerge not necessarily from climate hazards only but usually also depend on the exposure and vulnerability of people and ecosystems and are thus unevenly distributed and generally greater for disadvantaged people [IPCC, 2014]. However, ongoing global warming would amplify these existing risks, create new risks and increase the likelihood of severe, pervasive and irreversible impacts for natural and human systems [IPCC, 2014]. Further warming of the climate is largely determined by the cumulative future CO₂ emissions which in turn largely depend on socio-economic development and future climate policies. Thus, in order to mitigate global warming and its related risks, substantial and sustained reduction of greenhouse gas emissions are needed.

1.1.2 Global energy demand and climate change mitigation strategies

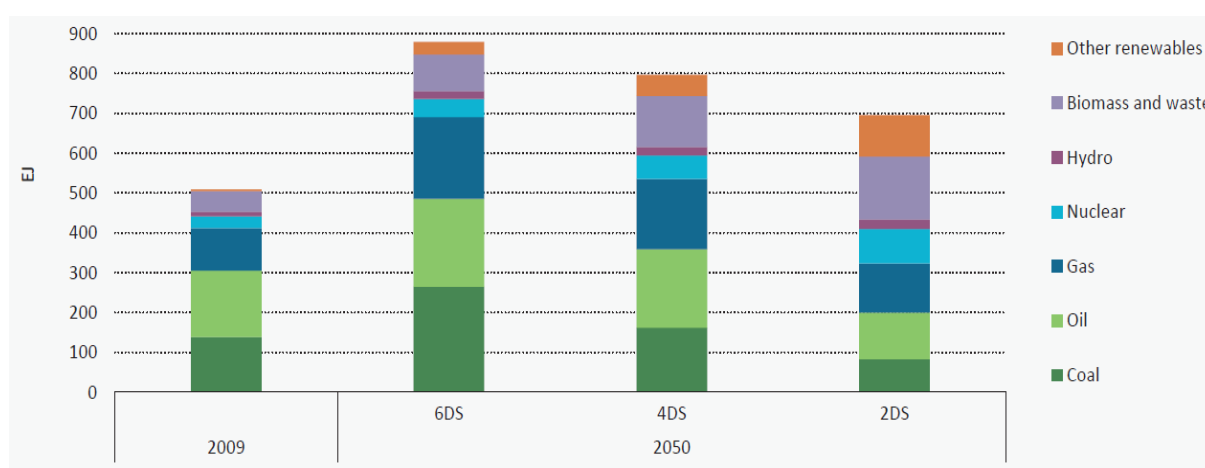
International societies and governments agreed to combat climate change and to limit global warming to a maximum of 2 °C. This global temperature increase (likely) corresponds to maximum atmospheric greenhouse gas concentrations of about 450 ppm CO₂-eq (or lower) at 2100 (assuming realistic emission pathways and absolute carbon budget). However, recent anthropogenic greenhouse gas emissions are the highest in history [IPCC, 2014] and substantial reductions of greenhouse gas emissions are thus required to achieve the two-degree goal.

The International Energy Agency (IEA) frequently publishes prospects of the world's primary energy demand and the corresponding CO₂ emissions that have to be taken into account if measures for climate mitigation should be elaborated. Moreover, prospective energy demands also depend on climate mitigation actions that may be taken in the future as they can lead to significantly reduction of energy consumption (e.g. by increasing process efficiencies). Thus, the IEA has considered three different future emission scenarios for their energy perspective assessment that have been referred to 6DS, 4DS and 2DS scenario. The 6DS scenario can be considered as "business as usual" scenario that extends current trends of primary energy demands and greenhouse gas emissions. Following this scenario would cause a long-term increase of global average temperature of 6 °C with all associated risks for natural and human systems. The 4DS scenario assumes that recent international pledges for reductions of greenhouse gas emissions will be achieved and that further efforts in the improvement of process efficiencies will be taken and it projects a long-term temperature rise of 4 °C. Finally, the 2DS scenario projects an energy system that, on a long-term would lead to a stabilization of global greenhouse gas concentrations to about 450 ppm and limit global temperature increase to 2 °C. This scenario requires that energy-related CO₂ emissions are cut by more than half till 2050 (compared to 2009) and continue to decrease thereafter. Furthermore, it requires additional reductions of greenhouse gas emissions in sectors apart from the energy sector. The corresponding emission pathways of the three scenarios are given in Figure 1.2. [IEA, 2012b]

The global primary energy demand of 2009 together with the projected energy demands in 2050 for all three emission scenarios are shown in Figure 1.3. Most important to note is that in all scenarios the contribution of fossil primary energy sources will remain dominant if not the largest in 2050. Furthermore, the total primary energy demand will increase in all three scenarios due to ongoing economic growth and increasing population. Even in the 2DS scenario the primary energy demand is about to increase by 35 %. The lower energy demand in the 2DS compared to the other scenarios arises from increasing utilization of electricity (e.g. in the transport section) whilst its production is decarbonized.

Figure 1.2: IEA ETP 2012 future emission scenarios (taken from [IEA, 2012b]).

Furthermore, most of the increasing primary energy demand will come from non-OECD countries while the primary energy demand of OECD countries will remain almost constant. The projected increase of primary energy demand of non-OECD countries in the 2DS scenario is by some 70 %. In OECD countries the utilization of fossil fuels in the electricity and transport sector will simultaneously drop by 60 %. These regional differences are important as they have implications on how the transformations of the respective energy systems can be achieved. [IEA, 2012b]

Figure 1.3: IEA ETP 2012-Future primary energy demand (taken from [IEA, 2012b]).

It has to be noted that in 2050 the distribution of greenhouse gas emissions among the different sectors will change significantly (see Figure 1.4). While the emissions arising from electricity generation will drop significantly in the 2DS, emissions from the transport and industry sector remain relatively high, revealing the difficulties associated with decarbonizing these sectors.

In either case, the 2DS will be only reached if global society manages to decouple the energy use from their economic activities which in turn requires development and deployment of the required technologies as well as changes of the economic structure and in individual behaviour [IEA, 2012b].

This implies that collective effort in climate mitigation has to be taken among all primary energy sources and sectors. Furthermore, a portfolio of different technologies will be required to achieve the 2DS target.

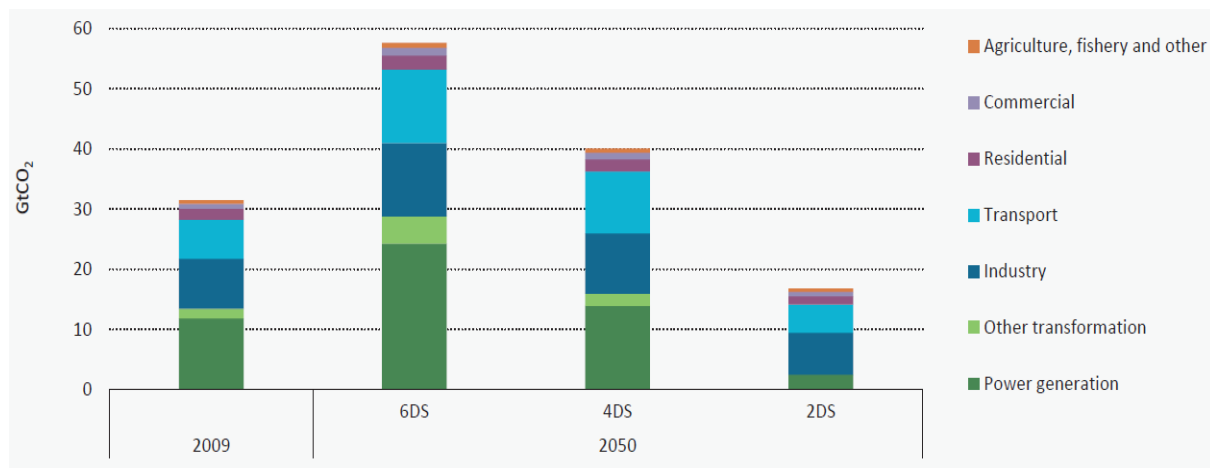
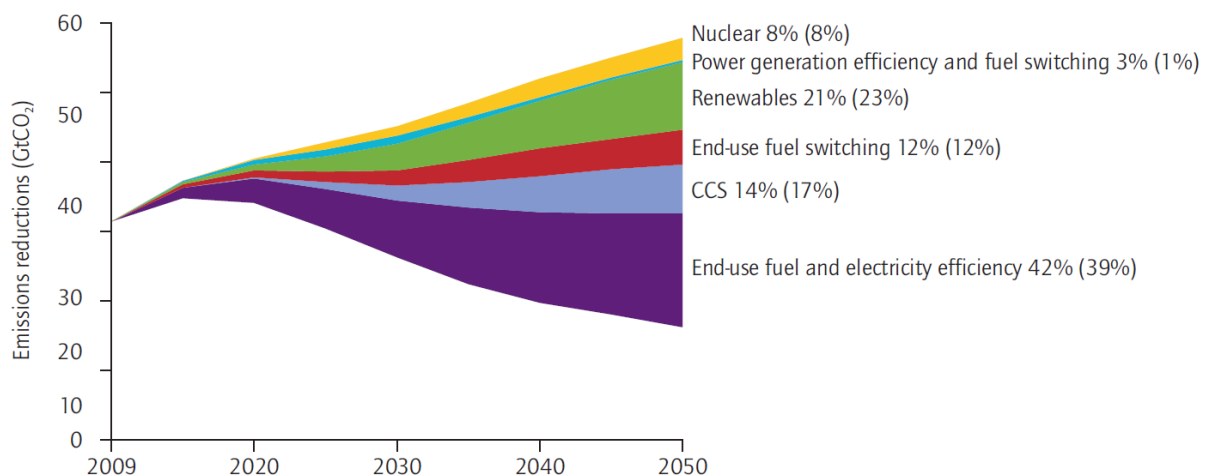
Figure 1.4: IEA ETP 2012-Greenhouse gas emissions per sector (taken from [IEA, 2012b]).

Figure 1.5 shows a potential technology portfolio that can facilitate emission reductions that are consistent with the 2DS scenario and related to the 6DS scenario. This technology portfolio can be considered as optimized in terms of abatement costs. This means that if one of the respective technologies fails to achieve the market penetration indicated in Figure 1.5 the other technologies need to contribute more to climate mitigation and thereby generate more abatement costs as compared to the given portfolio. [IEA, 2013b]

Figure 1.5: IEA cost effective portfolio of climate mitigation measures (taken from [IEA, 2013b]).

One important technology in this portfolio is carbon capture and storage (CCS) which is expected to contribute 14 % of the cumulative emission reductions till 2050. The IEA further expects that almost half of CCS related CO₂ abatement will take place in the industrial sector. [IEA, 2013b]

It is thus evident that CCS will be a critical component in the portfolio of climate mitigation measures and this thesis presents the development of a novel CO₂ capture system that has the potential to further decrease the costs associated with CCS. Hence, an introduction to CCS technology should be given in the following.

1.2 CARBON CAPTURE AND STORAGE

1.2.1 *General aspects and rationale of carbon capture and storage*

Carbon capture and storage (CCS) is a climate change mitigation method that refers to a number of different technologies that separate CO₂ at some process stage of large-point emission sources and subsequently isolate the captured CO₂ from the atmosphere through long-term sequestration into adequate storage sites [IPCC, 2005; Boot-Handford et al., 2013].

Even though the concept of CCS as option for mitigating CO₂ emissions was already evaluated around 1990 [Golomb et al., 1989; Booras, 1991] broad deployment of CCS is still far from being realized. One explanation for this is that in contrast to other climate change mitigation routes, the application of CCS yields no commercially valuable product. On the contrary, CCS causes significant investment and operational costs that are set against CO₂ emission savings as single benefit arising from CCS. Furthermore, storage of CO₂ implies safety risks that have to be managed on a long-term together with ethical concerns regarding future generations.

As a consequence, the deployment of CCS solely depends on how global society values the importance and priority of combating climate change and on policies and incentive mechanisms (e.g. price of CO₂) that can be developed basing on this opinion. However, while the provision of catalytic mechanisms are subject to decisions made by international societies and policy makers, the rationale behind the inclusion of CCS as important climate change mitigation method becomes evident from the following technological and economical aspects [IEA, 2013b]:

- Despite worldwide advances in the development and deployment of low-carbon technologies, coal has been the fastest growing source of primary energy, especially due to economic growth in China and India [IEA, 2012c]. Moreover, coal (and other fossil fuels) will remain to contribute a significant if not dominant part to the global primary energy demand. CCS represents the only technology (at least in the applicable sectors) that provides a solution for achieving deep CO₂ emission reductions even with continuing or increasing utilization of fossil fuels. [IEA, 2013b]
- If global average temperature increase should be limited to 2 °C, less than one-third of proven global reserves of fossil fuels can be utilized without CCS. The associated economic value of these reserves would thus get lost which affects governments and industries that derive incomes from fossil fuels. [IEA, 2012a]
- Discarding CCS from the list of mitigation measures would put pressure on all other mitigation routes and overall mitigation economics. For instance, mitigation efforts in the electricity sector would face a 40 % cost increase for the same CO₂ reduction targets in case CCS is not considered as mitigation option [IEA, 2012b]. Moreover, compared to cost-effective climate mitigation scenarios and depending on the global consumption growth, total climate change mitigation costs for stabilization of atmospheric greenhouse gas concentrations at 450 ppm CO₂-eq in 2100 could increase by up to 300 % if CCS is not available [IPCC, 2014].

- The industrial sectors currently contribute about 25 % of global CO₂ emissions and low reduction potentials are expected from (further) efforts in increasing process efficiencies or substitution of fossil fuel inputs. Thus, CCS currently represents the only mitigation concept that allows for deep CO₂ emission reductions in industrial sectors such as cement, iron and steel or chemicals and refining. [IEA, 2013a; IEA, 2013b].
- The combination of utilizing biofuels for generation of heat and power (or chemicals) with CCS (BECCS) represents a large-scale carbon dioxide removal (CDR) option as it would lead to a net negative CO₂ emission in case the process chain can be implemented in a sustainable way. [IPCC, 2014]

Furthermore, sufficient climate mitigation actions, especially in emerging countries such as China or India will most likely only be taken if global economic growth can be sustained or even increased and adequate living standards can be achieved globally throughout this century. Therefore it is crucial to perform climate mitigation in a cost-effective manner or even gain economic benefit from this evolving market. Basing on the aforementioned, it can be concluded that it is most likely to achieve this with inclusion of carbon capture and storage into the portfolio of climate mitigation options. In the following, the technological background of CCS, especially on the step of carbon capture should be briefly introduced.

1.2.2 Technological background

The complete CCS process chain can be separated into three individual tasks that are

1. Capture and subsequent compression of CO₂,
2. Transport of CO₂ to suitable storage sites and
3. Sequestration of CO₂.

The capture of CO₂ represents the most costly part accounting for 75 % of the overall CCS chain costs and is thus most critical in terms of overall process economics [Feron, 2005]. Transportation and storage of the CO₂ typically contribute only a minor fraction to the total costs of CO₂ sequestration [Figueroa et al., 2008]. Thus, most of the CCS related research focused on improving existing CO₂ capture technologies and on the development of novel CO₂ capture processes, respectively. The most critical aspect for CO₂ transportation is the purity of CO₂ achieved in the capture process since even low concentrations of impurities (e.g. O₂) can cause severe problems in pipelines or ship transport (e.g. corrosion or condensation). However, a great deal of practical experience exists from long distance pipeline transport of CO₂ in North America where CO₂ is utilized for enhanced oil recovery [Tanaka, 2008]. The economics of the individual transport methods (i.e. road and rail tankers, ship, onshore and offshore pipeline) typically depend on the quantities of CO₂ that need to be transported as well as on the transport distance [IPCC, 2005]. Storage of CO₂ is also performed since many years at different sites all around the world [Tanaka, 2008]. Potential sub-surface storage sites are deep saline formations, deep unminable coal seams as well as depleted or mature oil and gas fields. Storage within deep saline sites is, however, considered as most promising for CCS since such sites are evenly distributed around the world. Furthermore, compared to exploited oil- and gas fields they do not exhibit (multiple) production wells which represents a benefit for monitoring. Saline aquifers must exhibit sufficient storage capacity, porosity and permeability to be suitable for

CO₂ storage. Furthermore, they must be located at least 800 m below sea level to ensure stored CO₂ is stabilized in its dense phase and it must have a sealing cap rock that is impermeable to the passage of CO₂ on top of it [Bentham and Kirby, 2005]. In general, CO₂ storage is considered as most critical to public acceptance as it requires safe storage of massive amounts of CO₂ on a long-term.

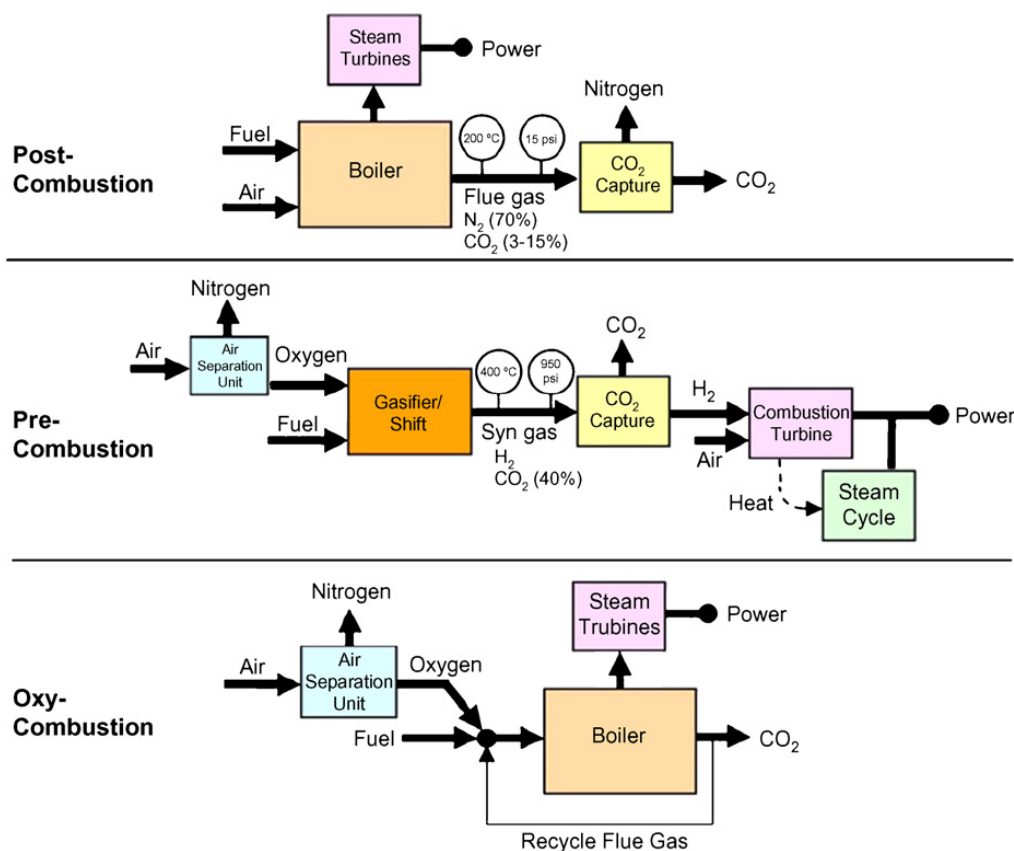
Successful deployment of CCS needs provision of technological solutions in each of the three sub-tasks. Furthermore, the provided technologies have to be feasible from an economic point of view. While CO₂ transport is already a relatively mature step in CCS, it is necessary to gain better understanding of risks and costs associated with geological CO₂ storage and to further reduce costs of CO₂ capture. Furthermore, legal and regulatory frameworks need to be elaborated for CCS and public awareness and understanding of CCS needs to be improved.

This thesis aims at developing a novel CO₂ capture technology that allows for significant reductions of CO₂ capture costs. Hence, in the following the technological background of CO₂ capture will be addressed in more detail. For detailed information regarding CO₂ transport and storage it is referred to the relevant literature (e.g. [IPCC, 2005; Tanaka, 2008; Boot-Handford et al., 2013]).

1.2.3 CO₂ capture processes

Typically, three different approaches are suggested for the task of CO₂ capture. Those are referred to post-combustion capture, pre-combustion capture and oxy-fuel combustion. Process schemes of all three approaches are given in Figure 1.6 and they should be briefly discussed in the following.

Figure 1.6: Proposed CO₂ capture routes (taken from [Figuerola et al., 2008]).



In **post-combustion** applications, CO₂ capture occurs downstream to the emitting process. Thus, this approach represents an end-of-pipe solution that can be applied to any kind of combustion, gasification or industrial process. For industrial processes it sometimes even represents the only

suitable option for CO₂ capture. However, the main drawback or challenge of this approach is that CO₂ partial pressures are usually low in the considered flue gas streams, which requires comparably large amounts of energy for separation. Typically, reversible reaction of CO₂ with aqueous amine solutions is suggested for post-combustion capture. This chemical absorption is a well-known technology that has been widely deployed in several industrial processes (e.g. gas purification) [MacDowell et al., 2010]. Chemical absorption is also considered as benchmark for the post-combustion CO₂ capture technology studied in this work and will thus be discussed in more detail in Section 1.2.4. Apart from chemical absorption, technologies basing on selective CO₂ adsorption, permeation through membranes and cryogenic separation or bio-mimetic approaches have been suggested for post-combustion CO₂ capture [Feron, 2005].

Pre-combustion CO₂ capture comprises any kind of process that decarbonizes utilized fossil fuels prior combustion. However, typically the term is connected to the so called integrated gasification combined cycle process (IGCC) where solid fuels are first gasified and where the purified syngas is sent to a water gas shift reactor to obtain a gas stream consisting predominantly of H₂ and CO₂. The CO₂ is then separated from the hydrogen again by means of physical or chemical absorption or by membranes. Thereafter, CO₂ is ready for compression and storage whereas the remaining hydrogen rich stream can be combusted in a turbine and used for power and steam generation. An advantage of this process is that compared to post-combustion applications the CO₂ partial pressure in the separation step is significantly higher (i.e. generally larger CO₂ concentration and potentially larger absolute pressure since gasification can occur at elevated pressure). This allows for more efficient separation (and compression) and typically lowers the overall parasitic energy demand of the capture process.

Oxy-fuel combustion refers to a process in which mixtures of almost pure O₂ (>95 %_{Vol}) and recycled flue gas are used to oxidize the utilized fuel. The use of this oxidizing agent leads to an exhaust gas stream that predominantly consists of CO₂ and water that can be simply separated through condensation of water. After condensation, the derived CO₂ typically exhibits impurities that arise from the utilized fuel and oxygen that need to be separated upstream to the compression unit. Furthermore, the utilization of high purity oxygen requires the application of an (cryogenic) air separation unit. The electrical energy demand of this unit represents the main energy penalty of oxy-fuel combustion compared to conventional combustion without carbon capture.

In addition to the discussed classical approaches for CO₂ capture several other approaches such as calcium looping, chemical looping or the use of ionic liquids instead of amine solutions have been proposed for CO₂ capture. These technologies show great potentials for reducing the CO₂ capture costs significantly. Nevertheless, the maturity level of the three classical approaches discussed above is significantly larger so that they are typically considered as benchmark technologies.

This work aims at the development of a novel technology for post-combustion CO₂ capture. Consequently, amine scrubbing has been selected as benchmark technology for evaluation of the developed CO₂ capture process and should thus be introduced in more detail in the following.

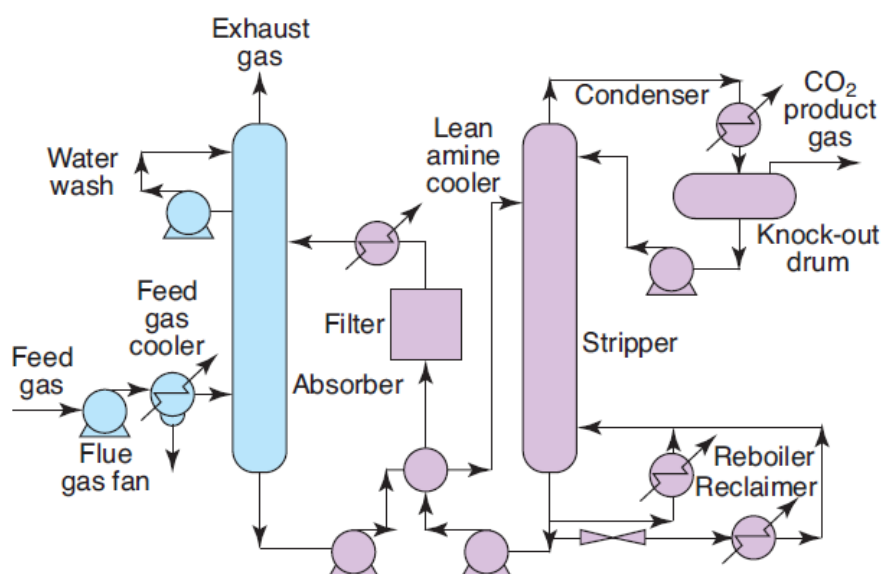
1.2.4 Post-combustion CO₂ capture via chemical absorption

The separation of CO₂ by chemical absorption is a mature and well-known technology and the basic process has been patented as early as 1930 [Bottoms, 1930; Rochelle, 2009]. In the late 1970s and early 1980s the process has been widely applied for flue gas CO₂ capture in the U.S. to serve as potential economic CO₂ source for industrial applications such as enhanced oil recovery (EOR) or the production of dry ice [Rao and Rubin, 2002]. However, for successful deployment in the field of CCS the process has yet to be demonstrated at scales that are sufficient for large-point emission sources in the power and industry sector.

The chemical absorption processes utilize liquid chemical solvents that can reversibly react with gaseous CO₂ by means of continuous temperature swing absorption in two separate columns. In this process a stream of “lean” solvent (i.e. solvent with low CO₂ loading) is introduced to the top of the absorption column where it flows down through the column and thereby selectively absorbs CO₂ from the upwards streaming flue gas stream. To improve the contact between the solvent and the CO₂ and thus the overall absorption kinetics the column is usually filled with packing materials. The packing material needs to facilitate large specific surfaces at lowest possible flow resistance to minimize the column pressure drop and the corresponding power demand of the flue gas blower. The power demand of the flue gas blower accounts for the main electricity demand of the scrubbing process [Rolker and Arlt, 2006]. The operating temperature of the absorber typically lies between 40-60 °C if aqueous alkanolamines are used as solvents [Bailey and Feron, 2005]. To avoid any entrainment of solvent droplets or solvent vapour emissions, the treated flue-gas is passed through a water wash section after reaching the top of the absorber column. At the bottom of the absorber column the CO₂ loaded “rich” solvent is extracted and pumped to the top of the regenerator column. Solvent regeneration is typically performed at 100-140 °C and slightly above atmospheric pressure [Bailey and Feron, 2005]. The regenerator column comprises a reboiler at the bottom that provides the required regeneration heat. The reboiler heat duty comprises the energy needed to heat up the solvent to regeneration conditions, the heat needed to break up the CO₂ bonds as well as the heat required for production of steam that acts as stripping agent within the regenerator and represents the main heat requirement of the process. At the top, the regenerator column comprises a condenser that is required for the recovery of stripping steam and to obtain an almost pure (>99 %) CO₂ product [Bailey and Feron, 2005]. The regenerated “lean” solvent can be extracted from the bottom of the regenerator column and pumped back to the top of the absorber column to capture CO₂ again. Typically, a so called “lean/rich” heat exchanger is applied to transfer heat between “lean” and “rich” solvent streams that are pumped between both columns. This heat integration measure allows for reducing the sensible heat demand for heating the “rich” solvent within the regenerator to a minimum. The described scrubbing process is illustrated within Figure 1.7.

Due to the acidic nature of CO₂, the use of amine containing liquid solvents has been suggested for CO₂ separation. Aqueous solutions of 30 %_w monoethanolamine (MEA) can thereby be considered as state-of-the-art solvents. However, novel solvents have been developed and utilized to achieve lower energy consumptions [Bailey and Feron, 2005]. Typically, sufficient CO₂ capture performances with efficiencies ranging from 75-90 % and CO₂ purities greater 99 % can be achieved using a MEA based solvent [Rao and Rubin, 2002].

Figure 1.7: Process scheme of MEA CO₂ scrubbing process (taken from [Bailey and Feron, 2005]).



However, the main drawback of this technology is the considerably large energy requirement for solvent regeneration amounting for 3.7 to 4.5 MJ per kg CO₂ captured [Tarka et al., 2006; Knudsen et al., 2009; Berger and Bhowan, 2011; Sjoström and Krutka, 2010; Pirngruber et al., 2013]. This relatively high energy demand would lead to a thermal efficiency reduction of about 10.6 % for a retrofitted coal fired power plant which corresponds to CO₂ avoidance costs of approximately 80 US\$ per tonne of captured CO₂ [Sjoström and Krutka, 2010]. Furthermore, due to the relatively slow absorption kinetics that are associated with dissolution and diffusion of CO₂ in the solvent, the capital expenses for the absorber of a full-scale amine scrubbing process would be considerably large [Heesink et al., 2013]. In addition to that, solvent degradation leads to typical solvent losses of between 0.5 to 2.0 kg per tonne of CO₂ captured [Rolker and Arlt, 2006]. This obviously leads to considerably large solvent make-up costs. A further drawback is that amines are irreversibly degraded by SO_x and O₂ and that some degradation products are corrosive or sometimes even potentially harmful to the environment or human health [MacDowell et al., 2010]. The corrosive nature of some degradation products as well as the solvent tendency to foam during operation could impact the integrity of plant operation and typically requires the addition of suitable inhibitors.

Hence, a lot of opportunities for improvement of the amine scrubbing process exist, especially with regard to process energy demand, capital costs or corrosion and emission issues. In the past, most of these issues have been subject to extensive research and development efforts and led to optimized process operation [Bailey and Feron, 2005; Rolker and Arlt, 2006; Rochelle, 2009; MacDowell et al., 2010]. Nevertheless, the technology exhibits various shortcomings that are intrinsic to the process and generally result in high CO₂ capture costs. This sets the need to develop alternative post combustion CO₂ capture technologies to obtain reduced CO₂ capture costs in the future.

1.3 PROBLEM DEFINITION

1.3.1 *Aim of this work*

The currently most mature post combustion CO₂ capture process is scrubbing by means of chemical solvents in continuous temperature swing absorption operation. One drawback of the scrubbing processes is, however, that they consume a lot of energy for heating the solvent to the desired regeneration temperature in the stripper and for supplying the required heat for regeneration of the solvent (i.e. heat of reaction plus heat for solvent evaporation). Another intrinsic problem of amine scrubbing systems is that transport of gas phase CO₂ into the solvent is based on dissolution and diffusion mechanisms that result in relatively low mass transfer coefficients. Hence, the application of sizeable and packed absorber columns is required to achieve practical CO₂ capture performance. Consequently, amine scrubbing systems exhibit high capital costs that in turn contribute to the overall CO₂ avoidance costs. In the past, researchers made substantial progress in the development of new solvents, optimized stripper configurations and advanced heat integration strategies that led to reduced energy demands and CO₂ avoidance costs of chemical scrubbing processes. However, the aforementioned drawbacks of amine scrubbing remain as they are intrinsic to the process. Breakthroughs in the reduction of CO₂ capture costs thus require the development of alternative technologies.

The capture of CO₂ via continuous temperature swing adsorption onto suitable solid adsorbent materials has been proposed as promising alternative to amine scrubbing technologies. Improved energy requirements can be expected from adsorption processes since the adsorbent materials typically exhibit higher CO₂ capacities and lower material heat capacities compared to chemical solvents. Furthermore, compared to amine scrubbing processes significantly larger mass transfer rates can be expected between highly porous adsorbent materials and bulk gas CO₂. As a consequence, the adsorber column could be comparably small which in turn implies reduced capital expenses.

Development of adsorptive CO₂ capture process has mainly focused on the development and analysis of different types of potential adsorbent materials. However, very little effort has been attributed to the development of suitable reactor designs for continuous temperature swing adsorption processes. The aim of this thesis is thus to elaborate a suitable reactor system for a CO₂ capture process that is based on temperature swing adsorption. The obtained CO₂ capture process should be evaluated from a thermodynamic point of view and derived performance figures should be used for comparison with state-of-the-art post-combustion CO₂ capture technologies. Furthermore, basing on the proposed reactor system a continuously operating bench scale unit should be designed, constructed and put into operation. CO₂ capture experiments should then be conducted within this unit to demonstrate the feasibility of the proposed design and to study the process experimentally under continuous operating conditions.

1.3.2 Key objectives

In accordance with the defined aims above the key objectives of this thesis can be formulated as follows:

1. Compare different classes of adsorbent materials that have been suggested for CO₂ separation from flue gases and select the most suitable material for further process design.
2. Elaborate and propose a reactor design that is suitable for continuous CO₂ capture from stack flue gas via temperature swing adsorption.
3. Assess the economics of the proposed temperature swing adsorption reactor system and compare obtained results with reported data from the benchmark technology.
4. Design and construct a bench scale unit for continuous CO₂ capture via temperature swing adsorption.
5. Conduct continuous CO₂ capture experiments within the bench scale unit in order to demonstrate the suitability of the proposed reactor system.
6. Perform parameter variations within the bench scale unit to study the process experimentally. Identify main operating parameters and their influence on the process performance. Identify performance limitations of the process and derive further process optimizations.
7. Propose next research and development steps that need to be taken in order to further push the temperature swing adsorption technology towards commercialization.

1.3.3 Organization of this thesis

In Chapter 2, the fundamentals of adsorption technology and fluidization engineering will be briefly introduced in order to provide the necessary theoretical background for the practical parts and discussions within this thesis.

Chapter 3 examines the key design aspects of temperature swing adsorption reactor systems for CO₂ capture from stack flue gas. The examination involves a comparison of properties of different existing adsorbent materials. Furthermore, process thermodynamics and heat management will be discussed and used to derive a suitable reactor system for continuous capture of diluted CO₂ streams via temperature swing adsorption.

Within Chapter 4 the temperature swing adsorption process that has been proposed in Chapter 3 is evaluated quantitatively. The evaluation is performed on the basis of mass- and energy balance calculations and available adsorption equilibrium data using a specially developed thermodynamic equilibrium model that will be introduced in the first part of this chapter. In the second part, the obtained process performance data will be discussed and compared with data from state-of-the-art technology. Finally, further process optimization strategies will be suggested and conclusions on the obtained results will be drawn.

A fluid-dynamic feasibility study of the proposed reactor system is conducted within Chapter 5. The feasibility study is performed within a cold flow model that has been designed in accordance with the reactor system proposals from the previous chapters as well as with desired operating parameters of

a planned continuously operating TSA bench scale unit. Results from the performed fluid-dynamic investigations will be presented and characteristics of the operation will be presented.

Chapter 6 introduces the bench scale unit for continuous CO₂ capture basing on TSA that has been designed, constructed and put into operation during execution of this doctoral thesis. Several experiments, including a vast variation of main operating parameters of the bench scale unit have been performed and results from these experiments will be presented in this chapter. The results will be discussed and taken up to draw conclusions on the function and operability of the proposed TSA reactor system.

Chapter 7 gives a short summary of the complete content of this thesis, whereas Chapter 8 highlights the main conclusions that can be derived from this thesis.

Finally, the author takes the liberty to suggest further research and development work regarding TSA processes in the outlook given in Chapter 9.

2. THEORETICAL BACKGROUND

2.1 ADSORPTION TECHNOLOGY

2.1.1 *Definitions and historical background*

Adsorption generally means the concentration of gaseous or dissolved substances on a boundary layer built up on the surface of a solid or liquid. The substance that exists in adsorbed state within the boundary layer is generally referred to as “adsorbate”, while the substance that is wished to be adsorbed is called the “adsorptive”. The material that provides the active surface at which adsorption takes place is defined as the “adsorbent”. The reverse process to adsorption, i.e. the removal of adsorbed species from the surface of an adsorbent is called desorption. In general, adsorption/desorption processes can take place at the interface of two phases that include liquid-liquid-, liquid-gas-, solid-liquid- and solid-gas systems. However, today's industrial scale adsorption processes are mainly based on systems that involve solid-liquid or solid-gas interfaces [Dąbrowski, 2001]. Since the technology of interest in this work is also based on adsorption in solid-gas interfaces, the following will primarily focus on such systems.

The very first exploitation of certain effects that can be connected to adsorption date back to ancient times [Dąbrowski, 2001]. Old nations, like the Egyptians, Greeks and Romans already utilized materials such as clay, sand or wood charcoal for various applications ranging from water desalination to oil clarification [Rouquerol et al., 2014]. It then took until the late 18th century before the first quantitative assessments of the uptake of gases by solids were reported by Scheele (1773) and Fontana (1777) [Freundlich, 1909]. The Swedish pharmacist and chemist Carl Wilhelm Scheele for example observed that gases desorbed from charcoal when it was heated and re-adsorbed when the charcoal was cooled back again. About half a century later, Pouillet (1822) was one of the first to discover the exothermic nature of adsorption. He reported that heat evolved from immersion of dry sand in water. Throughout the 19th century, the nature of adsorption was controversially discussed until Chappuis (1879; 1881) and Kayser (1881a; 1881b) found independently that the amount of adsorbed gas per mass of adsorbent material increased significantly with the specific surface area of the adsorbent [Masel, 1996]. It was thus concluded that adsorption is a surface phenomenon. It was further found by both authors, that the amount of adsorbed gas is related to the gas pressure. Kayser was also the first to introduce the term “adsorption” into literature. He further suggested distinguishing between the terms adsorption, where a gas binds onto the surface of an adsorbent and absorption where a gas dissolves into the bulk of a fluid. He found that both processes are fundamentally different since the amount of absorbed mass increases with the mass of absorbent, whereas the amount of adsorbed mass generally increases with the amount of available adsorbent surface, rather than with the adsorbent volume [Masel, 1996]. In 1909, McBain (1909) observed that the uptake of hydrogen by carbon can be separated into an initial step of rapid adsorption, followed by a slow process of absorption into the solids interior. He thus introduced the term “sorption” for such processes that involve both kinds of processes [Rouquerol et al., 2014]. At the end of the 19th century, researchers began to present results from adsorption experiments that have been conducted at constant temperature and the terms isotherm and isothermal-curve were introduced to the open literature. The first recorded adsorption isotherms have most likely been reported in

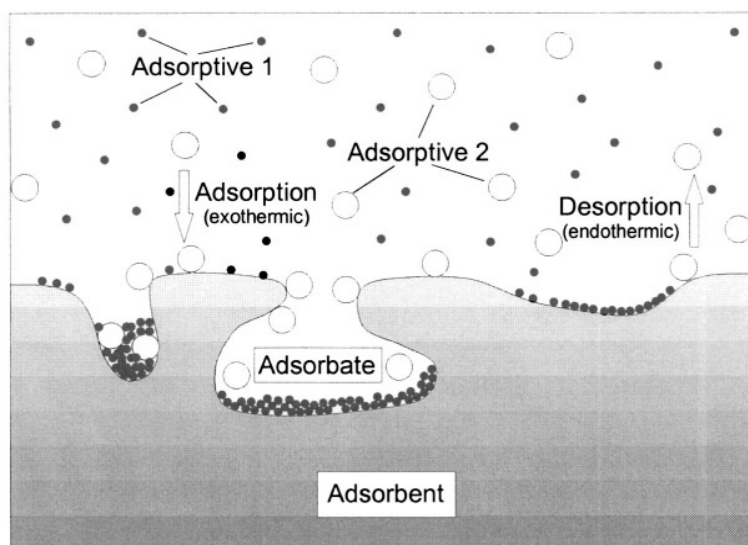
1881 and a further number of isotherms were then reported in the upcoming decades. It was thereby still believed by many investigators that uptake of components by adsorbent materials is accompanied by penetration of these components into the solid structure of the adsorbents [Rouquerol et al., 2014]. It was not until 1907, that the role of the adsorbent surface has been appreciated by Freundlich when he proposed his adsorption isotherm model nowadays known as Freundlich equation or isotherm [Freundlich, 1907]. Later, further effort has been put into the theoretical interpretation of adsorption till Langmuir's contributions [Langmuir, 1916; Langmuir, 1918] brought a radical change into the approaches of surface science [Rouquerol et al., 2014]. He proposed that adsorption is generally accompanied by the formation of a monomolecular layer (monolayer) of adsorbate on the surface of the solid or liquid adsorbent material, which delivered an explanation for the measured plateaus of different adsorption systems. A further important contribution to surface science was then delivered by Brunauer, Emmet and Teller that published an adsorption isotherm model that extended the Langmuir theory to multi-layer adsorption [Brunauer et al., 1938]. Nowadays, the BET-theory is applied in the standard procedure for the determination of the surface area of a wide range of powders and porous materials [Rouquerol et al., 2014]. It was also in the 1930, when the terms physisorption and chemisorption appeared in literature to distinguish between adsorption through van der Waals interactions and activated adsorption based on chemical reactions [Rouquerol et al., 2014].

Besides activities in the field of theoretical surface science, many industrial applications of adsorption technology evolved along the second half of the 20th century [Thomas and Crittenden, 1998]. In parallel, many new adsorbent materials and classes have been developed together with techniques to study the microporous structure of these materials and the state of adsorbates [Rouquerol et al., 2014]. The following will give a brief excursion into the fundamentals of adsorption and adsorptive gas-separation processes.

2.1.2 Fundamental aspects of adsorption

The phenomenon of adsorption occurs due to an attraction of adsorptive molecules to the surface of an adsorbent material where some sort of interaction takes place.

Figure 2.1: Adsorption system (taken from [Keller and Sautt, 2005]).



The concentration of molecules in the proximity of the surface occurs because the surface forces of the adsorbent are unsaturated, which leads to the formation of so called active sites where adsorption can take place (Figure 2.1). High adsorption capacities are provided by the large internal surface areas of the adsorbent materials that are typically in the range of $300\text{-}1200\text{ m}^2\cdot\text{g}^{-1}$. After adsorption took place, repulsive and attractive forces between the adsorbent and the adsorbate become balance. [Thomas and Crittenden, 1998].

The most important terms related to adsorption processes are indicated in Figure 2.1 and further defined in Table 2.1 whereby the definitions are consistent with the those proposed by the International Union of Pure and Applied Chemistry (IUPAC) [Sing et al., 1985; Rouquerol et al., 2014]

Table 2.1: Definitions of adsorption related terms (adapted from [Rouquerol et al., 2014]).

Term	Definition
Adsorption	Enrichment of one or more components in the vicinity of an interface
Adsorbate	Substance in the adsorbed state
Adsorptive	Adsorbable substance in the fluid phase
Chemisorption	Adsorption involving chemical bonding
Physisorption	Adsorption without chemical bonding

As already indicated in Table 2.1, adsorption could be either physical or chemical in nature, depending on the type and the intensity of interaction between the adsorbate and the adsorbent [Ruthven, 1984]. The corresponding adsorbent materials are commonly referred to as physisorbents and chemisorbents, whereas the related adsorption processes are known as physisorption and chemisorption. In physisorption, adsorption results from the universal van der Waals interactions, whereas in chemisorption valence forces are involved through the sharing or exchange of electrons between the adsorbent and the adsorbate [Thomas and Crittenden, 1998; Dąbrowski, 2001].

Physical adsorption processes are generally of exothermal nature as the free energy of the adsorptive reduces once it is bounded to the adsorbent surface [Thomas and Crittenden, 1998; Dąbrowski, 2001]. The reduced amount of free energy of the adsorptive is generally referred to as adsorption enthalpy. Chemisorption is characterized by chemical interaction between the adsorbate and the adsorbent and thus may be either exothermic or endothermic. Depending on the intensity of interaction between adsorbate and adsorbent (i.e. physisorptive or chemisorptive interaction) the adsorption enthalpy lies either in the range of the heat of condensation of the adsorptive (physisorption) or in the range of the chemical reaction that takes place between the adsorbent and the adsorptive (chemisorption) [Rouquerol et al., 2014]. The adsorption enthalpy thus sometimes represents a good indicator for the occurring adsorption mechanism. Chemisorption is typically characterized by a significantly larger adsorption enthalpy (typically -70 to $-200\text{ kJ}\cdot\text{mol}^{-1}$) as compared to physisorption (typically -10 to $-50\text{ kJ}\cdot\text{mol}^{-1}$) [Keller and Sautt, 2005]. However, it is not always easy to distinguish between both mechanisms as under favourable conditions they can either occur simultaneously or alternately [Dąbrowski, 2001]. Nevertheless, in chemisorption, adsorption occurs at distinct localized sites on the adsorbent's surface (i.e. active sites) where the adsorptive interacts chemically with the adsorbent [Ruthven, 1984]. The maximum amount of adsorptive that can adsorb on the adsorbent is thus limited by the number of available active sites on the adsorbent material. As the adsorptive can only interact with the adsorbent surface, this type of adsorption mechanism leads to the formation of single molecule layer of adsorbate on the adsorbent's surface (monomolecular

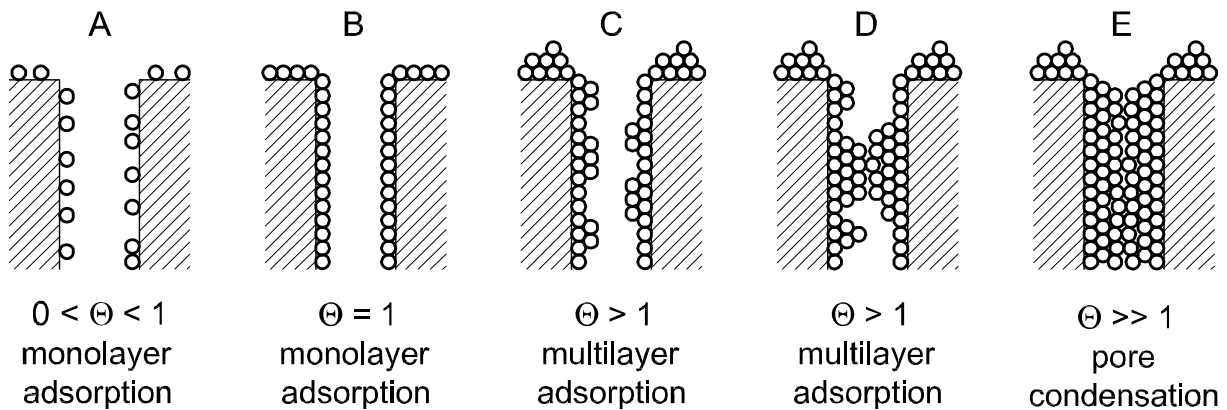
layer or monolayer). Physical adsorption, however, allows further for condensation of adsorptive molecules on top of the formed monolayer, leading to so called multilayer adsorption [Ruthven, 1984]. At high operating pressures, physical adsorption can even lead to capillary condensation in the pores of the adsorbent which leads to a further increase of the adsorption capacity [Ruthven, 1984].

If Θ is defined as the normalized number of occupied adsorption sites, the following two adsorption domains can thus be defined:

- $0 < \Theta \leq 1$: monolayer adsorption
- $\Theta > 1$: multilayer adsorption

For chemisorption, a value of $\Theta = 1$ relates to full occupation of all available adsorption sites on the adsorbent's surface, whereas in physisorption it corresponds to the amount of adsorbate required for complete coverage of the surface. A scheme for these adsorption domains is given in Figure 2.2, including an illustration for capillary condensation at high pressures (Figure 2.2, E).

Figure 2.2: Monolayer and multilayer adsorption.

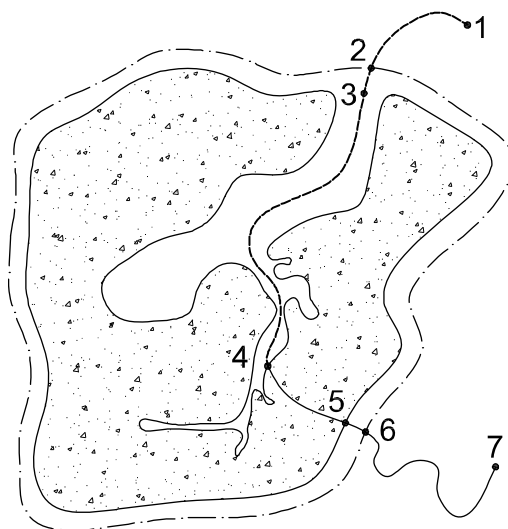


Another characteristic of chemisorption is that it can be an activated two-step mechanism where the chemical reaction occurs in the adsorbate. Depending on the value of the necessary activation energy, the rate of a chemisorptive process could be significantly smaller as the rates achievable by physisorptive processes. Compared to physisorption, which is always an associative process, chemisorption can involve dissociation of the adsorbate, which typically results in an irreversible adsorption process.

The adsorption process of an adsorptive on the surface of an adsorbent material is characterized through the following seven partial steps that are illustrated as a model in Figure 2.3. The first step is characterized by convective and diffusional transport of the adsorptive from the bulk phase to the boundary layer formed around the adsorbent material (Figure 2.3, 1-2). Afterwards the adsorptive needs to penetrate through this boundary layer by diffusion (Figure 2.3, 2-3) and then further through the porous structure of the adsorbent material, again driven by different diffusional transport mechanisms (Figure 2.3, 3-4), until the adsorptive finally adsorbs on an active site of the adsorbent's surface (Figure 2.3, 4). As already pointed out above, the adsorption step is accompanied by the release of heat which needs to be dissipated in the following steps. In the first step, the released heat is transported mainly via heat conductive transport mechanisms through the porous structure of the adsorbent material, till it reaches the adsorbent's surface (Figure 2.3, 4-5). From

there, the heat transport mechanism primarily governed by heat convective transport mechanisms (Figure 2.3, 5-6-7) [Bathen and Breitbach, 2001].

Figure 2.3: Model of adsorption process scheme (adapted from [Bathen and Breitbach, 2001]).

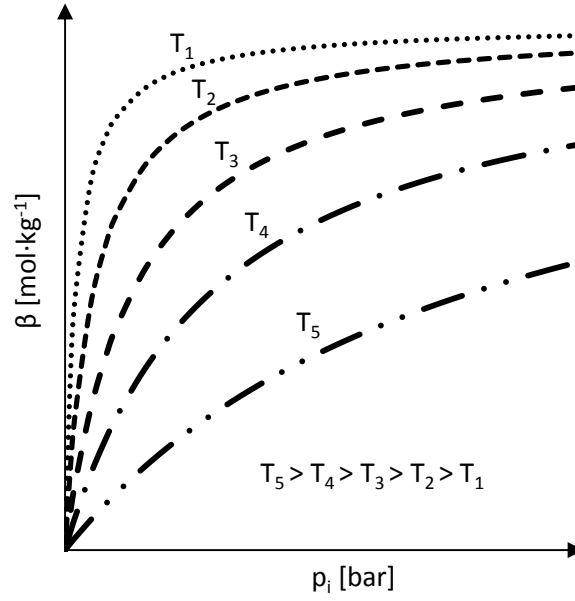


Depending on the operating conditions of the adsorption system (e.g. operating temperature, adsorbent texture, type of adsorptive, etc.) different steps within the adsorption scheme could limit the adsorption process. For example, the porosity and pore size distribution of the adsorbent material can have a significant impact on the mass transport within the particle. Mass transport within the porous adsorbent material could thereby become the rate governing step of the complete adsorption process. As indicated in Figure 2.3, the pores within the adsorbent material can be of different size. IUPAC recommends classifying the pores of an adsorbent based on their sizes into three different groups [Sing et al., 1985]:

- macropores: pores with widths exceeding about 50 nm,
- mesopores: pores with widths between 2 nm and 50 nm and
- micropores: pores with widths not exceeding about 2 nm

Due to the exothermic nature of adsorption, the adsorption capacity of an adsorbent material generally decreases with increasing temperature. Furthermore, the partial pressure of the adsorptive provides a driving force for the adsorption process so that the adsorption capacity of an adsorbent generally increases with increasing adsorptive partial pressure. The adsorbent equilibrium loading at constant temperature is thus characterized by the partial pressure of the bulk-phase adsorptive in the vicinity of the adsorbent material. This coherency is commonly used to report and interpret the performance of an adsorbent-adsorptive system. Since the relation between adsorbent loading and adsorptive partial pressure is illustrated at constant operating temperature, the resulting graphs are commonly referred to as adsorption isotherms. An exemplary set of adsorption isotherms is given Figure 2.4. The figure shows the adsorptive partial pressure versus the adsorbate loading on the adsorbent material given in mol of adsorbate per kg of adsorbent material.

Figure 2.4: Adsorption isotherms.



As can be seen, the adsorbate or adsorbent loading at constant adsorptive partial pressure decreases with increasing temperature. Furthermore, the adsorption isotherms show a rather steep rise at low adsorptive partial pressure and seem to approach some sort of saturation loading at larger adsorptive partial pressures. However, depending on the considered adsorbent-adsorptive system, the adsorption isotherms can have different shapes. Consequently, different models have been introduced to describe the different adsorption systems.

As the use of adsorption isotherms and their related calculation models is essential for the development and understanding of an adsorption process, the following discussions will focus on both topics.

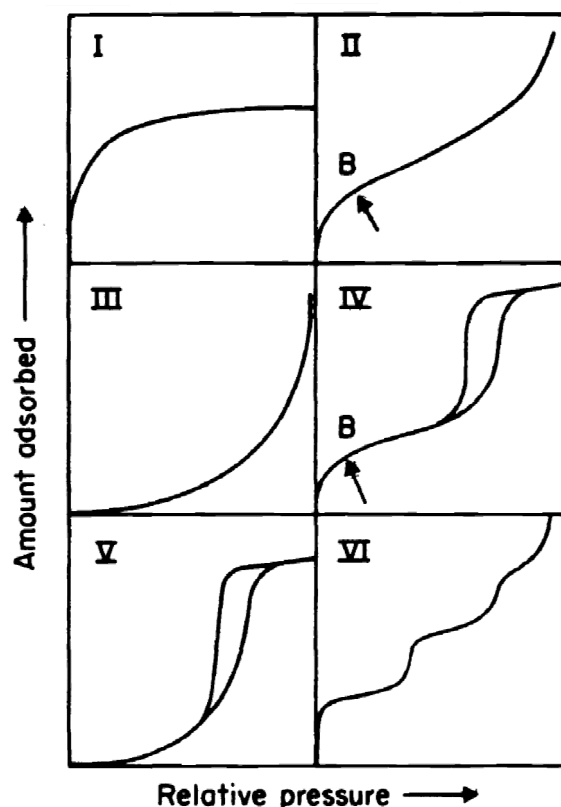
2.1.3 Adsorption isotherms and calculation models

In the sense of thermodynamics, the adsorption equilibrium under considered operating conditions could be described by the thermal equation of state for the adsorbed phase [Keller and Sautt, 2005]. In practice, however, the adsorption equilibrium is generally described with one of the state variables being held constant. For instance, the equilibrium relation between adsorptive pressure and operating temperature at constant adsorbate loading (adsorption isostere) is commonly used to derive the isosteric heat of adsorption. A more frequently used characterisation of the adsorption equilibrium state is the relation obtained for constant operating temperature; the so called adsorption isotherms that can generally be defined as

$$\beta = \beta(p_i)_T$$

As already pointed out above, the shape of an adsorption isotherm can differ from one adsorbent-adsorptive system to another. However, according to the IUPAC [Sing et al., 1985] the majority of physisorption isotherms can be grouped into six different types as shown in Figure 2.5. Among these types of physisorption isotherms, the types I, II and IV are the by far most common ones [Thomas and Crittenden, 1998]. Characteristic for these isotherm types is the almost linear correlation between the adsorbent loading and the adsorptive partial pressure for sufficiently low adsorbent coverage (Henry's Law region).

Figure 2.5: Types of physisorption isotherms (taken from [Sing et al., 1985]).



Type I isotherms are characterized by a horizontal plateau that maintains even at large adsorptive partial pressures and represents a maximum saturation loading. Such adsorption isotherms are typical for pure chemisorptive systems or for microporous adsorbents that show micropore filling without the formation of an adsorbate multilayer. Adsorption systems that behave according to Type II isotherms do not show a saturation loading but instead represent unrestricted monolayer-multilayer adsorption with Point B marking the end of monolayer adsorption. The adsorption process is characterized by the formation of successive adsorbate layers and through condensation of adsorptive within the larger pores of the adsorbent. This isotherm shape is typical for adsorbents that exhibit a wide pore size distribution. Type IV isotherms are similar to Type II isotherms except that they show a horizontal plateau at high adsorptive partial pressures. Furthermore, these types of isotherms typically show a hysteresis loop that can be associated with capillary condensation that takes place in mesopores. This isotherm type is typical for many industrial mesoporous adsorbent materials. [Sing et al., 1985; Thomas and Crittenden, 1998; Keller and Sautt, 2005].

Due to the different existing shapes of the adsorption isotherms, numerous models have been developed to mathematically describe the adsorption behaviour of adsorption systems. Some of the models have been derived on a theoretical basis whereas others are more of empirical nature. Furthermore, the ranges of validity of the individual models may be restricted to only small adsorbent loadings and adsorptive partial pressures. [Thomas and Crittenden, 1998].

Nevertheless, such models are essential for the design and assessment of adsorption processes. Thus, a selection of the most frequently used mathematical models for description of single component adsorption will be introduced in the following.

Langmuir isotherm

Langmuir derived this semi-empirical model already back in 1918 [Langmuir, 1918]. This model assumes that adsorption takes place at a finite number of localized active sites that are present on the adsorbent's surface. Thus, adsorption is only possible up to that point where the adsorbent's surface is completely covered by a single molecular layer of adsorbate. In contrast to physisorption, where multi-layer adsorption can occur, chemisorption involves direct chemical interaction between the adsorbate and the adsorbent's surface. Hence, the Langmuir isotherms are typically suitable for the description of the equilibrium state of chemisorption. Nevertheless, at low coverages the model is usually suitable for the description of a number of different adsorption systems. [Thomas and Crittenden, 1998]

A further assumption within the model is that independent from the actual adsorbate coverage no interaction occurs between adsorbate molecules. This in turn gives that the adsorption sites are equal from a thermodynamic point of view; i.e. with equal and constant heat of adsorption. As the model assumes a finite number of adsorption sites, the adsorption isotherms approach a saturation loading at large adsorptive partial pressures. [Thomas and Crittenden, 1998]

For an adsorbent material that exhibits a saturation loading of β_{max} , the model reads as follows:

$$\Theta = \frac{\beta}{\beta_{max}} = \frac{c(T) \cdot p_i}{1 + c(T) \cdot p_i} \quad (\text{Eq. 2.1})$$

The rate factor $c(T)$ in (Eq. 2.1) is defined as the ratio of the rates of adsorption and desorption. The temperature dependence of the rate factor $c(T)$ is typically expressed by the van't Hoff equation:

$$c(T) = c_0 \cdot e^{\frac{-\Delta H_{ads}}{R \cdot T}} \quad (\text{Eq. 2.2})$$

The parameter c_0 can be determined by fitting the Langmuir adsorption isotherms to experimental data. The (isosteric) heat of adsorption ΔH_{ads} can also be derived from experimental data by employing the Clausius-Clapeyron equation for two different equilibrium states at equal adsorbent coverage (e.g. see [Fauth et al., 2012])

$$\Delta H_{ads} = R \cdot \left(\frac{T_1 \cdot T_2}{T_2 - T_1} \right) \cdot \ln \left(\frac{p_2}{p_1} \right) \quad (\text{Eq. 2.3})$$

Henry's law

At sufficiently low adsorptive partial pressure, the Langmuir isotherm can be reduced to its linear form and one obtains an adsorption isotherm model that is commonly referred to as Henry's law (Eq. 2.4). The rate factor $c(T)$ can again be derived from the van't Hoff equation [Thomas and Crittenden, 1998].

$$\frac{\beta}{\beta_{max}} = c(T) \cdot p_i \quad (\text{Eq. 2.4})$$

BET isotherm

In 1938, Brunauer, Emmet and Teller [Brunauer et al., 1938] derived an adsorption isotherm that extends the classical Langmuir isotherm from monolayer to ideal multilayer adsorption. The BET-isotherm model is suitable to describe adsorption isotherms of Type II according to the IUPAC classification and reads as follows

$$\frac{\beta}{\beta_{ML}} = \frac{C_{BET} \cdot (p_i / p_{sat})}{(1 - p_i / p_{sat}) \cdot (1 - p_i / p_{sat} + C_{BET} \cdot p_i / p_{sat})} \quad (\text{Eq. 2.5})$$

In this equation, β_{ML} represents the maximum monolayer adsorbate loading per mass of adsorbent material, p_{sat} the saturation pressure of the adsorptive gas at the considered adsorption temperature and C_{BET} stands for the so called BET-parameter. The BET-parameter C_{BET} can be determined by relating it to the monolayer gas pressure or to the inflection point of the adsorption isotherm [Keller and Sautt, 2005].

The BET-theory inherently assumes that no interactions occur between neighbouring adsorbate molecules and that the heat evolved from adsorption of layers subsequent to the monolayer equals the heat of liquefaction of the adsorptive. Today, the BET-isotherm is widely used for the investigation of textural characteristics of porous materials. [Thomas and Crittenden, 1998]

2.1.4 Adsorption processes for gas separation

The fact that gaseous species can adsorb on the surface of porous materials has found widespread industrial use in gas separation processes [Ruthven, 1984]. The common task of any gas separation process is the selective removal or separation of one or more gaseous species from a bulk gas stream. However, the adsorption method that is used to achieve a selective separation of the desired component(s) can differ from application to application. Selective gas separation may be achieved through one or a combination of different adsorption effects that are listed in the following [Thomas and Crittenden, 1998]:

- Equilibrium effect: different equilibrium loadings exist for different adsorbate-adsorbent systems
- Kinetic effect: different adsorption rates exist for different adsorbate-adsorbent systems
- Molecular sieving effect: pore sizes of the adsorbent material may only allow the penetration of adsorptive molecules of specific size

The equilibrium effect strongly depends on the type of adsorbate-adsorbent interaction. For example, the affinity of adsorbent materials towards chemisorbed species is usually greater than towards physisorbed species. Thus, the selectivity towards species that react chemically with the adsorbent material is typically greater. Furthermore, the equilibrium effect can be exploited through targeted application of physisorbents that exhibit specific properties (e.g. hydrophilic, hydrophobic, polar or non-polar). The obtained selectivity from equilibrium effect based adsorption processes, however, depends on the process conditions such as the operating temperature and pressure or the gas-phase concentration of the different species. Figure 2.6 schematically shows the adsorption isotherms of nitrogen, oxygen and argon (i.e. the main components of air) for adsorption on a type 5A zeolite at 20 °C. The adsorbent material obviously allows for separation of N₂ from the other

species by means of the equilibrium effect. This property has been exploited commercially to obtain high purity oxygen streams from air. However, since the zeolite material also shows a weak affinity towards adsorption of argon the maximum oxygen purities that can be obtained with this process are typically limited to 96 %_{Vol} due to the presence of argon in the oxygen product. [Thomas and Crittenden, 1998]

Figure 2.6: Adsorption isotherms of different gas species on zeolite 5A at 20°C (taken from [Thomas and Crittenden, 1998]).

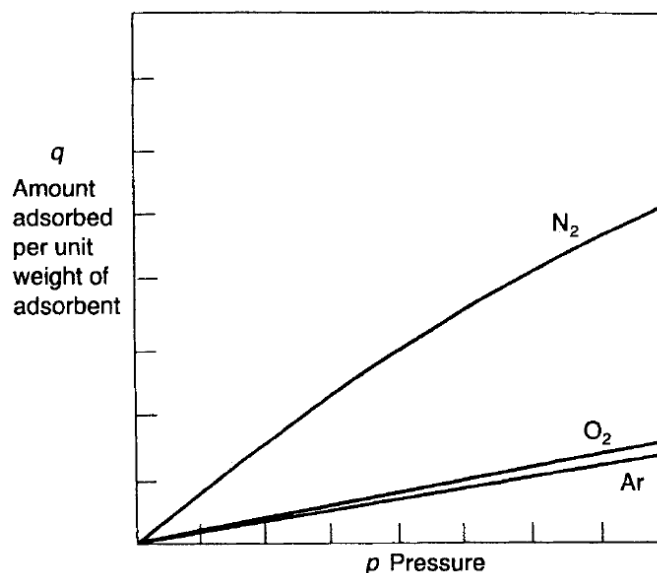
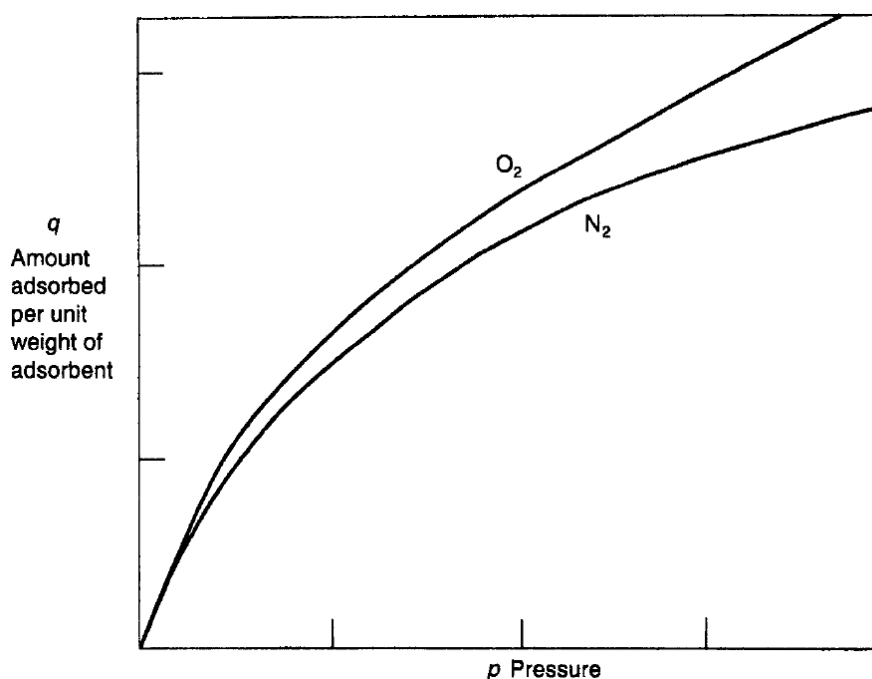


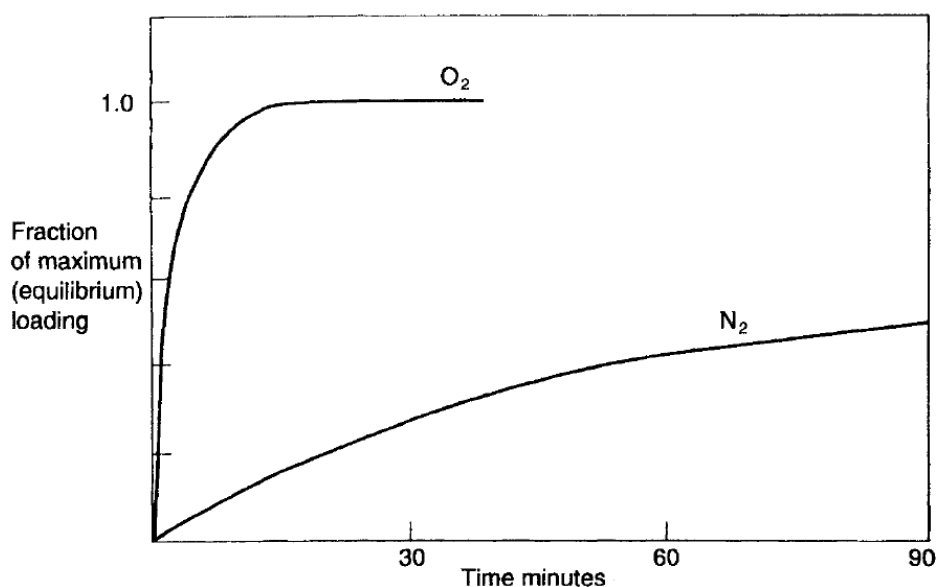
Figure 2.7 indicates the adsorption isotherms of oxygen and nitrogen on a carbon molecular sieve adsorbent material at 20 °C. It is clear from these isotherms that a separation of these gas species is not likely to be achieved through exploitation of the equilibrium effect as the difference in equilibrium loading of both species is rather small.

Figure 2.7: Adsorption isotherms of N₂ and O₂ on carbon molecular sieve at 20°C (taken from [Thomas and Crittenden, 1998]).



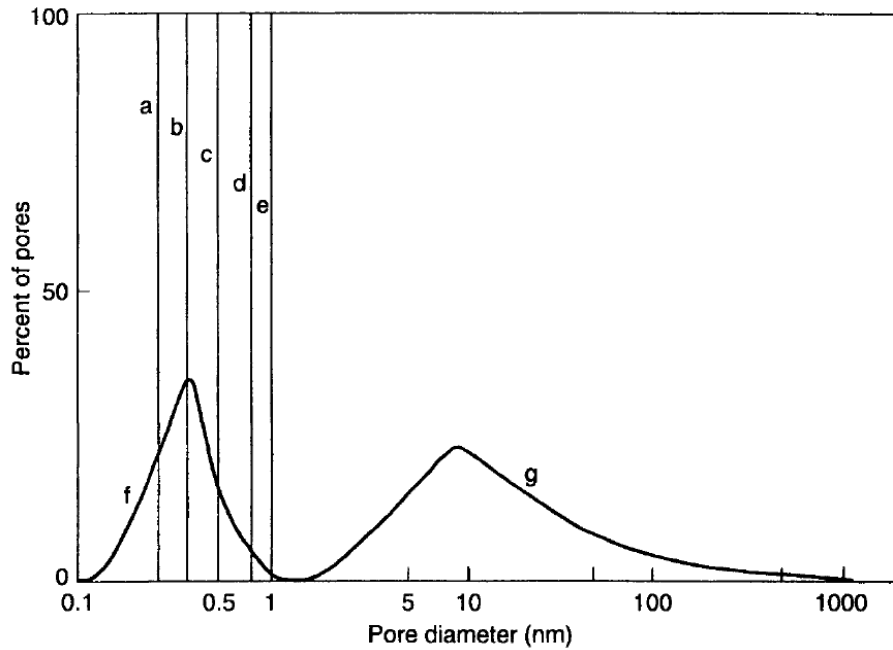
However, investigation of the adsorption rates of both species reveals that adsorption of oxygen on the carbon molecular sieve is by 40-50 times higher than adsorption of nitrogen. The micropore structure of the carbon molecular sieve affects the effective diffusive rates of both components so that diffusive transport of oxygen in the pores becomes significantly faster. This kinetic effect thus allows for effective separation of both gas species, given that the adsorption step is short enough. In general, for useful gas separation based on the kinetic effect, the size of the micropores of the adsorbent material need to be in the range of the dimensions of the diffusing adsorbate molecules. [Thomas and Crittenden, 1998]

Figure 2.8: Adsorption rates of N_2 and O_2 on carbon molecular sieve (taken from [Thomas and Crittenden, 1998]).



Tailoring of the adsorbent pore structure may allow for exploiting a true molecular sieving effect of the adsorbent material. Figure 2.9 show pore size distribution profiles of various adsorbent materials. The carbon based adsorbent materials shown in this figure exhibit a rather broad pore size distribution whereas zeolite type materials have one very precise pore size value. This precise pore size value arises from the crystal structure of zeolites and it qualifies these adsorbent materials for application in adsorption processes that are based on the molecular sieving effect. The drying of ethanol by a type 3A zeolite is a good example for such a process. This adsorbent material has a pore size of about 0.29 nm. The 3A zeolite pores permit the penetration of water molecules that have a diameter of about 0.26 nm, whereas the passage of the larger ethanol molecules (~ 0.45 nm) is prevented. [Thomas and Crittenden, 1998]

Figure 2.9: Pore size distribution of (a) zeolite type 3A, (b) 4A, (c) 5A, (d) 10X, (e) 13X, (f) carbon molecular sieve and (g) activated carbon (taken from [Thomas and Crittenden, 1998]).



In addition to a high adsorption selectivity, technological exploitation of adsorption typically requires the regeneration of the loaded adsorbent material or the recovery of adsorbed species, respectively [Brauer, 1985]. Thus, in continuous separation processes the adsorbent loading under adsorption conditions is larger than under desorption or regeneration conditions. The difference in adsorbent loading during continuous operation is referred to as working capacity:

$$\Delta\beta = \beta_{ads} - \beta_{des} \quad (\text{Eq. 2.6})$$

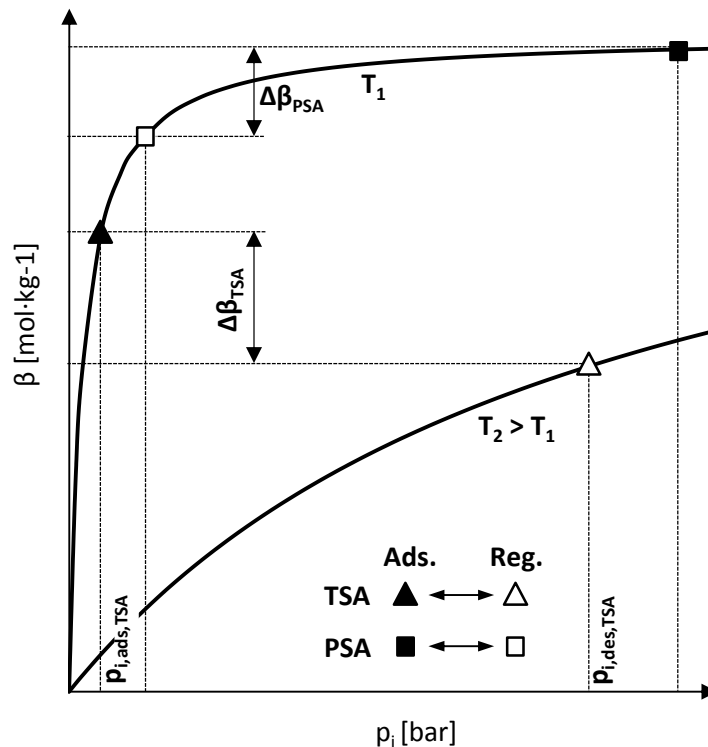
The regeneration or desorption step in turn should be performed in an economically sound manner in order to obtain a competitive separation process. In general, practical regeneration of the adsorbent material after adsorption may be achieved by the following approaches [Thomas and Crittenden, 1998]:

- increase in operating temperature
- reduction in pressure
- reduction in concentration (e.g. by purging with an inert fluid)
- displacement with a more strongly adsorbing species

Continuous and pseudo-continuous adsorption processes take advantage of either one or a combination of these regeneration approaches in order to perform continuous separation of one (or more) specific gas component(s) from bulk-gas streams.

Figure 2.10 illustrates the thermodynamic principle behind the two most commonly used regeneration approaches that are referred to as temperature swing adsorption (TSA) and pressure swing adsorption. As one can see from Figure 2.10, for both approaches the equilibrium adsorbent loading at regeneration conditions is lower than at adsorption conditions, which in turn allows for achieving a certain working capacity which is necessary for continuous process operation.

Figure 2.10: Continuous adsorption processes – TSA and PSA.



TSA processes take advantage of the fact that the equilibrium adsorbent loading decreases with increasing operating temperature. They are operated at constant pressure and adsorption takes place at lower temperatures than the adsorbent regeneration. The temperature swing demands continuous heating and cooling of the adsorbent material and the reactor equipment in case of pseudo-continuous processes. PSA processes take advantage of the fact that the equilibrium adsorbent loading decreases with decreasing adsorptive partial pressure. They are operated at constant temperature and the adsorption step takes place at a larger adsorptive partial pressure compared to the adsorbent regeneration step. The adsorptive partial pressure swing is either achieved by changing the absolute operating pressure (e.g. adsorption at elevated pressure or regeneration at reduced operating pressure) or by utilization of an inert stripping gas that dilutes the target gas stream within the regeneration step. If the pressure swing is achieved by reducing the pressure in the regeneration step to sub-atmospheric pressure, the process is commonly referred to as vacuum swing adsorption or vacuum pressure swing adsorption (VSA or VPSA). A reduction of the adsorptive partial pressure in the regeneration step may also be achieved through introduction of an inert stripping gas. As this approach results in a reduction of the adsorptive concentration in the bulk-gas the process is sometimes referred to as concentration swing adsorption (CSA). It is worth to note that in practical gas separation applications it is common to use combinations of the mentioned regeneration approaches in order to fulfil the separation task more effectively.

2.1.5 Adsorbent materials

The choice of suitable technical adsorbent materials represents the key aspect of any separation process as it essentially impacts the process separation performance and economics. For an ideal adsorbent material a set of requirements may be specified as follows:

- high selectivity and adsorption capacity
- fast adsorption/desorption kinetics
- favourable regeneration ability (economic regeneration conditions)
- good chemical stability (tolerant towards steam, contaminations)
- good mechanical stability (resistance towards attrition)
- inexpensive (abundant raw materials, low production costs)

Furthermore, these properties should be achieved in a wide range of operating conditions and ideally be maintained over an infinite number of adsorption/desorption cycles.

Practical adsorbent materials, however, exhibit certain trade-offs and an optimum adsorbent selection needs to be found for each considered separation task and process environment. Consequently, innumerable types of different adsorbent materials have been developed in the past. An overview of the basic types of adsorbents that have found practical use in industry are given in Table 2.2.

Table 2.2: Basic types of industrial adsorbents (adapted from [Dąbrowski, 2001]).

Carbon adsorbents	Mineral adsorbents	Other adsorbents
Active carbons	Silica gels	Synthetic polymers
Activated carbon fibres	Activated alumina	Composite adsorbents:
Molecular carbon sieves	Oxides of metals	(complex mineral-carbons,
Mesocarbon microbeads	Hydroxides of metals	X-elutrilite; X = Zn, Ca)
Fullerenes	Zeolites	Mixed sorbents
Heterofullerenes	Clay minerals	Organic-inorganic hybrids
Carbonaceous	Pillared clays	Metal-organic frameworks
nanomaterials	Porous clay hetero-structures (PCHs)	
	Inorganic nanomaterials	

In this work, an organic-inorganic hybrid adsorbent material, namely an amine-functionalized silica support material has been utilized for the purpose of CO₂ separation from simulated flue gas streams. A detailed review on this adsorbent material class is given in a later section of this work (see Section 3.2.3). For more detailed information regarding all other adsorbent classes it is referred to the related literature [Ruthven, 1984; Thomas and Crittenden, 1998; Bathen and Breitbach, 2001; Jones et al., 2009; Rouquerol et al., 2014].

However, to underline the importance and the variety of application fields for these kinds of adsorbent materials, a selection of industrial gas separation processes is given in Table 2.3.

Table 2.3: Selection of adsorption based gas separation processes (taken from [Dąbrowski, 2001]).

Separation ^a	Adsorbent
I. Gas bulk separations	
Normal paraffins/iso-paraffins, aromatics, olefins	Zeolites
N ₂ /O ₂	Zeolites
O ₂ /N ₂	Carbon molecular sieve
CO, CH ₄ , CO ₂ , N ₂ , NH ₃ /H ₂	Zeolites, activated carbons
Acetone/ vent streams	Activated carbon
C ₂ H ₄ /vent streams	Activated carbon
II. Gas purification	
H ₂ O/olefin-containing cracked gas, natural gas, air, synthesis gas, etc.	Silica, alumina, zeolite
CO ₂ /C ₂ H ₄ , natural gas, etc.	Zeolite
Organics/vent streams	Activated carbon, others
Sulfur compounds/natural gas, hydrogen, liquefied petroleum gas (LPG) , etc.	Zeolite
Solvents/air	Activated carbon, zeolites
Odors/air	Activated carbon
NO _x /N ₂	Zeolites, carbons
SO ₂ /vent streams	Zeolites, carbons
Hg/chlor-alkali cell gas effluent, other off gases	Zeolites, carbons

^aAdsorbates are listed first.

2.2 FLUIDIZATION ENGINEERING

2.2.1 General aspects of gas-solids contact

Numerous industrial processes exist where a gas is brought into contact with particulate solids to achieve a desired interaction of both phases. The type of interaction can thereby range from simple pneumatic transport of particles to complex heterogeneous catalytic reactions. Depending on the type of interaction, different aspects such as excellent gas-solids contact or good heat- and mass transfer are crucial for the technical realization of the desired process. Among the deployed gas-solid contactor systems, those based on fluidized bed technology can be considered as superior with respect to the aforementioned design aspects. This is because compared to fixed bed contactors the solids within a fluidized bed are not stationary but instead undergo a severe agitation which is beneficial for gas-solids contact as well as heat- and mass transfer.

The first commercial utilisation of the unique characteristics of fluidized bed systems goes back to 1926, where a fluidized bed reactor was deployed as gasifier for the production of synthesis gas from lignite. The gasifier was named after Fritz Winkler who first envisaged the reactor concept in his patent in 1922 [Winkler, 1922]. Since then, fluidized bed technology has been applied in numerous processes, extending from drying, cooling-heating, adsorption-desorption, coating and granulation or processes where heterogeneous catalytic and non-catalytic reactions take place [Werther, 2007].

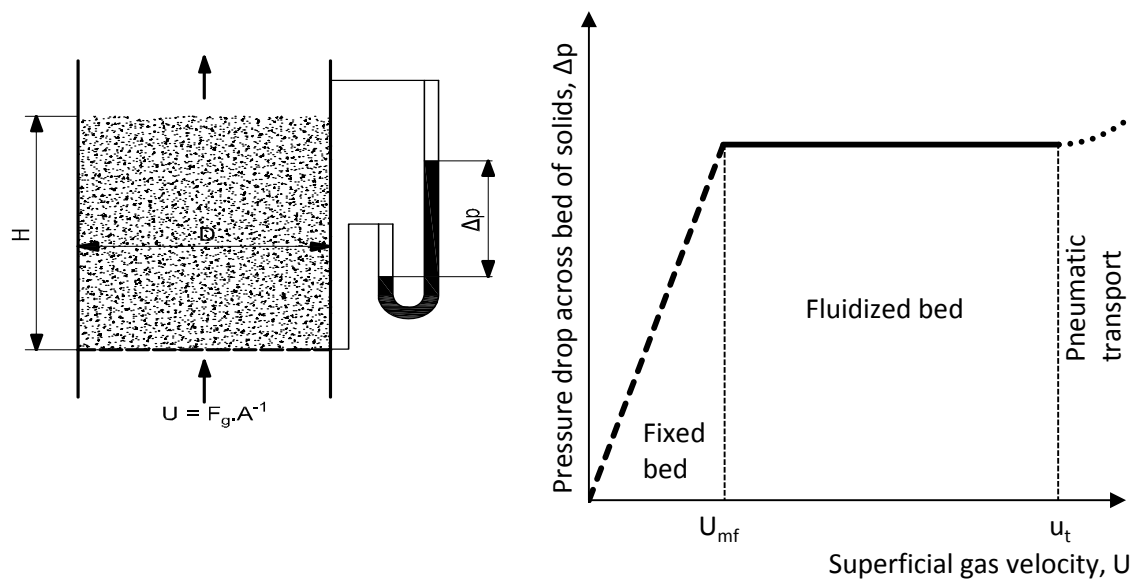
The following sections will present the fundamentals of gas-solid fluidized bed systems. It is worth to note that fluidized bed applications are not limited to gas-solid systems but can instead be realized in all different kinds of gas-liquid-solid phase combinations [Beránek et al., 1975]. Nevertheless, gas-solid fluidized beds represent the most commonly commercially applied systems. Thus, the discussions below will be limited to gas-solid fluidized bed systems.

2.2.2 Fluidized bed existence range

The sketch on the left hand side of Figure 2.11 shows a vessel that is filled with a stationary bed of solids of equal size and density. The solids rest on a porous plate through which gas is flowing at a superficial velocity of U . The superficial gas velocity U is thereby defined as the ratio between the total volumetric gas flow rate and the cross section of the empty vessel. As the gas is flowing through the bed it exerts a certain drag force to the particles within the bed. The magnitude of the drag force thereby depends on the gas flow rate or the superficial gas velocity U , respectively. If divided by the cross section of the vessel, the drag force can be expressed by the pressure drop Δp along the bed.

Figure 2.11 shows a typical course of the correlation between both parameters whereby the superficial gas velocity is plotted on the abscissa and the pressure drop on the ordinate of the diagram. As one can see from the figure, three different areas or gas-solids flow regimes can be distinguished. For sufficiently low gas velocities the bed of solids stays stationary. Thus, the corresponding flow regime is referred to as fixed bed regime. With increasing superficial gas velocity the pressure drop increases and the particles within the bed loosen up more and more. The pressure drop increases further till a point is reached where the drag force exerted by the gas counterbalances the weight of the, now completely suspended solids within the bed, minus their buoyancy. At this point the bed of solids switches into a fluid-like state and it marks the lower border of the existence range of a fluidized bed. The corresponding superficial gas velocity is thus commonly referred to as minimum fluidization velocity U_{mf} .

Figure 2.11: Pressure drop induced by a gas flowing through a bed of solids.



Since the mass of fluidized solids stays constant, the pressure drop along the bed stays constant even if the superficial gas velocity is further increased. However, at that point where the superficial gas velocity reaches the free-fall (or terminal) velocity u_t of the particles within the bed, the bed gets entrained out of the vessel and wall friction forces begin to dominate the pressure drop along the vessel. This point therefore marks the upper limit of the existence range of a fluidized bed and from there the flow regime switches to pneumatic transport which is characterized by a highly diluted flow of solids.

From the discussion above it becomes clear that proper design of fluidized beds requires knowledge of both superficial gas velocities limits. Suitable equations to assess the minimum fluidization velocity and the terminal velocity for a given bed of solids will thus be derived and presented in the following.

2.2.3 Minimum fluidization velocity and single particle terminal velocity

As shown in the previous section, the onset of fluidization is marked by that point where a further increase of the fluidization gas rate leads to no further increase of the bed pressure drop. It was further explained that this is because the pressure drop across a fluidized bed equals the weight of the solids within the bed minus their buoyancy divided by the cross section of bed:

$$\Delta p_{FB} = (1 - \varepsilon_{mf}) \cdot (\rho_p - \rho_g) \cdot g \cdot H \quad (\text{Eq. 2.7})$$

This correlation is also called the fundamental fluidization equation, whereby the first term in the equation includes the bed voidage at minimum fluidization conditions ε_{mf} which is defined as one minus the ratio between the volume occupied by particles within the bed and the total bed volume that includes void spaces between the particles:

$$\varepsilon_{mf} = \frac{\text{solids free bed volume}}{\text{total bed volume}} = \frac{V_{FB} - V_p}{V_{FB}} = 1 - \frac{V_p}{V_{FB}} = 1 - \frac{\rho_b}{\rho_p} \quad (\text{Eq. 2.8})$$

In (Eq. 2.8), ρ_b refers to the bulk density of the fluidized bed at minimum fluidization conditions and ρ_p to the apparent or hydrodynamic density of the particles that assumes a homogeneous particle without an internal porous structure. It is worth to mention that ρ_p must not be confused with the true density of the solid ρ_s that is larger and calculated by division of the particles mass by the particle volume minus the volume of the pores within the particle.

As the pressure drop over a fluidized bed is independent on the superficial gas velocity it is not possible to calculate the minimum fluidization velocity from (Eq. 2.7). However, at minimum fluidization state (Eq. 2.7) can be equated with the pressure drop over a fixed bed that is, according to Figure 2.11, obviously a function of the superficial gas velocity. The derivation of a general equation for prediction of the pressure drop across a fixed bed of solids that is caused by a gas stream flowing at a velocity of U should thus be derived in the following.

The pressure drop caused by a gas flow through an empty pipe of length L is generally given as

$$\Delta p_{pipe} = \zeta(\text{Re}) \cdot \frac{\rho_g \cdot U^2}{2} \cdot \frac{L}{D} \quad (\text{Eq. 2.9})$$

Now it is assumed that the pipe is filled with a bed of spherical particles with a diameter of d_p , whereas the bed exhibits a height of H and a voidage of ε . The gas then needs to flow through the void spaces within the bed, which changes the fluid-dynamic situation completely compared to the gas flow through an empty pipe. Hence, to still keep the analogy to (Eq. 2.9) in the equation for the fixed bed pressure drop, the superficial gas velocity U has first to be replaced by the average interstitial gas velocity defined as

$$U_{\text{int}} = \frac{F_g}{A_{\text{int}}} = \frac{F_g}{A \cdot \varepsilon} = \frac{U}{\varepsilon}$$

and the vessel diameter D has to be replaced by the hydraulic diameter defined as

$$D_h = \frac{4 \cdot A_{\text{int}}}{P} = \frac{4 \cdot A \cdot \varepsilon}{P}$$

The wetted perimeter P can be expressed by the known particle diameter d_p and the total number of particles n within the bed

$$n \cdot \frac{d_p^3 \cdot \pi}{6} = (1 - \varepsilon) \cdot \frac{d_p^2 \cdot \pi}{4} \cdot H \Rightarrow n = \frac{3}{2} \cdot \frac{1 - \varepsilon}{d_p}$$

as

$$P = n \cdot \frac{d_p}{H} \cdot \pi \cdot d_p$$

Finally, the pressure drop per height across a fixed bed of solids can be written as follows

$$\frac{\Delta p_{\text{fixB}}}{H} = \frac{3}{4} \zeta(\text{Re}) \cdot \frac{\rho_g \cdot U^2 \cdot (1 - \varepsilon)}{\varepsilon^3 \cdot d_p} \quad (\text{Eq. 2.10})$$

with the particle Reynolds number Re defined as

$$\text{Re} = \frac{U \cdot d_p \cdot \rho_g}{\mu} \quad (\text{Eq. 2.11})$$

For varying bed voidage ε , the frictional factor ξ can be expressed as $\zeta(Re, \varepsilon)$, whereby Ergun experimentally derived the following correlation for determination of the frictional factor [Ergun, 1952]:

$$\zeta(\text{Re}, \varepsilon) = \frac{4}{3} \cdot \zeta(\text{Re}) = 150 \cdot \frac{1 - \varepsilon}{\text{Re}} + 1.75 \quad (\text{Eq. 2.12a})$$

which, in combination with (Eq. 2.10) and (Eq. 2.11), finally yields an equation for the pressure drop over a fixed bed of solids that reads as follows:

$$\frac{\Delta p_{\text{fixB}}}{H} = 150 \cdot \frac{(1 - \varepsilon)^2}{\varepsilon^3} \cdot \frac{\mu \cdot U}{d_p^2} + 1.75 \cdot \frac{1 - \varepsilon}{\varepsilon^3} \cdot \frac{\rho_g \cdot U^2}{d_p} \quad (\text{Eq. 2.12b})$$

For laminar gas flow conditions ($Re < 1$) the first term in (Eq. 2.12b) is dominating the pressure drop. Thus, the second term can be neglected and (Eq. 2.10) rearranges to the well-known Carman-Kozeny equation:

$$\frac{\Delta p_{\text{fixB}}}{H} = 150 \cdot \frac{(1 - \varepsilon)^2}{\varepsilon^3} \cdot \frac{\mu \cdot U}{d_p^2}$$

However, typically the complete Ergun-equation is used to describe the pressure drop along a fixed bed. Equating thus (Eq. 2.7) and (Eq. 2.12b) and further introducing the Archimedes number Ar as additional dimensionless parameter as

$$Ar = \frac{d_p^3 \cdot (\rho_p - \rho_g) \cdot \rho_g \cdot g}{\mu^2} \quad (\text{Eq. 2.13})$$

a quadratic equation for the minimum fluidization velocity can be derived that reads as follows

$$Ar = \frac{1.75}{\varepsilon_{mf}^3} \cdot \text{Re}_{mf}^2 + \frac{150 \cdot (1 - \varepsilon_{mf})}{\varepsilon_{mf}^2} \cdot \text{Re}_{mf} \quad (\text{Eq. 2.14})$$

This equation can be used to directly calculate U_{mf} from Re_{mf} if the bed voidage and the particle diameter have been determined experimentally before. However, Wen and Yu (1966) showed that the coefficients of both Reynolds numbers in (Eq. 2.14) stay constant over a wide operating range and thus proposed to use the following equation in cases where U_{mf} cannot be calculated directly:

$$U_{mf} = \frac{\mu}{d_p \cdot \rho_g} \cdot \left(\sqrt{33.7^2 + 0.0408 \cdot Ar} - 33.7 \right) \quad (\text{Eq. 2.15a})$$

Later, Grace (1986) proposed different values for the coefficients in (Eq. 2.14), and ended up at the following equation

$$U_{mf} = \frac{\mu}{d_p \cdot \rho_g} \cdot \left(\sqrt{27.2^2 + 0.0408 \cdot Ar} - 27.2 \right) \quad (\text{Eq. 2.15b})$$

This equation will also be used for analytical estimation of the minimum fluidization velocity in this work. Another parameter that is linked to U_{mf} is the fluidization number that is commonly used as a measure for the level of fluidization and is defined as the ratio of the actual superficial gas velocity and the minimum fluidization velocity

$$\text{Fluidization number} = \frac{U}{U_{mf}} \quad (\text{Eq. 2.16})$$

The second important gas velocity in fluidization velocity is the particle free-fall or terminal velocity as it marks the transition from fluidized bed regime to dilute phase pneumatic transport. For a single (spheric) particle falling through a fluid, the terminal velocity can be derived from the balance of all forces acting on the particle. The force balance can be written as follows

$$\frac{d_p^3 \cdot \pi}{6} \cdot (\rho_p - \rho_g) \cdot g - C_D \cdot A_{p,proj} \cdot \frac{\rho_g \cdot u_t^2}{2} = m_p \cdot a_p = \frac{d_p^3 \cdot \pi}{6} \cdot \rho_p \cdot \frac{du_t}{dt} \quad (\text{Eq. 2.17})$$

Assuming now that the spherical particle with diameter d_p has reached its free fall velocity allows for setting the acceleration term on the right hand side of the force balance to zero. Rearranging (Eq. 2.17) finally gives a correlation that can be used to predict the terminal velocity of a single spheric particle:

$$u_t = \sqrt{\frac{4}{3} \cdot \frac{\rho_p - \rho_g}{\rho_g} \cdot \frac{d_p \cdot g}{C_D}} \quad (\text{Eq. 2.18})$$

The drag coefficient C_D in (Eq. 2.18) can be calculated from one of the following equations under consideration of the respective range of validity:

$$C_D = \frac{24}{Re} \quad Ar \leq 2 \text{ and } Re \leq 0.11 \quad (\text{Eq. 2.19a})$$

$$C_D = \frac{24}{Re} + \frac{4}{\sqrt{Re}} + 0.4 \quad 2 < Ar < 1.207 \cdot 10^8 \text{ and } 0.11 < Re < 19345 \quad (\text{Eq. 2.19b})$$

$$C_D = 0.43 \quad Ar \geq 1.207 \cdot 10^8 \text{ and } Re \geq 19345 \quad (\text{Eq. 2.19c})$$

2.2.4 Particle size definition

For the derivation of the correlations presented in Section 2.2.3 it was assumed that the considered bed of solids consists of ideally spherical particles with equal diameters. However, in practice this would never be the case, as the shape of the particle will usually deviate from the spherical shape

and the bed material will exhibit a certain particle size distribution (PSD) rather than consisting of particles with equal size. Thus, particle size definitions have been introduced that relate measured particle sizes to an equivalent spherical particle size that can be used within the correlations derived above. Different particle size definitions exist, but those that are most commonly used in fluidization technology are listed in Table 2.4

In general, the Sauter's diameter d_{SV} is used for design calculations of fluidized beds. The reason for this is that a bed of spheric particles with diameter d_{SV} should show similar pressure drop characteristics and bed voidages as compared to the corresponding aggregate of the non-spherical particles. In addition, the particle sphericity φ_s is commonly used to account for the actual particle shape and to correlate different particle size definitions, whereby it is defined as:

$$\varphi_s = \left(\frac{\text{surface of a sphere}}{\text{surface of the particle}} \right)_{\text{of same volume}} = \left(\frac{d_v}{d_s} \right)^2 \quad (\text{Eq. 2.20})$$

According to (Eq. 2.20) φ_s equals 1 if the particle has a spherical shape or lies between $0 < \varphi_s < 1$ for all other forms of particle shapes as a sphere shows the minimum possible surface to volume ratio. Particle sphericity values of technical relevant materials are usually within the range of $0.6 < \varphi_s < 1$. One approach to determine φ_s is to measure the pressure drop over a fixed bed of solids and further use this value to calculate d_{SV} from (Eq. 2.12b). Furthermore, d_v can be determined by measuring the mass of a known number of the same particles, in case the particle density is known. After both parameters have been determined, φ_s can be calculated from (Eq. 2.21).

$$d_{SV} = \varphi_s \cdot d_v \quad (\text{Eq. 2.21})$$

Table 2.4: Equivalent particle size definitions.

Designation	Description	Definition
sieve diameter d_{sieve}	width of the minimum square aperture that permits passing of the particle	
volume diameter d_v	diameter of a sphere with equivalent volume as the particle	$d_v = \sqrt[3]{\frac{6 \cdot V}{\pi}}$ (Eq. 2.22)
surface diameter d_s	diameter of a sphere with equivalent surface area as the particle	$d_s = \sqrt{\frac{A}{\pi}}$ (Eq. 2.23)
Sauter's diameter d_{SV}	diameter of a sphere with equivalent volume to surface area ratio as the particle	$d_{SV} = \frac{6 \cdot V}{A} = \frac{d_v^3}{d_s^2}$ (Eq. 2.24)
median diameter of the volumetric PSD d_{50} or $d(0.5)$	50% of the particles within the bed material have a smaller diameter than d_{50}	

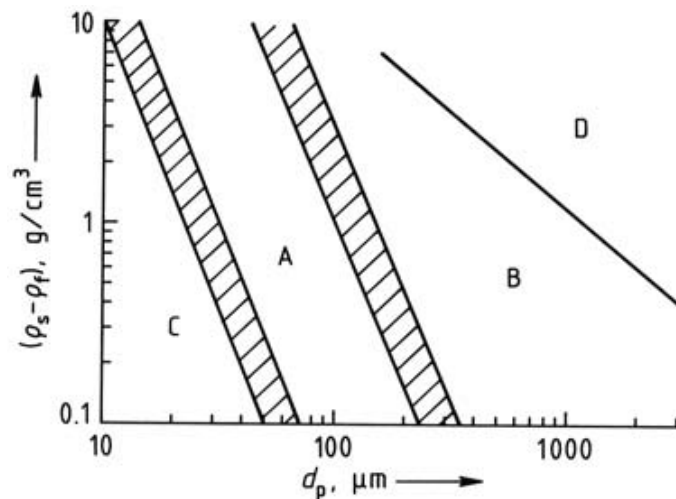
Even though the Sauter diameter is typically used as representative particle diameter for aggregates of non-spherical and non-uniform particles, the median diameter d_{50} has been selected as representative diameter for fluid-dynamic calculations in this work. This selection was considered as sufficient since the measured PSD's of the used materials in this work had a narrow and mono-modal

shape. However, it is worth to note that for broad and/or multi-modal PSD's the selection of the median diameter d_{50} as representative particle size would have not been suitable.

2.2.5 Particle classification according to Geldart

Depending on the mean size and density of the used bed material, different fluidization characteristics can be expected. That is because in addition to the forces exerted by the gas flow given in (Eq. 2.17) inter-particle adhesion forces are acting within the bed. For very fine and/or light particles these inter-particle forces can exceed the viscous forces from the gas flow. Hence, the fluidization behaviour of such powders will be significantly different from the behaviour of somewhat bigger and/or denser particles. In order to differentiate the fluidization behaviour of different kinds of powders, Geldart (1973) thus proposed an empirically derived classification of solids into four different groups. The parameters chosen for the classification were the mean particle diameter d_p within the bed and the density difference between particles and the fluidization agent ($\rho_p - \rho_s$). Geldart (1973) proposed boundaries between these for particle classes that are typically visualized within a diagram having d_p drawn on the abscissa and $(\rho_p - \rho_s)$ on the ordinate, as shown in Figure 2.12.

Figure 2.12: Geldart diagram (boundaries according to Molerus (1982)).



In order of increasing particle size and density are, the Geldart particle groups are referred to as Geldart C, A, B and D. The characteristic fluidization behaviour of each group will be described briefly in the following:

- Geldart C Particles:

Particles from this group are very fine, cohesive powders that can hardly be fluidized due to their strong inter-particle adhesion forces. In beds of such solids gas channels are usually formed and gas by-passes the bed through these channels, leading to a non-fluidized bed with significantly lower pressure drop as predicted from (Eq. 2.7). However, the fluidization behaviour can be improved through mechanical equipment such as agitators or vibrators or chemical additives. Typical powders that belong to this particle group are flours or fines obtained from downstream filter systems in solid fuel combustion units.

- Geldart group A particles:

Particles belonging to this group exhibit small mean size and/or low density. These particles can be easily fluidized, whereby at low fluidization velocities ($U \approx U_{mf}$) homogeneous bed fluidization without bubbles and with significant bed expansion is possible. Bubble formation occurs just at a specific fluidization velocity, called the minimum bubbling velocity U_{mb} . The bubbles formed within the bed are small. Even bubble growth due to coalescence of small bubbles is not significant as bubbles break up after they have reached a specific size. Typically, FCC catalysts belong to this particle group.

- Geldart group B particles:

Materials that belong to this group are characterized by moderate particle sizes and densities. These sand-like particles fluidize well and bubble formation occurs right after transition from fixed to fluidized bed regime. Bubbles can grow very large due to coalescence. In deep beds and small vessels they can even take up the complete cross section of the vessel (slugging regime) and bubble eruption can be vigorous in this regime. Bubble formation and growth within fluidized beds of this particle group is typically characterized in the following way:

- Small bubbles are formed at the gas distributor and grow and coalesce as they rise through the bed
- The bubble size increases roughly linearly with distance to the distributor and the amount of gas that is in excess to the minimum required gas flow for fluidization (i.e. $U - U_{mf} > 0$)
- The bubble size is more or less independent of the mean particle size and is not limited through bubble splitting
- Vigorous bubbling is typical for such beds, leading to better lateral mixing of solids

- Geldart group D particles:

This group of particles includes large and/or dense particles such as coffee beans or sand with average sizes > 0.5 mm. Deep beds of these solids are difficult to fluidize. Typically, large exploding bubbles or severe channeling, or spouting behaviour if the gas distribution is very uneven can be observed. Bubble formation and growth within fluidized beds of this particle group is typically characterized in the following way:

- Bubbles coalesce rapidly and grow to large size
- Bubbles rise more slowly than the rest of the gas percolating through the emulsion
- The dense phase has a low voidage
- When the bubble size approaches the bed diameter, flat slugs are observed

2.2.6 Fluidized bed regimes

Within the existence range of a fluidized bed, this means between the state of minimum fluidization and pneumatic transport of particles, a fluidized bed exhibits a sequence of different fluidization regimes as illustrated in Figure 2.13.

Starting from minimum fluidization state, the bed will expand as the fluidization rate increases and depending on the bed material (see Section 2.2.4) bubbles will start to be formed as soon as the fluidization velocity U exceeds $U_{mb} \geq U_{mf}$. This type of fluidized bed regime is called stationary or

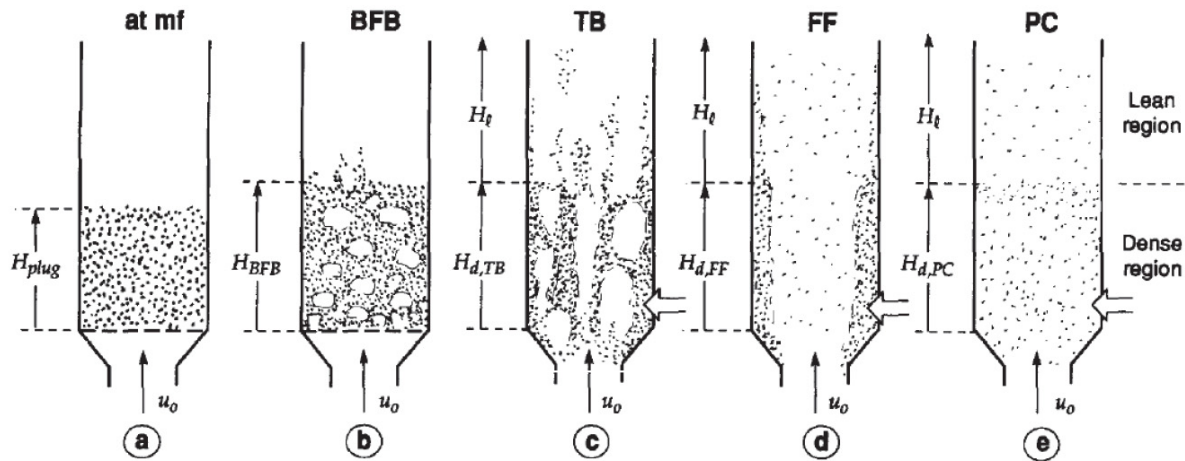
bubbling fluidized bed and is shown in (Figure 2.13 (b)). The bubbles formed in this regime agitate the solids and thereby lead to excellent gas-solids mixing conditions and moreover to good heat and mass transfer rates within the bed.

By increasing the velocity further, the excess gas starts to form solid free channels that exhibit lower pressure drops as compared to the rest of the solids suspension which in turn stays at almost minimum fluidization state. The local gas velocities within the channels are high enough to throw more and more particles into the freeboard of the vessel while the former bed surface vanishes. This regime is referred to as turbulent fluidization regime and pictured in Figure 2.13 (c)).

If the gas velocity is increased beyond turbulent fluidization conditions, the so called fast fluidization regime (Figure 2.13 (d)) will be reached. This regime typically exhibits a dense phase region in the bottom right above the gas distributor and the freeboard above the dense phase where the solids concentration decreases exponentially with height. The freeboard is further characterized by an upwards flowing disperse gas-solids phase within the core region of the riser cross section and a downwards flowing solids layer that is formed at the riser walls (core-annulus flow structure). In this regime significant particle entrainment out of the fluidized bed reactor can be observed and recirculation of particles is required in order to maintain the solids inventory within the system (circulating fluidized bed reactors (CFB)).

At the point where the fluidization velocity exceeds the terminal velocity of the largest particles within the fluidized bed the fluidization regime switches to pneumatic conveying (Figure 2.13 (e)) and the suspension density along the reactor drops significantly with a somewhat denser region again formed in the bottom region above the gas distributor.

Figure 2.13: Fluidized bed regimes [Kunii and Levenspiel, 1991]



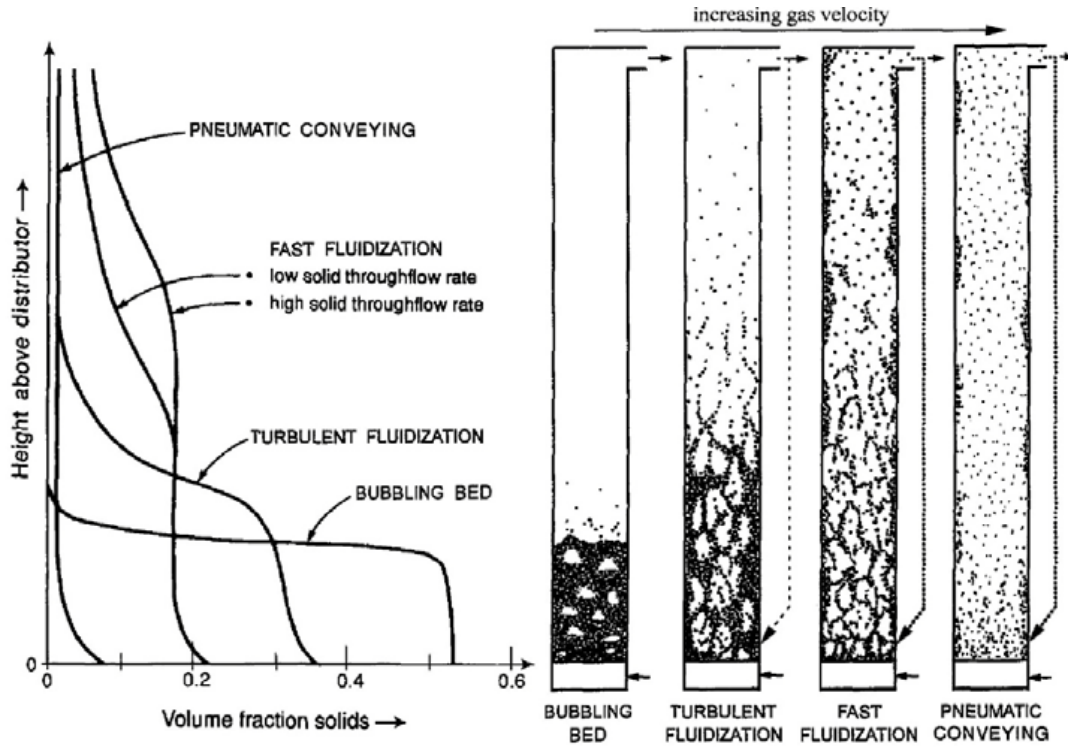
As indicated above, different fluidization regimes exhibit different solids distributions within a fluidized bed reactor. Typical solid volume fractions for the different fluidization regimes along the height of the fluidized bed reactor are shown in Figure 2.14. As one can see from this figure, in general a denser phase is formed in the bottom region right above the gas distributor. Above this dense region the solids volume fraction decreases more or less sharply depending on the respective fluidization regime.

For proper fluidized bed design it is of great importance to predict the fluidized bed regime that will be present at the desired operating conditions of the reactor. It was shown in the previous section, depending on the fluidized bed regime different typical distribution patterns of the solid inventory

within the fluidized bed and different solids concentrations at certain locations of the reactor can be expected. As the used material usually fulfils a certain purpose within the fluidized bed reactor (e.g. heat carrier, chemical reactant, catalyst, adsorbent etc.) the fluidized bed reactor design needs to account for the solids distribution within the system. In addition, heat and mass transfer rates strongly depend on the local solids concentration and the gas-solid contacting regime. Finally, knowledge about the solids concentration at the gas exit duct location of a fluidized bed reactor is crucial as it has a great impact on the design of the applied gas-solid separation as well as on the solids recirculation systems in case of CFBs.

The obvious need for a method that allows for prediction of fluidization regimes led to the development of so called fluidization regime maps. One of the most commonly used regime maps will be presented in the following.

Figure 2.14: Solids distribution along a fluidized bed reactor for different fluidization regimes (From Schmid et al. 2011, merged from Kunii and Levenspiel, 1991; Lim et al., 1995 and Grace, 1986)



2.2.7 Fluidized bed regime map

Grace (1986) proposed a regime map that illustrates the expected fluidization regimes in dependence on a dimensionless particle diameter defined as

$$d_p^* = Ar^{\frac{1}{3}} \quad (\text{Eq. 2.25})$$

and a dimensionless superficial gas velocity defined as

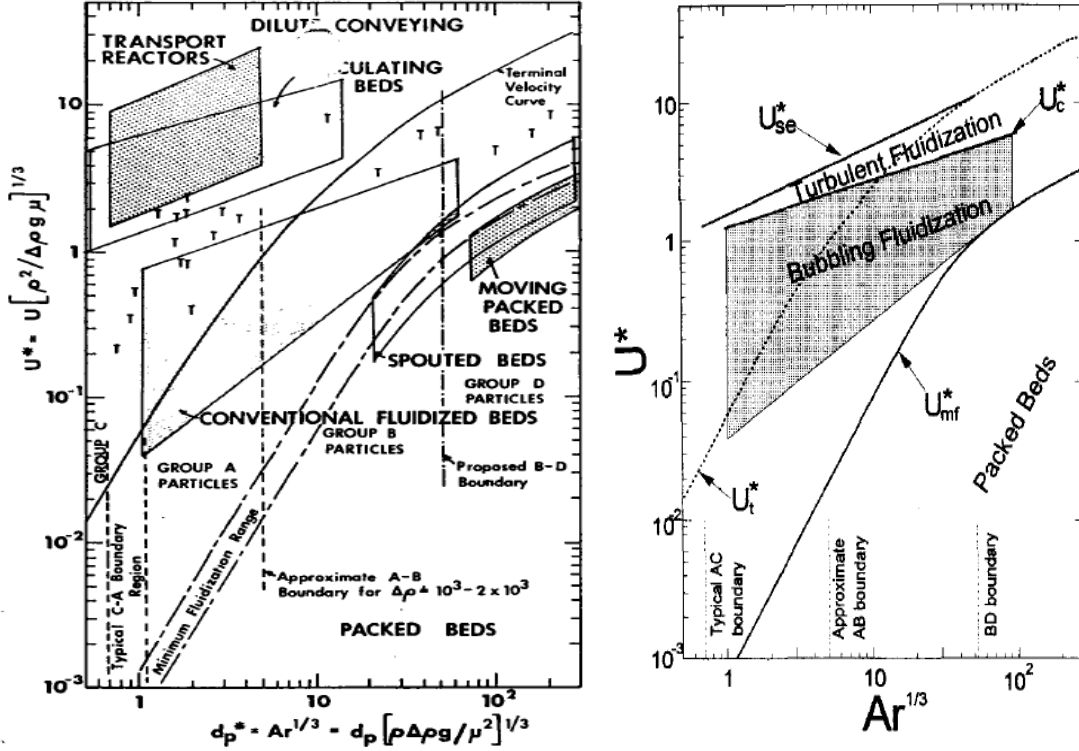
$$U^* = \frac{Re}{Ar^{\frac{1}{3}}} \quad (\text{Eq. 2.26})$$

Corresponding regime maps are shown in Figure 2.15. In these regime maps one can find the typical regions of existence for the above described fluidization regimes. The advantage of these regime

maps is that the choice of the axis allows for illustration of the characteristic fluidization gas velocities as well as for separation between different types of Geldart particle groups.

Such a regime map represents a powerful tool for design of fluidized bed reactors as it provides information about the expected fluidization regime and thus about the expected solids distribution within the system. Regime maps can further be used for rough scaling of a cold flow model of an actual fluidized bed reactor.

Figure 2.15: Fluidization regime map according to Grace [Grace, 1986 (left), Bi and Grace, 1995 (right)].



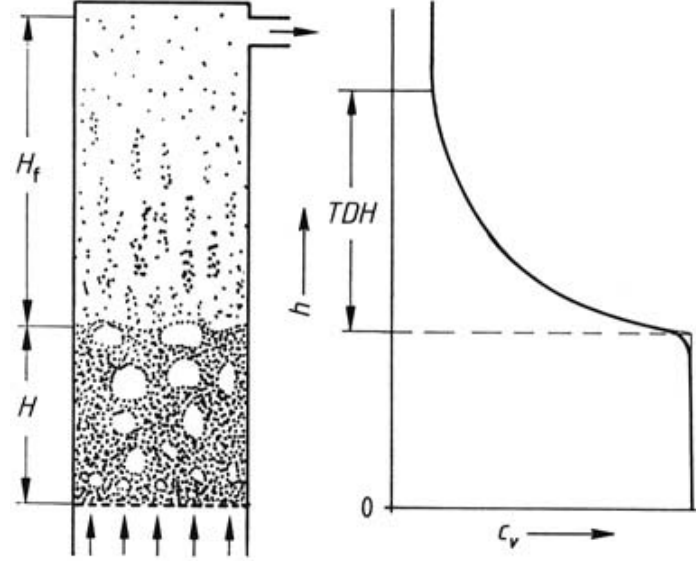
2.2.8 Bubbling fluidized beds

Bubble explosions at the apparent surface of the fluidized bed continuously throw particle clusters into the space above the bed. Within this space a classification of particles takes place; particles and particle clusters whose settling velocities are greater than the actual fluidization velocity fall back into the bed, whereas those particles and particle cluster that exhibit a smaller terminal velocity are elutriated by the gas stream. Right above the apparent bed surface the so called splash zone is formed which is governed by the ballistic movement of solid clusters. This zone exhibits a reduced density compared to the actual fluidized bed itself which is commonly referred to the dense phase of the fluidized bed. Above the splash zone the so called freeboard is formed which is also governed by solids backmixing due to local fluctuations of the gas velocity that arise from bubble explosions. The solids concentration along the freeboard height shows a characteristic exponential decay until a point is reached where local fluctuations of the gas velocity have decayed and the residual particles are small enough to be entrained with the gas stream (i.e. with $u_t < U$). Thus, at this point the solids concentration within the gas stream remains constant and the corresponding height is referred to as “transport disengaging height” and it is indicated in Figure 2.16.

For the design of the dust collecting systems of stationary fluidized beds it is essential to know the entrained solids mass flow rate at the height of the exit duct. Different models for the estimation of

entrainable particle size fractions, the solids concentration profile and the entrained mass flow rate can be found in the literature (e.g. [Kunii and Levenspiel, 1991]). However, the use of particle entrainment models, especially of those that have been derived on an empirical basis may lead to unsatisfactory assessment of the actual entrainment rates. This is mostly because particle entrainment out of a fluidized bed reactor is strongly affected by the exit duct geometry which can differ from one to another reactor system.

Figure 2.16: Solids distribution in bubbling fluidized bed reactors (taken from [Werther, 2007]).



2.2.9 Bed-to-surface heat transfer in bubbling fluidized beds

An outstanding characteristic of fluidized beds is that compared to other flow regimes such as fixed or moving beds the achievable heat transfer rates between bed material and heat exchanger (HEX) surfaces are usually by an order of magnitude higher. This characteristic can be attributed to severe agitation of the bed material caused by bubble formation, movement and explosion that in turn leads to a significant increase of the particle convective heat transport. Another characteristic of fluidized beds is that the bed material exhibits a high heat storage capacity. Consequently, occurring temperature gradients within a fluidized bed level out rapidly and conditions within the bed can generally be considered as uniform. The exchanged heat between an immersed HEX surfaces and a fluidized bed can generally be calculated by

$$\dot{Q}_{\text{HEX-FB}} = h_{\text{HEX-FB}} \cdot A_{\text{HEX}} \cdot (T_{\text{HEX}} - T_{\text{FB}}) \quad (\text{Eq. 2.27})$$

where A_{HEX} is the total HEX surface, T_{HEX} is the temperature at the surface of the HEX, T_{FB} is the uniform fluidized bed temperature at sufficient distance from the HEX and $h_{\text{HEX-FB}}$ is the average heat transfer coefficient between the HEX and the fluidized bed. Hence, in order to obtain an appropriate HEX design it is necessary to assess the heat transfer coefficient for the considered operating conditions. The average heat transfer coefficient is generally affected by three different heat transfer phenomena;

- Particle convective heat transfer,
- Gas convective heat transfer and
- Radiative heat transfer

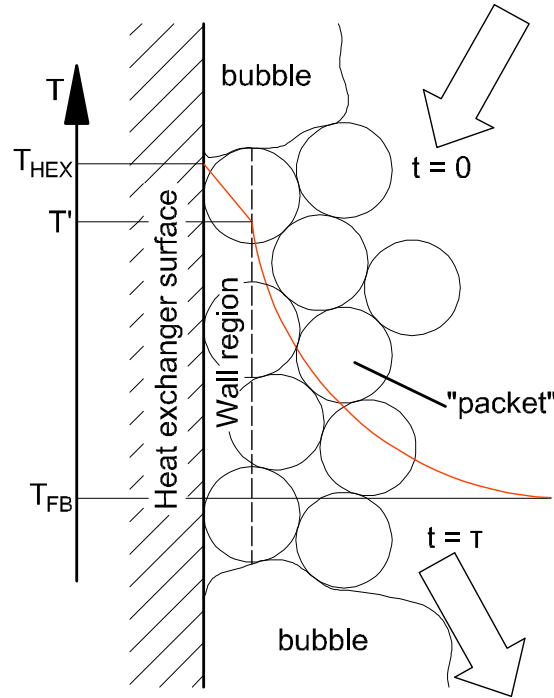
and can thus be given as

$$h_{HEX-FB} = h_p + h_g + h_{rad} \quad (\text{Eq. 2.28})$$

However, it is worth to note that the gas convective contribution for particle diameters $< 500 \mu\text{m}$ is comparably small and heat radiation effects can be neglected at temperatures below 500°C [Werther, 2007]. Thus, for (stationary/bubbling) fluidized beds of small particles, particle convection can be considered as the governing heat transfer phenomena and the average heat transfer coefficient h_{HEX-FB} roughly equals h_p .

Mickley and Fairbanks (1955) proposed the so called “(packet) renewal model” for assessment of the particle convective heat transfer coefficient. An illustration of the packet renewal model is shown in Figure 2.17.

Figure 2.17: HEX-FB heat transfer- packet renewal model.



This model assumes that an agglomerate of particles (packet) is temporary resting on the HEX surface till it gets swept away by a passing gas bubble. After the bubble passed the HEX surface, a new packet can contact the HEX. The expression for the heat transfer coefficient can then be given as

$$h_{HEX-FB} \approx h_p = h_b \cdot \delta_b + h_{packet} \cdot (1 - \delta_b) \quad (\text{Eq. 2.29})$$

When a bubble is present at the HEX surface, the heat transfer is governed by gas conductivity and radiation only and thus the contribution of bubbles to the average heat transfer can again be neglected ($h_b \approx 0$). On the other hand, if a packet contacts the HEX surface, particle convection starts to contribute to the heat transfer. For calculations of the heat transfer coefficient two different heat transfer zones can be assumed. At the HEX surface a wall region is formed that exhibits a larger voidage compared to the packet and thus gives a larger resistance towards heat transfer. However, for fluidized beds of small particles (or for long contact times between HEX surface and packets) the wall region resistance can be neglected and the particles at the HEX surface can be considered to be in thermal equilibrium with the HEX surface. In the packet itself thermal diffusion represents the

main resistance towards heat transfer. The packet heat transfer coefficient can be calculated using the following equation

$$h_{packet} = \sqrt{\frac{k_{packet} \cdot \rho_{packet} \cdot C_{packet}}{\pi \cdot t}} \quad (\text{Eq. 2.30})$$

The packet density ρ_{packet} can be estimated as follows

$$\rho_{packet} = (1 - \varepsilon_{mf}) \cdot \rho_p \quad (\text{Eq. 2.31})$$

whereas the heat capacity of the packet C_{packet} can be assumed to equal the heat capacity of the particles C_p . The effective thermal conductivity of the packet k_{packet} is taken as [Kunii and Levenspiel, 1991]

$$k_{packet} = \varepsilon_{mf} \cdot k_g \cdot (1 - \varepsilon_{mf}) \cdot k_p \cdot \left(\frac{1}{\varphi_w \cdot (k_p / k_g) + 2/3} \right) \quad (\text{Eq. 2.32})$$

where φ_w is the equivalent thickness of the wall region that can be assumed to equal half of the particle diameter. Assuming further an average contact time τ between packets and HEX surface the packet heat transfer rate can be given as follows

$$h_{packet} = 2 \cdot \sqrt{\frac{k_{packet} \cdot \rho_p \cdot (1 - \varepsilon_{mf}) \cdot C_p}{\pi \cdot \tau}} \quad (\text{Eq. 2.33})$$

Thus, the average heat transfer coefficient between an immersed HEX and a bubbling fluidized bed of small particles can finally be expressed as

$$h_{HEX-FB} = (1 - \delta_b) \cdot h_{packet} = 2 \cdot (1 - \delta_b) \cdot \sqrt{\frac{k_{packet} \cdot \rho_p \cdot (1 - \varepsilon_{mf}) \cdot C_p}{\pi \cdot \tau}} \quad (\text{Eq. 2.34})$$

To calculate h_{HEX-FB} from (Eq. 2.34) the values of the bubble fraction at the HEX surface δ_b and the average packet contact time τ are needed to be known. For immersed horizontal HEX, Kim et al. (2003) proposed to use the following correlations to predict both parameters

$$\delta_b = 0.19 \cdot \left[\frac{d_p \cdot g}{U_{mf}^2 \cdot (U_g / U_{mf} - A^*)^2} \right]^{-0.23} \quad (\text{Eq. 2.35})$$

$$\tau = 1.20 \cdot \left[\frac{d_p \cdot g}{U_{mf}^2 \cdot (U_g / U_{mf} - A^*)^2} \right]^{0.30} \cdot \left(\frac{d_p}{D_{HEX, pipe}} \right)^{0.225} \quad (\text{Eq. 2.36})$$

where A^* is used to account for local bubble formation between horizontal HEX pipes at superficial gas velocities below U_{mf} and can be calculated as follows

$$A^* = 1 - \frac{A_{HEX, proj.}}{A_{FB}} \quad (\text{Eq. 2.37})$$

In summary, one can state that the average heat transfer rate between an immersed HEX and a fluidized bed is primarily affected by the average contact time of the packets as well as by the bubble fraction around the HEX. According to (Eq. 2.35) and (Eq. 2.36) these parameters in turn are mainly dependent on the particle diameter and the fluidization state. The impacts of particle diameter and fluidization number on the average heat transfer coefficient are shown graphically in Figure 2.18 and Figure 2.19.

As indicated in Figure 2.18, in fluidized beds consisting of typical Geldart A and Geldart B particles the maximum heat transfer coefficient reached at optimum fluidization velocity increases with

decreasing average particle size. Note that the heat transfer coefficient drops significantly for Geldart C particles at particle diameters below about 20 μm .

On the other hand, a typical correlation between superficial gas velocity and heat transfer coefficient is shown in Figure 2.19.

Figure 2.18: Heat transfer coefficient between fluidized bed and immersed HEX surface (Dependency on particle diameter). [Kunii and Levenspiel, 1991]

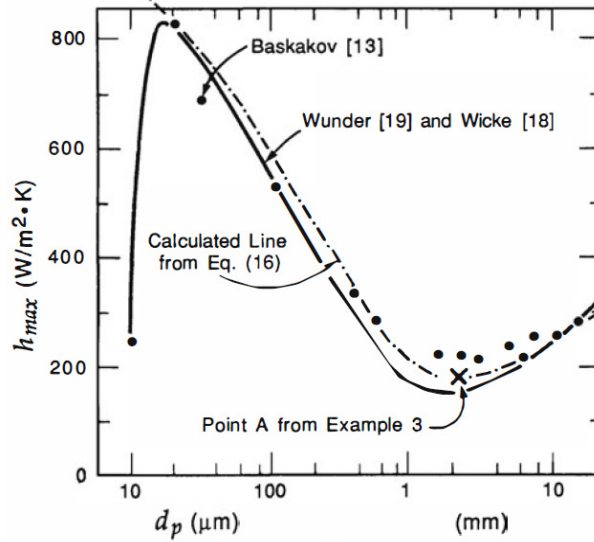
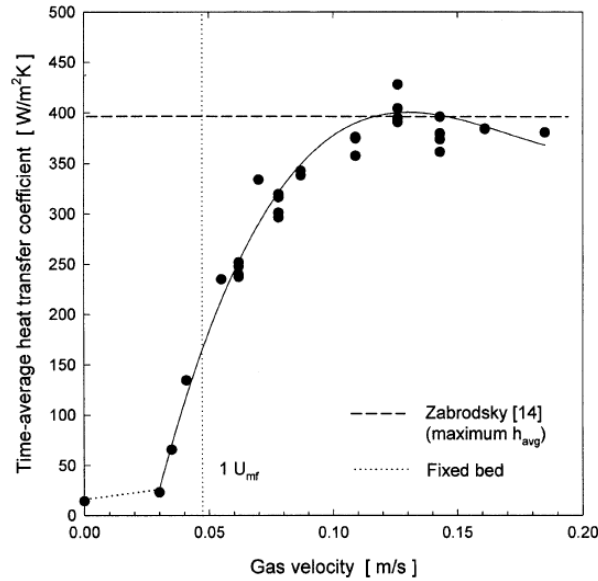


Figure 2.19: Heat transfer coefficient dependency on fluidization number [Kim et al., 2003].



As one can see from this figure, at gas velocities below U_{mf} (fixed bed) the heat transfer coefficient is significantly lower (it has to be noted that in Figure 2.19 the heat transfer coefficient increases significantly already for gas velocities lower than U_{mf} which can be attributed to local fluidization in the interstitial regions between the HEX tubes used in the considered experiment, see [Kim et al., 2003]). At superficial gas velocities above U_{mf} fluidization occurs and the achieved heat coefficient increases drastically. With increasing fluidization number the bubble formation within the bed (bubble fraction and bubble frequency) and thus the contact dynamics between the HEX surface and the particle packets changes which in turn affects the heat transfer between them.

The curve shown in Figure 2.19 exhibits a maximum at an optimum superficial gas velocity U_{opt} that can be estimated using the correlation proposed by Zabrodsky (1966)

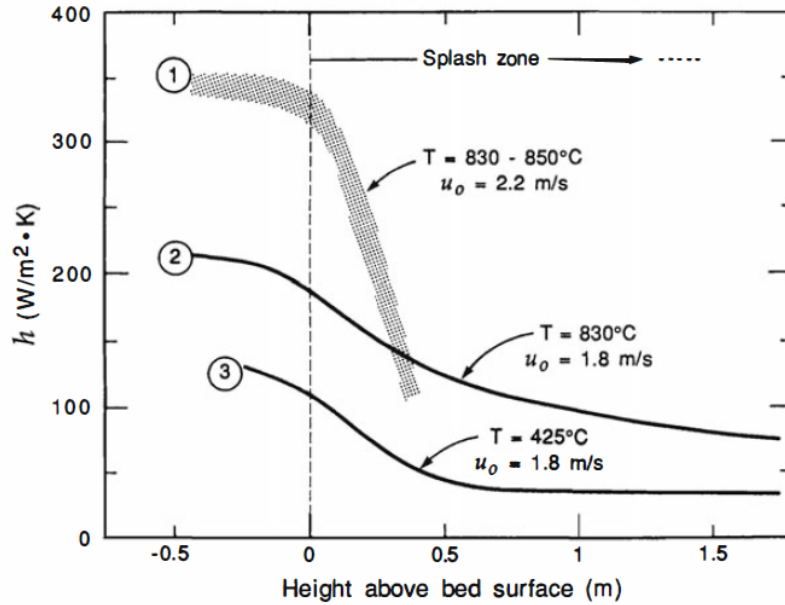
$$h_{\max} = 35.8 \cdot \rho_p^{0.2} \cdot k_g^{0.6} \cdot d_p^{-0.36} \quad (\text{Eq. 2.38})$$

At gas velocities beyond U_{opt} the increased bed bubble fraction leads to a reduced particle convective heat transfer and thus to an overall decrease of the average heat transfer coefficient.

Particle to HEX heat transfer in the splash zone

The models and theoretical backgrounds regarding bed-to-surface heat transfer coefficients presented above are more or less related to the dense phase region of the fluidized bed only. As pointed out above, the effective heat transfer rate achieved within this dense phase strongly depends on the bubbling characteristics and the solids concentration around the heat exchanger surface. In the splash zone of a stationary fluidized bed, however, no more bubbles are present and the solids concentration is reduced significantly compared to the dense phase region. Consequently, a reduced bed-to-surface heat transfer rate can be expected in the splash zone above a dense phase fluidized bed. This heat transfer characteristic is shown in Figure 2.20 that presents measured values of bed-to-surface heat transfer rates. As can be seen from this figure, the measured heat transfer coefficients within the splash zones have been significantly smaller as within the dense phase regions of the fluidized beds.

Figure 2.20: Measured heat transfer rates between horizontal tube banks and a fluidized bed of large particles (~1 mm) at high operating temperature (taken from [Kunii and Levenspiel, 1991]).



3. TEMPERATURE SWING ADSORPTION: REACTOR DESIGN

3.1 GENERAL ASPECTS

Post-combustion CO₂ capture from flue gases emitted by power plants or industrial processes is not likely to be performed within a PSA process since it would require compression of enormous gas quantities that are present at almost atmospheric pressure. A derivative of a PSA process where the adsorbent regeneration occurs at sub-atmospheric pressure (VPSA) has, however, been proposed as alternative route for post-combustion CO₂ capture [Chaffee et al., 2007]. Nevertheless, any kind of pressure swing process requires electric energy input for operation, which is not beneficial from an exergetic point of view. Furthermore, the options for the reactor design are expected to be limited as it will be difficult to run a continuous CO₂ capture process within a system of interconnected fluidized beds that operate at significantly different pressure levels.

On the other hand, TSA seems to be a feasible route as the proposed adsorbent materials can be regenerated at moderate operating temperatures and there are options to drive the process through utilization of low pressure steam. Moreover, intelligent heat integration measures could be implemented in order to further increase the process efficiency. In this work it is thus believed that CO₂ capture via TSA has the greatest potential and the following discussion will focus on TSA process related questions only.

Typically, the task of a CO₂ capture processes is to continuously separate a diluted CO₂ stream ($p_{\text{ads,in,CO}_2} \sim 5\text{-}15 \text{ kPa}$) with a high capture efficiency ($\eta_{\text{capt}} \sim 90 \%$) from a process flue gas and to subsequently provide the captured CO₂ at a high purity ($y_{\text{des,out,CO}_2} > 95 \text{ \%Vol}$). This task first of all sets certain demands on the used adsorbent material regarding its adsorption properties. These adsorption properties in turn may have implications on the TSA process and on the feasibility of certain reactor designs. However, the choice of the reactor design then again will set more or less critical demands on the shape, size or mechanical strength of the adsorbent material.

Thus, the selection of a suitable TSA reactor design is strongly connected to the properties of the utilized adsorbent material and vice versa. This chapter will thus first discuss the general requirements on adsorbent materials utilized in TSA CO₂ capture applications and introduce properties of existing adsorbents that are considered as suitable for this task. Basing on that, the requirements on a TSA reactor system that applies such adsorbent materials should be elaborated. Finally, a suitable reactor system for a continuously operating TSA process should be proposed.

3.2 ADSORBENT MATERIAL

3.2.1 General requirements on adsorbent materials for post-combustion CO₂ capture

The separation of a highly diluted CO₂ stream and the desired CO₂ purity requires adsorbent materials that are highly selective towards CO₂ adsorption even at low CO₂ partial pressures. Furthermore, sufficiently large CO₂ adsorption capacities within the range of relevant operating temperatures together with fast adsorption/desorption kinetics are desired as both parameters have implications on capital and operating costs of the CO₂ capture process. In addition, the

adsorbent material should allow for continuous CO₂ separation at lowest possible regeneration energy demand. Finally, an adequate adsorbent material needs to retain its mechanical and chemical integrity over a large number of adsorption/desorption cycles, even in the presence of flue gas contaminants (i.e. SO₂, NO_x) and should be abundant at low costs.

However, among the materials that have been developed up till now, there is no single adsorbent that fulfils the complete list of requirements given above. Instead, each material shows strengths and weaknesses that need to be considered for the conception of the actual TSA CO₂ capture process. Moreover, the suitability of an adsorbent material strongly depends on the CO₂ capture process itself. For example, the selection of the regeneration route affects the operating temperature and pressure under which adsorption and regeneration takes place and the operating conditions in turn have a strong impact on whether a considered adsorbent material is suitable for the process or not. Depending on the type of adsorption mechanism, adsorbent materials for CO₂ capture can be categorized into two different groups [Jones et al., 2009; Berger and Bhowan, 2011; Sayari et al., 2011; Samanta et al., 2012]:

- **Physisorbents**; where the interaction between the adsorbent and CO₂ is based on weak attractive forces (i.e. Van der Waals or electrostatic forces) and
- **Chemisorbents**; where the CO₂ covalently bonds to the adsorbent, typically through an acid-base reaction

Physisorbents exhibit rather low equilibrium loadings at low CO₂ partial pressures and commonly show a weak adsorption selectivity and sometimes favoured adsorption of species other than CO₂ [Sayari et al., 2011]. On the contrary chemisorbents (e.g. amine functionalized adsorbents) show a significantly improved CO₂ selectivity at low CO₂ partial pressures together with a generally great affinity towards CO₂ which is reflected by steep slopes of their adsorption isotherms [Sayari et al., 2011]. In the recent past, amine functionalized adsorbent materials have been introduced as chemisorbents for CO₂ capture applications [Jones et al., 2009]. The idea of immobilizing amines on a solid support actually represents an analogy to liquid amine solutions that proved to capture CO₂ in a highly selective manner. However, chemisorbents generally exhibit significantly larger CO₂ adsorption enthalpies compared to physisorbents. The heat of CO₂ adsorption on chemisorbents is typically in the range of the heat of the chemical reactions that take place (-60 to -90 kJ·mol_{CO₂}⁻¹), whereas the adsorption enthalpies of physisorbents are typically close to the heat of evaporation (-25 to -50 kJ·mol_{CO₂}⁻¹) [Samanta et al., 2012]. This encompasses a larger energy requirement in the regeneration step for chemisorbents compared to physisorbents.

In order to identify the appropriate group of adsorbent materials for continuous TSA processes, chemisorbents and physisorbents will be compared in more detail in the following.

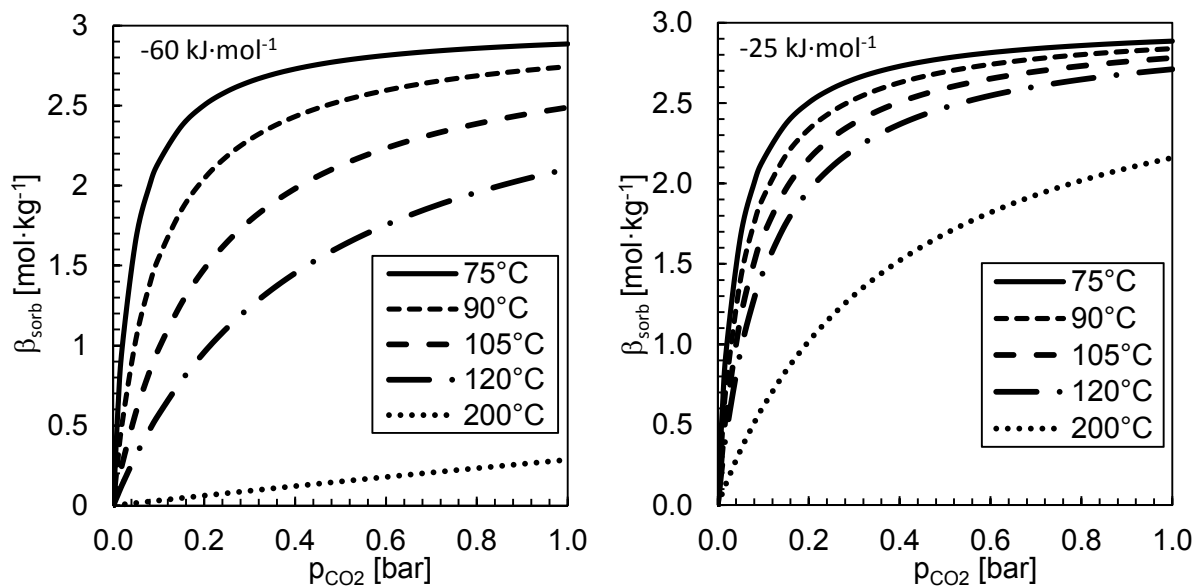
3.2.2 Adsorbents for continuous TSA- chemisorbents vs. physisorbents

Figure 3.1 shows Langmuir adsorption isotherms for adsorbent materials with different adsorption enthalpies. The isotherms on the left hand side are calculated for an adsorption enthalpy of -60 kJ·mol⁻¹ which lies in the range of chemisorbents. The isotherms on the right hand side are calculated with an adsorption enthalpy of -25 kJ·mol⁻¹ which represents a typical value for

physisorbents. For comparability the Langmuir parameters in the right figure ($-25 \text{ kJ}\cdot\text{mol}^{-1}$) are adapted in such a way that the adsorption isotherms at 75°C are equal in both plots.

At a first glance, it might appear that the use of physisorbents in a TSA process requires less regeneration energy compared to the use of chemisorbents due to their significantly lower adsorption enthalpies. However, the adsorption enthalpy of an adsorbent material also affects the temperature dependency of the adsorbent equilibrium loading and thus the necessary temperature swing between adsorption and regeneration conditions for transportation of a specific amount of CO_2 (see Figure 3.1). Obviously, if both sorbent materials shown in Figure 3.1 would be used in a TSA process, the chemisorbent material would need a significantly lower temperature difference between adsorption and regeneration conditions for transportation of the same amount of CO_2 per cycle. A larger temperature shift in turn would lead to larger regeneration energy demands of the TSA process.

Figure 3.1: Langmuir adsorption isotherms [adapted from Berger and Bhowan, 2011].



Berger and Bhowan (2011) showed that for a specific temperature shift in a TSA process, actually an optimum adsorption enthalpy that corresponds to a minimum regeneration energy requirement exists. They found that the optimum adsorption enthalpy, for constant and relevant adsorption conditions ($T_{\text{ads}} = 55^\circ\text{C}$ and $p_{\text{CO}_2, \text{ads}, \text{in}} = 0.14 \text{ bar}$) and a regeneration temperature of 160°C is at $-64 \text{ kJ}\cdot\text{mol}^{-1}$ and at $-87 \text{ kJ}\cdot\text{mol}^{-1}$ for a regeneration temperature of 110°C , respectively. Both adsorption enthalpies lie well in the range of those known from chemisorbent materials. It was thus concluded that despite their larger adsorption enthalpies the utilization of this class of adsorbent materials instead of physisorbents would potentially be more energy efficient for TSA processes [Berger and Bhowan, 2011].

Nevertheless, various types of both, physi- and chemisorbents have been suggested for the purpose of CO_2 capture and are currently under investigation in several research institutions around the world. Sjöström and Krutka (2010) have screened a number of different sorbents including supported amines, carbon-based sorbents and zeolites in a lab-scale facility using synthetic gas mixtures and actual flue gas from a coal fired power plant. The supported amines can be classified as chemisorbents and the latter two as physisorbents. Through the higher adsorption enthalpy, amine

based sorbents have a stronger CO₂ affinity especially at low partial pressures and thus show high selectivity towards CO₂. A good sorbent selectivity yields a high purity CO₂ stream from the desorber offgas, which is necessary to limit compression energy demands, to align with (pipeline) transport requirements and to save storage space. Carbon-based sorbents and zeolites exhibit rather weak selectivity with actually preferred adsorption of steam over CO₂. As flue gases from industrial facilities will always contain water to some extent, an extensive drying step prior to CO₂ removal has thus to be implemented if physisorbents are used commercially. In the case of amine sorbents, selectivity is generally not negatively affected by the presence of water. On the contrary, to the price of potentially larger cooling and regeneration demand the capacities of amine based sorbents increases under wet conditions, due to the formation of carbonates [Xu et al., 2005; Serna-Guerrero et al., 2008; Gray et al., 2009; Zhao et al., 2013].

At low CO₂ pressures, larger CO₂ working capacities can generally be achieved with supported amine sorbents compared to physisorbents. The working capacity is defined as the difference of adsorbed mass of CO₂ on the sorbents leaving the adsorber and the desorber. Thus, if a high working capacity is achieved, less of the adsorbent needs to be circulated to transport a specific amount of CO₂ between the adsorber and desorber. This in turn reduces the energy needed for heating and cooling of the adsorbent and thus the overall energy demand. Gray et al. (2009) suggested minimum working capacities of 3 mol_{CO2} per kg of adsorbent material in order to reduce the energy demand compared to the optimum MEA process by 30-50 %. The reported values for amine sorbents are generally close or even above this proposed limit [Xu et al., 2002; Xu et al. 2003; Son et al., 2008; Gray et al., 2009; Sjostrom and Krutka, 2010]. On the contrary, physisorbents and especially activated carbon adsorbents exhibit comparably low adsorption capacities at low CO₂ partial pressures [Sayari et al., 2011]. It is worth to note that it is crucial to distinguish both the working capacity and the dynamic loading from the sorbent saturation loading or adsorption capacity. While the saturation loading gives the theoretical maximum loading of a sorbent, the others are a result of how the continuous adsorption process is performed and strongly depend on the reactor system design. A reactor design that is expected to allow for achievement of high dynamic sorbent loadings will be introduced in a later section of this chapter.

One major advantage of physisorbents is their superior cyclic stability for applications with flue gases containing contaminants such as SO₂ or NO_x. Supported amines will irreversibly bind SO₂ and thus degrade, leading to larger material make-up [Sayari et al., 2011; Rezaei and Jones, 2013; Rezaei and Jones, 2014;]. To limit sorbent degradation, Ramezan et al. (2007) proposed an acceptable SO₂ threshold of 10 ppm_v. In a commercial system this would result in the implementation of further measures for SO₂ removal.

Summarizing, the comparison of state-of-the-art physi- and chemisorbents above, it is concluded here that the greatest potential for post-combustion CO₂ capture application can be attributed to amine functionalized chemisorbents. Depending on the type of immobilisation of the amine on the solid support the amine functionalized adsorbent materials are commonly separated into two different classes:

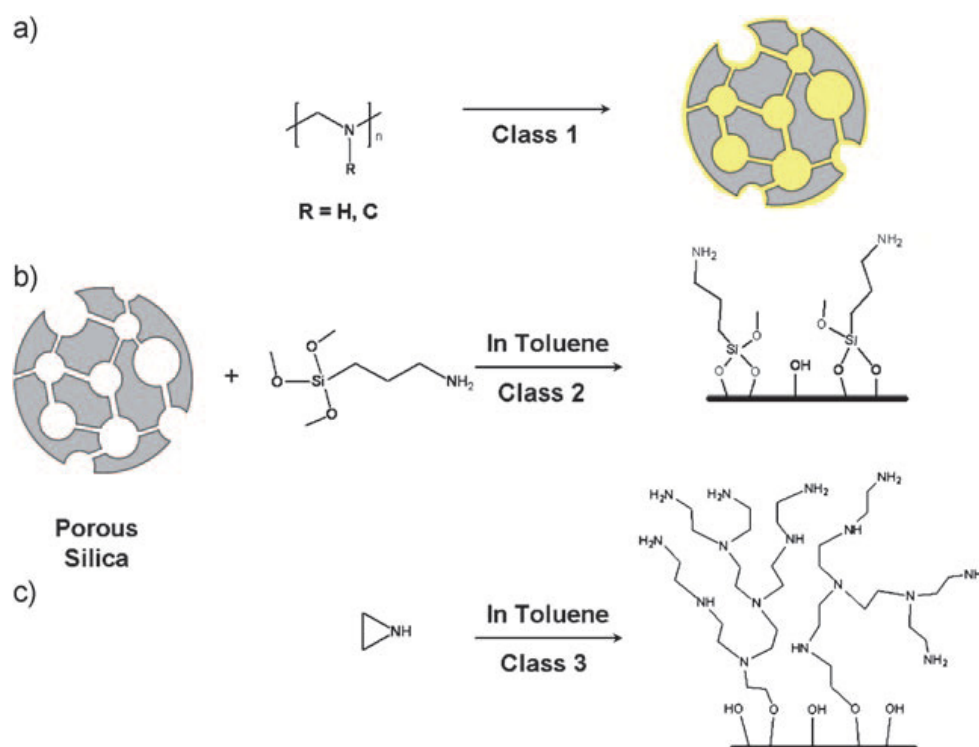
- adsorbents where the amine is **physically impregnated** onto the support material and
- adsorbents where the amine is **covalently bonded** to the solid support material

Within the group of adsorbents functionalized by covalently bonded amines, Li et al. (2010) further distinguish between adsorbent materials prepared by grafting or co-condensation method and those prepared by in-situ polymerization on the adsorbent's surface. Hence, they finally end up at three different classes of amine functionalized adsorbent as depicted in Figure 3.2.

It was reported that adsorbents of the latter two classes (Figure 3.2 b and c) are generally superior to impregnated adsorbents in terms of achievable amine efficiencies (moles of CO₂ adsorbed per 1 mol of N) long-term thermal stability and adsorption kinetics at temperatures below 75 °C [Jones et al., 2009; Sayari et al., 2011]. However, so far the adsorbent materials prepared with these methods exhibit rather low organic loadings and which in turn generally led to significantly smaller adsorption capacities compared to impregnated materials where the amine loadings are generally around 50 %_w. Furthermore, wet impregnation method is a comparably simple preparation method and can be considered as more suitable for commercial scale production of CO₂ adsorption materials [Jones et al., 2009; Bollini et al., 2011].

Since the adsorbent material that has been used within the experimental campaign presented in Chapter 6 was produced via wet impregnation, the following discussion will focus on this type of adsorbent materials only. For detailed information about the adsorbent classes it is referred to the excellent review from Jones et al. (2009).

Figure 3.2: Classification of amine functionalized CO₂ adsorbents (taken from [Li et al., 2010]).



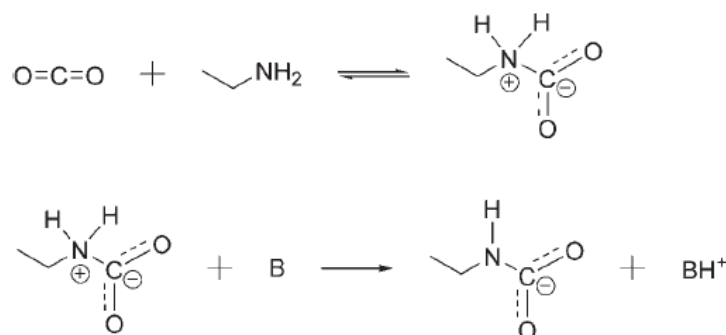
Among the amine impregnated adsorbents, poly(ethyleneimine) (PEI) has been identified as a promising amine compound for material functionalization and is the most commonly studied amine in literature [Jones et al, 2009; Bollini et al., 2011]. The adsorbent material that has been used in this work for the experimental campaign presented in Chapter 6 is also functionalized with PEI. Hence, the main properties of PEI based solid sorbents will be discussed in more detail in the following.

3.2.3 PEI impregnated solid sorbent materials

PEI can be considered as an aminopolymer that contains a mixture of primary, secondary and tertiary amines (branched) or a mixture of primary and secondary amines with primary amine termini (linear) [Jones et al., 2009]. Both PEI configurations exhibit high amine contents ($\sim 33\%_w$ of nitrogen) whereby the ratio of primary:secondary:tertiary amines for branched amines is usually assumed to be 1:1:1. However, for commercially available, low molecular weight PEI the proportion of tertiary amines is typically lower than that of primary and secondary amines [Jones et al., 2009]. The reaction mechanism between CO_2 and primary and secondary amines differs from the reaction path with tertiary amines, which is why the actual amine ratio is important to know. Furthermore, primary amines have a higher heat of adsorption compared to secondary amines. Thus, larger adsorption capacities and faster adsorption kinetics can be expected if a larger fraction of primary amines is used for adsorbent functionalization [Bollini et al., 2011].

Primary and secondary amines were found to react directly with CO_2 via a two-step zwitterion mechanism, whereas tertiary amines have a base-catalytic effect on the hydration of CO_2 [Vaidya and Kenig, 2007]. The two-step zwitterion reaction mechanism is illustrated for the reaction of a primary amine with CO_2 in Figure 3.3. In the first step of the reaction path the CO_2 forms a zwitterion with the lone pair on the amine. In the second step, a base is needed to deprotonate the zwitterion to form a carbamate. In humid environments this base can be H_2O or OH^- , whereas under dry conditions another amine is needed for the deprotonation of the zwitterion. Thus, under dry conditions the maximum amine efficiency (i.e. number of moles CO_2 bonded per mol N of the adsorbent) is 0.5.

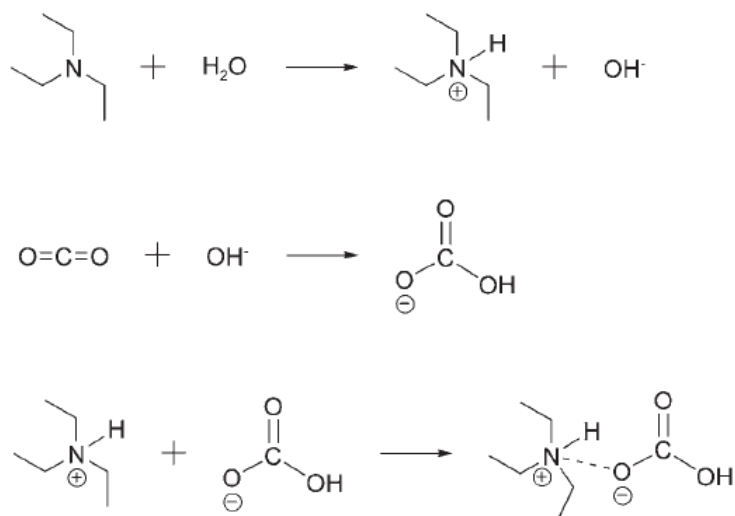
Figure 3.3: Carbamate formation- exemplarily illustrated for reaction of CO_2 with a primary amine (taken from [Jones et al., 2009].



The base-catalytic hydration mechanism for the reaction of CO_2 and a tertiary amine is shown in Figure 3.4. In contrast to primary and secondary amines, tertiary amines catalyse the formation of bicarbonate [Vaidya and Kenig, 2007]. Thereby, the amine first dissociates H_2O , which results in the protonation of the amine and the formation of a hydroxide ion. The hydroxide ion then reacts with CO_2 to form the bicarbonate anion that finally associates with the protonated amine to form a bicarbonate. In the same manner, primary and secondary amines can react with CO_2 and H_2O . However, typically carbamates are formed first and later converted to carbonates and bicarbonates, because the rate constant for carbamate formation is larger [Jones et al., 2009]. As for this pathway only one amine site is occupied by a CO_2 , the theoretical maximum amine efficiency doubles to 1 mol CO_2 per mol N. Thus, it is expected that in CO_2 capture processes that operate under humid adsorption conditions lower sorbent circulation rates and/or larger working capacities could be

achieved compared to processes where dry gases are treated [Harlick and Sayari, 2007; Sayari et al., 2011].

Figure 3.4: Base-catalytic hydration of CO₂ through tertiary amine (taken from [Jones et al., 2009]).

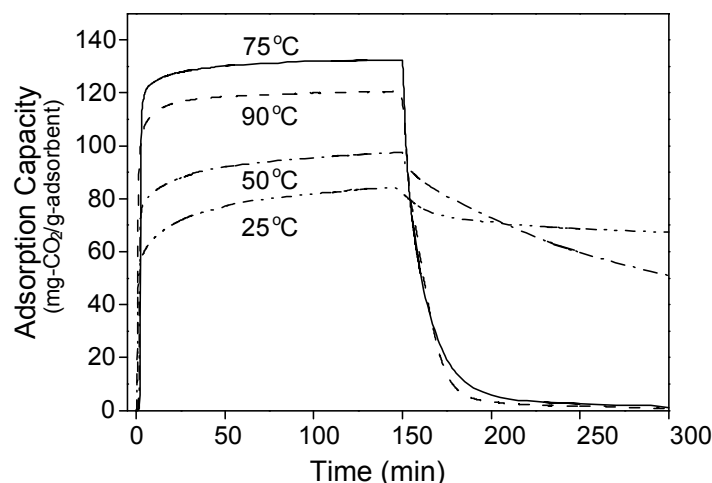


Saytyapal et al. (2001) were the first to publish a CO₂ capture performance study on PMMA beads functionalized with PEI. The tested material was initially developed and used to remove CO₂ from breathing air in space life support applications. The authors concluded that the material has significant potential for greenhouse gas control application as it was capable to capture CO₂ under ambient temperature and pressure and should be less cost intensive than membrane systems where the flue gas stream needs to be pressurized prior separation.

Later, Xu et al. (2002) studied the CO₂ adsorption performance of a mesoporous molecular sieve of MCM-41 type that had been modified by wet impregnation method with different PEI loadings. Their studies revealed a synergetic effect between the support and the amine that yields increased adsorption capacities compared to the pure substances. The measured adsorption capacities at 75 °C and within pure CO₂ atmosphere of the support (MCM-41) and the pure PEI were 14.3 and 109 mg·g_{adsorbent}⁻¹, whereas the maximum adsorption capacity achieved with the impregnated material was 133 mg·g_{adsorbent}⁻¹ (for a PEI loading of 75 %_w on the solid support, referred to as MCM-41-PEI-75). It was shown that the adsorption capacity increased with increasing loading. However, weighting the adsorption values with their corresponding PEI loading mass revealed an optimum PEI exploitation at a 50 %_w loading (MCM-41-PEI-50) with 215 mg·g_{PEI}⁻¹. This value was twice as much as the value for pure PEI, which clearly confirmed the synergetic effect between the support and the amine compounds. The reason why the optimum lied at 50 %_w has been explained with the fact that above this loading the total PEI volume (density of PEI ~ 1.0 g·ml⁻¹) exceeds the pore volume of the MCM-41 support (~ 1.0 ml·g⁻¹). Hence, at this value saturation loading had been achieved and addition of excess PEI led to the formation of a PEI-coating on the external surface of the support that behaved more similar to pure PEI. Xu et al. (2002) further studied the effect of the operating temperature on the adsorption performance of the MCM-41-PEI-50 material by exposing it to a pure CO₂ atmosphere for 150 min. They measured a maximum adsorption capacity at 75 °C and a significantly smaller capacity at 50 °C and an only somewhat smaller capacity at 100 °C. This result is in contrast to expectations as the adsorption of CO₂ on PEI or MCM-41 is a process of exothermic nature and adsorption capacity should therefore increase steadily with decreasing operating

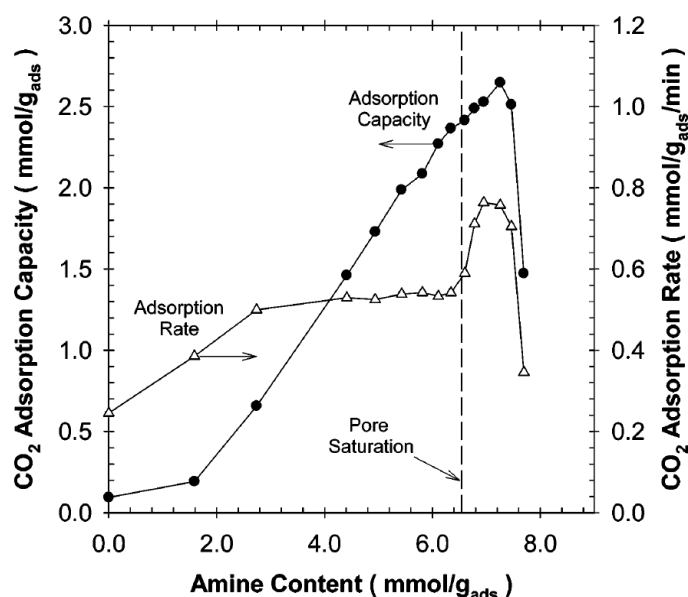
temperature. The authors attributed this effect to diffusion limitations caused by reduced flexibility of the active PEI adsorption sites together with reduced CO_2 exposure at temperatures below 75°C . Similar results have been obtained by Son et al. (2008) using a large-pore mesoporous silica (KIT-6) support impregnated with 50 %_w PEI loading. As can be seen from Figure 3.5 the maximum adsorption capacity has been achieved at 75°C during an exposure time of 150 min to pure CO_2 atmosphere. Further interesting to note is that desorption was not completed in this experiments during 150 min of desorption period under a stream of pure N_2 at equal temperatures levels as adsorption took place.

Figure 3.5: Effect of temperature on adsorption capacity of PEI impregnated KIT-6 (taken from [Son et al., 2008]).



The adsorption/desorption rates are, however, generally significantly increased through the immobilization of the amine on the solid support if they are compared with the respective rates of the pure amine compound [Xu et al., 2002; Son et al., 2008].

Figure 3.6: Effect of PEI loading on adsorption capacity and kinetics (taken from [Franchi et al. 2005]).

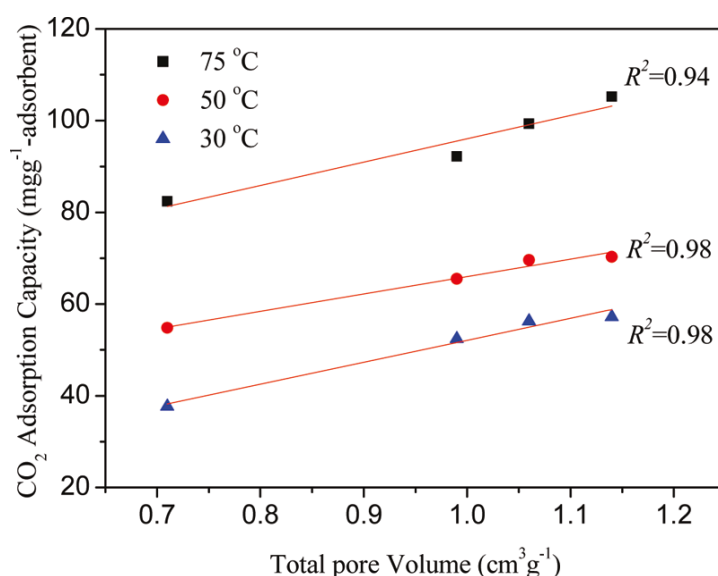


Franchi et al. (2005) showed that the adsorption rate of an impregnated adsorbent reaches a maximum at amine loadings somewhat larger than the saturation loading. If the amine loading is

further increased the adsorption rate drops down significantly as the diffusional resistance through the formed amine surface layer becomes dominant.

Son et al. (2008) synthesized a series of five different mesoporous silicas and impregnated the prepared supports with 50 %_w of PEI. All silica materials showed different textural properties with pore sizes ranging from 6.0 nm (KIT-6) to 2.8 nm (MCM-41) and pore volumes as large as 1.2 cm³·g⁻¹ (KIT-6). The authors measured the largest adsorption capacity and rate could be reached using the adsorbent material prepared with the largest pore size and volume. The measured adsorption capacities in pure CO₂ atmosphere and at 75 °C were 3.07 mmol·g⁻¹ for the KIT-6-PEI-50 and 2.52 mmol·g⁻¹ for MCM-41-PEI-50 material. The time periods measured to achieve 90 % of these stated equilibrium loadings were 4.2 min 59 min, respectively.

Figure 3.7: Correlation between adsorption capacity and pore volume for a series of different SBA-15 substrates impregnated with 50 %_w of PEI in 15.1 %_{vol} CO₂ (N₂ balance) atmosphere (taken from [Yan et al., 2011]).



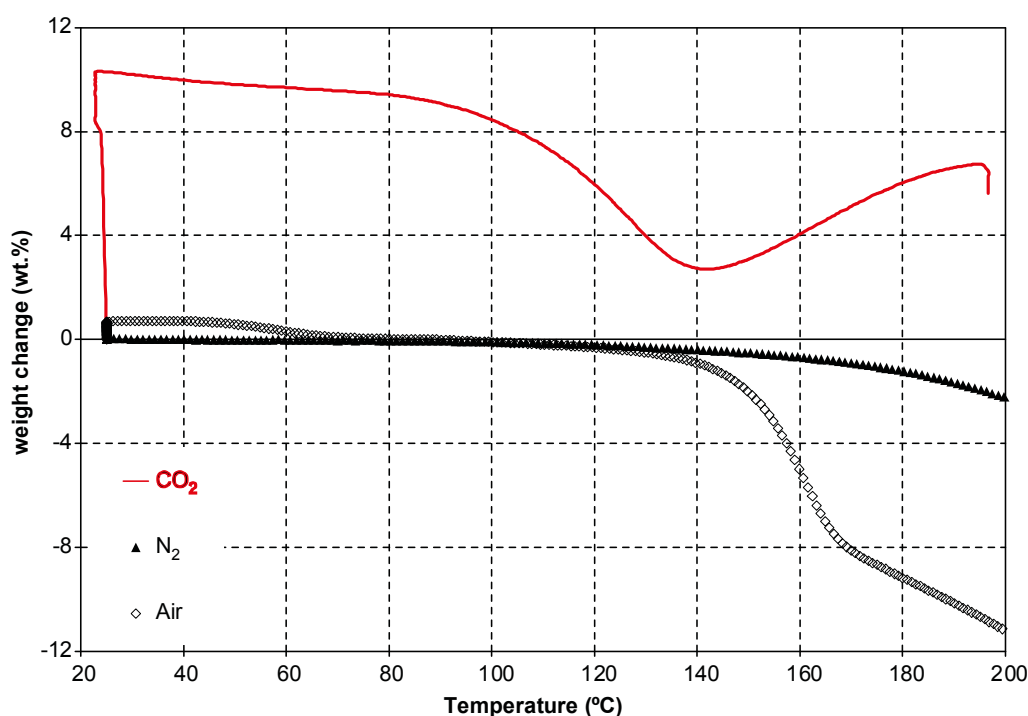
Similar test results have been obtained by Yan et al. (2011) using a series of SBA-15 substrates with textural properties and functionalized with 50 %_w PEI. As can be seen from Figure 3.7, the adsorption capacity of the substrates increases proportionally to the pore volume of the substrate. These results indicated that the textural properties of the amine support have a significant influence on the adsorption performance of the adsorbent.

As for continuous processes it is attempted to perform the regeneration of the adsorbent material through a temperature swing between adsorption and desorption conditions, several works have been attributed to study the thermal stability of the adsorbent material. In contrast to grafted amine adsorbents where the functional amine compounds are covalently bonded to the support's surface, adsorbent materials prepared by wet impregnation method show the disadvantage that part of the amine will always evaporate in accordance with their temperature dependent vapour pressure causing thermal decomposition of the adsorbent material. Xu et al. (2002) as well as Song et al. (2008) studied the decomposition temperature of pure PEI and compared it with decomposition temperatures of PEI impregnated on various mesoporous silicas. They reported that the decomposition temperature of PEI decreases significantly when immobilized on a solid support but the volatility of PEI is still small compared to commercially used amines such as monoethanolamine (MEA). Xu et al. (2002) measured a sharp weight loss of pure PEI at 205 °C,

whereas for the MCM-41-PEI-50 material they measured a similar weight loss rate at 125 °C. They ascribed this effect to the uniform dispersion of PEI on the support's surface and the fact that the decomposition temperature of substances decrease with their particle size.

Later, Drage et al. (2008) conducted TGA experiments to study the thermal stability of an PEI functionalized adsorbent by heating a material sample up to 200 °C. They further used three different atmospheres (air, CO₂ and nitrogen) to distinguish between different decomposition/degradation effects. The mass profiles obtained from these experiments are shown in Figure 3.8.

Figure 3.8: Adsorbent decomposition rate VS. temperature profiles for PEI impregnated adsorbent material (taken from [Drage et al., 2008]).



Similar to former studies, the experiments conducted in N₂ atmosphere showed that the PEI impregnated adsorbent material starts to degrade at temperatures above 120 °C due to amine evaporation. A similar weight loss has been observed between 90-135 °C using an air atmosphere. However, above 135 °C adsorbent weight loss drastically increased under air atmosphere compared to N₂ atmosphere, due evaporation and/or thermal degradation of the amine compounds in the presence of air oxygen. For the experiments conducted within CO₂ atmosphere a significant weight gain had been observed at ambient temperature due to adsorption of CO₂. The sample weight then decreased moderately up to a temperature of about 85 °C. At this temperature, the CO₂ adsorption capacity of the material started to drop significantly till a minimum was reached at about 135 °C. Above this temperature, unlike expected, the sample mass increased again which indicated that a secondary reaction product was obtained above 140 °C. To study this effect more closely, Drage et al. (2008) heated pure PEI in CO₂ up to 140 °C for 16 h, in order to obtain a material that almost exclusively consisted of the secondary reaction product. Post-test analysis of the obtained material revealed that reaction between PEI and CO₂ led to the formation of urea linkages between two adjacent amine sites and to the loss of water. However, it was also shown that the formation of urea linkages is small compared to the formation of carbamate and could be limited if the

regeneration time periods are kept small enough. Sayari and Belmabkhout (2010) studied the multi-cyclic stability of different amine functionalized adsorbent materials (including pore expanded MCM-41 impregnated with 55 %_w PEI) under dry and humid conditions. The adsorption/desorption cycles have been performed at different temperatures in pure CO₂ and N₂, respectively. They found that adsorbent deactivation in pure CO₂ atmosphere through formation of urea linkages occurs even under mild conditions, but at a smaller rate. However, after about 750 adsorption/desorption cycles at 70 °C one of the tested adsorbent materials lost around 15 % of its adsorption capacity. This result clearly reveals that regeneration of amine-functionalized adsorbent materials in pure CO₂ atmosphere is no viable route for commercial applications as it would result in excessive adsorbent make-up. The authors of this study, however, found that the presence of only small amounts of water inhibited the formation of urea linkages almost completely. They further found that hydrolysis allows for reversing the deactivation via formation and accumulation of urea groups completely. Heydari-Gorji and Sayari (2012) studied the long-term stability of mesoporous silicas impregnated with PEI of different molecular weights, namely branched ($M_n \sim 423$ and $M_n \sim 600$) and linear PEI ($M_w \sim 2500$). They studied the stability of the different adsorbent materials in the presence of carbon free air, simulated flue gas and different CO₂/N₂/O₂ mixtures. They reported that the thermal stability in pure N₂ atmosphere was greater for the adsorbents impregnated with PEI of large molecular weight. Furthermore, they also showed that exposure to dry CO₂ atmosphere leads to material deactivation due to formation of different urea groups. However, they showed that urea formation and thus the deactivation mechanism is strongly inhibited by the presence of water. Similar as in previous studies [Drage et al., 2008] the authors reported that PEI-impregnated materials degrade significantly faster in CO₂ free air as in N₂ due to oxidative degradation mechanisms. They inferred that in the presence of air (and absence of CO₂), PEI undergoes significant weight loss due to formation of volatile amine compounds. However, tests conducted with mixtures of CO₂/N₂/O₂ instead of CO₂ free air showed significantly smaller loss of adsorption activity. The authors thus concluded that present CO₂ protects amine groups from oxygen attack through an apparently faster formation of carbamates and bicarbonates that have enhanced oxygen stabilities.

It would be generally preferred to perform the regeneration step of a TSA process within a pure CO₂ atmosphere. This approach would eliminate the need for further gas separation steps as concentrated CO₂ would be obtained as the process product. However, regeneration in dry CO₂ atmosphere would ultimately lead to formation of urea linkages and thus to degradation of the adsorbent material (see discussion above). Furthermore, adsorbent regeneration in pure CO₂ atmosphere is not likely to result in deep reductions of the adsorbent loading and thus reduces the achievable working capacities. The use of an inert stripping gas instead of CO₂, however, is considered to significantly improve the adsorbent regeneration. While inert gases such as N₂ and He have been frequently used to study the performance of adsorbent materials at lab scale, the use of steam as stripping gas represents the only option relevant for practical applications. Nevertheless, so far only few studies have addressed the impact of stripping steam on the adsorbent material. Li et al. (2010) prepared three different adsorbent materials, one from each of the adsorbent classes shown in Figure 3.2. Among the prepared materials, the impregnated adsorbent material exhibited a loading of 35 %_w of low-molecular weight PEI. The different adsorbent materials were subjected to cyclic adsorption/desorption tests within a customized fixed bed configuration. During adsorption the adsorbent sample was exposed to a water-saturated mixture of CO₂ and N₂ until adsorbent

saturation occurred. The sample and the reactor vessel were then heated to 105 °C and subsequently saturated steam was introduced into the fixed bed. Fast desorption kinetics were observed for the impregnated material and the adsorption capacity of the material was retained over a number of three adsorption/desorption cycles. Even though this number of adsorption/desorption cycles is rather low, the obtained results indicated that impregnated materials are stable under steam-stripping conditions. It was thus concluded that steam-stripping seems to be a feasible method to improve regeneration performances in TSA processes. Hammache et al. (2013) also studied the steam stability of an adsorbent material prepared by wet-impregnation of a SiO₂ with 50 %_w of PEI. The adsorbent was exposed to multi-cycle adsorption/desorption conditions using a gas stream with 10 %_{vol} (He to balance) at 60 °C during adsorption and a stream of 90 %_{vol} saturated steam (He to balance) as stripping gas at 105 °C desorption conditions. Furthermore, the sorbent stability after long-time exposure to stripping-steam conditions was investigated in this study. It was shown that cyclic exposure to stripping-steam conditions led to decreasing adsorption capacities of the adsorbent material. The adsorbent degradation, however, levelled off after a number of four adsorption/desorption cycles. Long-term exposure did not have a significant impact on the adsorbent performance. The authors used different methods for characterization of the spent adsorbent material in order to determine the observed degradation mechanism. TGA analysis of fresh and spent adsorbents yielded similar organic loadings of both materials, revealing that the degradation mechanism was not subject to enhanced amine evaporation or leaching. Furthermore, SEM analysis of fresh and used support material showed that no degradation of the support material occurred. Finally, N₂ physisorption characterization was used to determine surface areas and pore volumes of fresh and used adsorbent materials. Results obtained from this characterization method revealed that both adsorbent parameters decreased significantly after the material has been exposed to steam-stripping conditions. The authors thus concluded that steam regeneration led to a reagglomeration of the amine compounds within the pores and on the surface of the adsorbent. This in turn caused pore blockage and reduced accessibility of active amine sites compared to the fresh material. Nevertheless, the adsorbent material maintained a sufficiently large adsorption capacity after multi-cycle exposure to steam-stripping conditions, labelling this method as feasible for adsorbent regeneration in continuous TSA processes.

3.3 HEAT MANAGEMENT AND PROCESS UP-SCALING

In a TSA process it is necessary to have an adequate control of the operating temperatures in the adsorption and regeneration step in order to exploit the advantageous properties of the adsorbent material [Krutka et al., 2013]. This is especially true for TSA processes that use chemisorbent materials with high heats of adsorption that need to be supplied and withdrawn, respectively. Deviations from the optimum operating temperatures could lead to smaller adsorption activities, to weak regeneration performance or, even worse, to adsorbent degradation. Hence, it can be expected that the TSA process performance would be negatively affected by any deviation from the optimum operating temperatures.

As adsorption onto amine functionalized chemisorbents is an exothermic process, the adsorption step in a TSA process requires active cooling of the adsorbent material in order to maintain the desired adsorption temperature. On the contrary, the same amount of energy needs to be supplied during the endothermic adsorbent regeneration step in order to maintain the desired elevated

regeneration temperature. These cooling and heating demands are further increased by the heating and cooling requirements that arise from the temperature shift of the adsorbent material and possibly also from the inert reactor equipment.

The parasitic energy demand for alternating cooling and heating of the inert reactor equipment represents an intrinsic disadvantage of fixed bed reactor configurations, making them appear as inappropriate reactor designs for TSA processes. A more suitable approach is obviously to circulate the adsorbent material between two individual gas-solid contacting zones that are operated at fixed temperature levels. Such a TSA system requires the application of either moving bed or fluidized bed contactors or combinations thereof in order to facilitate adsorbent circulation.

Assuming a TSA process with internal adsorbent circulation at steady-state conditions together with exclusive adsorption of CO₂ by the adsorbent material and further neglecting heat exchange with the inlet gas streams of both columns as well as heat losses, the heat that needs to be exchanged with the system can be expressed as follows

$$-\dot{Q}_{ads} = \dot{Q}_{des} = |\dot{Q}_{trans}| = \dot{m}_{sorb} \cdot [\Delta\beta_{CO_2} \cdot |\Delta H_{ads,CO_2}| + C_{p,sorb} \cdot (T_{des} - T_{ads})] \quad (\text{Eq. 3.1})$$

\dot{Q}_{trans} is commonly referred to as regeneration energy \dot{Q}_{reg} and values are typically reported in energy demand per kg of captured CO₂. Reported values for the regeneration energy of amine functionalized chemisorbents are in the range of 1100-3000 kJ per kg of CO₂ captured [Gray et al., 2009; Sjostrom and Krutka, 2010]. Even though the reported values are significantly lower compared to regeneration energies known from state-of-the-art amine scrubbing processes, the amount of heat that needs to be exchanged is still high.

As these heat flows deliver the thermodynamic driving force for the separation process, effective heat transfer becomes crucial for the overall performance and economics of a TSA process. Achievement of high heat transfer rates between adsorbent material and internal heat exchanger surfaces is important as this would allow for application of practical heat exchanger designs, thus, saving capital expenses (CAPEX) and Krutka et al. (2013) concluded that CAPEX and operating expenses (OPEX) of a TSA process running with amine functionalized adsorbent material will contribute almost equally to the final CO₂ capture costs.

Neither fixed bed nor moving bed regimes allow for achievement of satisfactory heat transfer rates because these regimes essentially rely on the gas phase to transport heat [Yang and Hoffman, 2009]. Even the application of indirect heating and cooling measures leads to rather low heat transfer rates [Bonjour et al., 2002; Clausse et al., 2011]. The fluidized bed regime, however, allows for particle convective heat transfer which results in particle to wall heat transfer rates that are larger by an order of magnitude as compared to heat transfer rates achieved in fixed or moving bed regimes [Yang and Hoffman, 2009; Krutka et al., 2013]. Furthermore, further design improvements such as finned tube designs can be applied to the immersed heat exchangers. This would allow for rather compact designs of the internal heat exchangers due to improved heat transfer surface to heat exchanger volume ratios [Grewal et al., 1985; Rasouli et al., 2005] and thus for reduced CAPEX.

From the important heat transfer point of view, fluidized beds are considered superior over all other contacting regimes and thus represent the first choice for TSA reactor systems. Therefore, the following discussions regarding suitable TSA reactor designs will focus on fluidized bed configurations.

3.4 THERMODYNAMIC CONSIDERATIONS

As already mentioned above, in PCC applications of continuous TSA processes it is required to remove highly diluted CO_2 from flue gases with capture efficiencies close to 90%. Furthermore, in cases where regeneration with CO_2 is not possible from a thermodynamic point of view or leads to adsorbent degradation (i.e. large regeneration temperature, urea formation, etc.) the utilization of stripping steam is usually considered. Steam is also usually available at CO_2 capture sites and it can be easily separated from the CO_2 stream through condensation. To optimize the process energy demand it is thus preferred to achieve the desired CO_2 capture performance with minimum stripping steam demand. The stripping steam demand will add to the OPEX of the TSA system, hence, making reactor systems with lower stripping steam demand attractive. The process energy demand could potentially be further improved through application of intelligent heat integration measures (see also discussions on heat integration measures in Chapter 4 of this thesis).

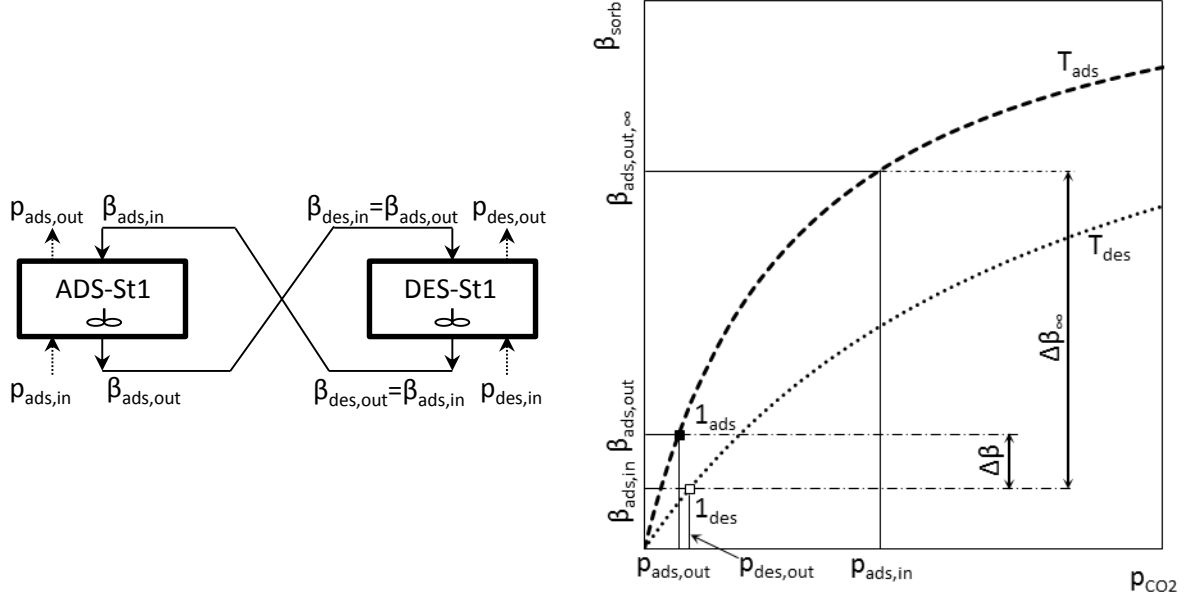
In order to reach a minimum energy demand of the TSA process it is further necessary to achieve the desired capture performance with the lowest possible sorbent circulation rate (SCR) between the adsorber and the desorber. As can be seen from (Eq. 3.1), lowering the SCR reduces the parasitic heating demand caused by the continuous temperature shift of the inert support material. A low SCR further allows for sufficient exploitation of the adsorbent CO_2 capacity since for a constant amount of captured CO_2 , it automatically results in high dynamic adsorbent loadings. The dynamic sorbent loading (dSL) is defined as the ratio of absolute CO_2 capture rate and the sorbent circulation rate between the adsorber and desorber.

It was shown above that due to the importance of heat management in TSA processes it is desired to apply reactor designs that are based on fluidized bed technology. The simplest continuously operated TSA reactor design consists of two individual, interconnected single-stage fluidized bed arrangements, such as previously proposed for biomass gasification or chemical looping combustion [Hofbauer et al., 1995; Pröll et al., 2009]. Such configurations comprise at least one entrained flow reactor to facilitate the internal circulation of solids to the second reactor that is either operated in bubbling bed or also in entrained flow regime. A simplified scheme of such a single-stage TSA configuration is given on the left hand side of Figure 3.9. The problem associated with the application of single-stage fluidized bed reactor systems is, however, that they induce certain thermodynamic limitations to the TSA process [Pirngruber et al. (2013)]. In order to find a suitable TSA reactor system that is based on fluidized bed technology it is essential to understand where this thermodynamic limitations come from. It should thus be discussed in more detail in the following using the adsorption isotherms shown in Figure 3.9.

Typically, in bubbling fluidized bed reactors ideal solids mixing may be assumed without measurable deviation [Guío-Pérez et al., 2013]. The excellent solids mixing, which is advantageous for heat transfer and gas-solids contact, implies a drawback for the continuous TSA capture process consisting of two interconnected single-stage fluidized beds. This is simply because the minimum CO_2 partial pressure in the adsorber off-gas is limited by the equilibrium CO_2 partial pressure, which in turn depends on the CO_2 sorbent loading in the ideally mixed fluidized bed. Since the solids are ideally mixed, the minimum CO_2 partial pressure that can be reached in the adsorber is connected to the loading of the loaded sorbents leaving the adsorber. The same applies to an entrained flow fluidized bed where the sorbents leaving the reactor at the top exhibit at maximum the equilibrium loading

that corresponds to the CO_2 partial pressure in the off-gas of the reactor. This circumstance is visualized on the right hand side of Figure 3.9.

Figure 3.9: TSA reactor system consisting of interconnected single-stage fluidized beds (adapted from [Ringhofer, 2014]).

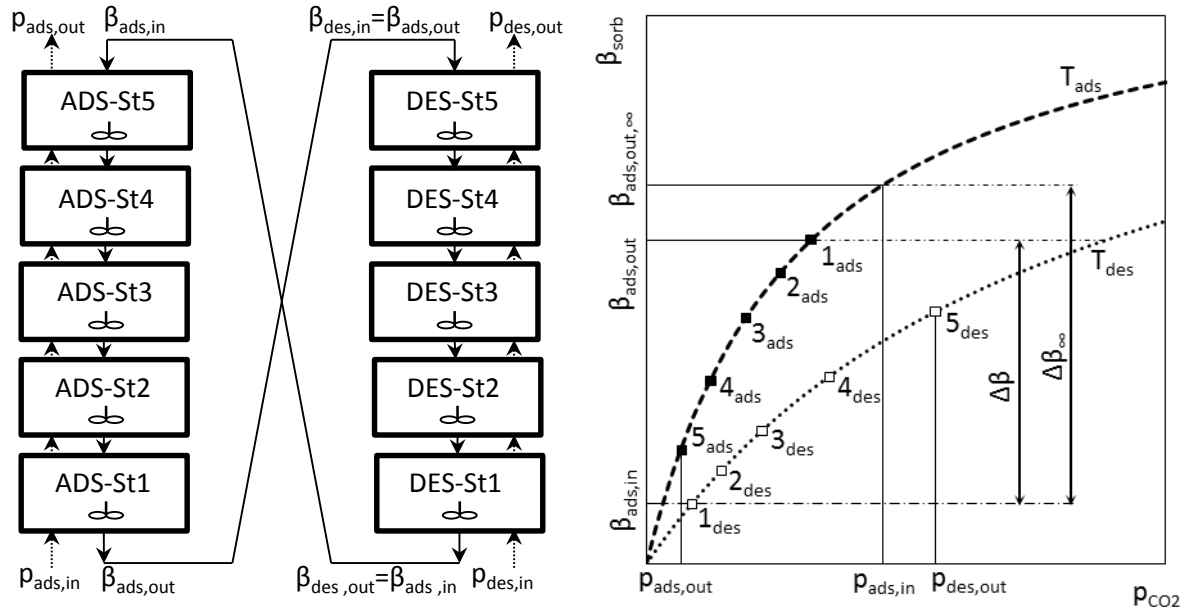


The figure shows the adsorption isotherms of a single-stage fluidized bed TSA reactor system that operates at T_{ads} in the adsorber and at T_{des} in the desorber. The isotherms indicate that on the desorber side, the maximum CO_2 concentration in the off-gas is limited by the equilibrium partial pressure of the lean sorbent leaving the desorber. This implies that in order to achieve high CO_2 capture efficiencies, large SCR and stripping steam demands are required. This in turn means that only very low dynamic loadings can be realized in single stage continuous fluidized bed processes according to Figure 3.9. The economics of a single-stage fluidized bed TSA system will be assessed in more detail within Chapter 4 of this work. Nevertheless, the considerations above already indicate that single-stage reactor designs for continuous TSA CO_2 capture applications can be discarded.

Nevertheless, due to its superior properties regarding heat transfer and its great up-scale potential, it would still be preferred to find a reactor design that applies fluidized bed technology. To overcome the thermodynamic limitations of the single-stage configuration, the gaseous and solid exit streams in both gas-solids contactors need to be disconnected. In continuously operating gas-liquid absorption units this is typically achieved through realization of a counter-current flow between gas and solvent streams. A counter-current flow of adsorbent material and gas streams would maintain a driving force for adsorption/desorption along the complete column. In the adsorber, the counter-current contact facilitates that regenerated particles (β is low) meet the off-gas of the adsorber with a desired small CO_2 partial pressure at the top of the column, while at the bottom of the column highly loaded sorbent material (β is high) is contacted with raw flue gas that exhibits a CO_2 partial pressure that is significantly larger than in the adsorber off-gas (e.g. about ten times larger for $\eta_{\text{capt}} = 90\%$). In fluidized bed systems, such a counter-current flow can be realized through stacking of several individual stationary fluidized beds (see scheme in Figure 3.10). In such systems, the sorbent loadings of the adsorbent material streams leaving the columns would no longer be connected to the off-gas CO_2 partial pressures of the columns. Instead the sorbent loading and CO_2 partial pressure in the off-gas of each individual stage are connected and reach at the best the equilibrium state that is

determined by the operating temperature of each stage. The adsorption isotherms shown in Figure 3.10 illustrate this circumstance for an ideal TSA system (i.e. adsorption equilibrium is reached) that comprises a adsorber and desorber column with each having 5 fluidized bed stages and that are operating at constant temperature (i.e. T_{ads} and T_{des} , respectively). The filled squares on the adsorption isotherm (T_{ads}) are marking the equilibrium states in each stage of the adsorber column. The same applies to the desorber, with the individual stage equilibrium states indicated as empty squares on the desorption isotherm (T_{des}). In both columns, stage 1 refers to the lowermost and stage 5 to the uppermost stage. This means that sorbent material extracted from stage 1 of one column enters into stage 5 of the respective other column. It is worth to mention that the drawn isotherms as well as the CO_2 partial pressures in the adsorber in- and outlet equal those from Figure 3.9.

Figure 3.10: TSA reactor system consisting of interconnected multi-stage fluidized bed columns (adapted from [Ringhofer, 2014]).



As one can see, by applying a multi-stage configuration, a significantly higher working capacity $\Delta\beta$ is achieved. In fact, for an infinite number of stages, $\Delta\beta$ would approach the theoretical maximum working capacity $\Delta\beta_{\infty}$ that is limited by the CO_2 partial pressure in the adsorber feed gas and the operating temperatures. Furthermore, high CO_2 offgas concentrations can be achieved in the desorber while at the same time particle regeneration down to essentially low loadings can occur in the lower part of the desorber. Depending on the desired temperature swing and the used adsorbent material, even concentration of the diluted CO_2 adsorber feed stream in the desorber off-gas stream is possible.

Hence, a TSA system that exhibits a multi-stage configuration in both gas-solid contactors allows for reaching high CO_2 capture efficiencies at low sorbent circulation and stripping steam rates. Thus, such a system should be capable to capture CO_2 with low regeneration energy demands while at the same time capital cost savings can be expected from reduced sizes of internal heat exchangers.

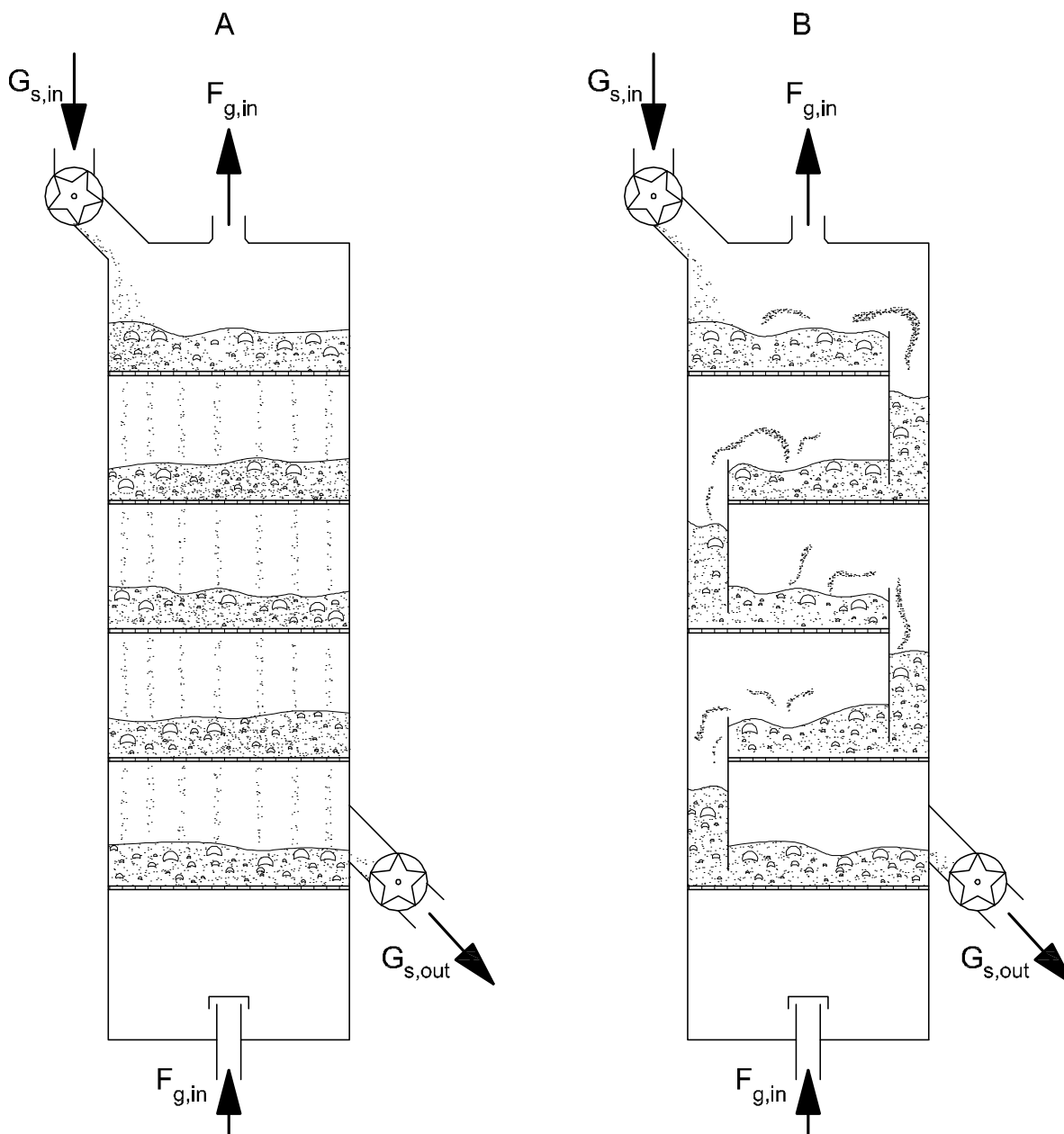
The following section will introduce the main aspects of multi-stage fluidization engineering and further elaborate an actual design concept for a multi-stage TSA system.

3.5 MULTI-STAGE FLUIDIZED BED SYSTEMS

3.5.1 General aspects of multi-stage fluidized bed systems

Efficient CO₂ capture within a continuously operating TSA process essentially requires a counter-current movement of sorbent material and gas streams in both, the adsorber and the desorber. The counter-current flow of both phases leads to an axial profile of gas concentration and sorbent loading within each contactor. This can be exploited in the adsorption process to achieve significant improvement of the process performance.

Figure 3.11: Multi-stage fluidized bed configurations.



Such a counter-current contactor can for example be realized in form of a fixed- or moving bed reactor. However, as stated above another crucial design criterion for both contactors is a proper heat transfer between heat exchangers and sorbent material and both of the mentioned reactor systems suffer from a very weak heat transfer. Fluidized bed reactors, however, offer high heat transfer coefficients between bed material and immersed heat exchanger surfaces.

Thus, it is proposed to use a system configuration in which both contactors are realized as multi-stage fluidized bed (MStFB) columns, with each of them comprising an internal heat exchanger. This design should allow for realization of an axial CO₂ concentration profile, respectively, an adsorbent loading gradient in inverse direction through counter-current movement of gas and solids while at the same time sufficiently large heat transfer rates can be achieved between sorbent material and immersed heating and cooling surfaces.

The simplest design of a column with several successive fluidized beds is a trickle flow reactor that makes use of horizontal perforated plates for sectioning of the reactor [Brauer et al., 1970; Srinivasa Kannan et al., 1994]. Such a reactor design is shown in Figure 3.11 (A). As trickle flow reactors exhibit no downcomers for connection of the individual stages, the design of the plate perforations need to permit simultaneous solid phase down- and gas phase up-flow. If the plates are designed properly and the gas and solid flow rates are within the limits of stable operation, a counter-current movement of gas and solid streams can be realized.

Despite of the simplicity of the trickle flow design a different design using downcomers for solid phase transport from stage to stage has been proposed. In such a system the downcomers hydraulically communicate between two adjacent stages via adjustment of their solids bed height.

Several studies on the fluid-dynamic behavior of MStFB systems with downcomers exist [Krishnaiah and Varma, 1982; Papadatos et al., 1975; Eleftheriades and Judd, 1978; Martín-Gullón et al., 1995; Mohanty and Meikap, 2009; Mohanty et al., 2010].

3.5.2 Design aspects of multi-stage fluidized bed systems with downcomers

From the above mentioned characteristics of MStFB systems with downcomers, two crucial design aspects can be extracted; the design of the downcomer as well as the gas distributor design. The design procedure of both components will be described in the following.

Gas distributor design (perforated plates)

A sufficient gas distributor design is essential for any fluidized bed system. For proper gas distribution over the entire bed cross section it is necessary that the ratio of distributor to bed pressure drop is sufficiently large. On the other hand, an increased distributor pressure drop causes increased total pressure drop of the fluidized bed column and thus larger operating costs. In the case of a post-combustion CO₂ capture unit, too large pressure drops may make retrofitting into an existing off-gas duct even impossible.

The pressure drop of a perforated plate gas distributor is generally given as

$$\Delta p_{distr} = \zeta \cdot \frac{\rho_g \cdot U_{g,or}^2}{2} \quad (\text{Eq. 3.2})$$

whereby in order to ensure uniform distribution of the fluidization gas over the cross section of the bed Zuiderweg (1967) suggested the following range

$$\Delta p_{distr} = 0.2 \div 0.4 \cdot \Delta p_{bed} \quad (\text{Eq. 3.3a})$$

Similar ranges have been proposed by other authors, e.g. Agarwal et al. (1962) suggested the following range

$$\Delta p_{distr} = 0.1 \div 0.3 \cdot \Delta p_{bed} \quad (\text{Eq. 3.3b})$$

Several correlations for the resistance factor of an orifice ξ can be found in literature. Applying the formulae used by Mohanty et al. (2010) and a triangular distributor perforation pattern, Δp_{distr} can be derived as follows

$$\Delta p_{distr} = 6 \cdot \rho_g \cdot \left(\frac{U_{g,col}}{\pi \cdot C_d} \right)^2 \left(\frac{p_{or}}{d_{or}} \right)^4 \quad (\text{Eq. 3.4})$$

using the following correlation for the coefficient of discharge

$$C_d = 0.6974 \cdot U_{g,col}^{0.2} \quad (\text{Eq. 3.5})$$

For perforated plate distributor designs it is furthermore important that the perforation diameter is on the one hand small enough to prevent solids from passing through them, but on the other hand large enough to prevent blocking through particles. A practically proven range of perforation sizes can be given as follows

$$3 \cdot d_p < d_{or} < 10 \cdot d_p \quad (\text{Eq. 3.6})$$

Downcomer design

As mentioned above a proper design of the downcomer is essential for stable operation of the MStFB column. Eleftheriades and Judd (1978) studied the influence of the downcomer solid mass flux on the downcomer solids flow regime for different values of superficial gas velocities within a two staged fluidized bed system using sand as bed material. They observed that if the downcomer solid mass flux is increased accordingly a moving bed regime within the downcomer can be preserved even at superficial gas velocities (i.e. total gas feed into the MStFB column) above the minimum fluidization velocity of the bed material. However, at a certain gas velocity the downcomer mass flux reached a maximum ($\sim 200 \text{ kg} \cdot \text{m}^{-2} \cdot \text{s}^{-1}$) and the flow regime within the downcomer switched to fluidized bed regime. The corresponding critical gas velocity was more or less independent on the downcomer to column area ratio, whereas the maximum solid flux increased with this ratio. For superficial gas velocities close to the minimum fluidization velocities it was shown that the moving bed flow regime within the downcomer can be retained at solid mass fluxes above $30 \text{ kg} \cdot \text{m}^{-2} \cdot \text{s}^{-1}$.

Figure 3.12 shows two individual stages of a MStFB column together with the main downcomer dimensions and the pressure drops indicated at their respective location of occurrence. Taking the notations from Eleftheriades and Judd (1978) studied the influence of the downcomer solid mass flux on the downcomer solids flow regime for different values of superficial gas velocities within a two staged fluidized bed system using sand as bed material. They observed that if the downcomer solid mass flux is increased accordingly a moving bed regime within the downcomer can be preserved even at superficial gas velocities (i.e. total gas feed into the MStFB column) above the minimum fluidization velocity of the bed material. However, at a certain gas velocity the downcomer mass flux reached a maximum ($\sim 200 \text{ kg} \cdot \text{m}^{-2} \cdot \text{s}^{-1}$) and the flow regime within the downcomer switched to fluidized bed regime. The corresponding critical gas velocity was more or less independent on the

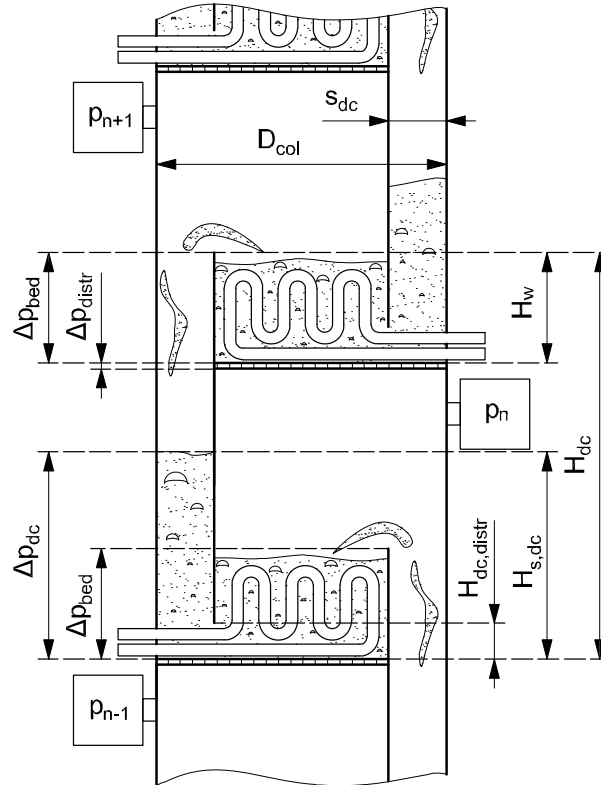
downcomer to column area ratio, whereas the maximum solid flux increased with this ratio. For superficial gas velocities close to the minimum fluidization velocities it was shown that the moving bed flow regime within the downcomer can be retained at solid mass fluxes above $30 \text{ kg} \cdot \text{m}^{-2} \cdot \text{s}^{-1}$.

Figure 3.12, for stable operation the pressure drop across the downcomer has to fulfil the following equation

$$\Delta p_{dc} = 2 \cdot \Delta p_{bed} + \Delta p_{distr} \quad (\text{Eq. 3.7})$$

Eleftheriades and Judd (1978) studied the influence of the downcomer solid mass flux on the downcomer solids flow regime for different values of superficial gas velocities within a two staged fluidized bed system using sand as bed material. They observed that if the downcomer solid mass flux is increased accordingly a moving bed regime within the downcomer can be preserved even at superficial gas velocities (i.e. total gas feed into the MStFB column) above the minimum fluidization velocity of the bed material. However, at a certain gas velocity the downcomer mass flux reached a maximum ($\sim 200 \text{ kg} \cdot \text{m}^{-2} \cdot \text{s}^{-1}$) and the flow regime within the downcomer switched to fluidized bed regime. The corresponding critical gas velocity was more or less independent on the downcomer to column area ratio, whereas the maximum solid flux increased with this ratio. For superficial gas velocities close to the minimum fluidization velocities it was shown that the moving bed flow regime within the downcomer can be retained at solid mass fluxes above $30 \text{ kg} \cdot \text{m}^{-2} \cdot \text{s}^{-1}$.

Figure 3.12: MStFB downcomer design.



In a TSA process one would try to operate the downcomer in fluidized bed regime. This would allow for good gas-solids contact also in the downcomers, thus, making the downcomer material contributing more actively to the adsorption process. Furthermore, in the fluidized bed regime the minimum downcomer bed height would be smaller than in the moving bed regime as the pressure drop along a stationary bed of solids reaches a maximum in the fluidized bed regime (see

Section 2.2). Thus, for the following derivations the downcomer is considered to be operated in the fluidized bed regime. Practically, the downcomer segment height s_{dc} needs to be chosen in a way to ensure a solids flux that is fairly below the transition limit for the given sorbent circulation rate.

Assuming, a fluidized bed regime within the downcomer, the pressure drop along the downcomer can be calculated as follows

$$\Delta p_{dc} = H_{s,dc} \cdot (1 - \varepsilon_{dc}) \cdot (\rho_s - \rho_g) \cdot g \quad (\text{Eq. 3.8})$$

The pressure drop across the fluidized bed of solids was reported to be equal in each stage (e.g. [Mohanty and Meikap, 2009]) and thus can be expressed as

$$\Delta p_{bed} = H_w \cdot (1 - \varepsilon_{bed}) \cdot (\rho_s - \rho_g) \cdot g \quad (\text{Eq. 3.9})$$

It is worth to note that the actual height of the formed dense phase is generally lower than the downcomer weir height [Papadatos et al., 1975]. Using the weir height H_w as dense phase height, however, leads to a conservative estimation of the minimum downcomer height. Furthermore, Martín-Gullón et al. (1995) assumed and experimentally verified that the mean gas velocities within the fluidized bed stage and the downcomer section are equal if the downcomer is operated in the fluidized bed and not in a slugging regime. Since, the voidage in a bubbling fluidized bed of particles with constant hydrodynamic properties just depends on the fluidizing gas velocity, both bed voidages can thus be considered to be equal. The bed voidage can be calculated using for instance the correlation given by Hsiung and Thodes (1977):

$$\varepsilon = \varepsilon_{dc} = \varepsilon_{bed} = \varepsilon_{mf} \cdot \left(\frac{\text{Re} - b'}{\text{Re}_{mf} - b'} \right)^{0.28} \quad (\text{Eq. 3.10})$$

where

$$b' = 0.216 \cdot \text{Re}_{mf}^{1.2} - 0.35 \quad (\text{Eq. 3.11})$$

During operation, the downcomer pressure drop will automatically adapt to fulfil (Eq. 3.7) by adjusting its solids bed height $H_{s,dc}$. For stable operation it is thus necessary that the following equation holds

$$H_{dc} \geq H_{s,dc} \quad (\text{Eq. 3.12})$$

If the solids height within the downcomer reaches the actual downcomer height, Δp_{dc} reaches a maximum. A further increase of the pressure drops of the right hand side of (Eq. 3.7) would lead to an unstable mode of operation [Martín-Gullón et al., 1995]. For stable operation of the MStFB column it is thus essential to have sufficiently large downcomer heights. On the contrary, too large downcomer heights lead to unnecessary capital costs as the increased freeboard heights are free of solid material and thus generally inactive in the TSA process.

Rearranging (Eq. 3.4) and (Eq. 3.7)-(Eq. 3.11), the downcomer solids height can be calculated as follows

$$H_{s,dc} = 2 \cdot H_w + \frac{6}{(1 - \varepsilon) \cdot g} \cdot \frac{\rho_g}{\rho_s - \rho_g} \cdot \left(\frac{U_{g,col}}{\pi \cdot C_d} \right)^2 \left(\frac{p_{or}}{d_{or}} \right)^4 \quad (\text{Eq. 3.13})$$

3.6 DOUBLE-LOOP MULTI-STAGE FLUIDIZED BED REACTOR DESIGN

Basing on the findings above, a TSA reactor system consisting of two interconnected multi-stage fluidized bed columns is introduced in the following. As the adsorbent material performs an overall figure-eight movement within the reactor systems, the proposed design is referred to as “Double-loop multi-stage fluidized bed system for continuous and effective temperature swing adsorption”.

Figure 3.13 shows the proposed double loop staged fluidized bed system. Both, the adsorber (Figure 3.13, A) and the desorber (Figure 3.13, B) consist of a series of bubbling fluidized beds where the net solids flow is downwards and gas is passing the contactor from the bottom to the top. The adsorber is fluidized with the flue gas to be treated in the TSA unit (Figure 3.13, 1), whereas the desorber is fluidized with a stripping gas agent that could be either steam, CO₂ or a combination thereof (Figure 3.13, 3). On the way through the adsorber column, the CO₂ concentration within flue gas gradually decreases as it is adsorbed by the passing adsorbent material so that the cleaned flue gas leaves the adsorber with the desired CO₂ concentration at the top of the column (Figure 3.13, 2). In the desorber, the adsorbent material gets regenerated, thereby, releasing CO₂ so that finally a mixture of CO₂ and steam is obtained in the offgas of the desorber (Figure 3.13, 4). The CO₂ concentration in the desorber off-gas will depend on the net CO₂ capture rate of the unit and the amount and composition of the stripping gas, whereby concentration of CO₂ is possible in this configuration and also desired.

Each of the individual fluidized bed stages features a gas distributor, a downcomer that enables controlled particle flow downwards adjacent stages, a weir plate as well as a heat exchanger for heat supply (Figure 3.13, 11) and cooling (Figure 3.13, 10), respectively. Solids are continuously discharged from the lowermost stages of both contactors under controlled conditions. L-valves as depicted in Figure 3.13 (E) can be used for this purpose but also mechanical flow control devices such as mechanical valves or screw conveyors may be used.

The respective flow control device further directs the sorbents into transport risers (Figure 3.13, C) that pneumatically lift the particles up to above the top stage of the respective other column. The transport risers additionally exhibit heat exchangers that enable heat exchange between hot particles leaving the desorber and colder particles leaving the adsorber (Figure 3.13, 12). Such a lean-rich heat exchanger is a key-component in any gas-liquid absorption scheme. Here, an additional increase of the TSA process economics should be achieved with such a configuration, even though it is expected that it would not be as significant as in liquid absorption process due to the lower heat capacity of the adsorbent material. The heat exchangers may be situated in the lower parts of the risers where a more or less dense bed of sorbent material will be formed and better heat transfer rates can be expected compared to the transport zones of the risers. Additional, counter-current heat exchange could be realized in the upper transporting zone of the risers, for example through a double wall design of the risers. At the top of the risers, the lifted particles enter a gas-solid separating device (Figure 3.13, D). Simple gravity separators or cyclone separators can be used here, potentially in combination with filter separators. The separated solids are directed into the top stage of the respective other column and thus circulate in a double loop through the system. The lift gas used in the transporting risers is continuously recycled by means of gas blowers (Figure 3.13, F). Part of the recycled gas can be used to adjust the sorbent throughput in the L-valves (Figure 3.13, 5 and 6)

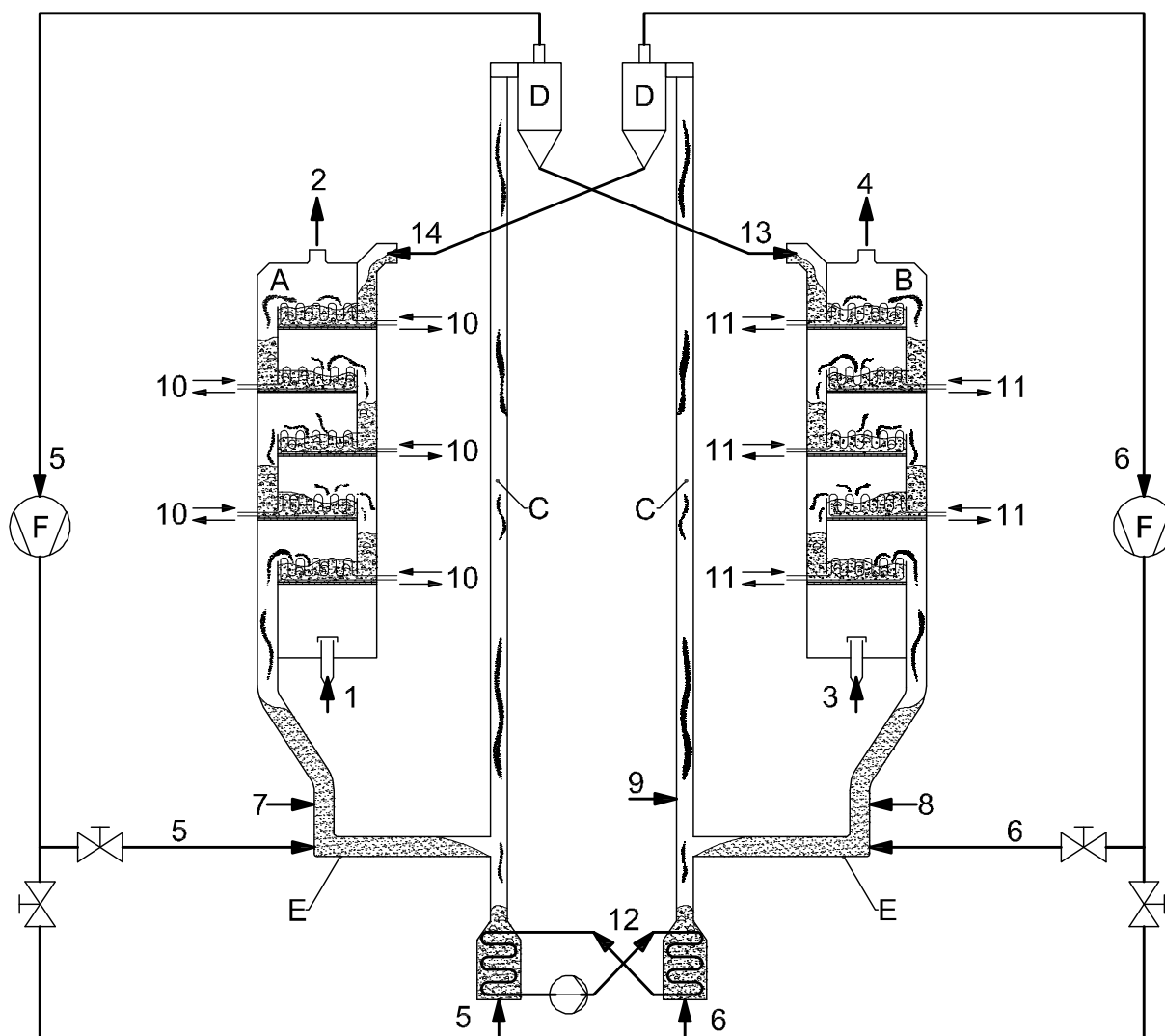
and thus to control the sorbent circulation rate and the distribution of the sorbent inventory between both columns.

It is worth to note that no gas sealing device is needed between the columns. The gas sealing between the two main gas streams, is accomplished by controlled introduction of a purge or sealing gas flow into the moving bed that will be formed between the lowermost contactor stage and the solids flow controlling devices between the columns and the risers (Figure 3.13, 7 and 8).

The introduced purge gas will split up with a part of it flowing towards the riser and the other part flowing counter-currently to the adsorbent material into the moving bed. Hence, it prevents any gas flow from the column into the riser section, thereby preventing exchange of the main gas flows in both columns. For constant operation of the recirculation blowers the amount of riser gas within the recycle system stays constant. Hence, the same amount of gas entering the closed riser system from the purge gas introduction (and potentially also through desorption of CO_2 from the adsorbent material) needs to leave the recycle system through the chute connecting the solids separator and the uppermost stage of the contactor. This means the gas used as purge needs to be acceptable in the inlet stream of one contactor and within the outlet stream of the respective other contactor. Moreover, as the recirculation gas composition will necessarily adapt to the purge gas composition it is important that no negative interaction between this gas and the circulating sorbents will occur. The proposed purge gas compositions are therefore dry CO_2 for the adsorber side (Figure 3.13, 7) and superheated steam for the desorber side (Figure 3.13, 8). The dry CO_2 purge will lead to an essentially pure CO_2 atmosphere in the riser section that transports the particle from the adsorber into the desorber. Therefore, the sorbents leaving the adsorber will slightly increase their CO_2 loading within the riser. In addition, a flow of pure CO_2 will enter the top stage of the desorber column and leave the system through the desorber exit duct. While the increased particle loading and the CO_2 stream into the desorber column do not represent a problem, the part of the CO_2 purge that enters the adsorber needs to be adsorbed by the particles in order to not decrease the capture performance. However, it is expected that the required purge gas streams for proper gas sealing are comparably small to the main gas streams and thus their influence on the performance of the lowermost stage of both columns can be neglected. The desorber purge nevertheless would represent a problem if the steam concentration within the closed riser gas system is not limited. As the lean-rich heat exchanger will cause a temperature drop (ideally down to the adsorber temperature) the introduced steam would condense within the riser which would have serious consequences for the solid sorbent material. Thus, it is proposed to introduce cleaned flue gas as diluting gas (Figure 3.13, 9) into the riser in order to keep the dewpoint of the gas mixture in the recirculation system below the present operating temperature.

From a thermodynamic point of view, the proposed system allows for achievement of low adsorber and high desorber CO_2 offgas concentrations, whilst reaching high dynamic sorbent loadings (high CO_2 loading on the rich sorbent leaving the lowermost adsorber stage and almost no CO_2 loading in the lean sorbent leaving the lowermost desorber stage). The high dynamic sorbent loading necessarily leads to low sorbent circulation rates, which in turn improves the efficiency of the TSA process. Hence, the proposed multi-stage arrangement seems to satisfy all of the requirements of an efficient solid sorbent post combustion CO_2 capture process. The actual potential of the process will be assessed within the following chapter by means of thermodynamic equilibrium modelling.

Figure 3.13: Double-loop multi-stage fluidized bed TSA reactor design.



A ... adsorber
 B ... desorber
 C ... riser
 D ... gas-solid separator
 E ... L-valve
 F ... recycle-gas blower
 1 ... raw flue gas
 2 ... clean flue gas
 3 ... stripping gas (steam)

4 ... CO₂ enriched stripping gas
 5 ... recirculation gas (CO₂)
 6 ... recirculation gas (clean flue gas)
 7 ... purge gas (CO₂)
 8 ... purge gas (steam)
 9 ... dilution stream (raw flue gas)
 10... adsorber stage cooling
 11... desorber stage heating
 12... lean-rich heat exchange
 13... high loaded solids
 14... regenerated solids

3.7 CONCLUSIONS

Exhaust gas streams from processes in the power or industry sector typically exhibit low CO₂ partial pressures. Consequently, the utilization of highly selective adsorbent materials is required in CO₂ separation based on temperature swing adsorption (TSA). Chemisorbents typically exhibit a good selectivity even at low adsorptive partial pressures and are thus most suitable for TSA processes. A further benefit of chemisorbents is that they allow for achieving comparably large working capacities at a given temperature swing due to their high adsorption enthalpies.

A new class of chemisorbents that comprise functional amine compounds on a porous support material has been developed in the recent past. Similar to the active amine compounds used in amine scrubbing processes, the amine functionalized adsorbent materials allow for reversible reaction with CO₂ that can be exploited at best within a TSA process. Depending on how the amine is applied to the porous support material, two different types of amine functionalized adsorbent materials can be identified; adsorbents impregnated with amine and adsorbents with active amine compounds covalently bonded to the surfaces of the porous support. The most commonly studied materials for TSA are polyethylenimine (PEI) impregnated adsorbents and main features of these materials have been presented.

The application of chemisorbents requires the exchange of large amounts of heat with the TSA system. Thus, heat transfer properties are crucial in such a system as they have implications on the final capital costs and thus on the process economics. Thus, a suitable TSA reactor design would allow for achieving maximum heat transfer rates. Fluidized bed reactor designs allow for achieving heat transfer coefficients that are by an order of magnitude larger compared to fixed or moving bed configurations. Hence, it was concluded that the application of fluidized bed technology is desired for TSA processes.

From a thermodynamic point of view a TSA process essentially requires counter-current movement of gas and sorbent materials, at least within the adsorber column. Depending on the used adsorbent material, regeneration within a single stage desorber, using CO₂ as stripping agent might be feasible. However, concerns have been raised that regeneration within a pure CO₂ atmosphere might lead to adsorbent degradation and that it is not likely that deep regeneration can be achieved within a pure CO₂ atmosphere. Thus, the use of steam as fluidization and stripping agent is typically suggested. In order to minimize the stripping steam demand it is beneficial to also apply a counter-current flow regime to the desorber.

Counter-current operation within a fluidized bed reactor can be achieved through sectioning of the fluidized bed reactor. The sectioning can be done with perforated plates with or without downcomers attached to them. The main design aspects of multi-stage fluidized bed columns with downcomers have been presented.

Basing on the findings in this chapter, a TSA reactor system consisting of two interconnected multi-stage fluidized bed columns has been introduced. In order to evaluate the feasibility of this system for post-combustion CO₂ capture it should be evaluated from a thermodynamic point of view in Chapter 4.

4. MODELLING AND PROCESS EVALUATION

4.1 MODEL DESCRIPTION

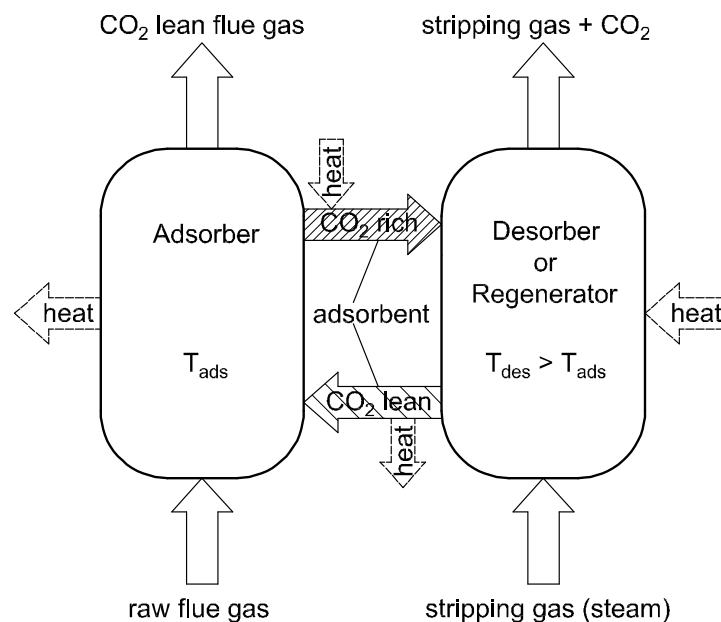
4.1.1 General aspects

A qualitative examination of potential TSA CO₂ capture processes designs in Chapter 3 resulted in a reactor system that is considered as optimal in terms of heat management and energy requirement. The proposed TSA reactor system comprises two interconnected multi-stage fluidized bed columns that facilitate counter-current contact of gas streams and adsorbent material. Furthermore, each of the individual stages is equipped with internal heat exchangers to enable heat exchange with highest heat transfer rates. The adsorbent transportation lines that connect both columns are equipped with additional heat transfer surfaces that allow for heat exchange between colder, CO₂ loaded (rich) and hotter, regenerated (lean) adsorbent material.

In order to quantitatively assess the energy requirement of such a TSA system an adequate simulation tool should be introduced and used within this chapter. The simulation tool is based on a simplified process scheme as given in Figure 4.1. The scheme includes all mass- and energy streams going in and out of the individual gas-solid contactors that are relevant for process evaluation. Each contactor is assumed to operate under isothermal conditions and with any number of internal fluidized bed stages.

The development of the simulation tool has been performed using the process simulation software IPSEpro. This software environment provides mathematical solvers that enable mass- and energy balance calculations within a graphical user interface.

Figure 4.1: Basic scheme of continuously operating temperature swing adsorption with regeneration.



4.1.2 Adsorption thermodynamics

For quantitative assessment of the energy requirement of the proposed TSA reactor system, a recently developed adsorbent material consisting of 25 %_w polyethyleneimine (PEI) and 25 %_w of 3-(aminopropyl)triethoxysilane (APTES) on a porous silica support [Fauth et al., 2012] is considered. An operating range for the TSA process between 75 °C and 120 °C has been selected based on recommendations for PEI-based sorbents, which were reported to perform worse at temperatures lower than 70 °C [Xu et al., 2002; Son et al., 2008] and show enhanced amine evaporation at temperatures above 130-140 °C [Drage et al. 2008; Drage et al., 2009; Zhao et al., 2013] (for more detailed information on amine functionalized solid sorbents see Section 3.2).

In order to consistently describe the adsorption thermodynamics of the material in the relevant temperature range, a Langmuir model is used according to:

$$\frac{\beta}{\beta_{\max}} = \frac{c(T) \cdot \varphi}{1 + c(T) \cdot \varphi} \quad (\text{Eq. 4.1})$$

$$\varphi = \frac{p_a}{p_0} \quad (\text{Eq. 4.2})$$

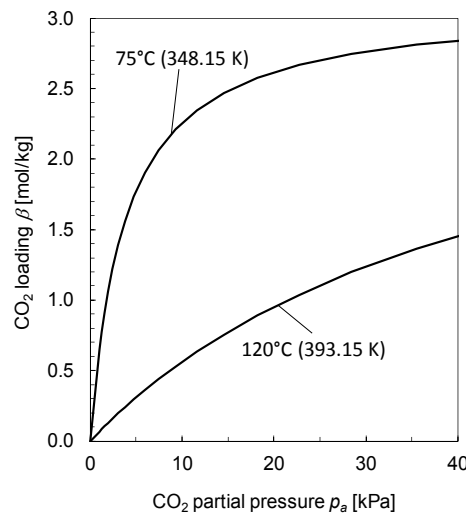
$$c(T) = c_0 \cdot e^{\frac{-\Delta H_{\text{ads}}}{R \cdot T}} \quad (\text{Eq. 4.3})$$

The three parameters β_{\max} , c_0 and ΔH_{ads} reported in Table 4.1 have been obtained from fitting raw data reported by Fauth et al. (2012) with (Eq.4.1)-(Eq.4.3). The adsorption isotherms of the adsorbent material for the selected operating temperatures, 75 °C and 120 °C, respectively, are shown in a range of relevant CO₂ pressures within Figure 4.2. It is worth to note that the enthalpy of adsorption given in Table 4.1 is, as expected, clearly in the range of chemisorbents which is relevant for the energy balance calculations and the evaluation of the process energy requirement that is going to be presented later in this chapter.

Table 4.1: Langmuir parameters describing the material assumed for the calculations.

Langmuir isotherm parameters of used adsorbent material		
Adsorbent saturation loading β_{\max}	3.11	[mol _{CO2} ·kg _{sorb} ⁻¹]
Langmuir constant c_0	9.84 · 10 ⁻⁹	[-]
Adsorption enthalpy ΔH_{ads}	-62.85	[kJ·mol _{CO2} ⁻¹]

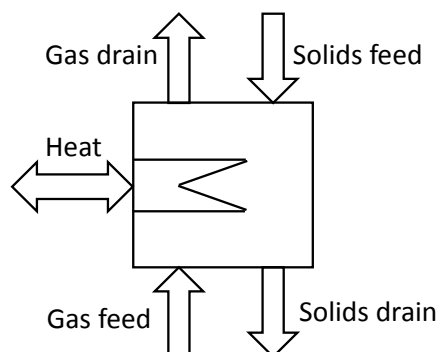
Figure 4.2: Adsorption isotherms of the material at the chosen operating temperatures of the TSA process.



4.1.3 Model of a fluidized bed gas-solid contacting stage

In order to allow calculation of fluidized bed adsorption and regeneration, a simple unit model (see Figure 4.3) of a gas-solid contacting stage is used and the assumptions underlying that model will be presented in the following.

Figure 4.3: Illustration of the simple equilibrium model of the gas-solids contacting stage assuming ideal solids mixing inside the stage.



As already mentioned above, the presented model is based on mass- and energy balance calculations. Consequently, this requires that the species mass balances for gas and solids as well as the energy balance are fulfilled. The energy balance within a stage unit accounts only for the heat of adsorption that is released/required during adsorption/desorption of CO_2 . The heat of adsorption is assumed as constant and independent of the adsorbent loading (Langmuir adsorption model). For reasons of simplicity and because thermo-data regarding co-adsorption effects of H_2O and CO_2 for the specific adsorbent is lacking, potential interactions between H_2O and the adsorbent material are neglected completely. In fact, the adsorbent material is assumed to interact exclusively with CO_2 .

Furthermore, the adsorbent material within a stage unit is assumed to be ideally mixed. This ideal solids mixing behaviour in turn results in equal CO_2 loadings of each adsorbent particle present within the stage. For a bubbling fluidized bed it was shown that this is a more or less realistic assumption [Guío-Pérez et al., 2013]. Because of the dominance of the solid phase in terms of heat capacity and due to the excellent heat transfer between gas and solids within fluidized beds, isothermal conditions have been assumed inside the stage. Heat exchange with a heating/cooling media is considered that allows for withdrawal of released heat of adsorption as well as supply of the necessary heat for regeneration and thus for control of the stage temperature. The heat exchange that is required to heat and cool the stream of adsorbent material circulating between adsorption and desorption zone is modelled outside of the stage unit model to distinguish between different energy requirements within the TSA process (see Section 4.1.4).

Adsorption and desorption reactions are assumed to be fast and sufficient gas-solid contact time is considered inside a stage unit so that equilibrium conditions according to the presented Langmuir adsorption model are approached. Together with the solids phase mixing assumption this requires that in each stage the two exiting streams of gas and sorbent material obey to equilibrium limitations.

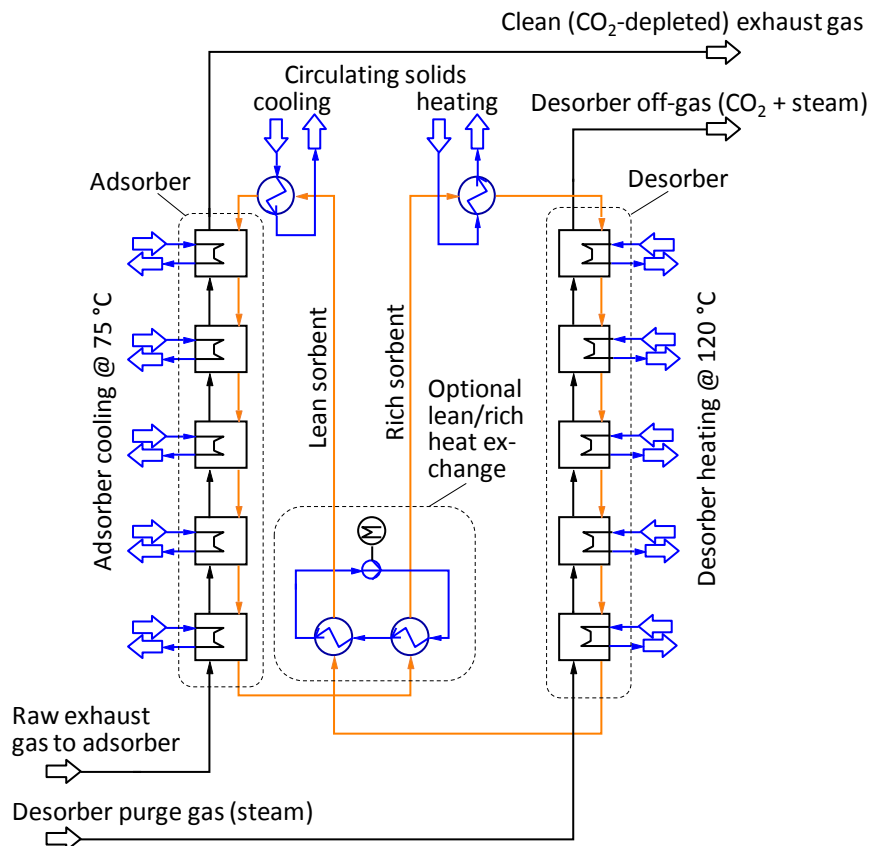
The model has been implemented in the process simulation software IPSEpro and used in combination with previously developed unit models for gas and solid stream handling [Pröll and Hofbauer, 2008a; Pröll and Hofbauer, 2008b; Bolhàr-Nordenkamp et al., 2009]. Gas phase enthalpies are calculated based on the NASA polynomial data [Burcat and McBride, 1997]. The lean solids heat

capacity used for solids enthalpy calculation is assumed to be constant between 75 °C (348.15 K) and 120 °C (393.15 K) at 1.3 kJ·kg⁻¹.

4.1.4 Models used for thermodynamic evaluation of the TSA process

In order to quantitatively assess the benefit of a multi-stage over a single-stage TSA process configuration, two different models will be used. For the single-stage configuration, two individual stage unit models will be connected, whereas in the multi-stage configuration several unit models of contacting stages are combined and connected to represent each gas-solids contactor column. In both configurations, heat exchangers are added to the sorbent circulation streams (riser systems) in order to obtain an overall thermodynamic model of the CO₂ separation process as shown in Figure 4.1. It is worth to note that no gas-streams are modelled in the recirculation systems. Hence, ideal gas sealing between both columns is assumed together with no adsorption/desorption activity of the adsorbent material within the recirculation systems. However, this model simplification should not affect the assessment of the process energy requirement. The final model of the multi-stage configuration is shown in Figure 4.4 and will be described exemplarily for both models in the following.

Figure 4.4: Simplified TSA process model featuring five theoretical stages in the adsorber and in the desorber: multi-stage configuration (streams: black = gas, blue = liquid, orange = solids).



In each gas-solids contactor, gas and solid streams flow counter-currently through a number of five consecutive stages that are described individually by the stage unit model described above. Individual heat exchange with each stage is assumed in order to keep the temperature constant at desired levels throughout each contactor. The circulating solids are formally cooled or heated, respectively, to the desired temperature prior to being fed to the contactor devices. This allows for

distinction between the heating or cooling requirement arising from the temperature swing and from the adsorption/desorption reaction, respectively. A certain lean/rich exchange effect may be achieved using the indicated arrangement featuring an intermediate heat carrier cycle. In contrast to the process design illustrated in Figure 3.13, the transporting gas cycles needed in the risers and the riser purge gas system are omitted from the simplified process model since little impact on the overall heat flows is expected.

4.2 RESULTS AND DISCUSSION

4.2.1 Specification of the separation task

In the following, the performance of continuously operated fluidized bed TSA systems will be investigated using the previously described sorbent properties and the introduced equilibrium model. In order to be capable to compare the obtained results with regeneration energy data of state-of-the-art amine scrubbing technology an adequate separation task for the equilibrium model should be defined beforehand. The application of post-combustion CO₂ capture amine scrubbing units has been mostly studied for treatment of flue gas streams derived from electricity generation. Among the different existing fossil fuel fired power plants, coal fired power plants represent the most critical emission sources as they cover a great share of the worldwide electricity generation and exhibit the largest energy specific CO₂ emissions [Chakma et al., 1995; Boot-Handford et al., 2013]. In the past, amine scrubbing units have been applied to coal fired power plants to study their process performance [Wilson et al., 2004; Knudsen et al., 2009]. Experimental data derived from tests within these units will be used for comparison with results obtained from modelling within this work. Considering the aforementioned, the separation task was defined according to Table 4.2, whereby the raw flue gas CO₂ concentration lies within the range of typical concentrations from coal-fired derived flue gas streams [Chakma et al, 1995; Rolker and Arlt, 2006].

Table 4.2: Definition of the gas separation task to capture 1 kg·s⁻¹ of CO₂ with a capture efficiency of 90 %.

Stream	Composition	Temperature	Pressure	Mass flow rate
Raw flue gas	10.0 % _{Vol} CO ₂ in N ₂	75 °C	105 kPa	7.47 kg·s ⁻¹
Clean flue gas	1.1 % _{Vol} CO ₂ in N ₂	75 °C	100 kPa	6.47 kg·s ⁻¹
Stripping gas	100 % steam	120 °C	105 kPa	variable
Desorber off-gas	variable CO ₂ content in steam	120 °C	100 kPa	variable

The numbers in Table 4.2 are based on an assumed CO₂ capture efficiency of 90 % and on a mass flow rate of captured CO₂ of 1 kg·s⁻¹. This allows for simple correlation of performance parameters such as required heat flows to the amount of CO₂ captured with 90 % capture rate (specific energy requirement). It is worth to note, that fixing the CO₂ capture efficiency at 90 % not necessarily leads to optimal process operation from an economic point of view. However, as this is also a matter of site specific conditions (e.g. availability of low-pressure steam) and because the target capture efficiency in the previously conducted studies has also been selected with 90 % making the choice of the CO₂ capture performance in the separation task reasonable.

Further, the pressure drop along each solids contactor is assumed to be equal at 5 kPa which is considered as the maximum allowable pressure drop for post-combustion CO₂ capture applications in the power sector. For the considered raw flue gas composition and CO₂ capture performance this

consequently leads to a CO_2 partial pressure of 10.5 kPa at the inlet and 1.0989 kPa at the outlet of the adsorber, respectively.

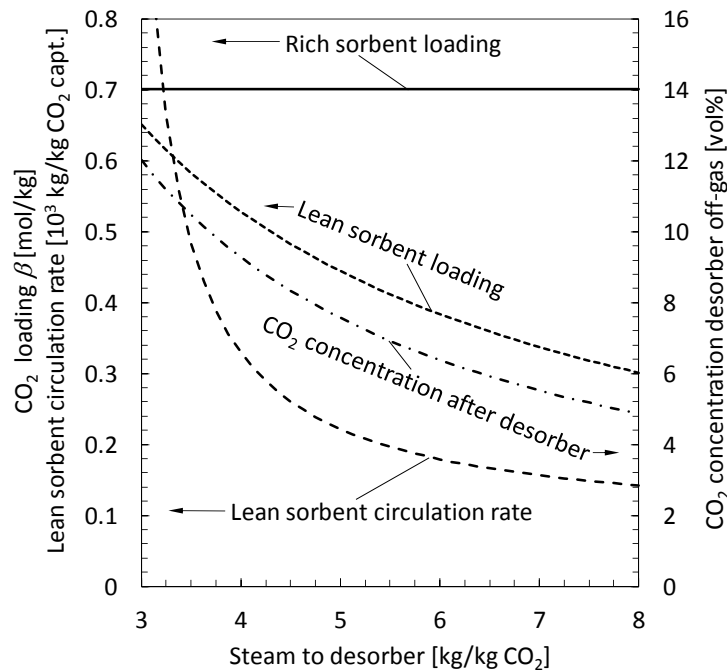
The stripping gas flow, sorbent circulation rate and the CO_2 concentration in the desorber off-gas will vary for the different configurations studied. For low energy penalties of the process, a low stripping gas demand and consequently high CO_2 concentrations in the desorber off-gas are of course desired. The feed water temperature for generation of stripping steam is assumed to be 100 °C (373.15 K) since it will be possible in most cases to obtain the feed water from condensing steam from the desorber off gas which is slightly above ambient pressure.

It should be pointed out again that the necessary steam quality in the TSA process is rather low and that the performed process assessment is only based on mass- and energy balance calculations, rather than on a more descriptive exergy analysis. This distinction is crucial as the utilization of low quality could even improve site specific parameters such as the fuel efficiency of a power plant. Hence, results obtained in this work give only numbers for the energy demand of the process itself, whereas the actual rating of the respective energy streams could be different for TSA applications at various power plant sites.

4.2.2 Performance evaluation of a single-stage TSA configuration

In order to point out the effect of the multi-stage approach, the behaviour of a process with a single stage in each contactor, i.e. adsorber and desorber, is investigated first. This process is set up similar to Figure 4.4, but with only one stage instead of the five stages as representations for the gas-solids contactors. Figure 4.5 shows the main process variables of the single stage system for the CO_2 capture target as specified in Table 4.2 as a function of the stripping steam flow rate between 3 and 8 kg per kg CO_2 captured.

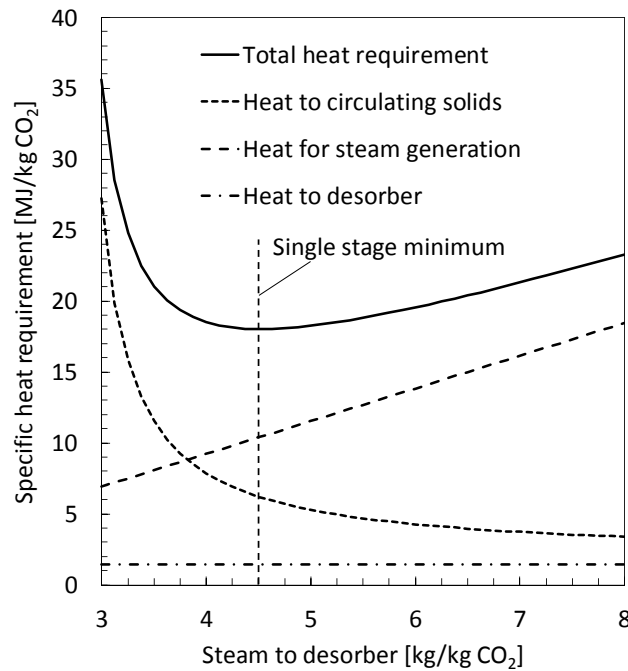
Figure 4.5: Sorbent loading, sorbent circulation and CO_2 concentration in the steam/ CO_2 stream after the desorber in the single-stage process during variation of the stripping steam flow rate for the separation task defined in Table 4.2.



The rich sorbent loading is constant as it is directly related to the target CO_2 concentration in the clean flue gas through (Eq. 4.1). On the contrary, the CO_2 concentration in the desorber off-gas and, consequently, the achievable lean sorbent loading, are functions of the stripping steam flow rate as this determines the CO_2 off-gas partial pressure in the desorber. Depending on the lean sorbent loading a certain sorbent circulation rate is turn required to transport the required amount of CO_2 from the adsorber into the desorber. As can be seen from Figure 4.5 due to increasing lean sorbent loadings the required sorbent circulation rate increases drastically with decreasing stripping gas flow rates. The corresponding heat demand of the single-stage configuration process without lean/rich heat exchange is given in Figure 4.6. The necessary heat for steam supply is proportional to the stripping steam flow rate while the heat to the desorber stage stays constant as the amount of desorbed CO_2 and consequently the heat of desorption are fixed. On the contrary, the heat supplied to the circulating solids before entering the desorber increases drastically with decreasing stripping steam feed into the desorber due to the drastic increase of the required sorbent circulation rate discussed above. For the case without lean/rich heat exchange, a minimum heat requirement of about 18 MJ per kg CO_2 captured occurs at a steam flow rate of 4.5 kg per kg CO_2 captured. A lean/rich heat exchanger might reduce the heat demand of the circulating solids. However, the remaining heat duty in the theoretical case of full lean/rich heat recovery, would still be significantly above the reported values for competing technologies. Moreover, high sorbent circulation rates in the range of several hundred kg per kg CO_2 captured would need to be accepted for the single-stage configuration.

These results clearly show that a continuous single-stage fluidized bed TSA system with well-mixed solid phases in adsorber and desorber cannot be proposed for post combustion CO_2 capture.

Figure 4.6: Heat requirement of the single-stage process during variation of the stripping steam flow rate without lean/rich heat exchange.



4.2.3 Performance of the multi-stage system with five stages in each contactor

In order to get an understanding of the basic behaviour of the multi-stage configuration, the process according to Figure 4.4 is studied first without using the lean/rich heat exchange option. The CO_2 loading on the circulating solid sorbent material, the composition of the desorber off-gas and the solid sorbent circulation rate are shown for a variation of the desorber purge steam flow rate in Figure 4.7.

The minimum stripping steam flow rate for this configuration is 0.55 kg per kg CO_2 captured. Below this value, the CO_2 loading on the lean sorbent gets too high to thermodynamically reach the desired CO_2 partial pressure at the adsorber outlet. At minimum steam supply, the CO_2 concentration in the desorber off-gas exceeds 40 % $_{\text{Vol}}$, clearly showing that concentration of CO_2 is possible using the staged design. Moreover, compared to the single-stage configuration the maximum adsorbent loading from the rich sorbent leaving the adsorber increased from 0.7 to above 2.3 mol $\cdot\text{kg}^{-1}$. The achievable working capacities in the multi-stage configuration are significantly higher leading to a much greater exploitation of the adsorption capacity of the adsorbent material. Consequently, the required sorbent circulation rate in the multi-stage configuration is only moderate between 10 and 15 kg per kg CO_2 captured and thus drops by an order of magnitude compared to sorbent circulation rate in the single-stage regeneration energy minimum.

Figure 4.7: Sorbent loading, sorbent circulation and CO_2 concentration in the steam/ CO_2 stream after the desorber in the multi-stage process during variation of the stripping steam flow rate for the separation task defined in Table 4.2.

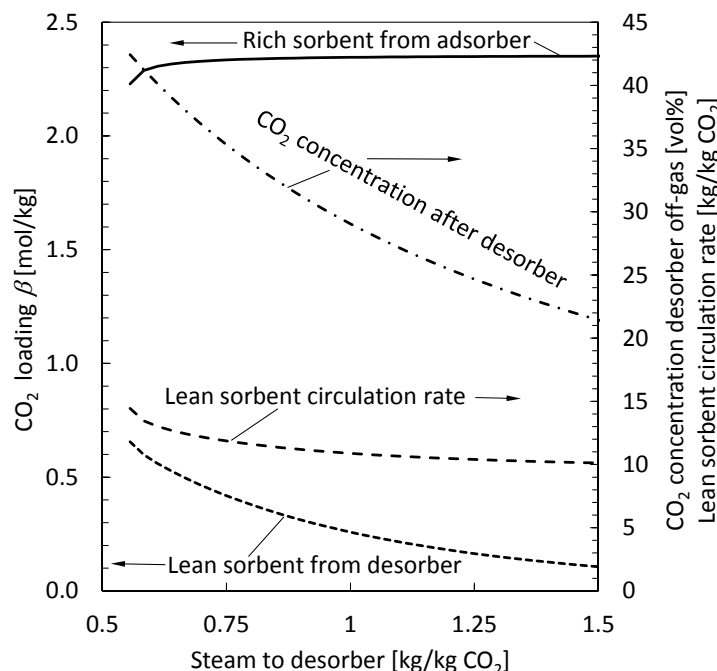
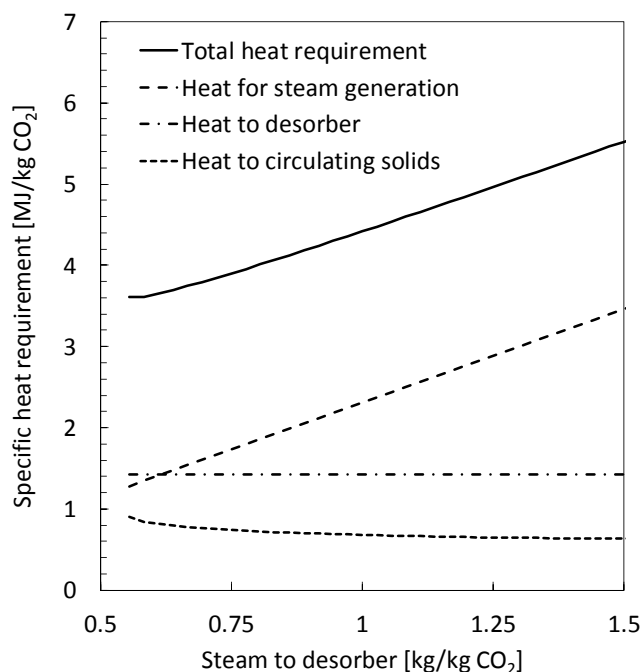


Figure 4.8 shows the related heat flows into the modelled multi-stage TSA system for the same stripping steam variation. Similar to the single-stage configuration, the heat for steam generation increases proportional to the amount of steam while the desorber heat demand stays constant. The energy for heating the circulating sorbent material correlates with the sorbent circulation rate. The sorbent circulation rate itself again depends on the stripping steam feeding rate that determines the equilibrium loading of the lean sorbent material leaving the desorber. However, as shown in Figure 4.7, compared to the single-stage configuration, the stripping steam rate has a rather small influence

on the lean sorbent loading and on the required sorbent circulation rate. Consequently, the considered stripping feeding rates were significantly smaller in the multi-stage configuration with values ranging from 0.5 to 1.5 kg per kg CO₂ captured. The minimum heat requirement obtained in the multi-stage configuration was around 3.6 MJ per kg CO₂ captured. This value is already in the range of reported values for state-of-the-art scrubbing technologies that are in the range of 3.7 to 4.5 MJ per kg CO₂ captured [Tarka et al., 2006; Knudsen et al., 2009; Berger and Bhowan, 2011; Sjostrom and Krutka, 2010; Pirngruber et al., 2013]

Figure 4.8: Heat requirement of the multi-stage TSA process during variation of the stripping steam flow rate without lean/rich heat exchange.



These results clearly proof that the multi-stage fluidized bed configuration is superior over a single-stage TSA design.

More detailed results from the multi-stage model derived for a practical desorber stripping steam flow rate of 0.75 kg per kg CO₂ captured are given in Table 4.3. The multi-stage configuration allows for reaching a working capacity as high as $2.26 - 0.39 = 1.87 \text{ mol} \cdot \text{kg}^{-1}$ whilst reaching a CO₂ content in the desorber off-gas of 35.3 %_{Vol}. The specific process heat requirement for this stripping steam rate amounts for about 3.9 MJ per kg CO₂ captured which is still in the range of reported values for amine scrubbing technologies.

It is important to note that equilibrium may not be reached within each stage of a real process. This effect can, however, be balanced by addition of more than five stages in real applications. Furthermore, insufficient stage efficiencies can always be balanced to a certain extent by increased sorbent circulation rates to the price of a lower working capacity and a greater energy requirement to heat the circulating sorbent material.

Table 4.3: Detailed results for a specific operating case with a stripping steam flow rate of 0.75 kg per kg CO₂ captured without lean/rich heat exchange derived from the equilibrium model of the multi-stage TSA configuration.

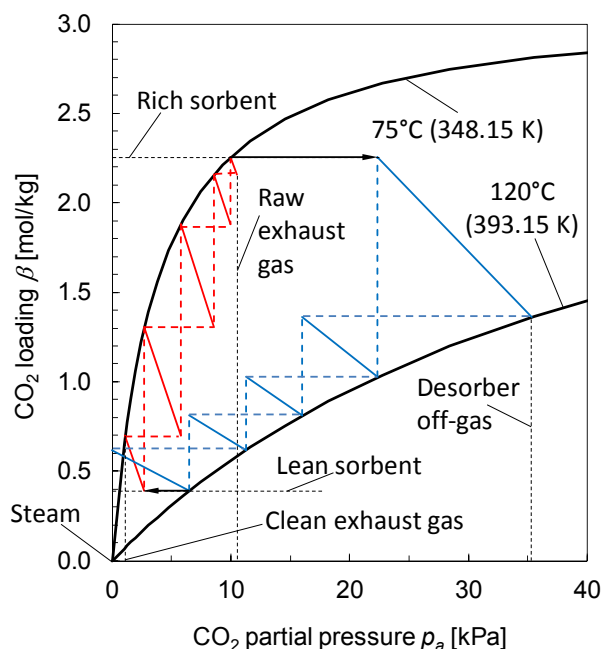
Overall TSA process data		
Mass rate of CO ₂ captured [kg·s ⁻¹]	1.00	
Desorber purge steam flow rate [kg·s ⁻¹]	0.75	
Unloaded sorbent circulation rate [kg·s ⁻¹]	12.19	
Heat duty steam generation [kW]	1730.5	
CO ₂ capture rate [%]	90.0	
Sorbent cycle data	Lean sorbent	Rich sorbent
CO ₂ loading on sorbent [mol·kg ⁻¹]	0.39	2.26
Loaded sorbent mass flow rate [kg·s ⁻¹]	12.40	13.40
Sorbent mean heat capacity (75...120°C) [kJ·(kg·K) ⁻¹] ^a	1.31	1.38
Lean sorbent heater / rich sorbent cooler duty [kW]	719.3	760.4
Specific contactor device data	Adsorber	Desorber
Contactor temperature (kept constant) [°C]	75.0	120.0
Absolute pressure contactor inlet [kPa]	105.0	105.0
Absolute pressure contactor outlet [kPa]	100.0	100.0
Total pressure drop contactor [kPa]	5.0	5.0
Gas operating volume flow contactor inlet [m ³ ·s ⁻¹]	5.66	0.93
Gas operating volume flow contactor outlet [m ³ ·s ⁻¹]	5.15	1.44
CO ₂ content inlet 1 st (bottom) stage [% _{vol}]	10.00	0.00
CO ₂ content inlet 2 nd stage [% _{vol}]	9.58	6.27
CO ₂ content inlet 3 rd stage [% _{vol}]	8.34	10.95
CO ₂ content inlet 4 th stage [% _{vol}]	5.66	15.69
CO ₂ content inlet 5 th (top) stage [% _{vol}]	2.70	22.12
CO ₂ content outlet 5 th (top) stage [% _{vol}]	1.10	35.31
Sorbent CO ₂ loading inlet 5 th (top) stage [mol·kg ⁻¹]	0.39	2.26
Sorbent CO ₂ loading inlet 4 th stage [mol·kg ⁻¹]	0.70	1.36
Sorbent CO ₂ loading inlet 3 rd stage [mol·kg ⁻¹]	1.30	1.03
Sorbent CO ₂ loading inlet 2 nd stage [mol·kg ⁻¹]	1.30	0.81
Sorbent CO ₂ loading inlet 1 st (bottom) stage [mol·kg ⁻¹]	1.88	0.62
Sorbent CO ₂ loading outlet 1 st (bottom) stage [mol·kg ⁻¹]	2.26	0.39
Cooling / heating duty 1 st (bottom) stage [kW] ^b	-72.9	175.0
Cooling / heating duty 2 nd stage [kW] ^b	-214.3	146.8
Cooling / heating duty 3 rd stage [kW] ^b	-442.1	165.0
Cooling / heating duty 4 th stage [kW] ^b	-461.4	256.5
Cooling / heating duty 5 th (top) stage [kW] ^b	-237.3	684.8
Total contactor cooling / heating duty [kW] ^b	-1428.1	1428.1

^a) Heat capacity of CO₂-loaded sorbent referring to mass of unloaded sorbent.

^b) Negative values indicate cooling requirement.

Figure 4.9 illustrates the adsorption/desorption activity of the individual stages within the 5-stage adsorber and desorber column. All intersections between the adsorption isotherms and the red and blue solid lines, respectively, represent the equilibrium states in the individual stages, similar to the equilibrium states illustrated in Figure 3.10. From Figure 4.9 it is immediately evident that the adsorption/desorption activities vary to a greater or lesser extent between the stages within of both columns. Generally, the stage activity seems to increase from the lowermost to the uppermost stage. Especially the lowermost adsorber stage has a rather low adsorption activity for the considered operating conditions. It is thus assumed, that a similar process performance would have been achieved within a system comprising only 4 adsorber stages.

Figure 4.9: Illustration of the effect of the five theoretical stage design for a specific operating case with a stripping steam flow rate of 0.75 kg per kg CO₂ captured.



The use of less adsorber stages would have consequently led to a lower loading of the rich sorbent material leaving the adsorber and thus to a larger sorbent circulation rate and process heat requirement. However, the actual process economics (i.e. CO₂ capture costs) depend not only on OPEX but also on CAPEX and in a real application of the technology the aim would most likely be to minimize the CO₂ capture costs rather than the process energy demand.

In addition, the overall process energy requirement could be significantly optimized through sufficient heat management within the process as well as through heat integration measures. This opportunity should be discussed in more detail below.

4.2.4 Heat integration measures

The reported process energy demands have been derived using a model that depicts only the core process of a TSA CO₂ capture system. However, it was shown that CO₂ capture costs can be significantly reduced through appropriate heat management and integration into existing process of the actual CO₂ emission source [Lively et al., 2010].

An example of a promising heat integration measure has been proposed by Kelley et al. (2010) where the heat generated during the CO₂ compression step is utilized within the CO₂ capture process. An

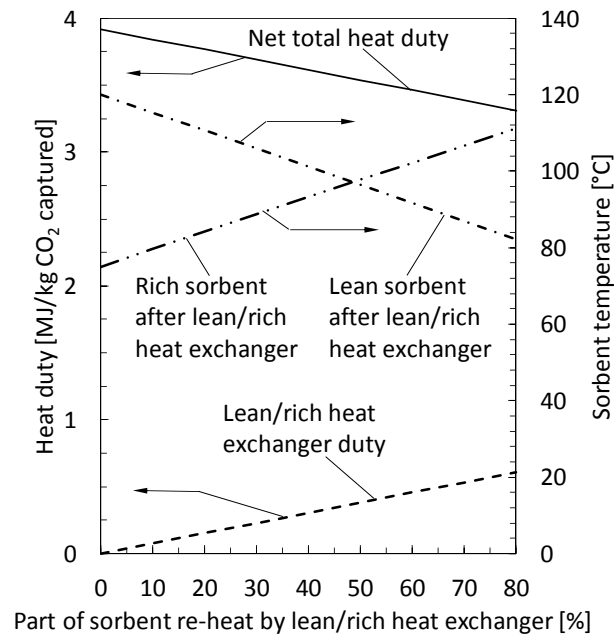
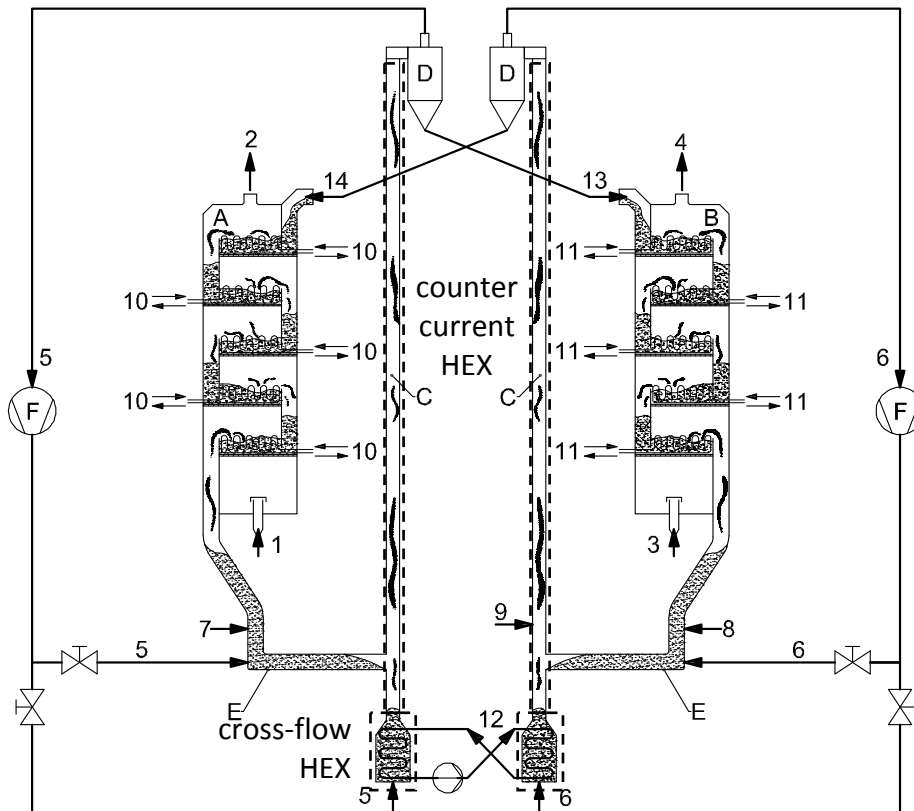
additional process optimization could be achieved from the application of a heat displacement system (i.e. process heat pump) that is capable to utilize the heat released by the exothermic adsorption reaction in the adsorber to drive the endothermic adsorbent regeneration step in the desorber. Such a system would meet both, the cooling requirement in the adsorber and the heat requirement in the desorber and thereby eliminate the demand of cooling water and heating steam completely. The fact that the exothermic heat is released at a lower temperature than it is needed for the regeneration step sets the need for application of a heat pump. Both concepts (i.e. heat recovery from CO₂ compression and process heat pump) make use of electric energy for active heat recovery and could reach coefficients of performance (COP) around 4. Thus, both concepts would allow for a significant energy demand reduction of the process. However, application will depend on the availability of compressors that are feasible to operate at the necessary temperature levels and on the economic situation regarding the availability of electricity at the capture site. Currently, there are no process heat pumps commercially available that can be operated in a temperature range that is required for the considered adsorbent material.

Another approach to optimize the heat management within the proposed TSA process would be to apply heat exchangers into the recirculation lines that allow for heat exchange between lean and rich adsorbent material. Such a lean/rich heat exchanger is a key component within any scrubbing process. It allows for partial recovery of the energy needed to heat/cool the circulating solvent. A similar heat exchange could be realized within the proposed adsorbent system and could partly reduce the energy requirement that has been referred to as “Heat to circulating solids” above. The application of such a lean/rich heat exchanger would allow for larger sorbent circulation rates if the need is set through insufficient adsorption efficiencies or lower working capacities (e.g. reduced stage number) and/or simply reduce the energy requirement of the process. The effect of a lean/rich heat exchanger on the TSA process energy requirement should thus be investigated in the following. The total low-temperature heat requirement of the multi-stage process without heat integration, including steam generation, amounts to 3.9 MJ per kg CO₂ captured for 0.75 kg steam per kg CO₂ case, what is well in the range of values reported for liquid amine CO₂ capture systems. This value can be further improved by application of a lean/rich heat exchanger device.

The energy needed to heat the rich sorbent to the desorber inlet temperature represents about 20 % of the total heat requirement (see Table 4.3) and can be partly contributed by heat exchange between the hot lean sorbent leaving the desorber and the cold rich sorbent coming from the adsorber. Since we deal with streams of fluidized solids, an intermediate heat carrier cycle will greatly increase design possibilities for such a lean/rich heat exchanger. Figure 4.10 shows the effect of adding a lean/rich heat exchanger depending on its share in heating the rich sorbent to the target temperature of 120 °C (393.15 K).

The net total heat requirement of the TSA process decreases by the amount of heat recovered in the lean/rich heat exchanger. A counter-current type heat exchange solution will be needed for more than 40 % lean/rich heat exchanger share in the sorbent re-heat. Below 40 % the heat recovery could be achieved e.g. by cross-flow fluidized bed heat exchanger in the dense phase region of the transport risers. The potential locations of the respective heat exchangers are given in Figure 4.11.

Figure 4.10: Effect of adding a lean/rich heat exchanger to the TSA process.


 Figure 4.11: TSA CO₂ capture system - application of lean/rich heat exchangers.


If an economically competitive device could contribute 50 % of the sorbent heat-up, the total heat requirement would decrease by about 10 % to 3.5 MJ per kg CO₂ captured.

In summary, the energy requirement for CO₂ capture using the continuous dual loop solid sorbent process is, without sophisticated heat integration, slightly lower as for liquid amine systems. However, some design aspects and especially the very low number of required theoretical stages in

the TSA system indicate there can be additional significant advantages over liquid amine systems coming from savings in capital expenditures.

4.3 CONCLUSIONS

TSA CO₂ capture within a single-stage fluidized bed reactor system is not economically feasible due to thermodynamic limitations that arise from the well-mixed particle phase. The proposed double loop multi-stage fluidized bed TSA system allows for effective counter-current movement of gas and solid phases at optimal heat transfer conditions. A principal thermodynamic evaluation of the proposed system has been conducted using a two times five stages TSA configuration and a polyethyleneimine (PEI) functionalized adsorbent material with Langmuir parameters known from literature.

The evaluation revealed that the process energy demand of this TSA configuration without application of any heat integration measures is 3.9 MJ per kg CO₂ captured. This energy demand is well within the range of reported values for amine scrubbing CO₂ capture systems using MEA.

Addition of a so called lean/rich heat exchanger that allows for heat recovery between the circulating sorbent materials led to significant improvement of the process energy demand. The minimum process energy demand dropped from 3.9 to 3.5 MJ per kg CO₂ captured which is slightly below reported values for MEA scrubbing systems.

It can be expected that additional heat integration would lead to further process optimization in terms of regeneration energy demand. Different heat integration measures have been suggested such as the application of a heat displacement system (i.e. process heat pump) that is capable to transfer the energy associated with the heat released from CO₂ adsorption in the adsorber to the desorber where it can drive the adsorbent regeneration. A further option for heat integration would be to recover the heat released during CO₂ compression and use it for the production of stripping steam and/or for heating of the desorber stages.

From a thermodynamic point of view, sufficient TSA process performance is possible using contactors that exhibit a number of only five theoretical stages. The related expectable low height of bubbling fluidized bed systems compared to scrubbing towers indicate great advantages with respect to capital costs. However, the question is whether adsorption/desorption kinetics are fast enough to approach thermodynamic equilibrium in a real application. In a next step it is thus needed to validate data from thermodynamic equilibrium modelling with experimental results obtained from a fully integrated TSA unit.

The next chapter will thus introduce a continuously operating TSA bench scale unit that has been designed, constructed and operated in the course of this thesis. Before designing of the actual bench scale unit a fluid-dynamic study has been conducted on the proposed multi-stage fluidized bed system in order to characterize the solid distribution within the system for different operating conditions and to prove the fluid-dynamic feasibility of the proposed design.

5. FLUID DYNAMIC STUDY ON THE MULTI-STAGE FLUIDIZED BED REACTOR SYSTEM

5.1 COLD FLOW MODEL DESIGN

5.1.1 General aspects

Cold flow models (CFM) are a commonly used tool for designing and upscaling of fluidized bed systems [Guío-Pérez, 2013; Marx, 2013]. They are generally built out of transparent material (e.g. perspex or glass) to permit direct view on the gas-solids movement inside the unit. Furthermore, they are typically operated at ambient conditions, with air as fluidizing gas agent. If designed properly, a CFM allows for observation of the actual fluid-dynamics that are present within a real fluidized bed reactor of virtually every size and mode of operation [Glicksman et al., 1993; Glicksman, 2003].

In this work, it was decided to conduct pre-tests within a CFM to study the fluid-dynamic feasibility of the proposed double loop multi-stage fluidized bed reactor design. Thereby, design of the used CFM has been derived from desired operating parameters of the planned bench scale unit (BSU) for continuous CO₂ capture (see Chapter 6). The design of the BSU itself is based on the TSA reactor concept that has been introduced in Section 3.6. As one can see from Figure 3.13, the basic design of both columns is similar and thus it is sufficient to conduct the fluid-dynamic study on half of the system only, i.e. one multi-stage column with internal recirculation.

In contrast to the common methodology of applying scaling criteria to design the CFM, a simplified approach has been used in this work. The reason for this is that the cold flow model will later be used as actual adsorber in the planned BSU, with rather similar operating temperature and properties of the fluidizing agent. Hence, it was decided to use borosilicate glass instead of typically used perspex material for the transparent parts of the CFM in order to allow for subsequent application of the CFM column as adsorber within the actual BSU.

5.1.2 Cold flow model design

Results derived from mass- and energy balance calculations in Chapter 4 show that a capture rate of 1 kg_{CO₂}·s⁻¹ at a capture efficiency of 90% can be achieved within a TSA system operated with a practical stripping steam demand of 0.75 kg·kg_{CO₂,capt}⁻¹ and a sorbent circulation rate of 12 kg·s⁻¹. These operating parameters have been used to derive the basic design parameters of the BSU adsorber column as given in Table 5.1, for a design CO₂ capture rate of 100 kg of CO₂ per day.

As the actual properties of the sorbent material used for BSU tests were unknown at the time the CFM design has been elaborated, it was assumed that the BSU will be operated with a solid sorbent material exhibiting hydrodynamic properties as given in Table 5.2. The assumed adsorbent diameter of 600 μm is rather large, but the choice can be seen as a trade-off between good heat and mass transfer characteristics within the individual fluidized beds and the overall TSA plant size. The feasibility of adsorbent material of that size for continuous TSA CO₂ capture, however, needs first to be proven experimentally.

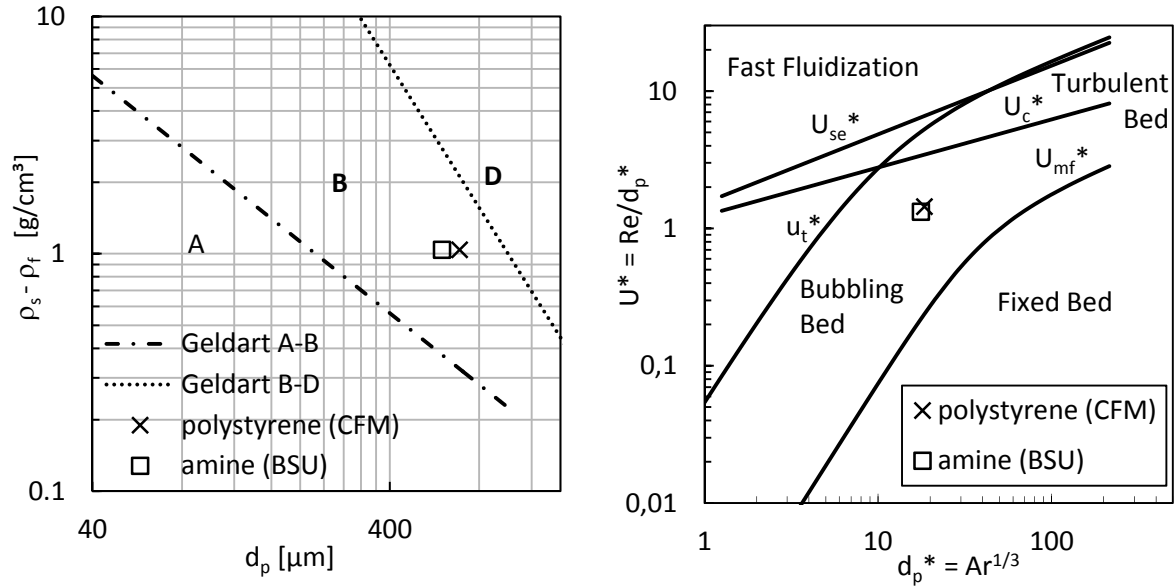
Table 5.1: BSU adsorber design parameters.

Adsorber parameters and dimensions		
absolute CO ₂ capture rate	100	[kg·day ⁻¹]
Flue gas flow ($y_{\text{CO}_2, \text{ads}, \text{in}} = 5 \text{ \%Vol}$, $\eta_{\text{capt}} = 90 \text{ \%}$)	46.8	[Nm ³ ·h ⁻¹]
inner diameter	0.150	[m]
weir height	0.06	[m]
solids circulation rate	50	[kg·h ⁻¹]
maximum column pressure drop	50	[mbar]

Table 5.2: BSU adsorbent material properties.

Hydrodynamic properties of BSU adsorbent		
mean particle diameter	600	[μm]
hydrodynamic particle density	1250	[kg·m ⁻³]
bulk particle density	700	[kg·m ⁻³]

Figure 5.1:- Simplified scaling approach:
Particle classification according to Geldart, 1973. (left),
CFM and BSU fluidized bed regime according to Bi and Grace (1995). (right)



For the CFM study it was decided to use inert particles made out of polystyrene as its material density is close to the expected apparent density of the adsorbent material. The average diameter of the CFM polystyrene material was derived using a simplified scaling approach in order to ensure fluid-dynamic similarity between the CFM and BSU. First of all, the CFM material and the BSU adsorbents material need to belong to the same particle class as defined by Geldart (1973). Secondly, the diameter was chosen in such a way, that the design operating points of the BSU using the adsorbent material and the CFM using the polystyrene particles match within a fluidized bed regime map. This approach is illustrated within Figure 5.1 and the corresponding hydrodynamic properties of the polystyrene material are given within Table 5.3.

The particle size distribution (PSD) of the finally used sieve fraction of polystyrene particles was determined within a Mastersizer 2000 (Malvern Instruments) via laser diffraction analysis method using a dry material probe (see volumetric PSD in Figure 5.2). The minimum fluidization velocity of

the polystyrene particles was determined experimentally (see Figure 5.3). From a hydrodynamic point of view the bed materials match quite well and both can be assigned to the Geldart-B particle category.

Table 5.3- CFM bed material properties.

Hydrodynamic properties of model polystyrene particles	
mean particle diameter	688 $[\mu\text{m}]$
hydrodynamic particle density	1040 $[\text{kg}\cdot\text{m}^{-3}]$
bulk density	640 $[\text{kg}\cdot\text{m}^{-3}]$
minimum fluidization velocity U_{mf} (measured for air, $t = 20\text{ }^{\circ}\text{C}$)	0.11 $[\text{m}\cdot\text{s}^{-1}]$

Figure 5.2: PSD of CFM bed material.

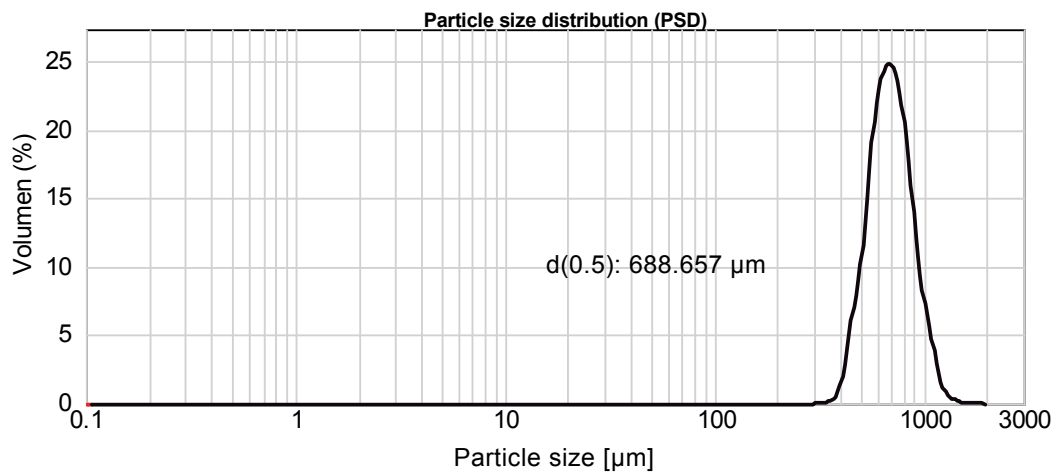
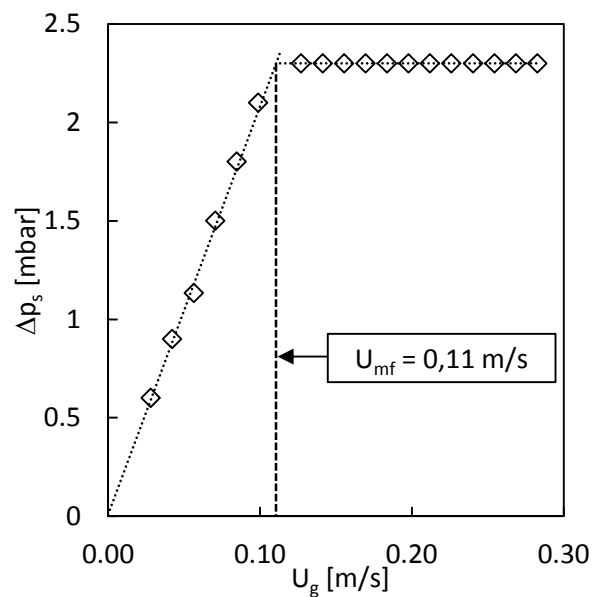


Figure 5.3: Minimum fluidization velocity of CFM bed material.



Finally, the geometry of the gas distributors (perforated plate design) and the downcomers were derived in accordance with Section 3.5.2. The final perforation diameter was selected with 3 mm together with a triangular perforation pattern with a pitch of 10mm and a perforation area ratio of

7.7 %. The downcomer height was selected with $H_{dc} = 200 \text{ mm} + H_w$ and the downcomer segment height with $s_{dc} = 25 \text{ mm}$, leading to a downcomer area ratio of $A_{dc} A_{ads}^{-1} = 11 \text{ \%}$.

5.2 EXPERIMENTAL

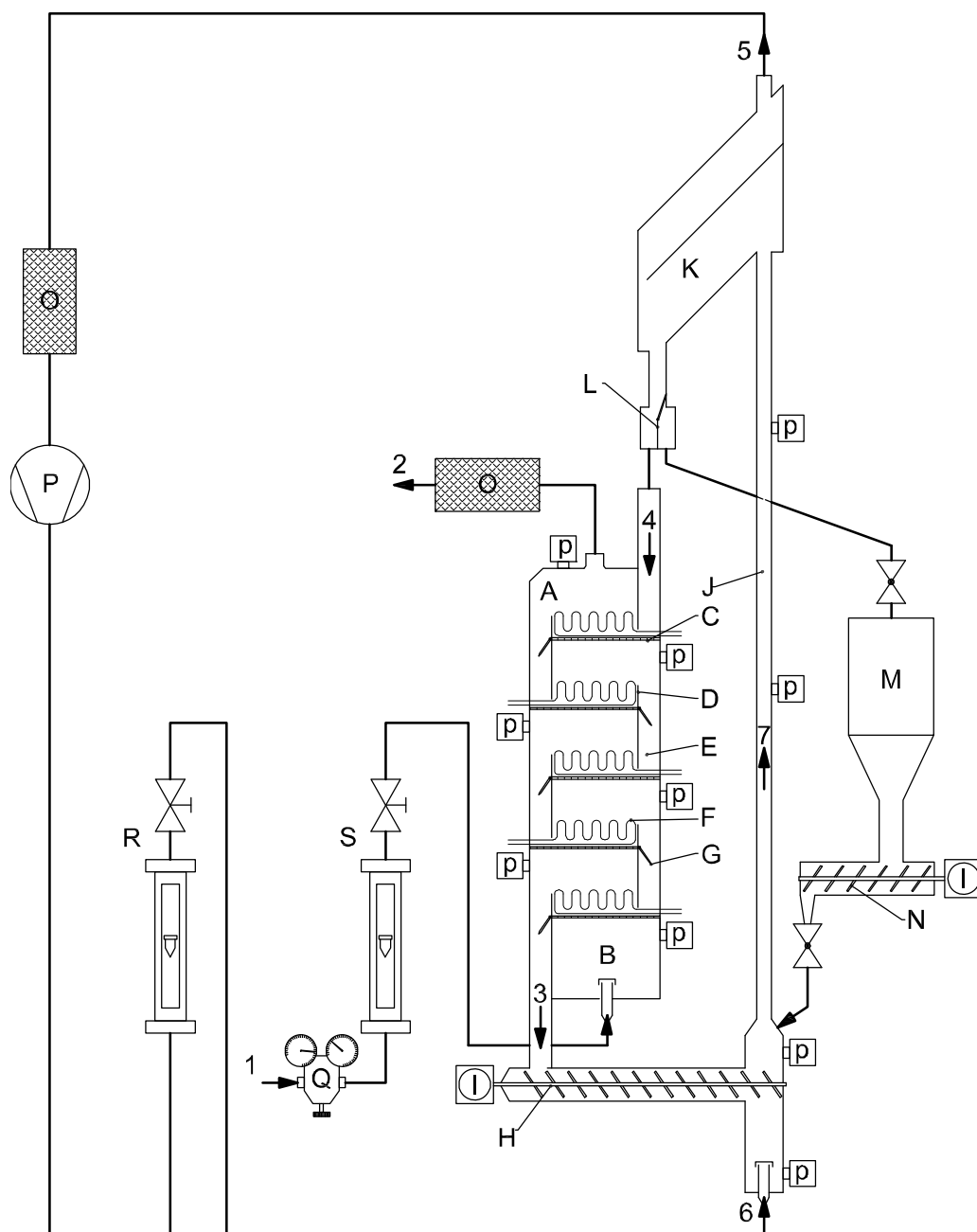
5.2.1 CFM setup

The present CFM serves as test facility for the investigation of the fluid-dynamic behaviour of a MStFB system with internal solids circulation. For this reason almost every element of the CFM is made out of transparent material in order to allow for observation of particles flowing within the system. The CFM comprises five individual stages that can be assembled in a modular form thus allowing for experiments with varying number of fluidized bed stages. The main components of the CFM are shown in Figure 5.4.

Each individual stage of the column (Figure 5.4, A) comprises a bubbling fluidized bed, a weir with adjustable height (Figure 5.4, D) as well as internal heat exchangers (Figure 5.4, F) that could later be used for adsorber cooling during the planned continuous capture tests. Solids enter the column at the top (Figure 5.4, 4) and flow counter-currently to the fluidizing gas stream through each downcomer and individual stationary fluidized bed (Stages 2-5) down to the lowermost stage (Stage 1). The fluidizing agent, which was dry air (Figure 5.4, 1), is introduced into the windbox (Figure 5.4, B) to approach even gas distribution prior the gas distributor of Stage 1. The column gas feed can be controlled by means of a needle valve and a variable area flowmeter (Figure 5.4, S). From Stage 1 solids are extracted through an exit duct where they flow in moving bed regime (Figure 5.4, 3) towards a screw conveyor at the bottom (Figure 5.4, H) of the CFM. The bottom screw conveyor (BSC) continuously transports the solids into a transport riser (Figure 5.4, J) that pneumatically lifts the solids into a particle separator (Figure 5.4, K) that is situated above the MStFB column. There, the particles are separated from the gas stream and are redirected towards the top of the column whilst the gas is recycled to the riser gas inlet nozzle by means of a gas compressor (Figure 5.4, P).

The amount of recycle-gas can also be adjusted via a needle valve and a variable area flowmeter (Figure 5.4, R). Since all of the solids entering the transport riser are entrained into the particle separator and redirected into the column, the solids circulation rate is controlled by the BSC only. Right after the particle separator, solids move through a mechanical flap valve (Figure 5.4, L) that leads the particles either back to the column or into a solids hopper (Figure 5.4, M) that is able to store the total solids inventory of the system. For system start-up or introduction of solids make-up during operation, material can be fed from the hopper into the system through a solids feeding screw conveyor (Figure 5.4, N). During operation the hopper system can be isolated from the rest of the CFM through ball valves. The CFM is equipped with ten pressure sensors that are attached beneath each gas distributor and at the top of the MStFB column as well as in the pneumatic transport riser (Figure 5.4, p). The maximum deviation from characteristic for the used pressure sensors is less than or equal to 1 % of full scale, whereby the used ranges were either 0-68.9 hPa (= 1 psi) or 0-100 hPa (in windbox and above Stage 1).

Figure 5.4: MStFB cold flow model.



A ... 5 stage adsorber column
 B ... windbox
 C ... gas distributor plate
 D ... stage weir plate
 E ... stage downcomer
 F ... stage heat exchanger
 G... downcomer flap
 H... bottom screw conveyor
 I ... driving motor
 J ... solids transport riser
 K ... gas-solids separator
 L ... solids directing flap
 M... solids hopper
 N... solids feeding screw

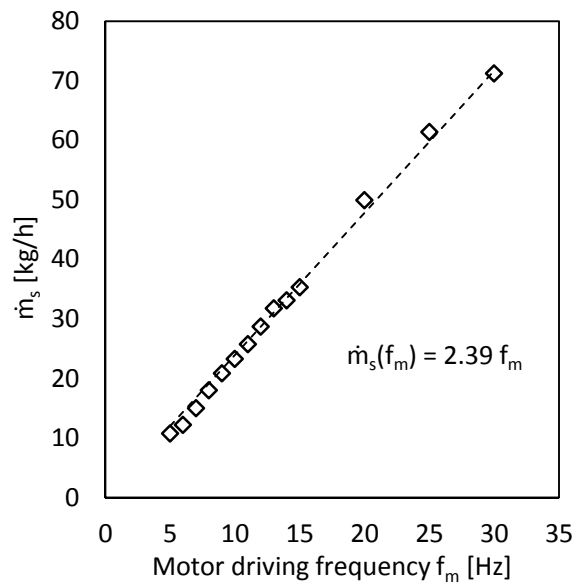
O... particle filter
 P... recycle-gas blower
 Q... pressure regulator
 R ... column air feed flow control
 S... recirculation gas flow control
 p ... pressure sensor
 1 ... pressurized air
 2 ... column offgas
 3 ... column particle drain
 4 ... column particle feed
 5 ... particle free recycle-gas flow
 6 ... recycle-gas riser feed
 7 ... gas-solid suspension flow

5.2.2 CFM start-up and commissioning

In the commissioning phase of the CFM, the start-up of the MStFB (i.e. filling of the individual stages) turned out to be quite difficult when using a configuration without active control of the downcomer pressure drop. Since in contrast to the gas distributor plates the downcomers exhibit practically no flow resistance, gas was preferably flowing through the downcomers as soon as a small diluted bed was formed above the gas distributors. This in turn led to immediate defluidization of the stages and thus to prevention of any further solids transport through the stages. Hence, no stable start-up of the system was possible at first place.

It was decided to apply restriction flaps inside the downcomers (Figure 5.4, G) in order to allow for active control of the downcomer flow resistance. During start-up, all restriction flaps are closed and solids are fed from the particle hopper into the riser and further into the empty column. The solids then remain within the top stage and start to form a fluidized bed. While the stage got filled, bubbles began to catapult more and more solids over the stage weir into the downcomer and a fixed bed of solids built up above the restriction flap in the top downcomer. As soon as the amount of solids within the closed downcomer was large enough, the restriction flap was opened and particles went down to the next stage below where a fluidized bed started to build up again. Thereby, the formerly opened restriction flap remained open and the pressure balance within the downcomer was maintained by the fluidized solids within it. This procedure was then repeated until the complete column was filled with the desired amount of solids.

Figure 5.5: Solids transport capacity of the bottom screw conveyor.



After start-up the solids feeding screw was turned off and the system was switched to internal particle circulation by starting up the BSC. The sorbent circulation rate was controlled by adjusting the rotational speed of the screw driving motor by means of a frequency converter. The BSC had an outer diameter of 38 mm and a pitch of 27 mm, resulting in a motor driving frequency dependent transport capacity as shown in Figure 5.5. During the experimental runs the actual solids circulation rate was calculated, using the linear relationship indicated in Figure 5.5. A similar linear correlation was determined for the solids feeding screw and used for calculation and control of the total system inventory.

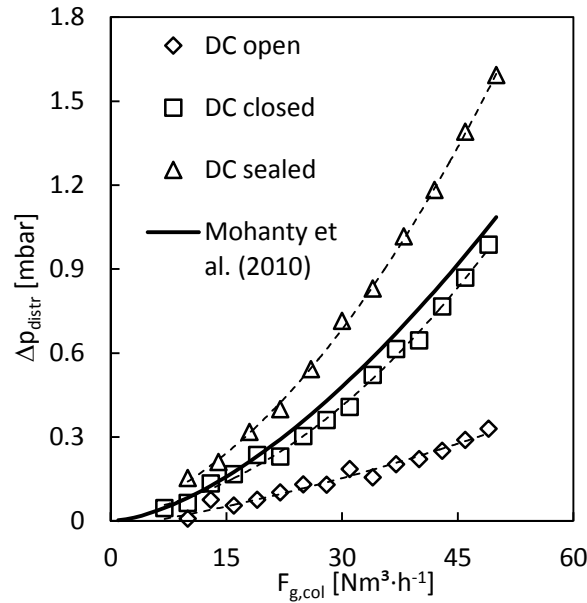
To determine the solids distribution within the system it is necessary to know the pressure drop offset caused by the installations within the empty column (i.e. the distributor pressure drops). The pressure drops caused by solids present within the column can then be determined by subtraction of the distributor pressure drop from the total pressures measured during CFM experiments. However, in empty column operation gas would primarily flow through the downcomer sections. This is in contrast to an operation of the filled column where the cross-sectional gas flow distribution can be considered as even. This means that if no counter-measures are applied, the empty column measurement would deliver distributor pressure drops that deviate from the pressure drops caused by these installations during normal operation of the column. In order to find a proper method for measuring the empty column pressure drop, measurements with three different downcomer configurations were performed and results have been compared with theoretically derived values.

The different downcomer configurations were:

1. Completely sealed downcomers,
2. Downcomers with closed restriction flaps and
3. Downcomers with opened restriction flaps.

The resulting pressure drop profiles for a gas distributor of a single empty stage are shown in Figure 5.6.

Figure 5.6: Stage pressure drop within the empty column.



As expected three different experimental pressure drop profiles have been identified, whereby the sealed downcomer configuration showed the largest and the open downcomer configuration showed the smallest values of distributor pressure drop. As mentioned above, during normal operation of the column an even cross-sectional gas velocity distribution is expected and thus neither the sealed nor the opened downcomer configuration is expected to deliver adequate values of the empty column pressure drop. The configuration with closed downcomer flaps, however, permitted restricted gas flow through the downcomers, leading to a more practical empty stage offset pressure drop profile. Finally, values predicted from (Eq. 3.4) have been used to calculate solid pressure drop values from measured absolute pressure values.

5.3 RESULTS FROM COLD FLOW MODEL TESTING

In order to study the multi-stage fluidized bed system with internal solids circulation, the influences of several operating parameters have been investigated individually. These investigations include variations of the following operating parameters:

1. Solids (sorbent) circulation rate (\dot{m}_s)
2. Variation of column feed gas flow rate (F_g)
3. Variation of solids inventory (Inv.)
4. Variation of bed height by changing stage weir heights (H_w)

The main focus of the CFM investigations was put on the fluid-dynamic behaviour of the column, as it represents the more critical component compared to the transport riser within the recirculation line. However, the distribution of the solids inventory between both fluidized bed systems turned out to depend on solids circulation rate and will, therefore, also be part of the discussions below. Reported values of solids pressure drops are averaged values from a time range of at least 2 min after steady state operation had been achieved. It is worth to note that except for Stage 1 the fluid-dynamic behaviour of all other stages was nearly identical. This means that more or less equal pressure drops have been measured within Stages 2-5 and thus average values of all these stages are presented below. The behaviour of Stage 1 is discussed separately. It is further worth mentioning, that trough all experiments, the stationary fluidized beds formed within Stages 2-5 showed a dense phase that was fairly below the edge of the bed weir with a distinct splash zone above it formed by exploding bubbles. Particle transport from the bed into the downcomer sections occurred out of the splash zone.

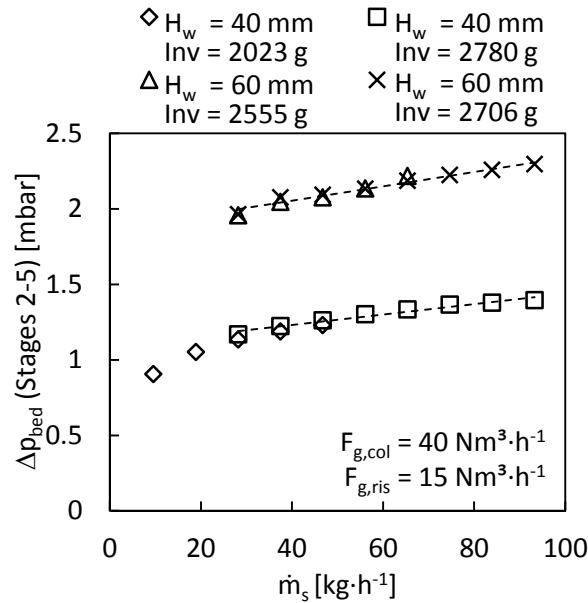
Results from the individual parameter variations will be presented and discussed in the following.

5.3.1 Variation of solids circulation rate

Figure 5.7 shows the averaged fluidized bed pressure drop of Stages 2-5 as a function of the solids circulation rate for a constant column fluidization rate.

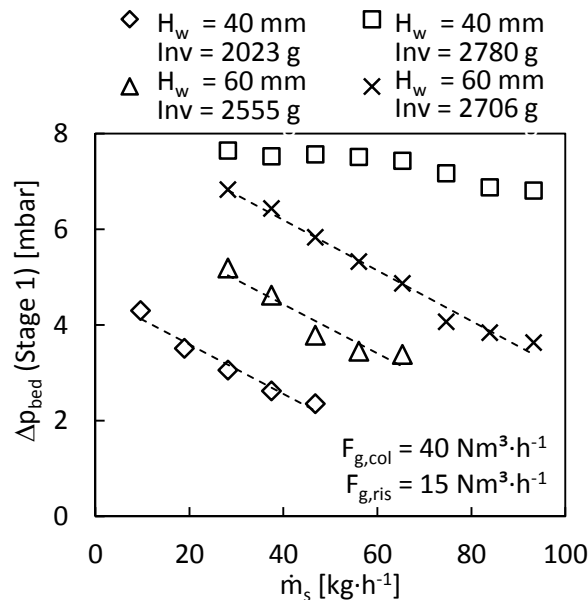
In addition, the solids inventory of the system as well as the stage weir heights have been varied within this experiment. Similar to the results reported in literature the bed pressure drops linearly increased with increasing solids throughput. Other researchers attributed this effect to a reduction of the actual bed voidage [Mohanty and Meikap, 2009] whereas here it is believed that the rise of pressure drop is caused by an increase of the dense bed height induced by a tailback effect at the weir plate. This is in analogy with the slope of the surface of any liquid flowing over a weir, where an increased slope can be observed if the flow rate is raised. Unfortunately, the slope is not easy to assess in the present fluidized bed column, since no distinct bed surfaces are formed. Instead, severe bubble eruptions that catapult solids into the freeboard area can be observed at the surface of the dense bed. However, it was decided to conduct another cold model study, dedicated to prove the assumption of increasing bed heights with increasing solids circulation. Results from this campaign will be presented in Section 5.3.4.

Figure 5.7: Stages 2-5 solids pressure drop vs. solids circulation rate.



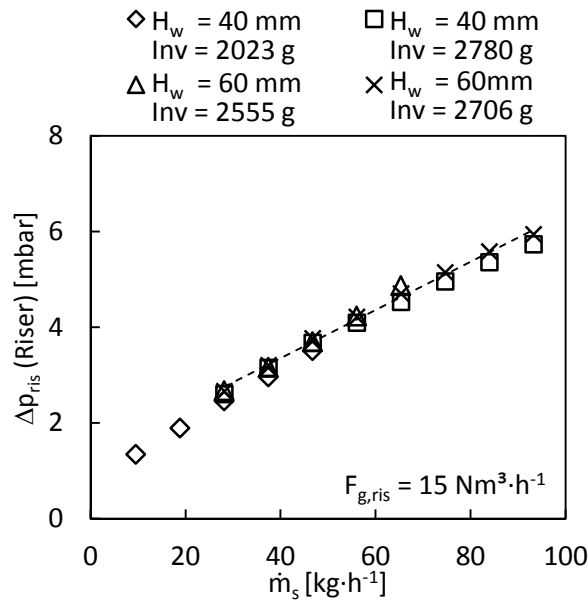
From Figure 5.7 it can be seen that an increasing weir height led to larger solids capacity of the individual stages, whereas the total system solids inventory had no impact on their fluid-dynamic behaviour. Figure 5.8 shows the influence of the solids circulation rate on the fluidized bed pressure drop along Stage 1 for four different system inventories and two different weir heights of the overlying stages. It is worth to note, that the used system inventory of 2706 g during the experiment conducted with a stage weir height of 40 mm was too large. In this experiment the lowermost stage was completely filled with solids and thus the experiment shows results that deviate from the other experimental results.

Figure 5.8: Stage 1 solids pressure drop vs. solids circulation rate.



Since the extraction of solids from the column is controlled by the BSC and the pressure drops of Stages 2-5 did not depend on the system inventory at constant weir height, any excess material fed into the column needs to accumulate within Stage 1 which in turn led to an increased solids pressure drop in this stage (see Figure 5.7).

Figure 5.9: Riser solids pressure drop vs. solids circulation rate.

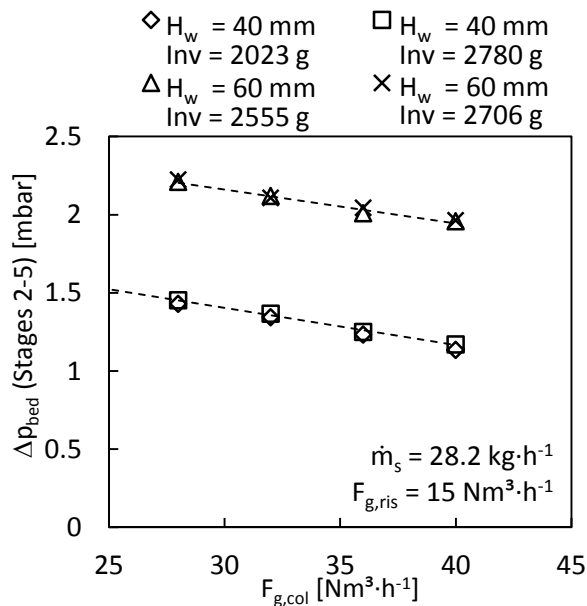


For a constant system inventory the share of excess material increased with decreasing stage weir height as the solids capacity of Stages 2-5 decreased. The measured pressure drops over Stage 1 confirmed that for increasing solids circulation rates less excess material is available since the capacities of Stages 2-5 and the riser system increase. The dependency of the riser solids capacity on the solids circulation rate can be seen for constant riser fluidization rate in Figure 5.9.

5.3.2 Variation of column fluidization rate

Figure 5.10 and Figure 5.11 show the dependency of the solids pressure drops within Stage 1 and Stages 2-5 on the column fluidization rate for a fixed solids circulation rate. Again the system inventories and the stage weir heights have been varied as additional parameters.

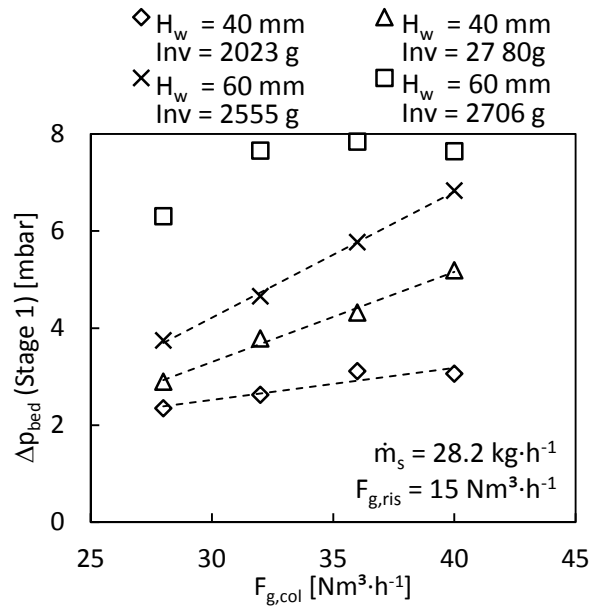
Figure 5.10: Stages 2-5 solids pressure drop vs. column gas feed flow.



As expected, increasing column fluidization rates led to decreasing solid pressure drops in Stages 2-5 due to an increase of the fluidized bed voidage (see Figure 5.10). As the total system inventory and

the solids circulation rate were kept constant during the experiment, the reduced solids capacity within Stages 2-5 led to an increase of excess material that accumulated within Stage 1 (see Figure 5.11). Again the experiment conducted with 2780 g total system inventory and 40 mm stage weir height led to deviating results as Stage 1 was completely filled with material.

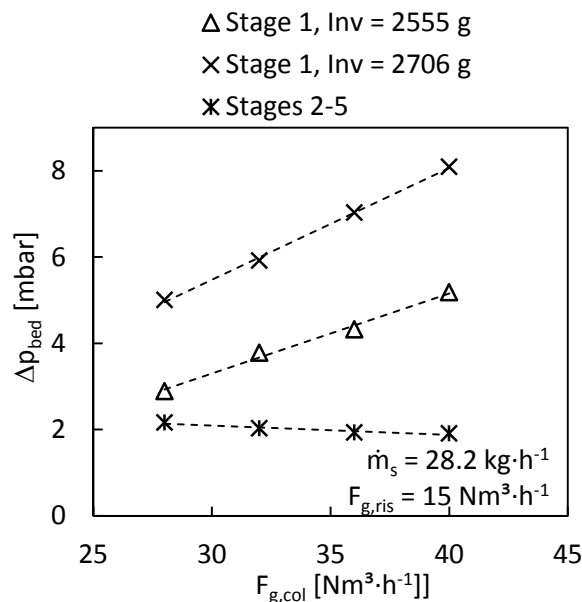
Figure 5.11: Stage 1 solids pressure drop vs. column gas feed flow.



5.3.3 Variation of total system solids inventory

Figure 5.12 illustrates the already discussed effect of system inventory on the solids capacity of the individual stages.

Figure 5.12: Effect of solids inventory on fluidized bed stage pressure drop.



The fluidized bed pressure drops within Stage 1 together with the averaged values for Stages 2-5 are shown for constant solids circulation rate, two different system inventories and varying column fluidization rate. As one can see for the larger inventory, the pressure drop along Stage 1 was four times larger than the pressure drop within one individual subsequent stage. The effect of system

inventory can be exploited within the continuously operating double loop system as it allows for sufficient control of the sorbent distribution between the adsorber and the desorber.

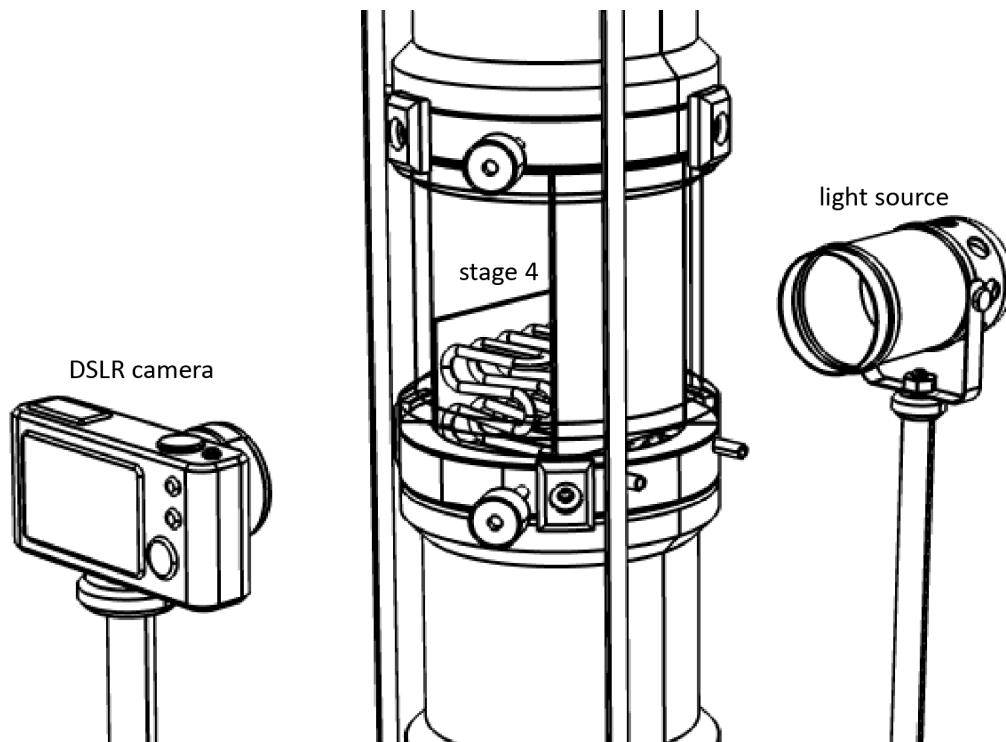
5.3.4 Study of dense bed expansion using long-time exposure photography

The first CFM test campaign showed that the main operating parameters of the multi-stage fluidized bed column have the following impact on the solids pressure drops along Stages 2-5:

- Increasing solids pressure drop with increasing solids circulation rate,
- Decreasing solids pressure drop with increasing column fluidization rate and
- Increasing solids pressure drop with increasing stage weir height.

While the latter two impacts can be attributed to an increased bed voidage and dense phase height, respectively, the impact of the solids circulation rate could not be explained sufficiently well after the first test campaign. Moreover, previously conducted CFM studies on multi-stage fluidized bed systems indicated that this effect can be correlated to a decreasing bed voidage [Mohanty and Meikap, 2009] which, however, conflicts with fluidization technology theory which states that the bed voidage of fluidized bed consisting of a specific bed material essentially depends on the fluidization velocity only. By taking further the fundamental fluidization equation (Eq. 2.7) into consideration, it was thus concluded that the increasing solids pressure drop can only be attributed to an increase of the fluidized bed height. However, as direct observation of the dense phase height within the individual stages was not possible it was decided to conduct another campaign, whereby an experimental configuration as shown in Figure 5.13 has been used to observe the height of the dense phase within Stage 4 of the fluidized bed column.

Figure 5.13: Experimental configuration for long-term exposure photography.



In this configuration a light source, the fluidized bed within Stage 4 and a digital single-lens reflex (DSLR) camera are aligned in a straight line. Both, the camera and the light source are mounted on a stand to allow for taking long-term exposure pictures of the fluidized bed formed within Stage 4. During the experiments the laboratory was darkened and the fluidized bed was only illuminated with the sketched light source. The pictures obtained from this configuration should allow for visual distinction of the dense phase region, the splash zone and the freeboard of the fluidized bed. This is because the solids density in these zones differs significantly, which in turn leads to different light transparency and thus to different colour-contrasts of all zones in the pictures.

The optimum time exposure for the used camera-light source configuration was found to be 5s. Figure 5.14 shows an exemplary picture that has been obtained from CFM testing. As expected, a more or less sharp contrast change can be identified between the three different zones of the stationary fluidized bed formed within the stage. Furthermore, the part of the heat exchanger that was obviously not immersed within the dense phase can be identified clearly. It is worth to note, that the grey stripe within the freeboard of the picture is the shadow of a threaded rod that is part of the adsorber column suspension which, unfortunately, could not be removed during the experiment.

After the optimum camera settings had been found a CFM test run, with variations of the solid circulation rate, the column fluidization rate and the stage weir height has been conducted. For each operating condition, two pictures of Stage 4 had been taken after the stage pressure drop stayed constant and thus revealed steady-state conditions. It is worth to note that the bed material used in the CFM campaign was the actual amine functionalized solid sorbent material that has been used for continuous CO₂ capture tests in Chapter 6. The exact fluid-dynamic properties of the material were, however, not important during these tests as the goal was to prove the explanation for the impact of the different column operating parameters on the solids pressure drop within the top stages of the column qualitatively only.

Figure 5.14: Description of stage picture obtained with long-term exposure photography.

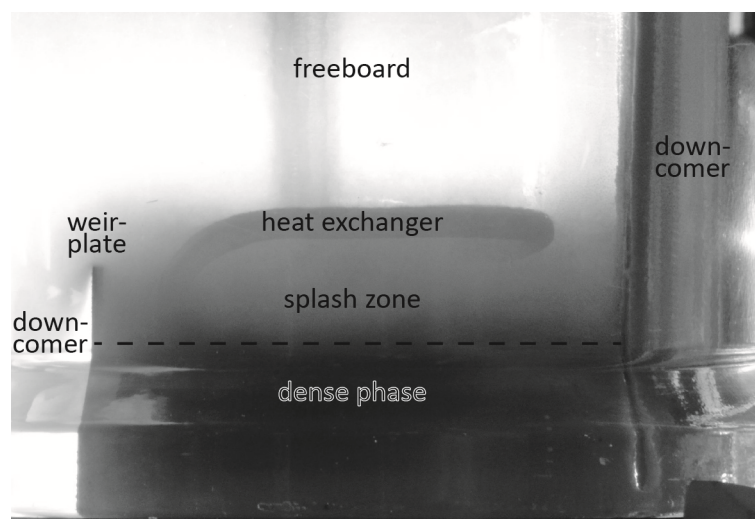
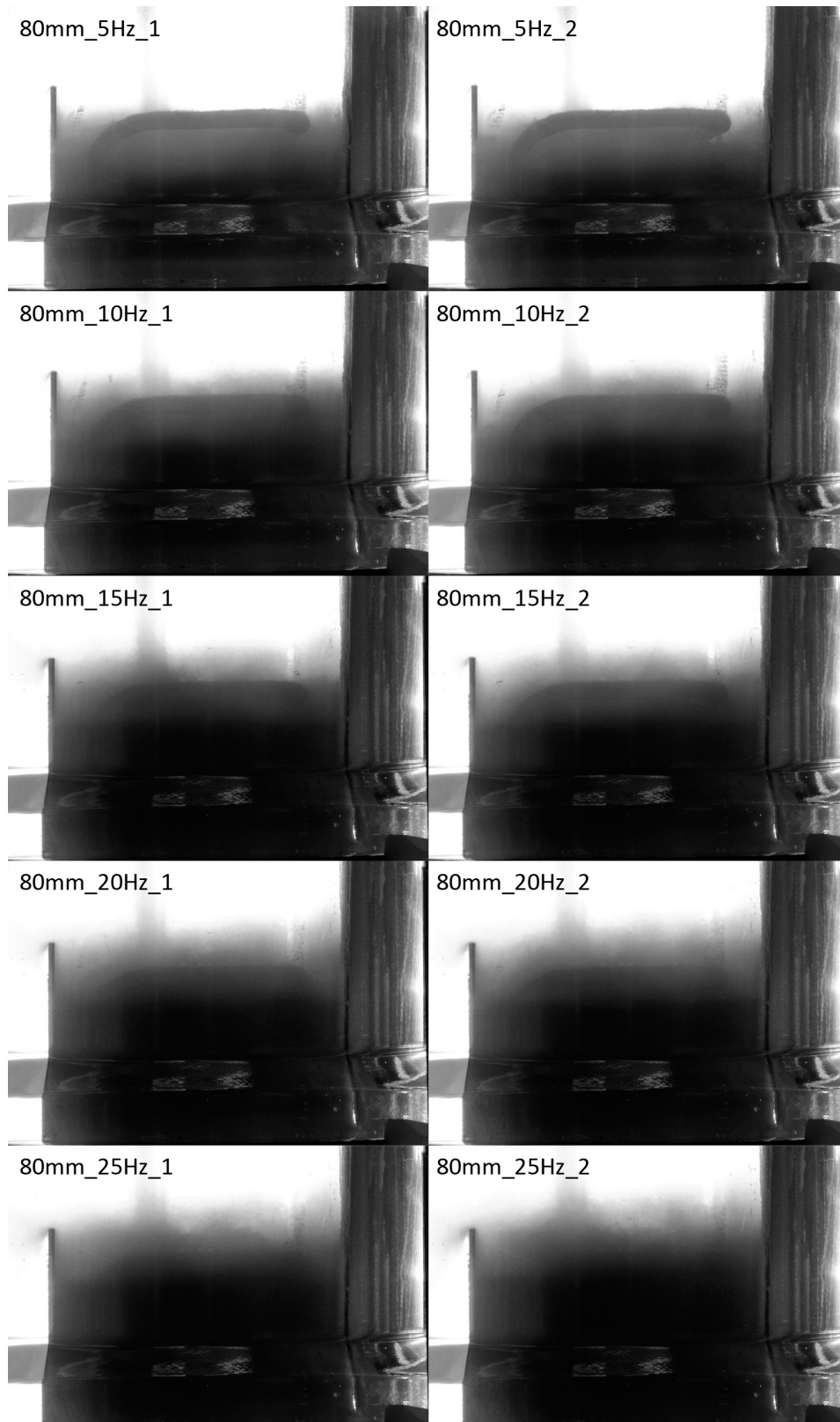


Figure 5.15 shows the picture series obtained from the variation of the solids circulation rate at constant fluidization rate for a stage weir height of 80mm. As already mentioned, two different pictures have been taken for each adjusted solids circulation rate and pictures with equal operating conditions are shown next to each other. The solids circulation rate increases from the pictures in the top to the lowermost row.

Figure 5.15: Pictures obtained from variation of the solid circulation rate.



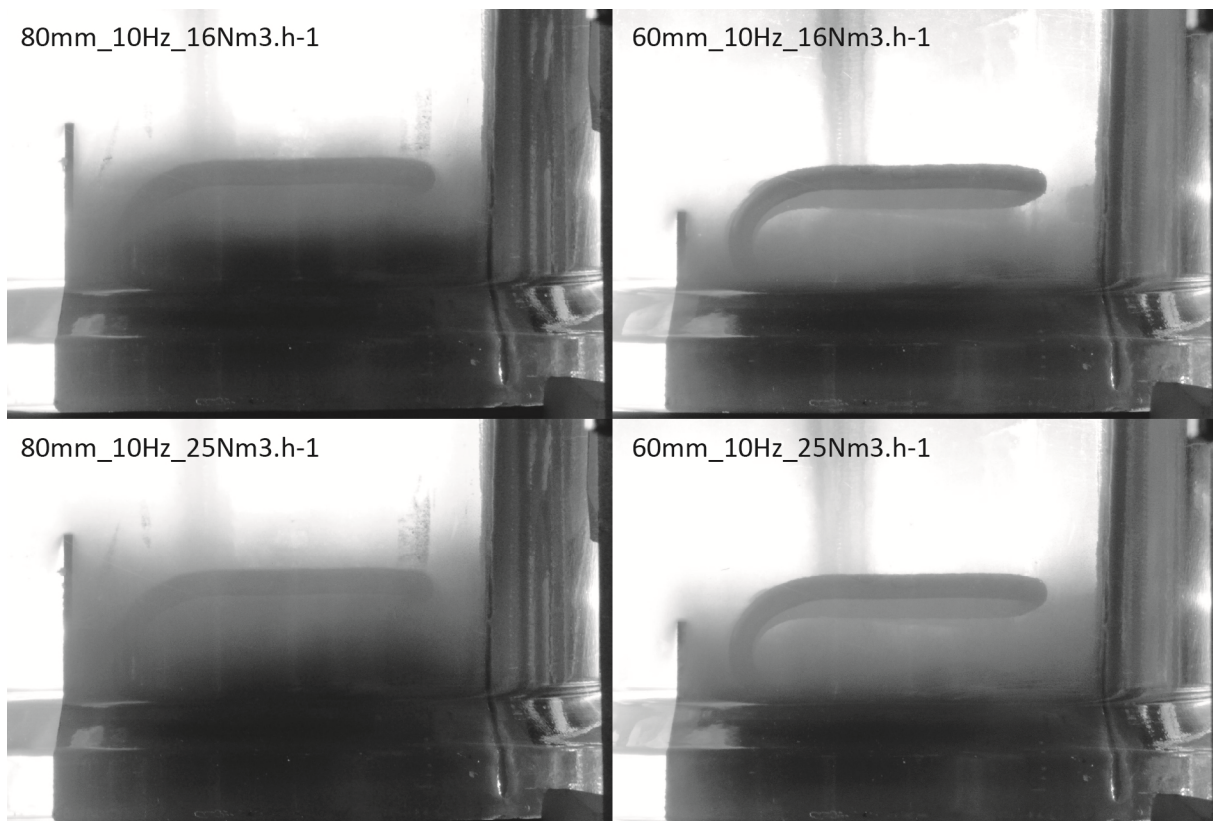
As one can clearly see from Figure 5.15, the dense phase (dark contrast zone) increased with increasing solids circulation rate which proves the assumption that has been made for explaining the increasing solid pressure drop with increasing solids circulation rate. Furthermore, it can be seen that the time-averaged dense phase surface height lies significantly below the weir plate edge, even for

high circulation rates. This has a strong impact on the design of the immersed heat exchangers, as instead of assuming good heat transfer conditions for the total weir height, only about a half to two thirds of the weir height can be assumed to be occupied by the dense phase. Thus, if the bed heat exchanger height matches the weir height, a significant part of the heat exchanger surface would end up in the splash zone where the achievable heat transfer rates can be lower by an order of magnitude.

Figure 5.16 shows a selection of pictures that have been derived from CFM tests with constant solid circulation rate, for two different column fluidization rates and stage weir heights. It can be seen that an increasing weir height led to an increasing dense phase height. This led to an increased coverage of the surface of the immersed bed heat exchanger which should lead to better heat transfer conditions during continuous CO₂ capture experiments.

Except for a more expanded splash zone, no significant difference can be identified between operating conditions with different column fluidization rates. It was expected that higher fluidization rates would lead to a “brighter” (because leaner) dense phase and thus to a weaker contrast between the dense phase and the splash zone without changing the height of the dense phase surface. However, under all operating conditions a layer of down-flowing solids was formed at the column wall within the dense phase zone. This wall-layer of solids was very dense as the gas velocity at the wall region approaches zero, which in turn prevents fluidization of solids within the wall-layer. Hence, the transparency of the wall-layer did not change with varying fluidization rate and it was not possible to observe the corresponding increase of the dense phase voidage.

Figure 5.16: Pictures obtained from variation of the weir height and the column fluidization rate.



5.4 CONCLUSIONS FROM THE COLD FLOW MODEL STUDY

The cold flow model study performed within a stacked five-stage fluidized bed system with internal solid circulation proved the fluid dynamic feasibility of the proposed TSA reactor system. The chosen design features weir plates, downcomer areas and a screw-conveyor-riser combination for particle return and shows robust operability. During start-up, however, it was found that active control of the empty downcomer pressure drops is necessary for chosen downcomer design. Without such a control measure the fluidization gas was preferably flowing through the empty downcomers which in turn led to defluidization of the stages. In the present cold flow model, the active control measure has been realized through mechanical flaps that had been placed in the downcomers of each stage. Alternatively to such flap valves, adjustable slide valves may be applied that cover the gas-distributor area below each downcomer section to control the gas flow through the empty downcomers during start-up.

An operating parameter variation revealed that the solids pressure drop in Stages 2-5 was almost identical throughout the study and a function of the solid circulation rate, the fluidization rate as well as the stage weir height. Qualitatively, the solids pressure drop correlates as follows with the mentioned operating parameters:

- Increasing solids pressure drop with increasing solids circulation rate,
- Decreasing solids pressure drop with increasing column fluidization rate and
- Increasing solids pressure drop with increasing stage weir height.

It was further shown that the solids pressure drop within Stage 1 was differently affected by the mentioned operating parameters and additionally influenced by the total solids inventory within the system. The solids pressure drop in Stage 1 qualitatively changes in the following way relative to the mentioned operating parameters:

- Decreasing solids pressure drop with increasing solids circulation rate (with accompanied partial shift of system solids inventory into the other stages and the transport riser),
- Increasing solids pressure drop with increasing column fluidization rate due to reduced solids capacities of all other stages above,
- Increasing solids pressure drop with increasing solids inventory

The characteristic solids hold-up within Stage 1 can be exploited for sufficient controllability of the solids inventory distribution between the desorber and adsorber.

The promising outcome of the investigations conducted within the CFM motivates the construction of a similar scale bench scale unit (BSU) for temperature swing adsorption (TSA) of CO₂. The design as well as first results from operation of the continuous TSA BSU will be presented in the following chapter.

6. TSA BENCH SCALE UNIT FOR CONTINUOUS CO₂ CAPTURE

6.1 BENCH SCALE UNIT DESIGN

6.1.1 General description

Figure 6.1 shows the proposed design of the TSA bench scale unit (BSU) which is based on the introduced double loop multi-stage fluidized bed system and optimized in accordance with the outcome of the previously conducted cold flow model study. The BSU has been constructed in order to deliver a proof of concept for the proposed continuous TSA CO₂ capture process and to further experimentally study said process and the effect of the relevant operating parameters on the process performance. As one can see from Figure 6.1, both, the adsorber and the desorber consist of five individual fluidized bed stages that are stacked on top of each other. The column stages are, however, built modularly, thus allowing for experiments with varying stage numbers in each column. The net-solids flow in both columns is downwards and gas passes the fluidized bed stages from bottom to top. Each of the individual stages features a gas distributor, a downcomer that enables controlled particle flow down to the underlying stage, downcomer flap valves for controlled system start-up, an exchangeable weir plate as well as an immersed heat exchanger for heat supply and removal, respectively. Solids are continuously discharged from the lowermost stages of both columns under controlled conditions (i.e. with an adjustable solids circulation rate) by means of mechanical screw conveyors. Transport of sorbent material between both columns is maintained via two individual transport lines, each of them consisting of a pneumatic transport riser and an impact-/gravitation separator. Both transport risers are further connected to an own particle tank and the exit ducts of both gas-solids separators comprise mechanical flap valves. This configuration allows for continuous addition or extraction of sorbent material while the unit is running and moreover serves as an appropriate sorbent storage while the system is shut-down.

Detailed information about the design and the specifications of the BSU will be given in the following.

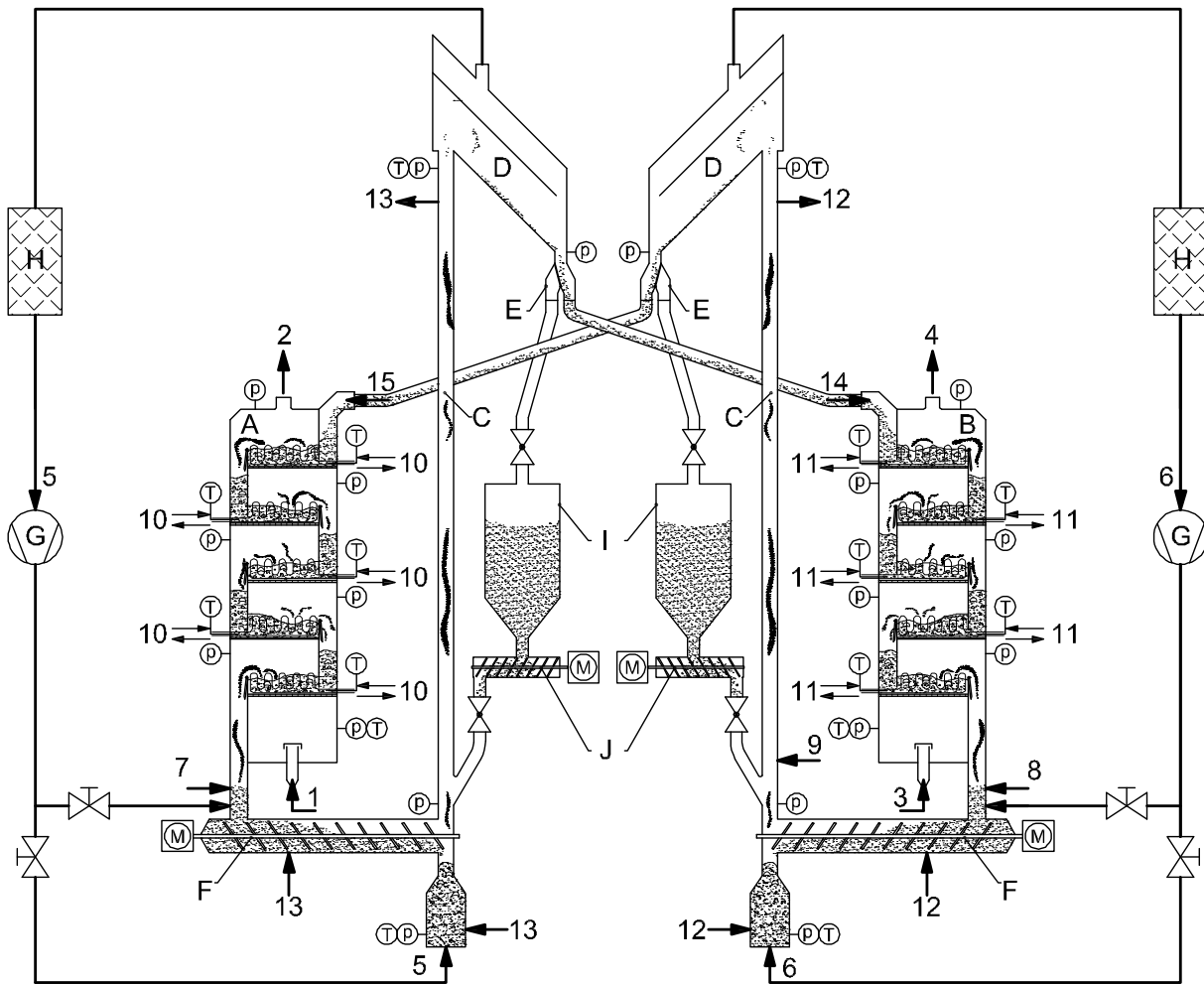
6.1.2 BSU design and specifications

The adsorber of the present TSA BSU has been used to study the fluid-dynamic behaviour of a multi-stage fluidized bed column with internal solid circulation. The adsorber was thereby designed for a CO₂ capture capacity of 100 kg·day⁻¹ with an assumed adsorbent size of 600 µm. However, prior the design of the BSU it turned out that an adsorbent batch of this size was not deliverable by our project partner. The fluid-dynamic properties of the finally received batch of adsorbent material are shown in Table 6.1 and the measured PSD of the material is given in Figure 6.2.

Table 6.1: Fluid-dynamic properties of final BSU adsorbent material.

Hydrodynamic properties of BSU adsorbent		
mean particle diameter d_{50}	300	[µm]
hydrodynamic particle density	1250	[kg·m ⁻³]
bulk particle density	700	[kg·m ⁻³]

Figure 6.1: Double loop staged fluidized bed bench scale unit design.



- | | | |
|-------------------------------|---|--|
| A ... adsorber | 1 ... raw flue gas | 11... desorber stage heating |
| B ... desorber | 2 ... clean flue gas | 12... riser cooling |
| C ... riser | 3 ... stripping gas (N ₂ , steam) | 13... riser heating |
| D ... gas-solid separator | 4 ... CO ₂ enriched stripping gas | 14... CO ₂ loaded adsorbent |
| E ... solids directing flap | 5 ... recirculation gas | 15... regenerated adsorbent |
| F ... bottom screw conveyor | 6 ... recirculation gas | |
| G ... recycle-gas blower | 7 ... purge gas (N ₂ , CO ₂) | Ⓟ ... pressure sensor |
| H ... particle filter | 8 ... purge gas (N ₂ , steam) | Ⓣ ... temperature sensor |
| I ... adsorbent tank | 9 ... dilution stream (N ₂) | Ⓜ ... driving motor |
| J ... adsorbent feeding screw | 10... adsorber stage cooling | |

The delivered adsorbent material is a chemisorbent that consists of a mesoporous ($d_{pore} = 4 - 35$ nm), almost pure silica precursor with a moderate BET surface area ($190 \text{ m}^2 \cdot \text{g}^{-1}$) and that is functionalized via impregnation with 50 %_w of polyethylenimine (PEI).

It is worth noting that the adsorbent size considered for design of the adsorber column in the CFM phase differs significantly from the size of the received adsorbent material. In order to ensure the fluid-dynamic functionality of the BSU, it was decided to keep the fluidization state (i.e. fluidization number) similar to the state tested in the CFM, rather than striving for achieving the same CO₂ capture capacity as considered in the CFM design phase.

On the desorber side, from a fluid-dynamic point of view it was not possible to optimize the stripping steam demand in accordance with results obtained from process performance assessment in

Chapter 4. It was decided to limit the minimum desorber column diameter to 110 mm, so that similar fluidization behaviour as in the adsorber column can be expected and wall friction (especially in the downcomer sections) still has no significant effect on the gas-solids flow within the column. The gas distributors within the desorber column have been realized as perforated plates, also with a perforation size of 3 mm, a triangular pitch of 10 mm and a perforation area ratio of 7.7 %. The downcomer segment height was chosen with 18.5 mm (downcomer area ratio: $A_{dc} \cdot A_{des}^{-1} = 11 \%$).

Figure 6.2: Particle size distribution of BSU adsorbent material.

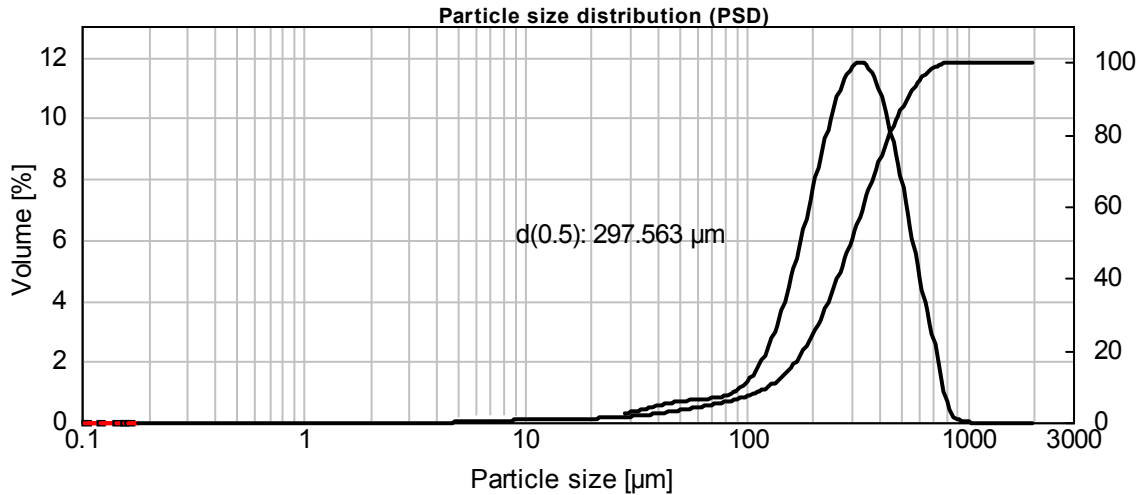


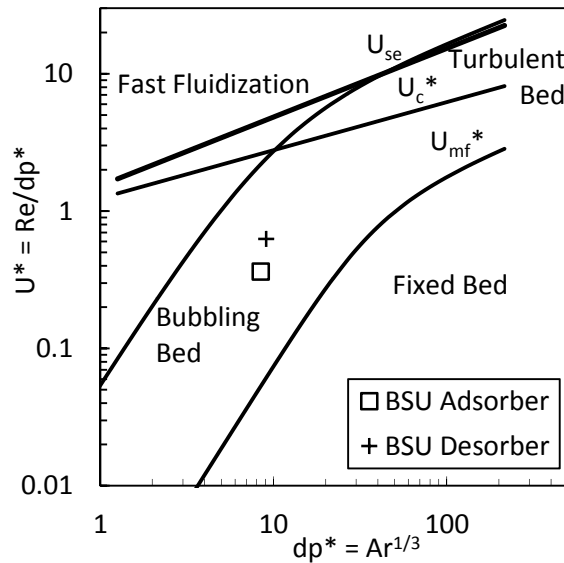
Table 6.2: Bench scale unit specifications

Adsorber column	
column diameter	150 [mm]
number of stages	1/2/3/4/5 [-]
weir height	40/60/80 [mm]
design operating temperature	75 [°C]
feeding gas components	N ₂ , CO ₂ , H ₂ O, Air [-]
design gas flow rate ($y_{N_2} = 95 \%_{vol.}$, $y_{CO_2} = 5 \%_{vol.}$)	15.8 [Nm ³ ·h ⁻¹]
design CO ₂ capture efficiency	90 [%]
design CO ₂ capture rate	35 [kg·day ⁻¹]
Desorber column	
column diameter	110 [mm]
number of stages	1/2/3/4/5 [-]
weir height	40/60/80 [mm]
design operating temperature	120 [°C]
feeding gas components	N ₂ , H ₂ O, Air [-]
design gas feeding rate (steam)	10 [kg·h ⁻¹]
design gas feeding rate (N ₂)	8 [Nm ³ ·h ⁻¹]

The main specifications of the BSU are given in

Table 6.2 and the fluid-dynamic states in both columns are marked within the regime map given in Figure 6.3.

Figure A 1 in the appendix shows two different isometric views of the final BSU design, both, with and without the framework of the unit. Figure A 2 shows additionally the main views of the BSU including dimensions of the BSU footprint. Figure A 3 shows a section view of the BSU that follows the adsorbent path within the system.

Figure 6.3: BSU fluidization regimes under design conditions.

Finally, Figure A 6 shows pictures of the commissioned BSU at the laboratories of the Institute of Chemical and Energy Engineering at the University of Natural Resources and Life Sciences, Vienna (BOKU) in March 2014.

In the following section the experimental setup will be introduced in more detail.

6.2 EXPERIMENTAL

6.2.1 Experimental setup

The present configuration of the experimental setup is illustrated in form of a process flow sheet in Figure A 4 in the appendix of this work. In the following, the experimental setup should be explained in more detail.

The adsorber can be fluidized with air, N₂, CO₂ and any combination of these components to obtain desired synthetic flue gas compositions. In addition, superheated steam can be added to the adsorber feed gas to adjust the humidity of the synthetic flue gas mixture. The flow rates of the individual fluidization gas components can be adjusted by means of variable area flowmeters and needle valves. The feed gas temperature can be controlled by means of electrical heat tracing, whereby the feed gas temperature is measured in the windbox of the adsorber column. Since the adsorber column is mainly built out of borosilicate glass and because observation of adsorbent movement within the column is desired during experimental runs, the adsorber column is not insulated.

The desorber column is made out of stainless steel and exhibits a double wall design for additional heating of the individual stages. The desorber can be fluidized with N₂, steam, air or any desired mixture of said gas species. Again, the flow rate of each fluidization gas component is adjusted by means of a combination of a variable area flowmeter and a needle valve. The desorber feed gas can be preheated also by means of electrical heat tracing. The desorber column is insulated to reduce heat losses to the environment.

The adsorbent circulation between both columns can be controlled via adjustment of the driving frequency of one (or both) bottom screw conveyors. The fluidization rate of the transport risers is

controlled via a variable area flowmeter and a needle valve, whereby the riser gases are constantly recycled via side channel blowers. Gas leakage between both columns can be prevented through introduction of purge or sealing gas streams into the moving bed section below the lowermost stages of each column. The purge gas flow rates are again adjusted through a variable area flowmeter and a needle valve and the selected purge gas media are CO₂ for the adsorber and steam for the desorber side.

For adjustment of the desired system temperatures, the BSU is cooled and heated by two independent thermal oil circuits. Compared to electrical heating, the use of such a thermo-oil system allows for secure control of the maximum system temperatures which is needed to limit adsorbent degradation through severe evaporation of active amine components. Beside the stage heat exchangers, the two bottom screw conveyors as well as the transport risers allow for heat exchange through a double wall design. The transport line directing adsorbent material from the adsorber to the desorber can be heated using the same thermo-oil supply as the internal desorber stage heat exchanger, whereas the transport line transporting adsorbent material from the desorber into the adsorber can be cooled using the same thermo-oil supply as the internal adsorber stage heat exchangers. The thermal-oil heating is implemented through electric heat cartridges introduced into an oil storage tank. Cooling of the cold thermo-oil circuit is performed within a freshwater cooled plate heat exchanger. Heating of the system can be controlled through adjustment of the thermal oil temperature which was limited to 140 °C. Cooling of the system can be controlled by adjustment of the thermo-oil temperature in the cold circuit and through adjustment of the thermo-oil flow rate which is done by means of pulse width controlled magnetic valves.

The gravitational gas-solid separators can be heated electrically in order to avoid problems with condensation in case of steam leakage into the transport lines. As a further measure to avoid condensation within the system, the fluidization gas within the riser that transports adsorbent material from the desorber into the adsorber can be diluted with N₂.

The steam that is used within both column gas feed streams is provided by an electric steam generator with a capacity of about 17 kg·h⁻¹ for saturated steam at 130 °C and 2.8 bar. While the offgas of the adsorber is directly vented to the stack, the desorber offgas is first passed over a condenser that is freshwater cooled. Since the required amount of steam for operation of the bench scale unit is quite low, the condensed steam is not recirculated. The expansion within the flowmeter and heat tracing leads to superheated steam at 130 °C and more or less ambient pressure before entering the desorber column.

6.2.2 Measurement and instrumentation

Pressure measurement

The locations of the integrated pressure measurement taps of the bench scale unit are shown in Figure 6.1.

Since proper fluidization of each individual stage is necessary to achieve continuous sorbent transport within the columns, the pressure drop over each stage is measured and monitored. An accurate pressure measurement can give information about the state of fluidisation and the amount of bed inventory in each stage and column. Additionally, pressure sensors are attached to the transport risers and the particle separators in order to allow for measurement of the riser inventory

and for detection of sorbent material blockage within the chutes connecting the particle separators and the uppermost column stages.

The pressure measurement has been performed via Kalinsky DS2 differential pressure sensors. The pressure sensors were connected to the unit's pressure taps via silicon tubes. For experiments where steam has been used as fluidizing gas agent, N₂ has been utilized as purge gas in the tubes in order to protect the pressure sensors from moisture, whereby the purge gas flow rates have been comparably small ($< 0.5 \text{ l}\cdot\text{min}^{-1}$). The linearity error of the applied sensors is less than or equal to 1 % of full scale which was 0 – 10 mbar, except for the pressure sensors connected to the pressure taps in the windboxes of both columns where the measurement range was 0 – 250 mbar.

Temperature measurement

The locations of the temperature sensors used for measurement of the adsorbent material temperature are shown in Figure 6.1. These temperatures were measured with CANtrans T RTD temperature probes from JUMO with CANopen output and an operating range of -50 °C to 150 °C with an accuracy of 0.2 % of full scale. In addition, temperature sensors have been applied to control the installed electrical trace heating as well as within the thermo-oil circuits to measure forward and return flow temperatures. The locations of these sensors are indicated within the process flow sheet provided in Figure A 4 in the appendix of this work. The type of temperature sensors that have been applied here were class B PT100 RTDs.

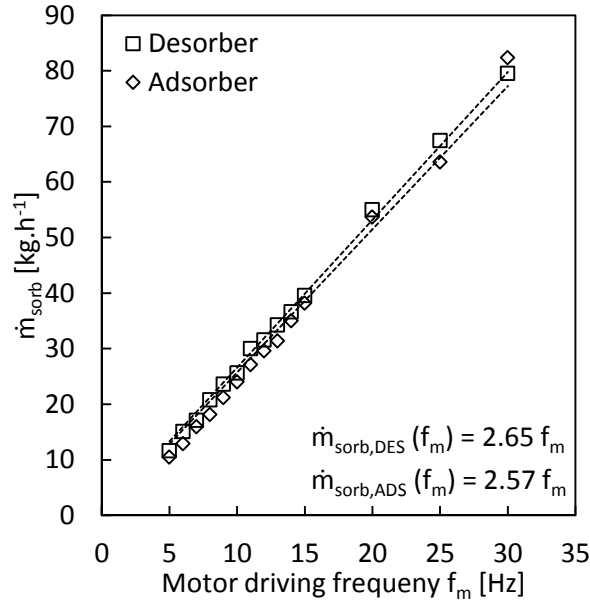
Gas analytics

The bench scale unit exhibits sample points for gas analytics in each stage of adsorber and desorber, in the exit ducts and in the gas inlets of both columns. All sample points are G 1/8" threaded connectors. The present configuration allows for measurement of CO₂ concentrations only, whereby in the present experimental study the analyser was just connected to the sample points located at the adsorber feed- and off-gas ducts. However, if necessary CO₂-measurement can be applied to each of the above mentioned sample points. The used CO₂-analytics was a X-STREAM X2GP from Emerson with a non-dispersive infrared detector. The analyser has a linearity error of less than or equal to 1 % of the calibrated range that was either 0.5 %, 5 % or 12 % CO₂.

6.3 COMMISSIONING OF THE BSU

6.3.1 Determination of screw conveying rates

Similar as to the CFM, the BSU features screw conveyors driven by gear motors for solids transport within the system. The actual driving speed of each screw and thus their solids transport capacities can be controlled via frequency converters. For determination of the transport capacity of all screws, the BSU was filled with the later used adsorbent material. For each screw the adsorbent material was then conveyed into a sample container and the conveying time was measured. The transport rate was then determined by measuring the weight of the sample container and by relating the measured mass with the conveying time. This procedure was repeated for different driving frequencies of the respective gear motors. The transport capacities of both bottom screw conveyors (BSC) are given in Figure 6.4. The actual transport rate and thus the sorbent circulation rate can be calculated by using the linear relationships printed in Figure 6.4.

Figure 6.4: Transport capacity of bottom screw conveyors.

6.3.2 BSU start-up procedure

In the beginning all downcomer flap valves within the adsorber and desorber need to be closed. Then the gas feed of both columns can be adjusted to a sufficiently large flow rate in order to ensure adsorbent material hold-up within the column (i.e. fluidization) during filling, whereby N₂ is used as fluidization agent. Next, the recirculation blowers within the transport lines are switched on. Adsorbent material is now fed from the particle tanks via the solids feeding screws into the individual transport lines and from there further entrained into the gas-solids separators that direct them into the top stages of each column. If the column gas feeding rates are sufficiently large, adsorbent material will immediately start to form a bed upon the uppermost gas distributor in each column. The dense bed height within the top stage increases while more and more material is fed into the system. After the dense phase reached a critical height exploding gas bubbles start to catapult adsorbent material into the downcomer, where they rest on the closed downcomer flap and form a fixed bed. When the fixed bed upon the flap valve is large enough, the flap can be opened and the downcomer directs the adsorbent material into the next stage below. There, again a bed starts to form immediately and the described procedure needs to be repeated until all stages are filled. At this point the solids feeding screws can be switched off and the bottom screw conveyors can be turned on in order to achieve sorbent circulation between both columns. The BSC below the desorber is operated at constant driving frequency, whereas the driving frequency of the BSC below the adsorber is adjusted in order to maintain a constant inventory distribution between both columns. Now that both columns are filled, the system can be started to be heated up via the stage heat exchangers located within the desorber as well as through pre-heating of the feed gas streams. If necessary, the adsorber can be cooled to achieve the required temperature difference between both columns. After the desired system temperatures have been reached the BSU is ready for CO₂ capture operation.

6.3.3 Assessment of gas leakage between both columns

The pressure drop across one column causes a positive pressure gradient between its lowermost stage (Stage 1) and the uppermost stage (Stage 5) of the respective other column. Without application of countermeasures, this circumstance would necessarily cause gas leakage between both columns. Any gas leakage will dilute (and contaminate) the off-gas streams.

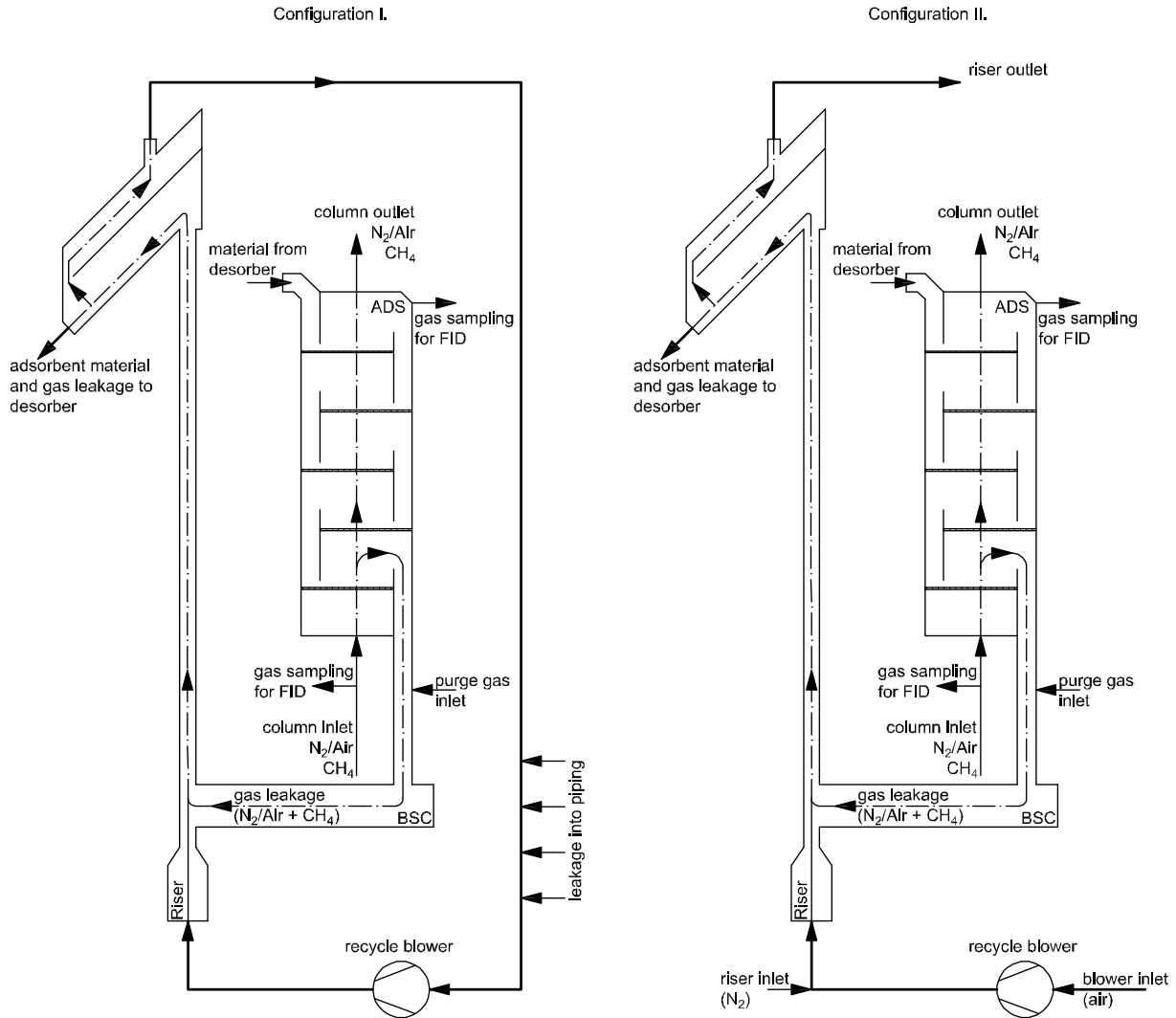
Hence, for a correct determination of the CO₂ capture performance of the BSU it is essential to assess the gas leakages quantitatively. For this reason a dedicated test campaign has been set up and the procedure and outcome of this campaign will be presented in the following.

The gas leakage from the adsorber column has been assessed at room temperature in two different test configurations as shown in Figure 6.5.

The experimental method in *Configuration I* is based on the fact that the riser transport gas is constantly recycled within a closed loop. Consequently, the riser gas composition needs to adapt to the composition of the gas flow leaking from the column (which was the adsorber in this campaign) into the transport line. Assuming further, that selective leaking of specific gas species, for example through adsorption on the bed material, can be neglected, the composition of the leaking gas stream equals the composition of the adsorber feed gas stream. Furthermore, as a consequence of mass conservation, the amount of gas that leaks into the closed transport system needs to leave through the chute connecting the gas-solids separator and the opposite column (desorber). There, the gas leakage stream gets diluted with the desorber fluidization gas. The use of a tracer gas within the fluidization gas feed of the adsorber should thus allow for assessment of the gas leakage, through measurement of the tracer gas concentration in the off-gas of the desorber. However, results obtained with this method have an inherent error as the desorber fluidization rate is measured at the inlet of the column and therefore this method does not account for gas leakages out of the desorber. However, if one assumes that the gas leakage is negligibly small compared to the desorber fluidization rate, sufficient assessment of the gas leakage should be possible with this method.

Nevertheless, a second method (*Configuration II* in Figure 6.5) has been applied to double-check the results obtained from the first method. Here, the transport line was opened and the tracer gas measurement was directly applied within the transport riser. The gas leakage was then assessed by accounting for the dilution obtained with the adjusted riser fluidization rate.

The fluidisation of the columns was realized with oil free pressurised dry air and later also with N₂ grade 5.0 (purity $\geq 99,999\%$). As tracer gas methane (CH₄) with a purity $\geq 99.5\%$ was used. As bed material inert glass beads with a diameter range between 300 μm and 400 μm were used. The flow rate of the fluidising gas was controlled by needle valves and measured with variable area flowmeters while tracer gas was supplied via a mass flow controller. The interfaces for the measurement of the gas concentration were installed at the inlet and outlet of the adsorber, the outlet of the desorber and in the transport riser with adequate distance to the screw conveyor to ensure a homogeneous composition of the riser gas. The determination of the concentrations was realised with a flame ionization detector (FID) 1230 from TESTA which was calibrated for the considered measurement ranges. All results of the FID below are average concentrations. The minimum time of measurement was 5 minutes with a sample rate of one measurement every 2 seconds.

Figure 6.5: Experimental configurations for leakage tests.

Results from leakage assessment

Both columns were fluidised with pressurised air. In the adsorber column the flow rate was set to $22 \text{ m}^3 \cdot \text{h}^{-1}$. The methane flow was set in such a way that a concentration of $800 \text{ ppm}_{\text{Vol}}$ has been obtained in the adsorber inlet (measured with FID). Unlike expected, the measured CH₄ concentration within the riser stabilized at $390 \text{ ppm}_{\text{Vol}}$ rather than adapting to the same concentration as within the adsorber feed. This indicated that the closed riser system was not completely leak proof and that the riser was sucking ambient air or even air from the desorber column. Therefore, an assessment of the gas leakage was not possible in *Configuration I* and the system was adapted to *Configuration II* to repeat the gas leakage measurement as described above.

In *Configuration II* a constant flow of riser fluidization gas was continuously mixed with the gas leakage out of the adsorber column. This allowed a direct detection of the gas leakage through FID measurement using sample gas extracted from the top section of the riser. Compared to *Configuration I* the gas leakage into the riser system could be neglected as the number of pipe fittings and thus the risk of potential leaks was reduced significantly. The pressure difference between the first stage of the adsorber and the bottom of the riser system was set to the same value as within *Configuration I*. Therefore, the gas leakage in *Configuration II* could be considered as equal to the leakage that occurred in *Configuration I*.

Two leakage measurements have been performed in the following, one with air and one with N₂ as fluidizing agent in the adsorber and the riser. The adsorber column was fluidised with a flow rate of 22 m³·h⁻¹, whereas the riser fluidization was set to 11.5 Nm³·h⁻¹. To get a significant response from FID measurement, the mass flow controller was set to its maximum flow rate leading to an adsorber inlet CH₄ concentration of 898 ppm_{Vol}. The riser offgas CH₄ concentration was measured with 1.83 ppm_{Vol}. Finally, the following equations have been used to calculate the gas leakage flow rate from the measured methane concentrations:

$$F_{riser,out} \cdot y_{CH_4,riser,out} = F_{Air/N_2,riser,in} \cdot y_{CH_4,riser,in} + F_{leak} \cdot y_{CH_4,leak} \quad (\text{Eq. 6.1})$$

$$F_{riser,out} = F_{Air/N_2,riser,in} + F_{leak} \quad (\text{Eq. 6.2})$$

$$F_{leak} = F_{Air/N_2,riser,in} \cdot \frac{y_{CH_4,riser,out} - y_{CH_4,riser,in}}{y_{CH_4,leak} - y_{CH_4,riser,out}} \quad (\text{Eq. 6.3})$$

The methane concentration in the riser feed gas can be set to zero whereas the methane concentration within the gas leakage stream was assumed to equal the measured methane concentration in the adsorber feed gas stream. With these assumptions, the gas leakage out of the adsorber column was determined with 23.5 l·h⁻¹.

A second test was performed with nitrogen grade 5.0 as fluidising agent within the adsorber and the riser. The fluidization flow rates of the adsorber and the riser were set to the same values as before. The CH₄ concentration in the adsorber inlet was measured with 861 ppm_v and the riser off-gas concentration was measured with 2.17 ppm_{Vol}. Using again (Eq. 6.3) together with the aforementioned assumptions, an average gas leakage of 29.0 l·h⁻¹ was derived from this measurement, which is very close to the value that has been obtained with air as fluidization agent.

The calculated gas leakage from the adsorber column into the transportation line was less than 0.15 % of the adsorber gas feeding rate. Thus, it was concluded that the effect of gas leakage on the assessment of the CO₂ capture performance can be neglected.

In addition to the quantitative assessment of the gas leakage, the function of the purge gas introduction as a gas sealing measure between both column gas streams has been tested. For this test, Configuration II was used again and a small amount (~ 0.1 m³·h⁻¹) of purge gas was injected into the moving bed formed below the adsorber solids exit duct (see Figure 6.1, 7). Right after introduction of the purge gas the CH₄ concentration measured within the transportation riser dropped from approximately 2 ppm_{Vol} to zero. Subsequently the purge gas was switched off again and the CH₄ concentration in the riser went back to its initial value, thus, clearly demonstrating the function of the purge gas sealing measure.

Nevertheless, it has to be stated that the tests have been performed with a single set of fluidization parameters only. A proper operation range of the purge gas sealing measure was beyond the scope of this first functionality assessment and needs to be identified within a dedicated experimental campaign.

6.4 RESULTS FROM CONTINUOUS CO₂ CAPTURE TESTS

6.4.1 Experimental plan

As already pointed out, the overall goal of the experimental campaign that will be presented in this work was to deliver a first proof of concept of the continuous CO₂ capture process via TSA within the proposed double loop multi-stage fluidized bed configuration. In addition to that, the influence of the main operating parameters on the process performance should be assessed. Among the operating parameters determining the TSA process performance, a variation of the parameters listed in Table 6.3 has been performed.

General comments on the conducted experimental campaign

In order to follow the result discussions in the next chapter, some general remarks should be made here:

- Except for the experiments where the stripping gas agent has been varied, N₂ has been used exclusively as stripping gas agent.
- Except for the experiments with humid adsorber feed gas, the simulated flue gas was dry and consisted of N₂ and CO₂ only (mixed from gas bottles).
- Unless stated otherwise the weir heights in all stages of both columns had been 60 mm throughout the conducted experiments.
- Unless stated otherwise the forward flow temperature of the thermal oil that is used for heating the desorber column was set to 140 °C. The thermal oil flow rate cannot be adjusted and can be considered as constant throughout the experiment.
- The presented results represent either measured raw data or parameter values that have been averaged over a sufficiently long period of time after reaching steady-state operation.
- The CO₂ concentration in the adsorber off-gas has been measured continuously whereas the CO₂ concentration in the adsorber feed-gas has been measured only after adjustment of a new CO₂ feed concentration to double check the flowmeter positions.
- The reported sorbent circulation rates correspond to a constant driving speed of the bottom screw conveyor below the desorber column that have been calculated using the linear relationship reported in Section 6.3.1.
- The CO₂ capture efficiency η_{capt} serves as process performance parameter that is defined as

$$\eta_{capt} = \frac{F_{CO_2,ads,in} - F_{CO_2,ads,out}}{F_{CO_2,ads,in}} \quad (\text{Eq. 6.4})$$

Table 6.3: BSU parameter study.

Parameter	Expected influence/ Aim of parameter variation
<i>Sorbent circulation rate</i>	The sorbent circulation rate should have a significant influence on the exploited working capacity of the used adsorbent material and thus on the achieved capture efficiency. However, it is desired to achieve high capture efficiencies with the lowest sorbent circulation possible, as it directly affects the regeneration energy demand of the process. Thus, the aim of this parameter variation was to identify an optimum sorbent circulation rate for the BSU.
<i>CO₂ feeding rate</i>	The CO ₂ feeding rate should be varied in two ways; first through variation of the CO ₂ concentration in the feeding gas at constant gas feeding (or fluidization) rate and second by variation of the gas feeding rate at constant CO ₂ concentration. An increasing CO ₂ feeding rate should enhance the CO ₂ capture performance as it generally improves the adsorption conditions. This parameter variation should assess the maximum CO ₂ capture rates that can be achieved within the current BSU configuration.
<i>Stripping gas agent</i>	The reason for the utilization of a stripping gas is to achieve a dilute CO ₂ atmosphere within the desorber and thus to improve the adsorbent regeneration. For the sake of simple BSU operation the very first experiments will utilize N ₂ as stripping gas agent rather than steam which is the required agent for commercial applications. Even though the composition of the stripping gas agent should not affect the regeneration step some unexpected interactions may occur with the adsorbent material if stripping gas changes from N ₂ to steam. Thus, the aim of this set of tests was to study whether the process performance is affected if the stripping gas agent is changed from N ₂ to steam.
<i>Humidity of synthetic flue gas</i>	It was reported that, compared to dry flue gas streams, the utilization of humid flue gas streams leads to increased CO ₂ adsorption capacities of amine functionalized adsorbent materials. It was claimed that this effect should improve the process performance as less sorbent circulation is required to capture a specific amount of CO ₂ . However, the influence of the flue gas humidity has never been studied within continuous operating configurations and should therefore be investigated in this experiment.

In the present BSU configuration, gas volume flows have only been measured at the column gas inlets, whereas CO₂ concentration has been measured in the adsorber feed- and off-gas. The flow rate of CO₂ in the feed- and off-gas of the adsorber can be correlated to the measured concentrations as follows:

$$F_{CO_2,ads,in} = y_{CO_2,ads,in} \cdot (F_{N_2,ads,in} + F_{CO_2,ads,in}) = \frac{y_{CO_2,ads,in} \cdot F_{N_2,ads,in}}{1 - y_{CO_2,ads,in}}$$

$$F_{CO_2,ads,out} = y_{CO_2,ads,out} \cdot (F_{N_2,ads,out} + F_{CO_2,ads,out}) = \frac{y_{CO_2,ads,out} \cdot F_{N_2,ads,out}}{1 - y_{CO_2,ads,out}}$$

Assuming further that no significant gas leakage out or into the adsorber column occurs (see results obtained from gas leakage measurement) and that the adsorbent material adsorbs CO₂ exclusively, the incoming and outgoing nitrogen flow in the adsorber can be set equal. The capture efficiency η_{capt} can then be calculated using the following correlation that comprises measured and thus known data only:

$$\eta_{capt} = \frac{\frac{y_{CO_2,ads,in} \cdot F_{N_2,ads,in}}{1 - y_{CO_2,ads,in}} - \frac{y_{CO_2,ads,out} \cdot F_{N_2,ads,in}}{1 - y_{CO_2,ads,out}}}{\frac{y_{CO_2,ads,in} \cdot F_{N_2,ads,in}}{1 - y_{CO_2,ads,in}}} \quad \text{or}$$

$$\eta_{capt} = 1 - \frac{y_{CO_2,ads,out} \cdot (1 - y_{CO_2,ads,in})}{y_{CO_2,ads,in} \cdot (1 - y_{CO_2,ads,out})} \quad (\text{Eq. 6.5})$$

- The second process performance parameter used in this work is the CO₂ capture rate \dot{m}_{capt} that is defined as

$$\dot{m}_{capt} = F_{CO_2,ads,in} \cdot \rho_{n,CO_2} \cdot \eta_{capt} \quad (\text{Eq. 6.6})$$

- In order to assess the exploitation of the adsorption capacity of the used adsorbent material, the so called dynamic sorbent loading dSL has been defined as

$$dSL = \frac{\dot{m}_{capt}}{\dot{m}_{sorb}} \quad (\text{Eq. 6.7})$$

6.4.2 First continuous CO₂ capture test

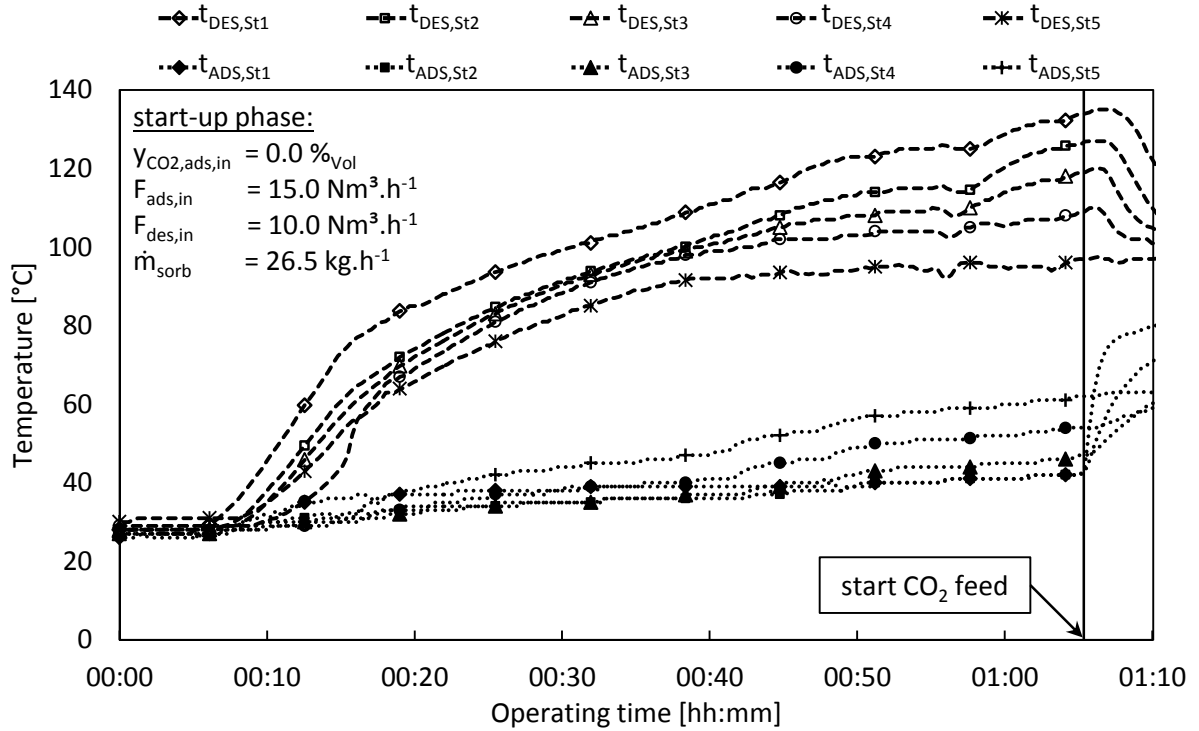
The aim of this very first CO₂ capture experiment within the constructed BSU was to deliver a proof of concept for the developed TSA process design.

In the beginning of the experiment the BSU was filled under ambient conditions as described in the start-up procedure above. After stable sorbent circulation between both fluidized bed columns had been established, the thermo-oil heating (forward flow temperature 140 °C) as well as the electrical heat tracing for gas pre-heating was switched on. The temperatures of the individual fluidized bed stages during the start-up phase are shown in Figure 6.6. Most noticeable from this figure is the axial temperature profile that developed within both fluidized bed columns. These profiles resulted from

the multi-stage fluidized bed configuration (i.e. reduced axial mixing of sorbent material) and the fact that hot/ cold particles constantly entered the adsorber/ desorber column at the top and had been cooled/ heated on their way down to the bottom of the column by means of the applied internal heat exchangers.

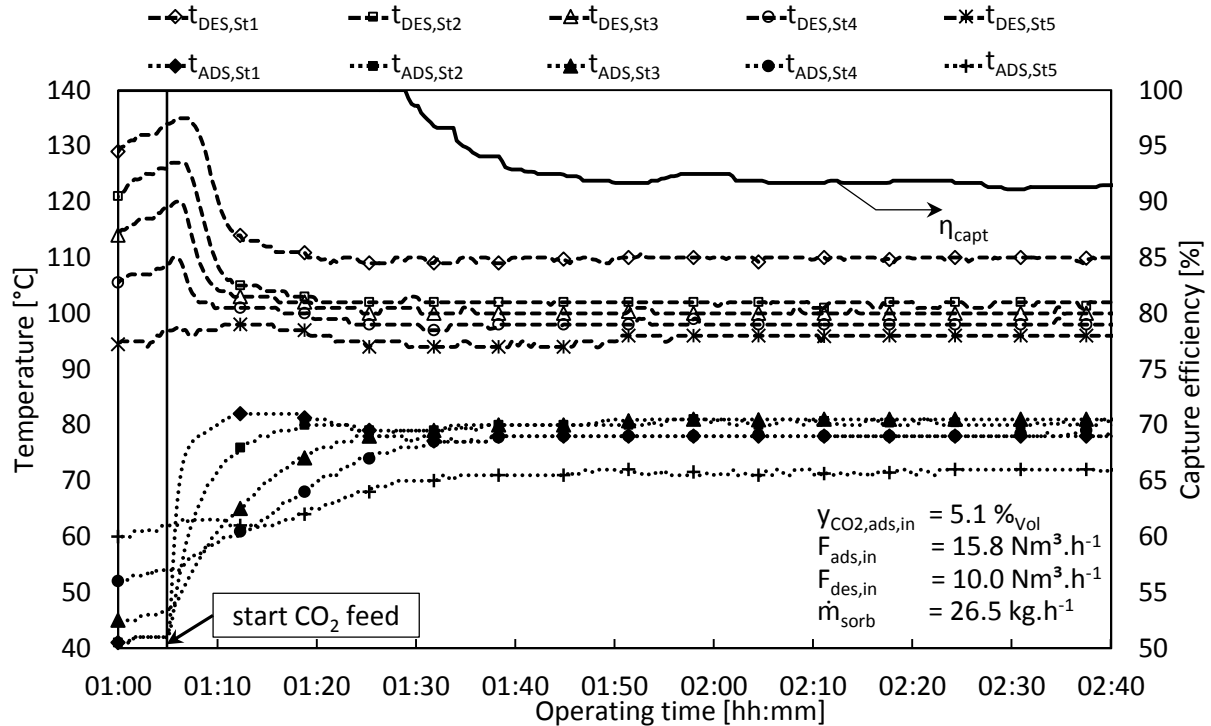
After about one hour the highest system temperature (desorber, Stage 1) approached 140 °C that correspond to the maximum tolerable adsorbent temperature. It is worth to note that at that time the lowest temperature in the desorber column (Stage 5) was about 97 °C which strongly differs from the design temperature of 120 °C. This indicates an insufficient heat transfer between the adsorbent material and the internal heat exchangers, especially within the desorber column. However, in order to avoid severe adsorbent degradation through evaporation of amine compounds in the desorber, the actual experiment was started after the adsorbent material temperature in the lowermost desorber stage reached 135 °C. From that point on, CO₂ was introduced into the adsorber column with a concentration of approximately 5 %_{Vol}.

Figure 6.6: First continuous CO₂ capture experiment - start-up phase.



Right after the CO₂ feed was started the temperatures within the adsorber stages increased drastically as heat from CO₂ adsorption was released as shown in Figure 6.7.

Thereby, most of the heat was obviously released in the bottom section of the adsorber and since the adsorbent material was fresh and completely unloaded in the beginning, no CO₂ was detected within the adsorber off-gas leading to an initial capture efficiency of 100 %. Only a short time after CO₂ introduction had been started the desorber temperatures dropped significantly. It is worth to note that the most drastic decrease was observed in the lower stages that exhibited the largest temperatures prior introduction of CO₂. The temperature decrease derived from the heat demand for regeneration of the adsorbent material.

Figure 6.7: First continuous CO₂ capture experiment – steady state operation.

After a few minutes of operation the adsorber cooling was switched on and the cooling media flow rate was adjusted to approximate the desired operating temperature of 75 °C in the individual adsorber stages. Interesting to note is that similar to the results obtained from equilibrium modelling the largest cooling demand occurred in the top stage of the adsorber. The cooling of the lowermost stage, however, had to be switched off occasionally, thus, revealing weaker adsorption activity in this stage.

After about 25 minutes of continuous CO₂ capture a breakthrough of CO₂ was detected and the CO₂ concentration increased. About further 30 minutes later it stagnated around 0.41 %Vol. This off-gas concentration corresponds to a CO₂ capture efficiency of 92 % and a CO₂ capture rate of 35.2 kg·day⁻¹. Obviously the adsorption and regeneration kinetics are very fast as the design capture rate has been achieved with only five practical fluidized bed stages applied in each column. However, it was achieved with a rather high specific adsorbent circulation of around 18 kg per kg of captured CO₂ as well as a large specific stripping gas feed of about 5.5 kg steam equivalent per kg of captured CO₂. These values are fairly above the optimum that has been predicted from thermodynamic equilibrium modelling. On the other hand, the regeneration temperatures in the desorber were significantly lower than the desired 120 °C, with temperatures ranging from 96 to 110 °C only. Consequently, a larger sorbent circulation rate was required to achieve the desired capture performance. This result indicates that the practical limits for BSU operation lie in the amount of heat that can be exchanged with the adsorbent material rather than in the adsorption kinetics.

Nevertheless, a first proof of concept was clearly delivered with this experiment and paved the way for further parameter studies within the BSU.

6.4.3 Results from performed dry gas parameter variations

Overview of all parameter variations

Table 6.4 gives an overview of all results obtained from the parameter study conducted compositions within the BSU using dry feed gas streams in both columns.

Operating point EXP 1 refers to the first continuous CO₂ capture experiment that has been discussed above. All operating points with starting number 1, 2 and 3 have been obtained during variation of the operating parameter named in the first column of Table 6.4.

Finally, the results from operating point OPt 4 have been obtained from an experiment where the initial heat exchangers had been replaced by heat exchangers of a different design.

In the following, results obtained from parameter variations as well as from tests with the new heat exchanger design should be discussed in more detail.

Table 6.4: Summary of results obtained from performed BSU parameter variations.

varied parameter	Operating point	$y_{\text{CO}_2, \text{ads}, \text{in}}$ [% _{Vol}]	$F_{\text{ads}, \text{in}}$ [Nm ³ ·h ⁻¹]	$F_{\text{des}, \text{in}}$ [Nm ³ ·h ⁻¹]	\dot{m}_{sorb} [kg·h ⁻¹]	η_{capt} [%]	\dot{m}_{capt} [kg·day ⁻¹]	dSI [% _w]	$T_{\text{DES}, \text{St1}}$ [°C]	$T_{\text{ADS}, \text{St5}}$ [°C]
-	EXP 1	5.06	15.80	8.00	26.50	91.58	34.76	5.47	109.93	71.60
\dot{m}_{sorb}	OPt 1.1	5.06	15.80	8.00	18.55	78.10	29.65	6.66	115.78	78.91
	OPt 1.2	5.06	15.80	8.00	22.52	85.02	32.27	5.97	111.30	75.75
	OPt 1.3	5.06	15.80	8.00	25.18	90.05	34.18	5.66	110.16	74.46
$y_{\text{CO}_2, \text{ads}, \text{in}}$	OPt 2.1	7.89	15.85	8.00	25.18	69.96	41.49	6.87	109.14	83.32
	OPt 2.2	10.13	15.80	8.00	25.18	57.99	44.02	7.29	109.13	88.76
$F_{\text{CO}_2, \text{ads}, \text{in}}$	OPt 3.1	5.06	15.80	8.00	31.88	96.01	36.44	4.76	108.89	69.00
	OPt 3.2	5.00	20.00	8.00	33.13	83.70	39.72	5.00	107.02	77.27
	OPt 3.3	5.17	23.20	8.00	26.50	72.70	41.39	6.51	108.10	80.30
	OPt 3.4	5.06	31.60	8.00	33.39	56.21	42.67	5.32	106.45	81.96
-	OPt 4	4.86	16.92	8.00	16.43	91.82	35.72	9.06	119.08	68.15

Variation of solid circulation rate

The goal of this experiment was to investigate the effect of the sorbent circulation rate between the adsorber and desorber column on the process performance.

The CO₂ concentration within the adsorber feed gas, consisting of N₂ and CO₂, was held constant at about 5 %_{Vol} and the total gas feeding rate was 15.8 Nm³·h⁻¹. In the desorber column the stripping gas feeding rate was held constant at 8 Nm³·h⁻¹, using N₂ as stripping gas agent. An adsorber temperature of 75 °C has been approximated by adjustment of the cooling media flow rate through each internal stage cooler whereby the cooling media forward flow temperature was set to 20 °C. The thermal-oil forward flow temperature for the desorber heating was set to 140 °C whereby the desired desorber operating temperature was 120 °C. The sorbent circulation rate between both contactors was varied in five different operating points, ranging from 18.55 kg·h⁻¹ to 31.88 kg·h⁻¹.

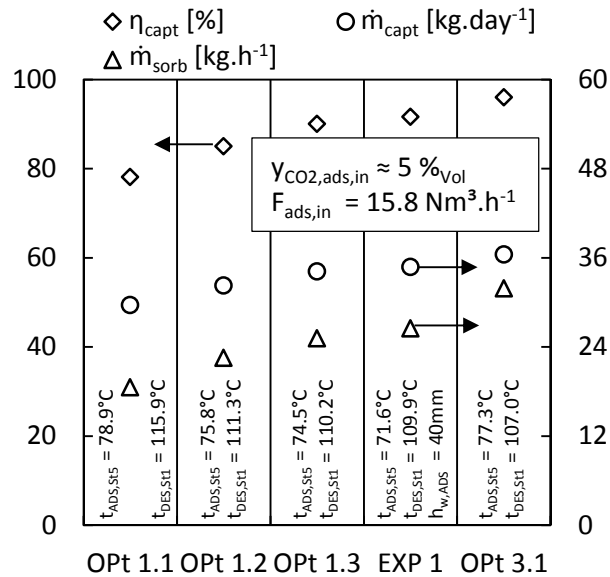
Figure 6.8 shows the obtained process performance data for the individual operating parameters together with their respective sorbent circulation rate. Furthermore, the operating temperatures within adsorber Stage 5 and desorber Stage 1 are indicated as additional parameters. These temperatures are the most important ones as they determine the equilibrium conditions in the final

regeneration step in the desorber and the final adsorption step in the adsorber, respectively. Values of the obtained dynamic sorbent loading, which is defined as the ratio of the captured amount of CO₂ and the sorbent circulation rate, are listed in Table 6.4.

The capture efficiency and the amount of CO₂ captured per day showed a clear rise with increasing circulation rate. The capture efficiency went from 78.1 % at 18.55 kg·h⁻¹ to 96.0 % at 31.88 kg·h⁻¹ and the amount of CO₂ captured by day increased from 29.65 kg·day⁻¹ to 36.44 kg·day⁻¹. On the other hand, the sorbent dynamic loading dropped from 6.66 %_w at a circulation rate of 18.55 kg·h⁻¹ to only 4.76 %_w at 31.88 kg·h⁻¹.

Furthermore, the solid circulation rate shows a significant effect on the stage operating temperatures. The average temperature of the desorber column decreased with increasing circulation rate. Interesting to note is that the temperature gradient between the uppermost and the lowermost stage is dropped also with increasing sorbent circulation rate. In the adsorber the increasing cooling demand for higher circulation rates was covered by increasing flow rates of the cooling media. However, similar as within the desorber column the temperature difference between the stages in the column decreased.

Figure 6.8: BSU parameter assessment - variation of sorbent circulation rate.



Variation of CO₂ feeding rate

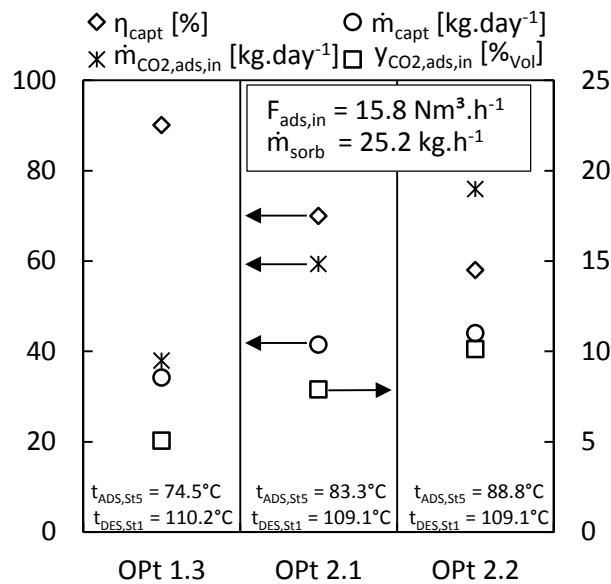
The goal of this experiment was to investigate the system behaviour of the bench scale unit (BSU) for different absolute CO₂ feeding rates. The absolute CO₂ feeding rate has been varied in two different ways:

1. Through variation of the CO₂ concentration in the adsorber feed gas at constant gas feeding rate and
2. Through variation of the gas feeding rate into the adsorber with constant CO₂ concentration.

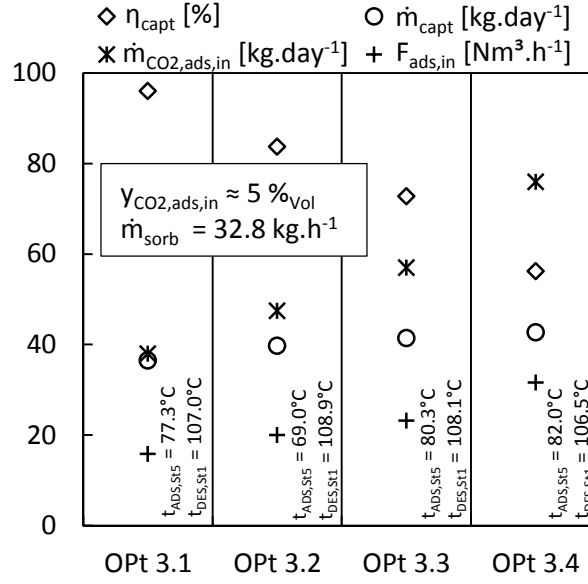
The first variation has been performed to simulate different flue gas sources such as combined cycle gas or coal/biomass power plants that represent sites where the developed TSA CO₂ capture technology can be applied to. The second variation has been performed to assess the influence on the TSA CO₂ capture system if the CO₂ emitting source changes from full- to part-load operation, hence, if the flow rate of the treated flue gas stream changes.

In the first variation of the CO₂ feed the adsorber gas feeding rate was held constant at 15.8 Nm³·h⁻¹ while the CO₂ concentration in the gas flow was selected with 5.06, 7.89 and 10.13 %_{Vol} respectively. The sorbent circulation rate was held constant at 25.18 kg·h⁻¹. The performance parameters obtained from this parameter variation are shown in Figure 6.9. As one can see from this figure, the capture rate increased with increasing CO₂ concentration in the feed. An increased CO₂ concentration corresponds to a larger CO₂ partial pressure within the adsorber, which in turn led to a higher driving force for the adsorption process. However, if the performance increase between the respective operating points is related to the CO₂ capture rate achieved in OPT 2.2, it seems that the capture rate approximated a maximum. An increase of the CO₂ concentration in the adsorber feed from 5.06 %_{Vol} in OPT 1.3 to 7.89 %_{Vol} in OPT 2.1 led to an 16.6 % increase of the CO₂ capture rate, whereas an increase from 7.89 to 10.13 %_{Vol} resulted in an increase of only 5.7 %. Furthermore, the indicated stage temperatures show that the desorber temperatures dropped while the adsorber temperatures increased with increasing CO₂ concentration in the adsorber feed. Thus, it is believed that the capture rate was limited by insufficient heat transfer between adsorbent material and the internal heat exchangers which in turn caused an insufficient regeneration of the adsorbent material as well as unfavourable operating temperatures within the adsorber. This is supported by the fact that the dynamic sorbent loading increased from 5.66 %_w in OPT 1.3 to 7.29 %_w in OPT 2.2. As a consequence, the capture efficiency dropped significantly from 90.05 % in OPT 1.3 to only 57.99 % in OPT 2.2.

Figure 6.9: BSU parameter assessment - variation of flue gas CO₂ concentration.



In the second CO₂ feed variation the CO₂ concentration was held constant at about 5 %_{Vol} and the total feed gas rate was adjusted to 15.8, 20.0, 23.2 and 31.6 Nm³·h⁻¹ in four different operating points. The sorbent circulation rate was kept constant at 32.8 kg·h⁻¹ in all operating points. The results obtained from this parameter variation are shown in Figure 6.10.

Figure 6.10: BSU parameter assessment - variation of flue gas flow rate.

Similarly to the above discussed CO₂ feed variation, the CO₂ capture rate increased with increasing CO₂ feed into the system.

A plausible explanation for the improved capture rate is that at low CO₂ capture efficiencies, the CO₂ partial pressures in the top stages are larger compared to optimum operation and thus driving force for adsorption is enhanced. Comparison of OPT 2.2 and OPT 3.4, two operating points with the same CO₂ feeding rate of 75.9 kg·day⁻¹, shows that a higher capture rate or capture efficiency has been achieved with larger CO₂ feed concentrations (OPT 2.2) even though, the sorbent circulation rate has been significantly lower in this case (25.18 kg·h⁻¹ compared to 32.8 kg·h⁻¹).

Another reason for the increasing capture rate was that the upper stages became more active as more CO₂ was present compared to the experiments with lower gas feeding rate. This is indicated by the increasing temperature of the uppermost stage within the adsorber. Beside the increased adsorber temperatures, the desorber temperatures dropped simultaneously which again indicated insufficient heat exchange between the adsorbent material and the internal heat exchangers that led in turn again to insufficient adsorbent regeneration in the desorber and improper adsorption conditions in the adsorber.

The variation of the adsorber CO₂ feeding rate clearly revealed that heat exchange with the adsorbent material (i.e. desorber desorber and adsorber cooling) is the limiting factor for continuous operation of the BSU. In order to improve the heat exchange, it was decided to redesign the existing heat exchanger and replace them. The design of the new heat exchangers in both columns should thus be introduced in the following and results obtained with the new heat exchanger design will be compared with aforementioned results.

Tests with new heat exchanger design

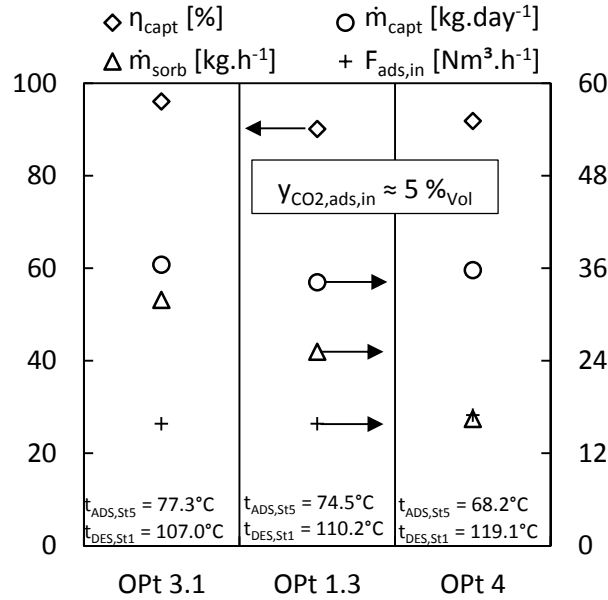
Figure A 5 in the appendix of this thesis illustrates the old and the new heat exchanger designs that have been applied to the stages of the adsorber and desorber column. Section drawings of the column stages are shown on the left side of the figure, together with values of the total immersed surface area of the heat exchangers. Compared to the old designs the heat transfer surfaces increased by a factor of 2.1 in the adsorber and by 2.85 in the desorber. The distance between the

gas distributors and the top edges of the heat exchangers increased slightly in the adsorber from 61 mm to 68 mm and more significantly in the desorber from 42 mm to 58 mm. This means not the complete additional heat transfer surface can be expected to be immersed into the dense phase of the bed under standard operating conditions. However, for 60 mm weir plate heights it can be assumed that the heat exchanger surface that is not immersed within the dense phase lies at least within the splash zone of the fluidized beds.

If the conclusion that heat transfer is the limiting factor for the capture performance of the BSU is valid, then a noticeable difference in the system performance can be expected with the new heat exchanger designs.

Figure 6.11, shows the results obtained from an BSU operation with the new heat exchanger designs (OPT 4) in comparison with results obtained with the previous heat exchanger configuration (OPT 1.3 and OPT 3.1).

Figure 6.11: Benchmark test with new heat exchanger design.



The three operating points have been selected for comparison as almost the same CO₂ feeding rate (at about $y_{\text{CO}_2,\text{in}} = 5 \%_{\text{Vol}}$) has been used during measurement of their performance data. Furthermore, a capture rate of about 36 kg day⁻¹ at a capture efficiency > 90 % has been achieved in all operating points.

However, the sorbent circulation rate in the experiment with new heat exchangers has been significantly lower as compared to the former experiments. This resulted in a significantly larger dynamic sorbent loading of 9.06 %_w (see Table 6.4) and thus to a better exploitation of the adsorption capacity of the used adsorbent.

The combination of larger heat transfer surfaces and lower sorbent circulation rate resulted in a significant improvement of the operating temperatures within the BSU. In average the stage temperatures within the desorber increased by about 10 °C. Due to the excellent CO₂ capture performance achieved in OPT 4, the adsorption activity in the uppermost adsorber stage (Stage 5) was very low and the improved cooling situation led to a temperature drop below 70 °C. Nevertheless, the new heat exchangers within the adsorber led to a better controllability of the stage temperatures.

Comparison of the results obtained from the experiments with the new heat exchanger design showed a clear and significant improvement of the process performance. Thus, the previous assumption that the heat exchange with the system limits the BSU operating performance can be seen as validated.

6.4.4 Variation of stripping gas composition

The aim of the conducted experiment was to investigate the influence of the stripping gas composition on the performance parameters of the CO₂ capture system. The used stripping gases have been N₂ (dry regeneration), steam and mixtures thereof.

Throughout the experiment, the flow rate of the (dry) adsorber feed gas has been held constant at 16.8 Nm³·h⁻¹. The composition of the synthetic flue gas was adjusted to a constant mixture of CO₂ (7.67 %_{Vol}) and N₂ (balance to 100 %_{Vol}). The desired adsorber temperature was again 75°C and has been controlled by adjusting the cooling media flow rate through the individual adsorber stage heat exchangers. The desired operating temperature of the desorber was 120°C, whereas the thermal-oil forward flow temperature of the heating circuit was set to 145 °C. The sorbent circulation rate between both contactors was held constant at 31.6 kg·h⁻¹.

For system start-up and for the first period of the actual experiment, N₂ served as stripping gas. During the experiment N₂ was continuously replaced by superheated steam (from 0 to 100 %_{Vol} in steps of 25 %_{Vol}). For dry regeneration the total stripping gas feed flow was 8 Nm³·h⁻¹, whereas during steam regeneration about 10 kg·h⁻¹ of steam was fed into the desorber.

Figure 6.12: BSU parameter assessment – variation of the stripping gas composition (adapted from [Dietrich, 2014]).

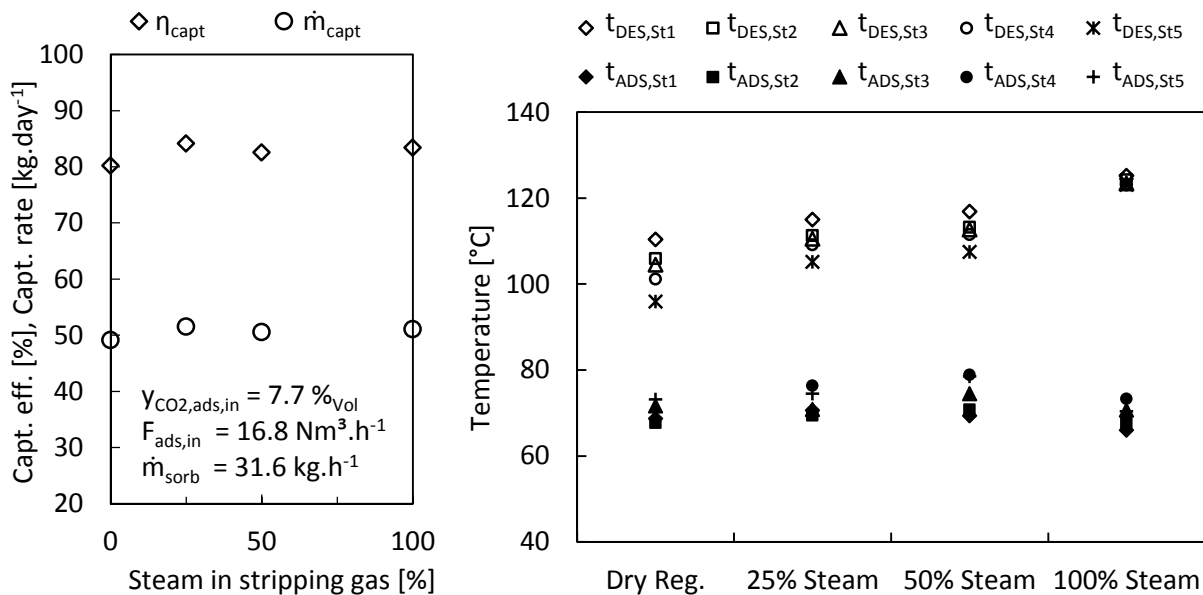


Figure 6.12 shows the results obtained from the variation of the stripping gas composition. The figure on the right shows the temperature distribution within the adsorber and desorber column, whereas the left figure illustrates the unit performance data in terms of the obtained CO₂ capture efficiency and capture rate.

As one can see from Figure 6.12, increasing steam concentrations had a positive effect on both BSU performance parameters. Moreover, as soon as steam was present within the stripping gas, a significant change of the operating temperatures of each desorber stage has been observed. For dry

regeneration a temperature distribution from 96°C (uppermost stage, Stage 5) to 110°C (lowermost stage, Stage 1) was measured in the desorber. Dry regeneration led to a capture efficiency of 80 %. The maximum capture efficiency (84 %) was measured with 25 %_{Vol} steam content within the stripping gas. For a further increase of the steam concentration the capture efficiency decreased to 82 % (50 %_{Vol} steam) and 83 % (100 % steam). However, with increasing steam concentration in the stripping gas a significant increase of the desorber temperatures with decreasing axial temperature difference has been observed.

The obtained results clearly indicate that the adsorbent material interacted with steam fed into the desorber. It is assumed that steam was continuously adsorbed onto the sorbent material within the desorber column. Steam adsorption activity increased with increasing steam content of the stripping gas since this led to an increased steam partial pressure which represents the driving force for steam adsorption.

The adsorption of CO₂ delivered as well as the sensible heat stored within the adsorbent material delivered the required heat for desorption of steam. As the adsorber feed gas was completely dry, no severe condensation of desorbed steam has been observed. The desorbed steam only increased the relative humidity of the adsorber off-gas. However, some condensation was observed on the surface of the adsorber stage heat exchangers as their surface temperatures had been significantly lower than the bed temperatures shown in Figure 6.12. The formed film of condensate led to some coverage of the cooler surfaces with adsorbent material that adhered on the film.

In contrast to the interaction between sorbent material and CO₂, interaction with steam led to a heat release within the desorber and a heat demand within the adsorber, hence causing a desirable internal heat displacement effect. This seems to be highly promising for large scale applications of the TSA system as this effect could drastically improve the heat transfer situation within both reaction zones. It is obviously possible to achieve the desired operating temperatures with less required internal heat transfer surface. In other words, the use of steam as stripping agent reduces the heating and cooling duty of the individual heat exchangers. It could potentially even reduce the overall energy requirement of the TSA system if steam is chemisorbed onto the adsorbent surface (heat of reaction > heat of evaporation). However, this needs to be validated within dedicated steam adsorption tests that are accompanied by mass and energy balance calculations. Furthermore, the achieved process temperatures did not lead to the expected performance increase compared to dry regeneration performance. It is believed that this is most likely caused by occupation of potential CO₂ adsorption sites through co-adsorbed steam, which is especially the case in the uppermost adsorber stage that in turn determines the finally achieved CO₂ capture performance.

Another aspect is that the treated flue gas in this experiment was completely dry. This will never be the case in practical applications even if significant efforts for drying are being made. It is expected that the water content within a typical industrial flue gas could diminish the internal heat displacement effect.

6.4.5 Variation of flue gas humidity

The aim of this experiment was to assess the influence of flue gas humidity on the operation of the BSU. For this reason steam was added to the dry adsorber feed gas stream that has been fed at a constant rate of 16.8 Nm³·h⁻¹ and with a constant CO₂ feed concentration of 7.65 %_{Vol}. For humid feed gas tests, N₂ in the adsorber feed gas has been replaced partly by steam so that the desired

steam concentration was achieved. During the complete experiment, the sorbent circulation rate was kept constant at $31.5 \text{ kg}\cdot\text{h}^{-1}$. The desired adsorber temperature was again 75°C and it has been controlled by adjusting the cooling media flow rate through the individual adsorber stage heat exchangers. The cooling media forward flow temperature was adjusted to 20°C by means of a fresh water cooled plate heat exchanger. The desired operating temperature of the desorber was 120°C , whereas the thermo-oil forward flow temperature of the heating circuit was set to 145°C .

The influence of the flue gas humidity has been studied in two different experiments. In the first experiment, pure nitrogen was used as stripping gas agent (later referred to as dry regeneration experiment), whereas in the second experiment steam was used as stripping gas agent (later referred to as steam regeneration experiment). For the dry regeneration experiment the stripping gas flow rate was set to $11 \text{ Nm}^3\cdot\text{h}^{-1}$, whereas in the steam regeneration experiment it was set to about $9.5 \text{ kg}\cdot\text{h}^{-1}$. The results obtained from both experiments will be discussed in the following.

Dry regeneration

This experiment was conducted with dry and humid adsorber feed gas streams. For humid adsorber feed gas conditions, the steam feed concentration was adjusted to $5\%_{\text{vol}}$. The resulting gas stream had a dew point temperature of 33.1°C and a relative humidity of 13% (for $t = 75^\circ\text{C}$ and $p = 101325 \text{ Pa}$).

Figure 6.13: BSU parameter assessment - variation of flue gas humidity (dry regeneration).

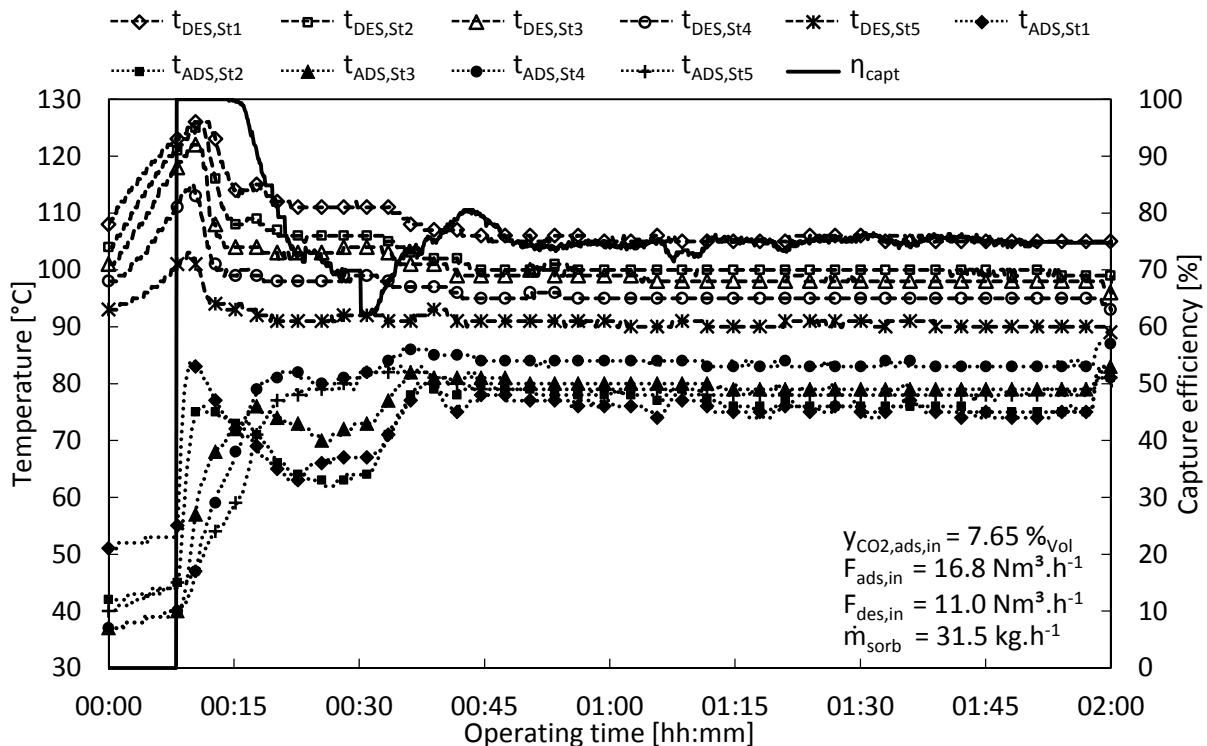
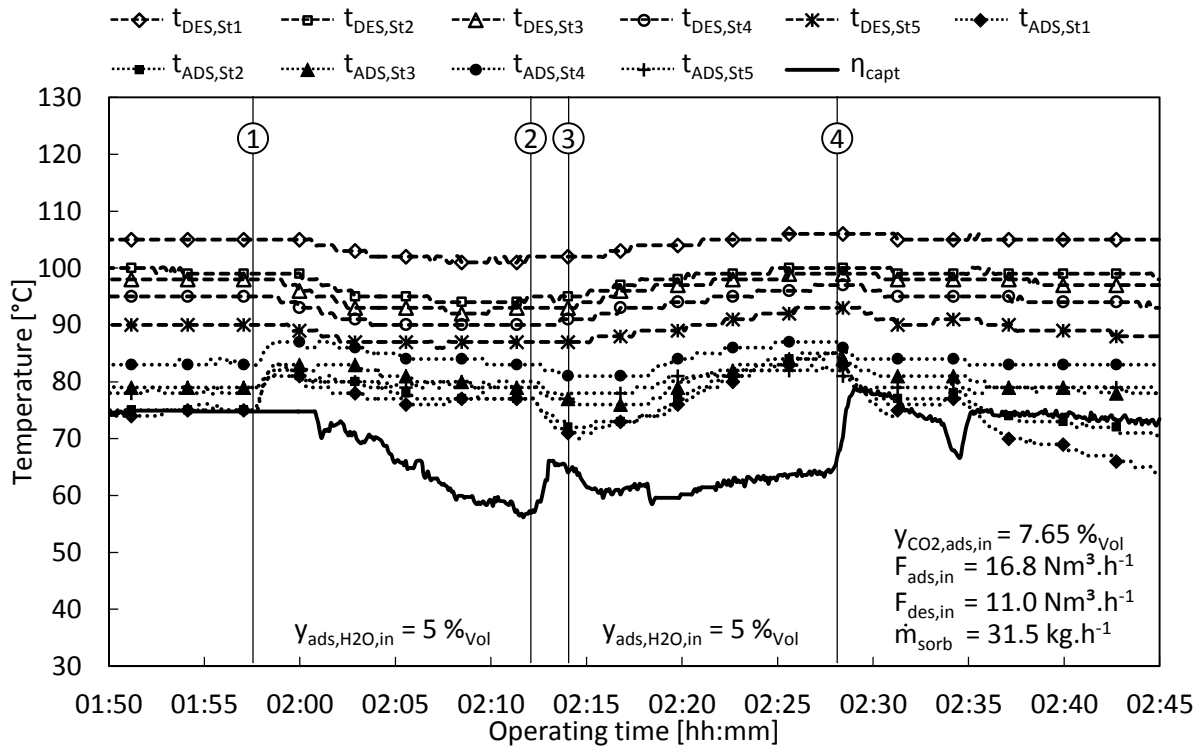


Figure 6.13 and Figure 6.14 show the time course of the individual bed temperatures within the ad- and desorber together with the achieved CO₂ capture efficiency. The first few minutes in Figure 6.13 show the last period of the BSU start-up phase. Then, at about 10 minutes of operation, CO₂ was fed into the adsorber at the aforementioned concentration. At this time the adsorber feed gas was completely dry and after about 50 minutes, steady state operation at a CO₂ capture efficiency of 75% was reached. This operation mode was maintained for a further hour, till it was started to add

steam into the adsorber feed gas. The beginning of the humid flue gas feed is marked as point “1” within Figure 6.14.

Figure 6.14: BSU parameter assessment - variation of flue gas humidity (dry regeneration).



Immediately after switching from a dry to a humid adsorber feed gas stream the temperatures within the adsorber increased significantly and the cooling media flow had to be increased in order to get back to the desired adsorber operating temperature of 75 °C. After a few minutes of operation the desorber temperatures began to decrease, which was accompanied by a significant decrease of the CO₂ capture performance.

From this result it is clear that again an interaction between the steam present within the adsorber feed gas and the adsorbent material occurred. Again it is most likely that steam adsorbed onto the adsorbent material, but this time within the adsorber, whereas desorption of steam occurred within the desorber. Consequently, the interaction between steam and adsorbent material caused an additional cooling demand in the adsorber as well as an increased heating demand within the desorber.

After about 15 minutes of operation with humid adsorber feed gas the CO₂ capture efficiency dropped down to a value of 55 %. Meanwhile, a layer of adsorbent material was built up on the internal adsorber stage heat exchangers as a film of condensate was formed on their surfaces and adsorbent material adhered to this film. Thus, the steam feed into the adsorber was turned off (time mark “2”). Virtually instantaneously, the adsorber temperatures dropped again and the CO₂ capture efficiency increased significantly. After only a short period of time steam was again added to the system (time mark “3”) and the capture efficiency dropped similar as before. However, this time the adsorber temperatures increased only slowly as the cooling flow rate was significantly larger as compared to time mark “1”.

Immediately after steam introduction into the adsorber feed gas, adsorbent layers began again to form on the surfaces of the adsorber stage heat exchangers. Consequently, the adsorber cooling

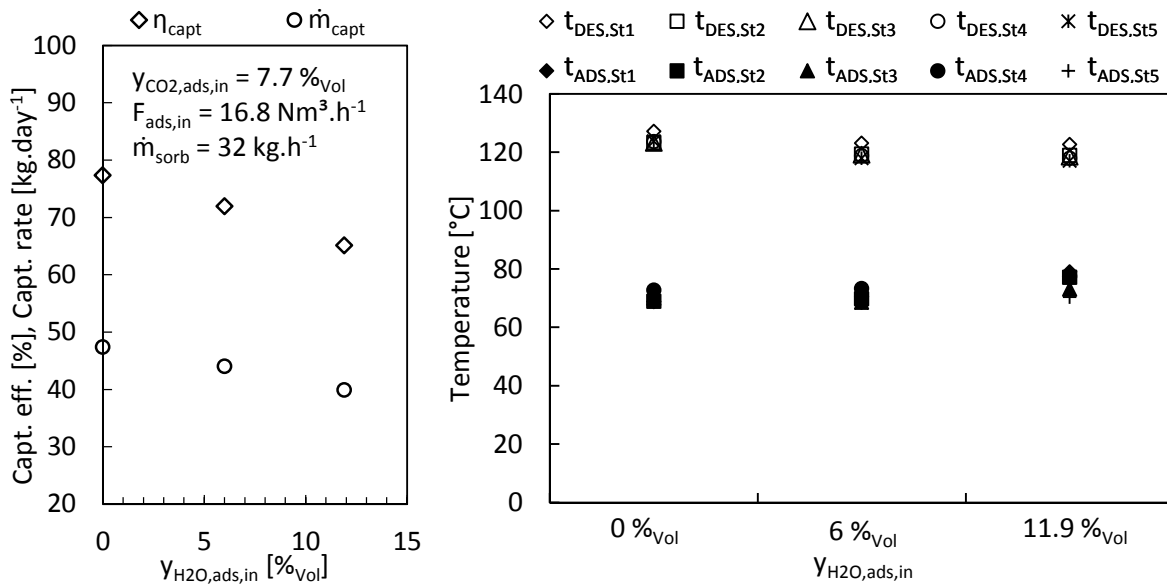
performance dropped and the temperatures within the complete system began to rise, whereby the CO₂ capture efficiency increased slightly. After further 15 minutes of operation with humid feed gas, the adsorbent layer around the adsorber stage heat exchangers had grown to a size that impeded proper operation of the BSU. Thus, it was decided to stop the experiment and to switch back to operation with dry adsorber feed gas (time mark “4”). Again the CO₂ capture efficiency increased significantly, right after the introduction of the humid adsorber feed was stopped. Introduction of dry gas feeds in both columns led to drying of the surfaces within the adsorber and after several minutes of operation the adsorbent layers on the heat exchanger surfaces started to shrink again. At the end of the time scale shown in Figure 6.14, the same operating performance as prior introduction of humid adsorber feed gas was reached. This indicates that the adsorbent material did not degrade through contact with the humid feed gas during this short period of operation. However, adsorbent material from the heat exchanger layers had to be removed as they had formed stable agglomerates that were not fluidizable.

Steam regeneration

In this experiment the relative humidity of the adsorber feed gas was changed in three steps, from 0 to 16 and 31 %, which corresponds to volumetric steam feed concentrations of 0 to 6 and 11.9 %_{Vol}. The resulting dew point temperatures for the individual humid feed gas streams were 36.4 °C and 49.5 °C, respectively (for $t = 75$ °C and $p = 101325$ Pa).

Figure 6.15 shows the obtained BSU performance parameters (left figure) and operating temperatures (right figure) for the three studied relative humidities of the adsorber feed gas.

Figure 6.15: BSU parameter assessment - variation of flue gas humidity (steam regeneration) (adapted from [Dietrich, 2014]).



As compared to the dry regeneration experiment, the obtained operating temperatures of the desorber stages have been significantly higher for all three tested flue gas humidities. As discussed already in Section 6.4.4 this temperature difference is most likely caused by continuous adsorption of steam within the desorber and desorption of steam within the adsorber column. However, considering the course of the operating temperatures, it seems like the introduction of humid adsorber feed gases weakened this heat displacement effect from steam regeneration. Comparison

of the obtained desorber operating temperatures identifies a temperature decrease from $t_{DES,St1} - t_{DES,St5} = 127\text{ }^{\circ}\text{C} - 123\text{ }^{\circ}\text{C}$ for dry adsorber feed gas to $t_{DES,St1} - t_{DES,St5} = 123\text{ }^{\circ}\text{C} - 117\text{ }^{\circ}\text{C}$ for a relative adsorber feed gas humidity of 31 %. On the other hand, the corresponding adsorber temperatures increased from $t_{ADS,St1} - t_{ADS,St5} = 69\text{ }^{\circ}\text{C} - 73\text{ }^{\circ}\text{C}$ to $t_{ADS,St1} - t_{ADS,St5} = 70\text{ }^{\circ}\text{C} - 79\text{ }^{\circ}\text{C}$. This indicates, that desorption of steam became more and more unfavourable in the already humid environment of the adsorber and consequently the obtained adsorbent working capacity with regard to steam adsorption was reduced. Consequently, control of the operating temperatures became more difficult which in turn resulted in increased axial temperature gradients within both columns. The temperature changes in both columns in turn caused a performance drop of the BSU. However, the capture efficiency did not drop as significant as within the dry regeneration experiment. Even after increasing the feed gas humidity in the adsorber to 31 %, the achieved CO₂ capture efficiency was 65 % and thus larger than under dry regeneration conditions and at a relative flue gas humidity of 13 %. Hence, it seems that the negative effect of the flue gas humidity on the BSU performance was significantly smaller when steam was used as stripping gas.

The increased cooling duty within the adsorber that resulted from larger feed gas humidities was again covered by increasing the cooling media flow rates through all adsorber stage heat exchangers. As the forward flow temperature of the cooling media was again significantly lower as the dew point temperatures of the humid feed gases, once more condensation occurred on the surfaces of the adsorber heat exchangers. Adsorbent material again began to adhere onto the condensate film and until a thick layer of adsorbent material was formed around the heat exchangers. As the adsorber feed gas humidity had been increased gradually, the adsorbent layer around the heat exchangers was insignificant during the operation with flue gas humidity of 16 % but increased to an inadmissible size. Consequently, the experiment had to be stopped again and it was concluded that BSU operation with humid adsorber feed gas streams requires measures to control the cooling media forward flow temperature. In order to avoid condensation on the adsorber stage heat exchangers and the resulting formation of adsorbent layers around them, it is essential to lift the cooling media forward flow temperature above the dew point temperature of the adsorber feed gas.

6.5 CONCLUSIONS FROM CONTINUOUS CO₂ CAPTURE TESTS

Successful operation of the constructed bench scale unit clearly proved the feasibility of the proposed double loop multi-stage fluidized bed system for continuous CO₂ capture via temperature swing adsorption.

The desired CO₂ capture efficiency of 90 % together with the target CO₂ capture rate of 34 kg·day⁻¹ have been reached or even surpassed in several experiments. The fact that this performance was achieved with a number of only five practical stages applied to each BSU column indicates that adsorption/desorption kinetics were fast for the used adsorbent material and the studied operating conditions. Moreover, the experiments have been conducted with specific stripping gas feeding and sorbent circulation rates that were close to the rates derived from thermodynamic equilibrium calculations. This implies that equilibrium adsorbent loadings and CO₂ partial pressures have been reached or at least nearly approached inside the BSU.

Altogether, the BSU has been operated for 53 hours including a total of 33.5 hours of continuous CO₂ capture operation. Throughout this experimental campaign the adsorbent material retained its chemical and mechanical integrity. Hence, from continuous BSU operation it can be assumed that

neither amine evaporation nor attrition of adsorbent material seemed to be critical for the used adsorbent material. Nevertheless, a dedicated experimental campaign with long-term operation under realistic operating conditions, using a single batch of adsorbent material, is needed to obtain concrete figures of the needed adsorbent material make-up.

Even though the attrition of adsorbent material has been insignificant, quite a lot of make-up material was needed within the very first experiments. The make-up demand arose from considerable material entrainment out of the columns into the off-gas particle filters. Analysis of the filter material size distribution revealed that the majority of the material was in the size range of the fresh adsorbent material. After the first experiments had been conducted it was thus decided to adapt the freeboards and gas exits ducts of the uppermost stages of both columns in order to reduce the entrainment of viable adsorbent material. These adaptations led to a significantly reduced entrainment of adsorbent material in all following experiments. It was concluded that up-scaled designs of the double loop reactor system will most likely need to comprise suitable particle separators (e.g. cyclones) applied to the gas exit ducts of both columns combined with sufficiently large freeboards of the uppermost stages.

After the functionality of the BSU has been demonstrated successfully, a parameter variation has been conducted in order to assess the influence of selected process parameters on the CO₂ capture performance. The parameters selected for this study were the sorbent circulation rate as well as the relative and absolute CO₂ feeding rate while the process performance was assessed using the CO₂ capture rate and the CO₂ capture efficiency as indicators.

Variation of the sorbent circulation rate showed that both, the CO₂ capture rate and the CO₂ capture efficiency increased with increasing sorbent circulation rate. This aligns with predictions obtained from thermodynamic equilibrium modelling. However, the improved process performance was achieved to the price of a reduced exploitation of the adsorption capacity of the adsorbent material as well as an increased heating/cooling demand within the system. In a commercial application the actual sorbent circulation rate will thus result from a trade-off between a desired minimum CO₂ capture performance and a maximum allowable parasitic energy demand of the process.

It was further shown that increased CO₂ feeding rates led to increasing CO₂ capture rates. In both variations the achieved CO₂ capture rates seemed to approach a maximum while the corresponding CO₂ capture efficiencies dropped drastically with increasing CO₂ feeding rates. This performance limitation was attributed to insufficient heat exchange with the system that was in turn caused by insufficient surface area of the internal stage heat exchangers. This was confirmed in experiments conducted after replacing the initial heat exchangers with heat exchangers of larger heat transfer area as it was possible to achieve a significant improvement of the BSU performance in these tests.

Variation of the stripping gas composition from pure N₂ to pure steam led to increased operating temperatures within the desorber and to a reduced cooling duty within the adsorber column. Utilization of steam as stripping gas agent even facilitated the achievement of desired operating temperatures within both columns. Furthermore, the axial temperature gradients along the individual stages decreased significantly leading to more or less isothermal operating conditions in both columns. This effect on the operating temperatures was most likely caused by continuous adsorption of steam within the desorber column and desorption of said steam inside the adsorber column. The heat for steam desorption was thereby provided by the heat released from CO₂ adsorption which reduced the total cooling duty within the adsorber. The adsorption of steam in the

desorber, however, led to a release of heat that partly compensated the heat demand for CO₂ desorption and heating of the adsorbent material. This effect has thus been referred to as internal heat displacement effect. It had a positive effect on the BSU process performance parameters; even though the performance increase has been comparatively small if one considers that the process operating temperatures had improved significantly. It is believed that adsorbed steam led to a partial blockage of active CO₂ adsorption sites which in turn partly compensated the beneficial effect of a larger temperature swing between adsorber and desorber.

In contrast to predictions from the open literature, a change from dry to humid adsorber feed gas led to a drastic drop of the process performance in all experiments. However, the performance drop was more pronounced in experiments where N₂ was used as stripping gas. The performance drop was obviously caused by an interaction of steam and the adsorbent material, with similar effects on the process heat management as observed in the previously conducted variation of the stripping gas composition. However, in contrast to the beneficial internal heat displacement effect that is obtained by utilization of steam as stripping gas, the adsorber feed gas humidity had a detrimental effect on the process performance. This is because steam was adsorbed by the adsorbent material within the adsorber and needed to be subsequently desorbed within the desorber. Hence, the introduction of humid synthetic flue gas into the adsorber led to an additional cooling duty and heating demand in the adsorber and desorber, respectively. As the installed, internal heat exchanger surface was fixed within the BSU, it was not possible to cover this additional heat exchange requirement in the conducted experiment, which in turn led to a weaker process performance. On top of this, introduction of humid flue gas led to condensation on the internal stage heat exchangers within the adsorber. Adsorbent material adhered onto the formed condensate film until a thick and stable layer of adsorbent material had been formed around the adsorber stage heat exchangers that impeded further operation of the BSU. The reason why condensation occurred was that the forward flow temperature of the cooling media has been below the dew point of the introduced synthetic flue gas. It was thus concluded that for proper operation of the BSU it is either needed to use dried flue gas or to adjust the cooling media forward flow temperature of the adsorber heat exchangers in accordance to the dew point of the treated flue gas.

7. SUMMARY

Most recently published climate change assessment reports emphasized again that anthropogenic greenhouse gas emissions are the main drivers for the observable changes of global temperature levels and global and regional climates. Among the climate active greenhouse gas emissions, CO₂ that arise from the utilization of fossil fuels in power generation, industry or transport has the greatest impact on climate change. However, the contribution of fossil fuels to the world's primary energy demand will remain and most likely even increase in the next decades to come. Thus, policy makers together with international organisations proposed different strategies and technologies to achieve CO₂ emission reductions and mitigation of global climate change.

Among those measures, carbon capture and storage (CCS) may play a significant role for climate change mitigation on a mid-term basis as this technology allows for continued utilization of fossil fuels whilst the emission of CO₂ into the atmosphere is reduced significantly. CCS provides that CO₂ from large point emission sources such as power plants or industrial facilities is separated from the flue gas stream and subsequently transported to a suitable storage site (e.g. depleted oil or gas field) where the CO₂ can be stored and kept out of the atmosphere on a long term. The capture of CO₂ is the most energy-intensive step in the whole CCS process chain, while underground storage is most critical with respect to public acceptance and transport in pipelines or containers require high purity CO₂ to avoid corrosion problems. Deployment of CCS thus relies essentially on the availability of efficient CO₂ capture technologies (CCT) that are capable to capture CO₂ at low costs.

Different CO₂ capture routes have been proposed, whereas post-combustion CO₂ capture (PCC) seems to exhibit many advantages such as simple end-of-pipe application or retrofitting potential for existing CO₂ sources in both power production and industry. Among the PCC technologies discussed today, absorption in aqueous amine solvents is considered as the most mature technology. However, amine scrubbing technologies exhibit several disadvantages that typically result in large process heat demands and CO₂ capture costs. The large process heat demands arise from high heat capacities of the aqueous amine solutions, from the heat of reaction that needs to be supplied during regeneration of the loaded solvent and from the fact that this regeneration step is accompanied by water evaporation. Due to rather low absorption rates, sizeable, packed absorption columns are required to achieve high CO₂ capture rates. Furthermore, solvent degradation products are corrosive, which sets high demands on the utilized materials as well as on off-gas treatment facilities. The corresponding capital costs are thus high and add to the comparably large overall CO₂ capture costs. In the past decades, the development of novel amine solvents together with the elaboration of optimized heat integration strategies led to process improvements and reduced CO₂ capture costs. However, the aforementioned drawbacks of amine scrubbing remain as they are intrinsic to the process so that breakthroughs in the reduction of CO₂ capture costs require the development of alternative capture technologies.

A world-wide effort has thus been put into the search and development of alternative CO₂ capture routes that are capable to capture CO₂ with lower parasitic energy demand and at significantly lower costs. The application of adsorption based processes has been proposed as viable route to achieve this goal. Solid sorbents usually exhibit higher CO₂ working capacities, lower material heat capacities

and lower heat of reaction compared to chemical solvents. Furthermore, evaporation of water in the regeneration step could be avoided completely. Thus, the process energy demand of an adsorption based CO₂ capture process should be markedly smaller compared to an amine scrubbing process which in turn should allow for CO₂ capture at lower costs.

Commercially available physisorbents like activated carbons or zeolites are known to be capable to adsorb CO₂. However, physisorbents typically show weak CO₂ selectivity especially in the presence of water and low adsorption capacities at small CO₂ partial pressures; i.e. at conditions relevant for CO₂ capture from stack flue gas. This circumstance promoted a world-wide effort in the development of novel CO₂ adsorbents. Inspired by the excellent CO₂ absorption properties of amine-based solvents, researchers immobilized amines onto solid support materials and thereby developed a new class of highly selective CO₂ adsorbent materials. This good selectivity is reached through chemical reactions (i.e. chemisorption) that take place between active amine sites on the adsorbent's surface and CO₂ from the bulk gas. The price for this good selectivity is, however, that the chemisorption step is accompanied by the release of comparably large amounts of heat. This heat needs to be withdrawn in the adsorption step and subsequently supplied during desorption of CO₂ in the adsorbent regeneration step. This in turn sets high demands on the heat management capabilities of the adsorption process. On the other hand, it has been shown that larger adsorption enthalpies lead to stronger temperature dependencies of the adsorbent's adsorption capacity. This in turn is beneficial for efficient operation in temperature swing adsorption (TSA) based processes that are, from a techno-economic point of view, considered as superior over pressure swing adsorption (PSA) based processes for stack flue gas CO₂ capture applications. This is because TSA processes require heat input at moderate temperature levels that can be supplied by low-quality steam that is typically available at considered sites for PCC applications while PSA processes would require large amounts of pure exergy (i.e. compressor power) to elevate the pressure of the enormously large flue gas rates.

Up till now not much work has been dedicated to the development of suitable reactor designs for continuous CO₂ capture processes basing on TSA. Performed experiments for adsorbent development were conducted in TGA's and within lab units like fixed beds for batch or single-stage fluidized beds for continuous operation. Even though it is an important step to demonstrate the feasibility of CO₂ adsorbent materials in such lab units, the used configurations cannot be considered as suitable for commercial applications. While fixed bed configurations have the problem of weak up-scale potential through limitations in heat transfer and process control (i.e. quantity of fixed beds and control valves), single-stage fluidized bed configurations face thermodynamic limitations that arise from almost ideal gas-solids mixing behaviour in fluidized beds and that induce uneconomic process operation with low adsorbent working capacities and/or large amounts. Nevertheless, due to their superior heat transfer properties fluidized bed systems are excellently suited for TSA applications, making it worth to find fluidized bed reactor designs that are capable to overcome the aforementioned thermodynamic limitations of single-stage fluidized bed configurations.

The aim of this thesis was thus to develop a TSA reactor system for CO₂ separation from stack flue gas that applies fluidized bed technology and further allows for economic process operation. Basing on thermodynamic considerations, it has been concluded that for economic TSA process operation within a fluidized bed reactor system it is key to provide counter-current contact between gas and adsorbent streams in both gas-solids contactors (i.e. within adsorber and desorber). In fluidized bed

reactors, such a counter-current contact between gas and solid phases can be realized within multi-stage fluidized bed columns. The sectioning of the column into individual fluidized bed stages is achieved through application of gas distributors that permit downwards flow of solids (e.g. through suitable perforations or downcomers) and upwards flow of the gas phase, i.e. the fluidizing agent.

According to these findings, a novel TSA reactor system consisting of interconnected stacked fluidized bed columns serving as adsorber and desorber has been introduced in this work. Both columns consist of a number of individual fluidized stages stacked on top of each other. The individual stages are built up by gas distributors (e.g. perforated plates) and feature bed weirs, immersed bed heat exchangers for indirect cooling/heating of the sorbent material as well as downcomers for controlled solids transport to adjacent stages below. The adsorber is fluidized with the flue gas to be treated in the TSA unit, whereas the desorber is fluidized with a stripping gas agent that could be either steam, CO₂ or a combination thereof. Controlled transport of sorbent material from the bottom stage of one column to the top stage of the respective other column is performed in two separate recirculation lines. Each of these transport lines consists of an adjustable adsorbent conveyor (e.g. L-valve or mechanical screw), a pneumatic transport riser as well as a gas-solids separator at the top of the transport riser that directs the sorbent material into the top stage of the column. The lifting gases within the transport risers are recirculated in closed loops and gas sealing between the columns is achieved through controlled introduction of purge gas streams into the moving beds that are formed between the solids exit ducts of the columns and the adsorbent conveyors. The transport risers may additionally exhibit heat exchangers that enable heat exchange between hot particles leaving the desorber and colder particles leaving the adsorber (i.e. lean/rich heat exchanger). As the adsorbent material performs an overall figure-eight movement within this proposed reactor systems it has been named "Double-loop multi-stage fluidized bed system for continuous and effective temperature swing adsorption".

The key role of the counter-current contact within a TSA fluidized bed system has been confirmed in this work using a mass and energy balance based thermodynamic equilibrium model. The simulations clearly showed that multi-stage configuration is essentially needed as single-stage configurations would lead to enormous regeneration energy demands due to significantly large sorbent circulation rates and stripping steam demands. The equilibrium model has further been used to evaluate the proposed TSA process within the proposed reactor system against state-of-the-art amine scrubbing technologies on the basis of their respective process energy requirements. The simulations showed that the TSA technology is at least competitive in terms of regeneration energy demand compared to state-of-the-art MEA. However, the regeneration energy demand of the TSA process has been determined without considering energy recovery from high level heat integration measures (except from lean-rich heat exchange).

In order to assess the fluid-dynamic feasibility of the proposed double-loop multi-stage fluidized bed reactor system, a cold flow model (CFM) has been designed, constructed and put into operation. The design of the used CFM has been determined using desired operating parameters of the planned, continuously operating TSA bench scale unit (BSU). Since the double-loop multi-stage fluidized bed reactor system exhibits a symmetrically design it was sufficient to conduct the fluid-dynamic study on one half of the system only. Hence, the CFM consisted of only one multi-stage fluidized bed column and a single transportation line that redirected the particulate solids back to the top of the column. The column comprised five individual fluidized bed stages built up above perforated plate gas

distributors. The stages exhibited exchangeable weir plates and downcomers as well as copper coils as dummy heat exchangers. Polystyrene particles have been used as bed material during the CFM experiments, whereby an adequate particle size has been selected to achieve fluid-dynamic similarity between the operating conditions in the CFM and those present within the adsorber of the BSU. During commissioning of the CFM it turned out that the application of downcomer flap valves (or alternative measures to control the empty downcomer pressure drop) is essential for start-up of the multi-stage fluidized bed column. The conducted CFM campaign clearly proved the fluid-dynamic function of the proposed reactor system. Variations of the solid circulation, the column fluidization rate, the stage weir height and the solids inventory have been conducted to assess the influence of the respective operating parameter on the solids distribution within the reactor system. It was shown that the solids capacities of the upper stages is a function of the first three stated operating parameters, whereas the solids capacity within the lowermost stage is additionally affected by the total solids inventory within the system. This circumstance helps to control the distribution of the solids inventory between both columns in the double-loop system. An additional parameter variation has been conducted to study the dense phase expansion of a single fluidized bed within the column using long-time exposure photography. Obtained results revealed that the dense phase expands with increasing weir height and sorbent circulation, whereas it stays almost constant with varying column fluidization rate and solids inventory. However, increasing column fluidization rates led to a dilution of the dense phase, i.e. to an increasing voidage within the dense phase. The promising outcome of the CFM test campaign motivated the construction of a continuous TSA bench scale unit (BSU) in order to demonstrate continuous CO₂ capture operation within the proposed reactor system.

Basing on the findings from CFM experiments a fully integrated TSA-BSU has been designed, constructed and put into operation. The BSU consists of two columns, each of them comprising a series of five fluidized bed stages. The individual stages feature perforated plate gas distributors, adjustable bed weirs, immersed bed heat exchangers for indirect cooling/heating and downcomers to permit downwards transport of adsorbent material. Synthetic flue gas mixtures and N₂ or steam serve as fluidizing agents in the adsorber and desorber, respectively. Controlled transport of sorbent material between the columns is performed via adjustment of the driving speed of the mechanical screw conveyors located within each recirculation line.

Prior conducting continuous CO₂ capture experiments within the BSU, a pre-test has been dedicated to the assessment of gas leakages between both fluidized bed columns as well as of the function of the purge gas sealing method. Results from this pre-test revealed that for the operating ranges of interest, the gas leakage between both columns can be neglected. After introduction of purge gas it was not possible to detect any gas leakage, which proved the feasibility of this sealing measure. After the completion of the commissioning phase the BSU has been put into operation. One of the very first experiments conducted in the BSU delivered a successful proof of concept for the TSA process within the proposed reactor system. Stable operation with CO₂ capture efficiencies above 90 % at a total CO₂ capture rate of 35 kg·day⁻¹ and an dynamic sorbent loading of 5.5 %_w has been achieved using a synthetic flue gas mixture with 5 %_{vol} CO₂ feed concentration and N₂ as stripping gas agent. Further experiments included variations of the main operating parameters, i.e. the sorbent circulation rate, the relative CO₂ feeding rate (CO₂ concentration in treated flue gas) and the absolute CO₂ feeding rate (flue gas feeding rate at constant CO₂ concentration). The assessment of these operating parameters revealed that the process performance in terms of absolute CO₂ capture rate

increases with increasing sorbent circulation and CO₂ feeding rate. The CO₂ capture efficiency also increased with increasing sorbent circulation rate to the price of lower dynamic sorbent loadings, whereas it dropped significantly with increasing CO₂ feeding rates. This performance limitation has been attributed to insufficient heat exchange with the system that was in turn caused by insufficient surface area of the internal stage heat exchangers. This explanation has been confirmed in experiments conducted after replacing the initial heat exchangers with heat exchangers of larger heat transfer area as it was possible to achieve a significant improvement of the BSU performance in these tests. The first experimental campaign within the BSU has been conducted with completely dry synthetic flue gas mixtures as adsorber feed gas and with pure N₂ as stripping gas within the desorber. Thus, the last experimental campaign within the BSU has been dedicated to demonstrate the feasibility of steam as stripping gas agent in the desorber and to assess the impact of the presence of water in the adsorber feed gas. Replacement of N₂ as stripping agent by steam revealed an internal heat displacement effect that caused a temperature increase in the desorber and a reduced cooling demand in the adsorber. It has been concluded that this effect is most likely based on steam adsorption that takes place within the desorber and subsequent desorption of steam in the adsorber. The corresponding steam adsorption enthalpy led to an overall heat input in the desorber that helped to achieve the desired desorber operating temperatures for the first time during continuous operation of the BSU. On the adsorber side, the released heat from CO₂ adsorption provided the necessary energy required for desorption of steam and led to an overall reduced cooling demand in the adsorber. Unlike expected, only a slight performance improvement has been observed with increased temperature swing between adsorber and desorber. It is expected that pre-adsorbed steam partially blocked active adsorption sites on the adsorbent material so that they have not been available for CO₂ adsorption in the upper stages of the adsorber. Contrary to the beneficial internal heat displacement obtained by utilization of steam as stripping gas, the introduction of humid adsorber feed gas had a detrimental effect on the process performance. Two different experiments with humid adsorber feed gas have been conducted; the first with N₂ (dry regeneration) and the second using steam (steam regeneration) as stripping gas. During dry regeneration adsorption of water from the adsorber feed gas stream adsorbed within the adsorber and subsequently desorbed within the desorber. Hence, the introduction of humid synthetic flue gas into the adsorber led to an increased cooling and heating demand in the adsorber and desorber, respectively. As a consequence of the limited heating and cooling capacity within the BSU, the process performance dropped significantly. However, the performance drop was more pronounced in experiments where N₂ was used as stripping gas. A further performance drop occurred due to formation of an adsorbent layer on the adsorber heat exchangers after water started to condense at that point where dew point of the introduced synthetic flue gas was higher than the forward flow temperature of the cooling media. It was thus concluded that for proper operation of the BSU it is either needed to use dried flue gas or to adjust the cooling media forward flow temperature of the adsorber stage heat exchangers in accordance to the dew point of the treated flue gas.

The results obtained from theoretical process evaluation and continuous CO₂ capture experiments at bench scale clearly indicated the suitability of the proposed double-loop multi-stage fluidized bed reactor design for the continuous CO₂ capture process basing on TSA. In the following the main conclusions from this work should be drawn and an outlook on potential next steps in the TSA process development should be given.

8. CONCLUSIONS

Within this thesis, a novel reactor system for continuous CO₂ capture from stack flue gas via temperature swing adsorption has been proposed, evaluated in terms of thermodynamic equilibrium calculations and fluid-dynamic cold flow modelling and further investigated during continuous operation at bench scale. The main conclusions that can be drawn from this work should be given in the following.

Fundamental thermodynamic considerations indicated that single stage fluidized bed reactor designs are not advantageous for TSA CO₂ capture because of thermodynamic limitations that arise from the well-mixed particle phase. From a thermodynamic point of view a TSA process essentially requires counter-current movement of gas and sorbents within both contactors. Such reactor designs can easily be achieved by application of fixed or moving bed systems. However, a TSA process additionally requires exchange of large amounts of heat per captured mass of CO₂ and fluidized bed systems are superior over fixed or moving bed configurations in terms of heat transfer. Thus, a reactor system of interconnected multi-stage fluidized bed columns has been proposed that allows for both counter-current movement of phases in both contactors and achievement of maximum heat transfer rates between adsorbent material and internal heat transfer surfaces. Furthermore, the design proposal includes aspects of solids transport and gas sealing between the two contacting devices.

A principal thermodynamic evaluation of a two times five stage concept using reported Langmuir parameters of a polyethyleneimine (PEI) impregnated adsorbent revealed an energy demand of the TSA process of 3.5 MJ per kg CO₂ captured, which is slightly lower than reported values for liquid amine CO₂ capture systems. This means, in terms of process energy demand the TSA technology is at least competitive to state-of-the-art technology. However, it can be expected that application of improved heat integration measures to the TSA process will lead to further reductions of the process energy demand (examples for potential heat integration measures are given in the outlook of this thesis). Moreover, the low number of only five theoretical stages that has been used for process evaluation together with the expectable low heights of the bubbling fluidized bed stages indicates great advantages over scrubbing technology with respect to capital costs. Last but not least, the utilization of amine functionalized adsorbent materials instead of aqueous amine solutions is expected to significantly reduce corrosion issues which represents an additional potential for cost reductions. Therefore, from a techno-economic point of view it can be concluded that the proposed TSA process can be considered as promising alternative to state-of-the-art post combustion CO₂ capture technologies.

Results obtained from cold flow model testing showed that from a fluid-dynamic point of view stable operation within a broad range is possible within the chosen design of the multi-stage fluidized bed column. For system start-up, however, an active control of the empty downcomer pressure drop is needed in order to avoid defluidization of the stages and to enable stepwise filling of the column from the top to the bottom stage. The dense phase within the fluidized bed of a single stage has been investigated using long-time exposure photography. Results from this study revealed that the dense phase expansion is a function of the used stage weir height and the solids mass flow through

the stage. Furthermore, the dense phase expansion has been significantly below the edge of the used weir plates under all operating conditions studied. Variation of the column fluidization rate seemed to have almost no effect on the dense phase expansion. However, the apparent dense bed voidage seemed to increase with increasing fluidization rate. It is important to know these dense phase characteristics when it comes to correct estimation of the solids pressure drop within the column (i.e. maximum weir height per stage under given operating conditions) or designing of the internal heat exchangers sufficiently as large heat transfer coefficients can only be expected within the dense phase itself.

The suitability of the proposed TSA process design for continuous capture of CO₂ has been demonstrated in several experiments that have been conducted within a fully integrated bench scale unit (BSU). Results obtained from continuous CO₂ capture experiments showed that CO₂ capture efficiencies above 90 % can be achieved with comparably large dynamic sorbent loadings and sufficiently low stripping gas demands. These excellent results have been achieved with a number of only five stages within both contactors of the BSU, which indicates that adsorption/desorption kinetics are fast and adsorption equilibrium is approached within the system. The fast adsorption/desorption kinetics have a large impact on the design of commercial scale TSA units, as they allow for application of rather compact designs. This confirms that significantly lower capital costs and plant footprints can be expected from TSA plants compared to amine scrubbing units.

The CO₂ capture capacity within the BSU, however, exhibited a maximum that increased after replacing the initial stage heat exchangers by heat exchangers with larger heat transfer surface. This clearly indicated that the CO₂ capture capacity of a TSA process is limited by the heat exchange capabilities of the process equipment rather than by the adsorption/desorption kinetics. In order to maximise the CO₂ capture capacity of a TSA process it is thus crucial to optimise the heat transfer conditions within the system. For instance, this can be done by increasing the surface to volume ratio of the internal stage heat exchangers so that more surface area contributes to the heat exchange. Furthermore, the achievable heat transfer coefficients between internal heat exchanger surfaces and adsorbent material can be increased through proper choice of the adsorbent material size and fluidization state. It can be expected that smaller particle would lead to increased heat (and mass) transfer coefficients and thus to enhanced process performance. For a given fluidization number, smaller adsorbent particles, however, would require larger cross sections of the contactors in order to treat the same flue gas volume flow. On the other hand, the improved heat transfer would allow for smaller sized internal heat exchangers. Thus, the choice of a suitable adsorbent particle size is not a straight-forward procedure since it has a direct impact on achievable heat and mass transfer rates, on the TSA plant footprint and on the overall capital costs. However, it can be expected that for a required CO₂ capture capacity (i.e. for a given number of required heat transfer surface) it will be intended to minimize the overall capital costs and/or to achieve a TSA plant footprint that fits into the available installation space at the considered erection site.

Changing the stripping gas composition in the desorber from pure N₂ to steam had a great impact on the operating temperatures and the overall heating and cooling requirements within the BSU. It appears that co-adsorption of steam took place in the desorber which in turn led to the release of adsorption heat. The “wet” adsorbent material was continuously regenerated within the dry atmosphere of the adsorber where the heat released from CO₂ adsorption led to desorption of steam. This led to an overall reduced cooling demand within the adsorber. Consequently, the

operating temperatures within all stages of both contactors approached the desired operating temperatures for the first time. While during dry regeneration experiments the operating temperatures along the stages of both contactors exhibited a more or less significant temperature gradient, the gradient narrowed in both columns during steam regeneration. This effect was more pronounced when the synthetic flue gas feed into the adsorber was dry compared to the experiments where humidified flue gas has been introduced. Since the internal heat displacement effect from steam co-adsorption led to larger temperature swing between the contactors of the BSU one would have expected an improved CO₂ capture performance compared to dry regeneration. However, in fact only a small performance increase has been observed during steam regeneration

No significant adsorbent degradation has been observed during more than 30 h of continuous CO₂ capture experiments. However, adsorbent make-up had to be added during this operation period as a result of significant material entrainment out of the top stages of both columns. For assessment of the mechanical stability of the adsorbent material during continuous operation it is thus required to reduce the adsorbent entrainment out of the BSU and to conduct further dedicated long-term tests. The same applies for the assessment of the chemical stability of the adsorbent material. However, as it was possible to reproduce individual BSU operating points after several hours of operation and with almost no adsorbent make-up, it appears as if adsorbent degradation is within an acceptable range. Furthermore, it has been shown in continuous BSU experiments that condensation of water within the TSA system leads to immediate adhesion of adsorbent materials and to formation of agglomerates that can cause malfunction of the CO₂ capture unit. Hence, it is crucial to avoid water condensation at any location of the TSA system at any time.

9. OUTLOOK

It was of course impossible to cover all necessary development steps of the TSA technology and to address all related research questions within the context of this thesis. Within this chapter, the author would thus like to take the liberty to give some suggestions for further work that needs to be done from his perspective to bring TSA CO₂ separation processes towards commercialization. Thereby, a distinction is made between suggestions for additional experimental bench scale studies and further development and optimization of the TSA process:

Additional experimental studies at bench scale

Additional BSU experiments should be conducted to obtain further operating experience and understanding of the TSA process. These experiments should include detailed parameter studies to characterize the BSU operation and to assess operation limits of the process.

Dry regeneration experiments should be conducted to confirm that adsorption equilibrium is approached within the BSU or to assess the derivation from adsorption equilibrium, respectively. This would require the measurement of CO₂ concentrations and/or the heat exchange in each stage as well as knowledge of the thermodynamic equilibrium data (i.e. Langmuir parameters) of the used adsorbent material. The CO₂ adsorption equilibrium data can be derived from separated TGA or fixed bed experiments. Experimentally derived data can then be compared with results obtained from the developed thermodynamic equilibrium model using the derived adsorbent data and operating conditions that had been measured within the respective BSU experiment (i.e. temperatures, pressures, gas compositions, volume flow rates and sorbent circulation rate). If it turns out that adsorption equilibrium is approached within the BSU, then the assumptions made in the developed equilibrium model can be considered as correct and the model could be directly used for future tasks in TSA process design.

The interaction between steam and the PEI impregnated adsorbent material should be studied and the underlying mechanism (i.e. chemisorption or physisorption) should be identified. Multi-component adsorption equilibrium data for CO₂ and steam should be derived for the used adsorbent material. Derived adsorption equilibrium parameters should then be integrated into the existing thermodynamic equilibrium model. The updated model can then be used to assess the impact of the internal heat displacement effect on the process economics as well as for further tasks regarding process design. An obvious benefit derived from co-adsorption of steam is that it helps to achieve the desired operating temperatures within the regenerator. This in turn could help to reduce the required heat exchanger surface and thus the capital expenses. However, the benefit could be even greater in case that steam chemically interacts with the adsorbent material. The corresponding adsorption enthalpy would then be in the range of the reaction heat. As a consequence the co-adsorbed steam would release more heat within the desorber as required for steam production. The difference between both enthalpies is supplied by the released heat from CO₂ adsorption in the adsorber and thereby reduces the cooling demand of the process significantly. The exploitation of this benefit would require that the dew point temperature of the treated lies far below the adsorber operating temperature so that the relative humidity of the adsorber off-gas is small enough to give

enough driving force for steam desorption. Adjustment of the flue gas dew point temperature could be achieved through a sub-cooling step upstream to the TSA unit, whereas it is worth to mention that cooling of the flue gas is anyway required. Another advantage of controlling the flue gas dew point is that it helps to avoid water condensation within the adsorber.

So far, synthetic flue gas mixed from N_2 and CO_2 bundles has been used as adsorber feed gas during the conducted BSU experiments. Thus, the effect of oxygen and other species, such as nitrogen-oxides (NO_x) or sulphur-oxides (SO_x) on the TSA process performance has not been studied in these experiments. However, these species are typical constituents of flue-gases and it has been reported that these components may lead to degradation of amine functionalized adsorbent materials. Prior further actions are taken towards up-scaling of the TSA process it is thus considered necessary to study the process performance under realistic operating conditions, i.e. with practical synthetic flue gas mixtures or even with real flue gas derived from an industrial facility.

Further BSU experiments should be dedicated to the assessment of amine emissions from the unit. The off-gas streams of both columns should be examined for amine contaminations under different operating conditions (e.g. synthetic vs. real flue gas, dry vs. steam regeneration, etc.) and conclusions on off-gas treatment measures should be drawn.

Long-term BSU experiments should be conducted under practical operating conditions in order to assess the mechanical and chemical stability of the used adsorbent material. Particle life-time figures should be derived from these tests and used for more detailed techno-economic process evaluations.

As pointed out in Section 3.2 of this thesis, numerous amine functionalized adsorbent materials that are suitable for selective CO_2 capture from stack flue gas have been developed over recent years and further material development and optimization is still in progress. Thus, it is highly recommended to have alternative adsorbent materials tested within the BSU. This would allow for studying the performance of separate adsorbent materials under practical operating conditions and to identify optimal adsorbent properties for further adsorbent development.

TSA process development and optimization

Conducted BSU experiments revealed that heat transfer between internal heat exchanger surfaces and adsorbent material may be the limiting factor within the TSA process. In order to achieve maximum CO_2 capture rates within a TSA system it is thus required to maximize the heat transfer rates within the system. Beside the optimization of adsorbent diameter and fluidization conditions this can be achieved through maximizing the available heat exchanger surface for a given bed volume. Thus, optimized heat exchanger designs should be developed and enhanced heat transfer properties should be confirmed experimentally. Advanced designs may comprise finned tubes or tubes with pins welded onto their surface.

It has been pointed out that application of sufficient heat integration measures can reduce or even completely eliminate individual heating or cooling demands of the TSA process and thereby lead to optimized process economics. However, the opportunities for application of such heat integration measures will most likely differ from site to site. The feasibility of some heat integration measures may depend on the availability of related process equipment that needs to be developed first. Moreover, application of such heat integration measures might increase the process capital expenses to such an extent that the overall CO_2 capture costs increase even though the process energy requirement drops. Thus, it is necessary to assess the potential of different heat integration

measures prior application. This in turn requires the development of suitable process simulation tools and the availability of concrete figures concerning additional equipment costs.

The following heat integration measures are expected to have a great potential for process optimization and may be considered within the first assessments:

1. Staged **wet compression** of total desorber off-gas stream for generation of stripping steam demand and partial generation of desorber heating steam.
2. Efficient **lean/rich heat exchange** in the adsorbent recirculation lines from regenerated adsorbent material extracted from the desorber to loaded adsorbent material extracted from the adsorber.
3. Application of a **heat displacement system** (i.e. process heat pump) that is capable to utilize heat released from CO₂ adsorption that takes place at moderate temperature levels within the adsorber to provide the necessary heat for adsorbent regeneration at elevated temperature within the desorber.

Even though the suitability of the double-loop multi-stage fluidized bed reactor system for continuous CO₂ capture via TSA has been demonstrated successfully, further process design optimizations should be considered and investigated for future applications.

Two potential alternative TSA process designs that are improved with respect to overall capital costs are given in Figure A 7. In both designs, the individual gas-solids contactors of the TSA system have been placed on top of each other with a sealing section between them. Compared to the proposed double-loop design, both alternative designs comprise only one transportation line and thus exhibit overall smaller capital costs and plant footprints.

In the design on the left hand side of Figure A 7, the adsorber is stacked on top of the desorber and both columns are connected via a loop seal. If one assumes that the backpressures of the adsorber and the desorber are almost equal, the loop seal would need to balance almost the complete adsorber pressure drop and as a consequence it would need to be very deep. Thus, it is suggested to operate the desorber at slightly elevated pressure so that the loop seal size is of the same size as one individual stage of the columns. Operating the desorber at slightly elevated pressure should be possible without any additional operating costs as stripping steam is available at sufficiently large pressure. Instead of recycling the transportation gas within the transport riser, the riser may be fluidized with clean flue gas to avoid concentration of water and water condensation within the transportation line. This would also eliminate the need for utilization of a purge gas in the moving bed section above the L-valve in Figure A 7. The second alternative TSA process design on the right hand side of Figure A 7 exhibits the advantage that the bigger adsorber column is placed below the desorber. This could have benefits for the stability and the support of the construction. However, the operation of the sealing section between both columns is more critical as it is potentially not economic to operate the adsorber at elevated pressure. Furthermore, the transport riser would require a gas recycle and the utilization of CO₂ as purge gas.

NOTATION

List of symbols:

Symbol	Description	Unit
A	cross section	$[\text{m}^2]$
A^*	dimensionless surface ratio as defined in (Eq. 2.37)	$[-]$
A_0	sum of perforation cross section	$[\text{m}^2]$
a_0	perforation cross section	$[\text{m}^2]$
a_p	particle acceleration	$[\text{m}\cdot\text{s}^{-2}]$
Ar	Archimedes number	$[-]$
C	heat capacity	$[\text{J}\cdot(\text{kg}\cdot\text{K})^{-1}]$
$c(T)$	temperature dependent Langmuir rate factor	$[-]$
c_0	pre-exponential factor	$[-]$
C_{BET}	BET-parameter	$[-]$
C_D	drag coefficient	$[-]$
C_d	coefficient of discharge	$[\text{m}^2\cdot\text{s}^{-2}]$
c_v	volumetric solids concentration	$[\text{kg}\cdot\text{m}^{-3}]$
D, d	pipe/reactor diameter, diameter	$[\text{m}]$
D_h	hydraulic pipe/reactor diameter	$[\text{m}]$
d_0	perforation diameter	$[\text{m}]$
d_{50}	median diameter	$[\text{m}]$
d_p	diameter of spherical particle	$[\text{m}]$
d_p^*	dimensionless particle diameter	$[-]$
d_s	surface diameter	$[\text{m}]$
d_{sieve}	sieve diameter	$[\text{m}]$
d_{SV}	Sauter diameter	$[\text{m}]$
d_v	volume diameter	$[\text{m}]$
dSL	dynamic sorbent loading	$[\%_w]$
F	gas flow rate	$[\text{Nm}^3\cdot\text{h}^{-1}]$
f_0	free area ratio	$[-]$
f_m	motor driving frequency	$[\text{Hz}]$
g	acceleration due to gravity	$[\text{m}\cdot\text{s}^{-2}]$
G_s	solids flux	$[\text{kg}\cdot(\text{m}^2\cdot\text{s})^{-1}]$
H	height	$[\text{m}]$
h	heat transfer coefficient	$[\text{W}\cdot(\text{m}^2\cdot\text{K})^{-1}]$
h_g	gas convective heat transfer coefficient	$[\text{W}\cdot(\text{m}^2\cdot\text{K})^{-1}]$
h_p	particle convective heat transfer coefficient	$[\text{W}\cdot(\text{m}^2\cdot\text{K})^{-1}]$
h_{max}	maximum heat transfer coefficient	$[\text{W}\cdot(\text{m}^2\cdot\text{K})^{-1}]$
h_r	radiative heat transfer coefficient	$[\text{W}\cdot(\text{m}^2\cdot\text{K})^{-1}]$
H_w	weir height	$[\text{m}]$
ΔH_{ads}	adsorption enthalpy, heat of adsorption	$[\text{J}\cdot\text{mol}^{-1}]$

Symbol	Description	Unit
i	gear ratio	[-]
k	thermal conductivity	[W·(m·K) ⁻¹]
L	characteristic length	[m]
M	molecular weight	[g·mol ⁻¹]
m_{capt}	CO ₂ capture rate	[kg·day ⁻¹]
m_{circ}, m_s	solids circulation rate	[kg·h ⁻¹]
m_p	mass of single particle	[kg]
m_{sorb}	adsorbent circulation rate	[kg·h ⁻¹]
n	number of particles within bed	[-]
N	number of perforations in distributor plate	[-]
P	wetted perimeter	[m]
p	pressure	[Pa] or [mbar]
p_i	partial pressure of species i	[Pa]
p_{sat}	saturation pressure of adsorptive	[Pa]
Δp	pressure difference/drop	[Pa] or [mbar]
q	amount of adsorbate per adsorbent mass	[mol·kg ⁻¹]
R	ideal gas constant	[kJ·(mol·K) ⁻¹]
Re	Reynolds number	[-]
s_{dc}	downcomer segment height	[m]
T	temperature	[K]
t	time or temperature	[s] or [°C]
$U (u_0)$	superficial gas velocity	[m·s ⁻¹]
U^*	dimensionless gas velocity	[-]
U_0	velocity in perforation	[m·s ⁻¹]
U_{mf}	minimum fluidization gas velocity	[m·s ⁻¹]
u_t	free fall or terminal velocity	[m·s ⁻¹]
Q	heat flow	[W]
y	volumetric gas concentration	[% _{vol}]

Abbreviations:

Symbol	Description
<i>ADS</i>	adsorber
<i>BECCS</i>	bio-energy combined with carbon capture and storage
<i>BFB</i>	bubbling fluidized bed regime
<i>BSC</i>	bottom screw conveyor
<i>BSU</i>	bench scale unit
<i>CCS</i>	carbon capture and storage
<i>CCT</i>	CO ₂ capture technology
<i>CFB</i>	circulating fluidized bed
<i>CFM</i>	cold flow model
<i>CSA</i>	concentration swing adsorption
<i>DC</i>	downcomer
<i>DCFB</i>	dual circulating fluidized bed
<i>DES</i>	desorber
<i>DSLR</i>	digital single-lens reflex camera
<i>EOR</i>	enhanced oil recovery
<i>FCC</i>	fluid catalytic cracking
<i>FF</i>	fast fluidized bed regime
<i>FID</i>	flame ionization detector
<i>HEX</i>	heat exchanger
<i>IEA</i>	International Energy Agency
<i>IGCC</i>	integrated gasification combined cycle process
<i>Inv.</i>	total solids inventory
<i>IPCC</i>	Intergovernmental Panel on Climate Change
<i>IUPAC</i>	International Union of Pure and Applied Chemistry
<i>MEA</i>	monoethanolamine
<i>MStFB</i>	multi-stage fluidized bed
<i>OECD</i>	Organisation for Economic Co-operation and Development
<i>OPt</i>	operating point
<i>PC</i>	pneumatic conveying regime
<i>PCC</i>	post-combustion CO ₂ capture
<i>PEI</i>	polyethylenimine
<i>PMMA</i>	polymethylmethacrylat
<i>PSA</i>	pressure swing adsorption
<i>PSD</i>	particle size distribution
<i>TB</i>	turbulent fluidized bed regime
<i>TDH</i>	transport disengaging height
<i>TGA</i>	thermogravimetric analysis
<i>TSA</i>	temperature swing adsorption
<i>VSA, VPSA</i>	vacuum swing adsorption

Subscripts:

Symbol	Description
<i>ads</i>	referring to the adsorber
<i>b</i>	bubble phase
<i>col</i>	values within the multi-stage fluidized bed column
<i>d</i>	dense bed region
<i>dc</i>	downcomer
<i>des</i>	referring to the desorber
<i>distr</i>	gas distributor
<i>f</i>	fluid, freeboard
<i>FB</i>	fluidized bed
<i>FixB</i>	fixed bed
<i>g</i>	gas phase
<i>HEX</i>	heat exchanger
<i>HEX-FB</i>	between heat exchanger and fluidized bed
<i>in</i>	inlet streams
<i>int</i>	interstitial region between particles
<i>l</i>	lean bed region
<i>leak</i>	leakage
<i>mb</i>	fluidization conditions at which bubbles start to appear within the bed
<i>mf</i>	minimum fluidization conditions (transition fixed bed to fluidized bed)
<i>n</i>	value at standard conditions
<i>opt</i>	optimum fluidization conditions at $h = h_{max}$
<i>or</i>	orifice
<i>out</i>	outlet streams
<i>p</i>	particle
<i>packet</i>	referring to an agglomeration of particles (= packet)
<i>pipe</i>	referring to flow conditions within an empty pipe
<i>proj</i>	projected surface area
<i>PSA</i>	pressure swing adsorption
<i>reg</i>	regeneration
<i>ris, riser</i>	values within the solid transport riser
<i>s</i>	solids
<i>sorb</i>	adsorbent material
<i>Sti</i>	stage number i
<i>t</i>	values at $U = u_t$
<i>TSA</i>	temperature swing adsorption
<i>trans</i>	transferred with system
∞	theoretical maximum

Greek symbols:

Symbol	Description	Unit
β	adsorbent loading	[mol·kg ⁻¹]
β_{\max}	adsorbent saturation loading	[mol·kg ⁻¹]
β_{ML}	maximum monolayer adsorbent loading	[mol·kg ⁻¹]
$\Delta\beta$	working capacity	[mol·kg ⁻¹]
δ_b	volumetric bubble fraction	[-]
ε	fluidized bed voidage	[-]
ε_{mf}	fluidized bed voidage at $U = U_{mf}$	[-]
ζ	pressure loss coefficient	[-]
η_{capt}	CO ₂ capture efficiency	[%]
θ	fraction of occupied adsorption sites	[-]
μ	dynamic gas viscosity	[Pa·s]
ρ_g	gas density	[kg·m ⁻³]
ρ_p	particle density	[kg·m ⁻³]
τ	average residence time	[s]
φ	pressure ratio	[-]
φ_s	particle sphericity	[-]
φ_w	equivalent thickness of wall region	[-]

REFERENCES

- Agarwal, J. C., Davis, W. L., King, D. T., (1962). Fluidized-bed coal dryer. *Chem. Eng. Prog.* 58, 85-90.
- APCC, (2014). Summary for Policymakers (SPM). In: Österreichischer Sachstandsbericht Klimawandel (AAR14), Asutrian Panel on Climate Change (APCC), Verlag der Österreichischen Akademien der Wissenschaften, Vienna, Austria.
- Arrhenius, S., (1886). On the influence of carbonic acid in the air upon the temperature of the ground. *Philos. Mag.* 41, 237-277.
- Bailey, D. W., Feron, P. H. M., (2005). Post-Combustion Decarbonisation Processes. *Oil Gas Sci. Technol.* 60 (3), 461-474.
- Bathen, D., Breitbach, M., (2001). Adsorptionstechnik. Springer Verlag, Berlin Heidelberg, 2001.
- Bentham, M., Kirby, G., (2005). CO₂ Storage in Saline Aquifers. *Oil & Gas Science and Technology – Rev. IFP* 60 (3), 559-567.
- Beránek, J. Rose, K., Winterstein, G., (1975). Grundlagen der Wirbelschicht-Technik. Leipzig: Krausskopf.
- Berger, A. H., Bhowan, A. S., (2011). Comparing Physisorption and Chemisorption Solid Sorbents for use Separating CO₂ from Flue Gas using Temperature Swing Adsorption. *Energy Procedia* 4, 562-567.
- Bi, H. T., Grace, J. R., (1995). Flow regime diagrams for gas-solid fluidization and upward transport. *Int. J. Multiphase Flow* 21 (6), 1229-1236.
- Bolhár-Nordenkamp, J., Pröll, T., Kolbitsch, P., Hofbauer, H., (2009). Comprehensive Modeling Tool for Chemical Looping Based Processes. *Chem. Eng. Technol.* 32 (3), 410-417.
- Bollini, P., Didas, S. A., Jones, C. W., (2011). Amine-oxide hybrid materials for acid gas separations. *J. Mater. Chem.* 21, 15100-15120.
- Bonjour, J., Chalfen, J.-B., Meunier, F., (2002). Temperature Swing Adsorption Process with Indirect Cooling and Heating. *Ind. Eng. Chem. Res.* 41 (23), 5802-5811.
- Booras, G. S., (1991). An engineering and economic evaluation of CO₂ removal from fossil-fuel-fired power plants. *Energy* 16 (11-12), 1295-1305.
- Boot-Handford, M. E., Abanades, J. C., Anthony, E. J., Blunt, M. J., Brandani, S., Mac Dowell, N., Fernández, J. R., Ferrari, M.-C., Gross, R., Hallett, J. P., Haszeldine, R. S., Heptonstall, P., Lyngfelt, A., Makuch, Z., Mangano, E., Porter, R. T. J., Pourkashanian, M., Rochelle, G. T., Shah, N., Yao, J. G., Fennell, P. S., (2013). Carbon capture and storage update. *Energy Environ. Sci.* 7, 130-189.
- Bottoms, R. R., (1930). Process for separating acidic gases. Girdler Corp., U.S. patent 1783901.
- Brauer, H., (1985). Die Adsorptionstechnik – ein Gebiet mit Zukunft. *Chem.-Ing.-Tech.* 57 (8), 650-663. (article in German).
- Brauer, H., Mühle, J., Schmidt, M., (1970). Untersuchungen an einer mehrstufigen Rieselboden-Wirbelschicht. *Chemie-Ingenieur-Technik* 42 (7), 494-502. (article in German).

- Brunauer, S., Emmett, P. H., Teller, E., (1938). Adsorption of Gases in Multimolecular Layers. *J. Am. Chem. Soc.* 60 (2), 309-319.
- Burcat, A., McBride, B., (1997). Ideal gas thermodynamic data for combustion and air pollution use. Technion Israel Institute of Technology, Aerospace Engineering Report, TAE 804 (garfield.chem.elte.hu/Burcat/burcat.html, last accessed October 2014).
- Chaffee, A. L., Knowles, G. P., Liang, Z., Zhang, J., Xiao, P., Webley, P. A., (2007). CO₂ capture by adsorption: Materials and process development.
- Chakma, A., Mehrotra, A. K., Nielsen, B., (1995). Comparison of chemical solvents for mitigating CO₂ emissions from coal-fired power plants. *Heat Recovery Systems & CHP* 15 (2), 231-240.
- Chappuis, P., (1879). *Wied. Ann.* 8, 1.
- Chappuis, P., (1881). *Wied. Ann.* 12, 161.
- Clausse, M., Merel, J., Meunier, F., (2011). Numerical parametric study on CO₂ capture by indirect thermal swing adsorption. *International Journal of Greenhouse Gas Control* 5, 1206-1213.
- Dąbrowski, A., (2001). Adsorption – from theory to practice. *Advances in Colloid and Interface Science* 93, 135-224.
- Dietrich, F., (2014). A novel system for continuous temperature swing adsorption: parameter study at bench scale. Master Thesis, Institute of Chemical Engineering, Vienna University of Technology, Vienna, Austria.
- Drage, T. C., Arenillas, A., Smith, K. M., Snape, C. E., (2008). Thermal stability of polyethylenimine based carbon dioxide adsorbents and its influence on selection of regeneration strategies. *Microporous and Mesoporous Materials* 116, 504-512.
- Drage, T. C., Smith, K. M., Arenillas, A., Snape, C. E., (2009). Developing strategies for the regeneration of polyethylenimine based CO₂ adsorbents. *Energy Procedia* 1 (1), 875-880.
- Eleftheriades, C. M., Judd, M. R., (1978). The design of downcomers joining gas-fluidized beds in multistage systems. *Powder Technology* 21 (2), 217-225.
- Ergun, S., (1952). Fluid flow through packed columns. *Chemical Engineering Progress* 48, 89-94.
- ESRL, (2015). Full Mauna Loa CO₂ record. U.S. Department of Commerce, National Oceanic and Atmospheric Administration, Earth System Research Laboratory, Global Monitoring Division, <http://www.esrl.noaa.gov/gmd/ccgg/trends/index.html> (link last accessed January 2015).
- Fauth, D. J., Gray, M. L., Pennline, H. W., Krutka, H. M., Sjoström, S., Ault, A. M., (2012). Investigation of Porous Silica Supported Mixed-Amine Sorbents for Post-Combustion CO₂ Capture. *Energy Fuels* 26, 2483-2496.
- Feron, P. H. M., (2005). Challenges in Capture Processes: The Way Forward. *Oil Gas Sci. Technol.* 60 (3), 509-510.
- Figuerola, J. D., Fout, T., Plasynski, S., McIlvried, H., Srivastava, R. D., (2008). Advances in CO₂ capture technology – The U.S. Department of Energy's Carbon Sequestration Program. *International Journal of Greenhouse Gas Control* 2, 9-20.
- Fontana, F., (1777). *Mem. Mat. Fis. Soc. Ital.* 1, 679.

- Franchi, R. S., Harlick, P. J. E., Sayari, A., (2005). Application of Pore-Expanded Mesoporous Silica. 2. Development of a High-Capacity, Water-Tolerant Adsorbent for CO₂. *Ind. Eng. Chem. Res.* 44, 8007-8013.
- Freundlich, H., (1907). Über die Adsorption in Lösungen. *Z. Phys. Chem.* 57, 385-470.
- Freundlich, H., (1909). *Kapillarchemie*. Akademische Verlagsgesellschaft, Leipzig, Germany.
- Geldart, D., (1973). Types of Gas Fluidization. *Powder Technology* 7, 494-502.
- Glicksman, L. R., (2003). Fluidized bed scaleup, in *Handbook of Fluidization and Fluid-Particle Systems*. W.C. Yang, ed., New York: Marcel Dekker.
- Glicksman, L. R., Hyre, M., Woloshun, K., (1993). Simplified scaling relationships for fluidized beds. *Powder Technology* 77, 177-199.
- Golomb, D., Herzog, H., Tester, J., White, D., Zemba, S., (1989). Feasibility, Modelling and Economics of Sequestering Power Plant CO₂ Emissions In the Deep Ocean. Massachusetts Institute of Technology, Energy Laboratory, MIT-EL 89-003.
- Grace, J. R., (1986). Contacting Modes and Behaviour Classification of Gas-Solid and Other Two-Phase Suspensions. *Can. J. Chem. Eng.* 64, 353-363.
- Gray, M. L., Hoffman, J. S., Hreha, D. C., Fauth, D. J., Hedges, S. W., Champagne, K. J., Pennline, H. W., (2009). Parametric Study of Solid Amine Sorbents for the Capture of Carbon Dioxide. *Energy Fuels* 23, 4840-4844.
- Grewal, N. S., Cheung, T. K., Saxena, S. C., (1985). Heat transfer between Horizontal Finned Tubes and a Gas-Solid Fluidized Bed. *Ind. Eng. Chem. Proc. Des. Dev.* 24 (2), 458-471.
- Guío-Pérez, D. C., (2013). Cold flow model assisted evaluation of an improved dual circulating fluidized bed design for chemical looping processes including solids residence time measurements. PhD Thesis, Institute of Chemical Engineering, Vienna University of Technology, Vienna, Austria.
- Guío-Pérez, D. C., Pröll, T., Wassermann, J., Hofbauer, H., (2013). Design of an inductance measurement system for determination of particle residence time in a dual circulating fluidized bed cold flow model, *Ind. Eng. Chem. Res.* 52 (31) , 10732-10740.
- Hammache, S., Hoffman, J. S., Gray, M. L., Fauth, D. J., Howard, B. H., Pennline, H. W., (2013). Comprehensive Study of the Impact of Steam on Polyethyleneimine on Silica for CO₂ Capture. *Energy Fuels* 27, 6899-6905.
- Harlick, P. J. E., Sayari, A., (2007). Application of Pore-Expanded Mesoporous Silica. 5. Triamine Grafted Material with Exceptional CO₂ Dynamic and Equilibrium Adsorption Performance. *Ind. Eng. Chem. Res.* 46, 446-458.
- Heesink, A. B. M., Veneman, R., Magneschi, G., Brilman, D. W. F., (2013). Cutting the cost of carbon capture. *Power Engineering International* 21 (8), 52-61.
- Heydari-Gorji, A., Sayari, A., (2012). Thermal, Oxidative, and CO₂-Induced Degradation of Supported Polyethylenimine Adsorbents. *Ind. Eng. Chem. Res.* 51, 6887-6894.
- Hofbauer, H., Stoiber, H., Veronik, G., (1995). Gasification of organic material in a novel fluidised bed system. In: *Proceedings of the First SCEJ Symposium on Fluidisation*, The Society of Chemical Engineers, Tokyo, Japan, 291-299.

- Hsiung, T. H., Thodos, G., (1977). Expansion characteristics of gas-fluidized beds. *Canadian Journal of Chemical Engineering* 55 (2), 221-224.
- IEA, (2012a). *World Energy Outlook 2012*. OECD/IEA, Paris.
- IEA, (2012b). *Energy Technology Perspectives 2012*. OECD/IEA, Paris.
- IEA, (2012c). *Medium-Term Coal Market Report 2012*. OECD/IEA, Paris.
- IEA, (2013a). *Global Action to Advance Carbon Capture and Storage: A Focus on Industrial Applications*. OECD/IEA, Paris.
- IEA, (2013b). *Technology Roadmap: Carbon capture and storage*. OECD/IEA, Paris.
- IPCC, (2005). *IPCC Special Report on Carbon Dioxide Capture and Storage*. Prepared by Working Group III of the Intergovernmental Panel on Climate Change. Cambridge University Press, Cambridge, United Kingdom and New York, NY, USA.
- IPCC, (2014). *Climate Change 2014: Synthesis Report of the Fifth Assessment Report of the Intergovernmental Panel on Climate Change*, http://www.ipcc.ch/pdf/assessment-report/ar5/syr/SYR_AR5_LONGERREPORT_Corr2.pdf (link last accessed January 2015).
- Jones, C. W., Drese, J. H., Choi, S., (2009). Adsorbent Materials for Carbon Dioxide Capture from Large Anthropogenic Point Sources. *ChemSusChem* 2, 796-854.
- Kayser, H., (1881a). *Wied. Ann. Phys.* 12, 526.
- Kayser, H., (1881b). *Wied. Ann. Phys.* 14, 450.
- Keller, J., Sautdt, R., (2005). *Gas Adsorption Equilibria – Experimental Methods and Adsorption Isotherms*. Springer Science & Business Media.
- Kelley, B. T., Deckman, H. W., Hershkowitz, F., Northrop, P. S., Ravikovitch, P. I., (2010). Temperature swing adsorption of CO₂ from flue gas utilizing heat from compression. U.S. Patent US 7731782 B2.
- Kim, S. W., Ahn, J. Y., Kim, S. D., Lee, D. H., (2003). Heat transfer and bubble characteristics in a fluidized bed with immersed horizontal tube bundle. *Int. J. of Heat and Mass Transfer* 46, 399-409.
- Knudsen, J., Jensen, J., Vilhelmsen, P. J., Biede, O., (2009). Experience with CO₂ capture from coal flue gas in pilot-scale: Testing of different amine solvents. *Energy Procedia* 1, 783-790.
- Krishnaiah, K., Varma, Y. G., (1982). Pressure Drop, Solids Concentration and Mean Holding Time in Multistage Fluidisation. *The Canadian Journal of Chemical Engineering* 60, 346-352.
- Krutka, H., Sjostrom, S., Starns, T., Dillon, M., Silverman, R., (2013). Post-Combustion CO₂ Capture Using Solid Sorbents: 1 MWe Pilot Evaluation. *Energy Procedia* 37, 73-88.
- Kunii, D., Levenspiel, O., (1991). *Fluidization Engineering*. Butterworth-Heinemann, USA, 2nd Ed., 491.
- Langmuir, I., (1916). The constitution and fundamental properties of solids and liquids. Part I. Solids. *J. Am. Chem. Soc.* 37, 2221-2295.
- Langmuir, I., (1918). The adsorption of gases on plane surfaces of glass, mica and platinum. *J. Am. Chem. Soc.* 40, 1361-1403.

-
- Li, W., Choi, S., Drese, J. H., Hornbostel, M., Krishnan, G., Eisenberger, P. M., Jones, C. W., (2010). Steam-Stripping for Regeneration of Supported Amine-Based CO₂ Adsorbents. *ChemSusChem* 3, 899-903.
- Lim, K. S., Zhu, J. X., Grace, J. R., (1995). Hydrodynamics of gas-solid fluidization. *International Journal of Multiphase Flow* 21, 141-193.
- Lively, R. P., Chance, R. R., Koros, W. J., (2010). Enabling Low-Cost CO₂ Capture via Heat Integration. *Ind. Eng. Chem. Res.* 49, 7550-7562.
- MacDowell, N., Florin, N., Buchard, A., Hallett, J., Galindo, A., Jackson, G., Adjiman, C. S., Williams, C. K., Shah, N., Fennell, P., (2010). An overview of CO₂ capture technologies. *Energy & Environmental Science* 3(11), 1645-1669.
- Martín-Gullón, I., Marcilla, A., Font, R., Asensio, M., (1995). Stable operating velocity range for multistage fluidized bed reactors with downcomers. *Powder Technology* 85, 193-201.
- Marx, K., (2013). Next scale Chemical Looping Combustion – Overall Plant Design. PhD Thesis, Institute of Chemical Engineering, Vienna University of Technology, Vienna, Austria.
- Masel, R. I., (1996). Principles of Adsorption and Reaction on Solid Surfaces. John Wiley & Sons, New York, USA.
- McBain, J. W., (1909). *Phil. Mag.* 18, 916.
- Mickley, H. S., Fairbanks, D. F., (1955). Mechanism of heat transfer to fluidized beds. *AIChE J.* 1 (3), 374-384.
- Mohanty, C. R., Meikap, B. C., (2009). Pressure drop characteristics of a multi-stage counter-current fluidized bed reactor for control of gaseous pollutants. *Chemical Engineering and Processing* 48, 209-216.
- Mohanty, C., R., Rajmohan, B., Meikap, B., C., (2010). Identification of stable operating ranges of a counter-current multistage fluidized bed reactor with downcomer. *Chemical Engineering and Processing* 49, 104-112.
- Molerus, O., (1982). Interpretation of Geldart's type A, B, C and D powders by taking into account interparticle cohesion forces. *Powder Technology* 33 (1), 81-87.
- Papadatos, K., Svrcek, W. Y., Bergougnou, M. A., (1975). Holdup dynamics of a single stage gas-solid fluidized bed adsorber. *Can. J. Chem. Eng.* 53, 686.
- Pirngruber, G. D., Guillou, F., Gomez, A., Clausse, M., (2013). A theoretical analysis of the energy consumption of post-combustion CO₂ capture processes by temperature swing adsorption using solid sorbents. *International Journal of Greenhouse Gas Control* 14, 74-83.
- Pouillet, C. M., (1822). *Ann. Chim. Phys.* 20, 141.
- Pröll, T., Hofbauer, H., (2008a). Development and Application of a Simulation Tool for Biomass Gasification Based Processes. *International Journal of Chemical Reactor Engineering* 6 (1).
- Pröll, T., Hofbauer, H., (2008b). H₂ rich syngas by selective CO₂ removal from biomass gasification in a dual fluidized bed system – Process modelling approach. *Fuel Processing Technology* 89, 1207-1217.
- Pröll, T., Kolbitsch, P., Bolhàr-Nordenkampf, J., Hofbauer, H., (2009). A Novel Dual Circulating Fluidized Bed System for Chemical Looping Processes. *AIChE Journal* Vol. 55 (12), 3255-3266.
-

- Ramezan, M., Skone, T. J., Nsakala, N., Liljedahl, G. N., (2007). Carbon dioxide capture from existing coal-fired power plants. Final Report DOE/NETL-401/110907.
- Rao, A. B., Rubin, E. S., (2002). A Technical, Economic, and Environmental Assessment of Amine-Based CO₂ Capture Technology for Power Plant Greenhouse Gas Control. *Environ. Sci. Technol.* 36, 4467-4475.
- Rasouli, S., Golriz, M. R., Hamidi, A. A., (2005). Effect of annular fins on heat transfer of a horizontal immersed tube in bubbling fluidized beds. *Powder Technology* 154, 9-13.
- Rezaei, F., Jones, C. W., (2013). Stability of Supported Amine Adsorbents to SO₂ and NO_x in Postcombustion CO₂ Capture. 1. Single-Component Adsorption. *Ind. Eng. Chem. Res.* 52, 12192-12201.
- Rezaei, F., Jones, C. W., (2014). Stability of Supported Amine Adsorbents to SO₂ and NO_x in Postcombustion CO₂ Capture. 2. Multicomponent Adsorption. *Ind. Eng. Chem. Res.* 53 (30), 12103-12110.
- Ringhofer, T., (2014). First Operation of a Novel Fluidized Bed Reactor System for Continuous Solid-Sorbent CO₂ Capture. Master Thesis, Institute of Chemical Engineering, Vienna University of Technology, Vienna, Austria.
- Rochelle, G. T., (2009). Amine Scrubbing for CO₂ capture. *Science* 235, 1652-1654.
- Rolker, J., Arlt, W., (2006). Abtrennung von Kohlendioxid aus Rauchgasen mittels Absorption. *Chemie Ingenieur Technik* 78 (4), 416-424.
- Rouquerol, F., Rouquerol, J., Sing, K. S. W., Llewellyn, P., Maurin, G., (2014). Adsorption by powders and porous solids: Principles, Methodology and Applications. 2nd ed., San Diego: Academic Press.
- Ruthven, D. M., (1984). Principles of Adsorption and Adsorption Processes. John Wiley & Sons, New York, USA.
- Samanta, A., Zhao, A., Shimizu, G. K. H., Sarkar, P., Gupta, R., (2012). Post-Combustion CO₂ Capture Using Solid Sorbents: A Review. *Ind. Eng. Chem. Res.* 51, 1438-1463.
- Satyapal, S., Filburn, T., Trela, J., Strange, J., (2001). Performance and Properties of a Solid Amine Sorbent for Carbon Dioxide Removal in Space Life Support Applications. *Energy Fuels* 15, 250-255.
- Sayari, A., Belmabkhout, Y., (2010). Stabilization of Amine-Containing CO₂ Adsorbents: Dramatic Effect of Water Vapor. *J. AM. CHEM. SOC.* 132, 6312-6314.
- Sayari, A., Belmabkhout, Y., Serna-Guerrero, R., (2011). Flue gas treatment via CO₂ adsorption. *Chem. Eng. J.* 171, 760-774.
- Scheele, C. W., (1773). Chemische Abhandlung von der Luft und dem Feuer. see: Ostwald's Klassiker der exakten Wiss. 58.
- Schmid, J. C., Pröll, T., Pfeifer, C., Hofbauer, H., (2011). Improvement of gas-solid interaction in dual circulating fluidized bed systems. In: Proceedings of the 9th European Conference on Industrial Furnaces and Boilers (INFUB), Reis et al. Eds., Estoril, Portugal, April 26-29, 2011.
- Serna-Guerrero, R., Da'na, E., Sayari, A., (2008). New Insights into the Interactions of CO₂ with Amine-Functionalized Silica. *Ind. Eng. Chem. Res.* 47, 9406-9412.

- Sing, K. S. W., Everett, D. H., Haul, R. A. W., Moscou, L., Pierotti, R. A., Roquérol, J., Siemieniewska, T., (1985). Reporting physisorption data for gas/solid systems with special reference to the determination of surface area and porosity. IUPAC, Pure & Appl. Chem. Vol. 57 No. 4, 603-619.
- Sjostrom, S., Krutka, H., (2010). Evaluation of solid sorbents as a retrofit technology for CO₂ capture. Fuel 89, 1298-1306.
- Son, W.-J., Choi, J.-S., Ahn, W.-S., (2008). Adsorptive removal of carbon dioxide using polyethyleneimine-loaded mesoporous silica materials. Microporous and Mesoporous Materials 113, 31-40.
- Srinivasa Kannan, C., Subba Rao, S., Varma, Y. B. G., (1994). A study of stable range of operation in multistage fluidised beds. Powder Technology 18, 203-211.
- Tanaka, N., (2008). CO₂ capture and storage: A key carbon abatement option. OECD/IEA, Paris.
- Tarka, T.J., Ciferno, J. P., Gray, M. L., Fauth, D, (2006). CO₂ capture systems using amine enhanced solid sorbents. Presented at the Fifth Annual Conference on Carbon Capture & Sequestration, Alexandria, VA, USA, May 8-11, Paper No. 152, 30pp (Available via the Internet at <http://www.netl.doe.gov/publications/proceedings/06/carbon-seq/Tech%20Session%20152.pdf>. (last access February 2014)).
- Thomas, W. J., Crittenden, B., (1998). Adsorption Technology & Design. 1st Ed., Butterworth-Heinemann.
- Tyndall, J., (1861). On the absorption and radiation of heat by gases and vapours. Philos. Mag. 4, 273-285.
- Vaidya, P. D., Kenig, E. Y., (2007). CO₂-Alkanolamine Reaction Kinetics: A Review of Recent Studies. Chem.Eng.Technol. 30 (11), 1467-1474.
- Wen, C. Y., Yu, Y. H., (1966). A generalized method for predicting the minimum fluidization velocity. AIChE Journal 12 (3), 610-612.
- Werther, J., (2007). Fluidized-Bed Reactors. Ullmann's Encyclopedia of Industrial Chemistry.
- Wilson, M., Tontiwachwuthikul, P., Chakma, A., Idem, R., Veawab, A., Aroonwilas, A., Gelowitz, D., Barrie, J., Mariz, C., (2004). Test results from a CO₂ extraction pilot plant at boundary dam coal-fired power station. Energy 29, 1259-1267.
- Winkler, F, (1922). Verfahren zum Herstellen von Wassergas, Deutsches Reich Patent 437970.
- Xu, X., Song, C., Andresen, J. M., Miller, B. G., Scaroni, A. W., (2002). Novel polyethylenimine-modified mesoporous molecular sieve of MCM-41 type as high capacity adsorbent for CO₂ capture. Energy Fuels 16, 1463-1469.
- Xu, X., Song, C., Andrésen, J. M., Miller, B. G., Scaroni, A. W., (2003). Preparation and characterization of novel CO₂ "molecular basket" adsorbents based on polymer-modified mesoporous molecular sieve MCM-41. Microporous and Mesoporous Materials 62, 29-45.
- Xu, X., Song, C., Miller, B. G., Scaroni, A. W., (2005). Influence of Moisture on CO₂ Separation from Gas Mixtures by a Nanoporous Adsorbent Based on Polyethylenimine-Modified Molecular Sieve MCM-41. Ind. Eng. Chem. Res. 44, 8113-8119.
- Yan, X., Zhang, L., Zhang, Y., Yang, G., Yan, Z., 2011. Amine-Modified SBA-15: Effect of Pore Structure on the Performance for CO₂ Capture. Ind. Eng. Chem. Res. 50, 3220-3226.

- Yang, W.-C., Hoffman, J., (2009). Exploratory Design Study on Reactor Configurations for Carbon Dioxide Capture from Conventional Power Plants Employing Regenerable Solid Sorbents. *Ind. Eng. Chem. Res.* 48, 341-351.
- Zabrodsky, S.S., (1966), *Hydrodynamics and heat transfer in fluidized beds*, MIT Press, Cambridge, MA, 379.
- Zhao, W., Zhang, Z., Li, Z., Cai, N., (2013). Investigation of Thermal Stability and Continuous CO₂ Capture from Flue Gases with Supported Amine Sorbent. *Ind. Eng. Chem. Res.* 52, 2084-2093.
- Zuiderweg, F. J., (1967). Session Report. In: *Proceedings of International Symposium on Fluidization*, Netherlands University Press, Amsterdam, 739-750.

APPENDIX

Figure A 1: Isometric view of TSA BSU design.

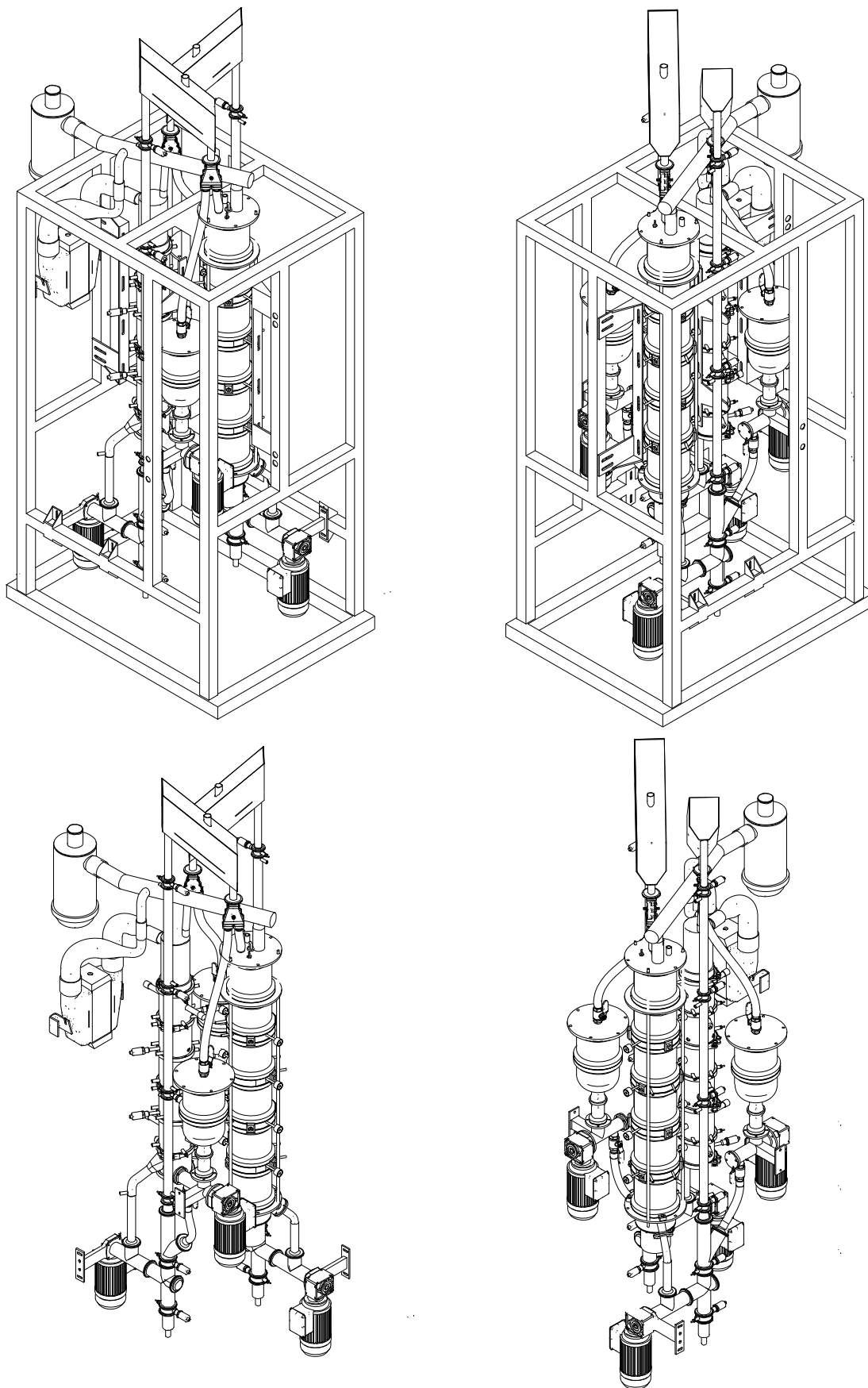


Figure A 2: Main views of TSA BSU design.

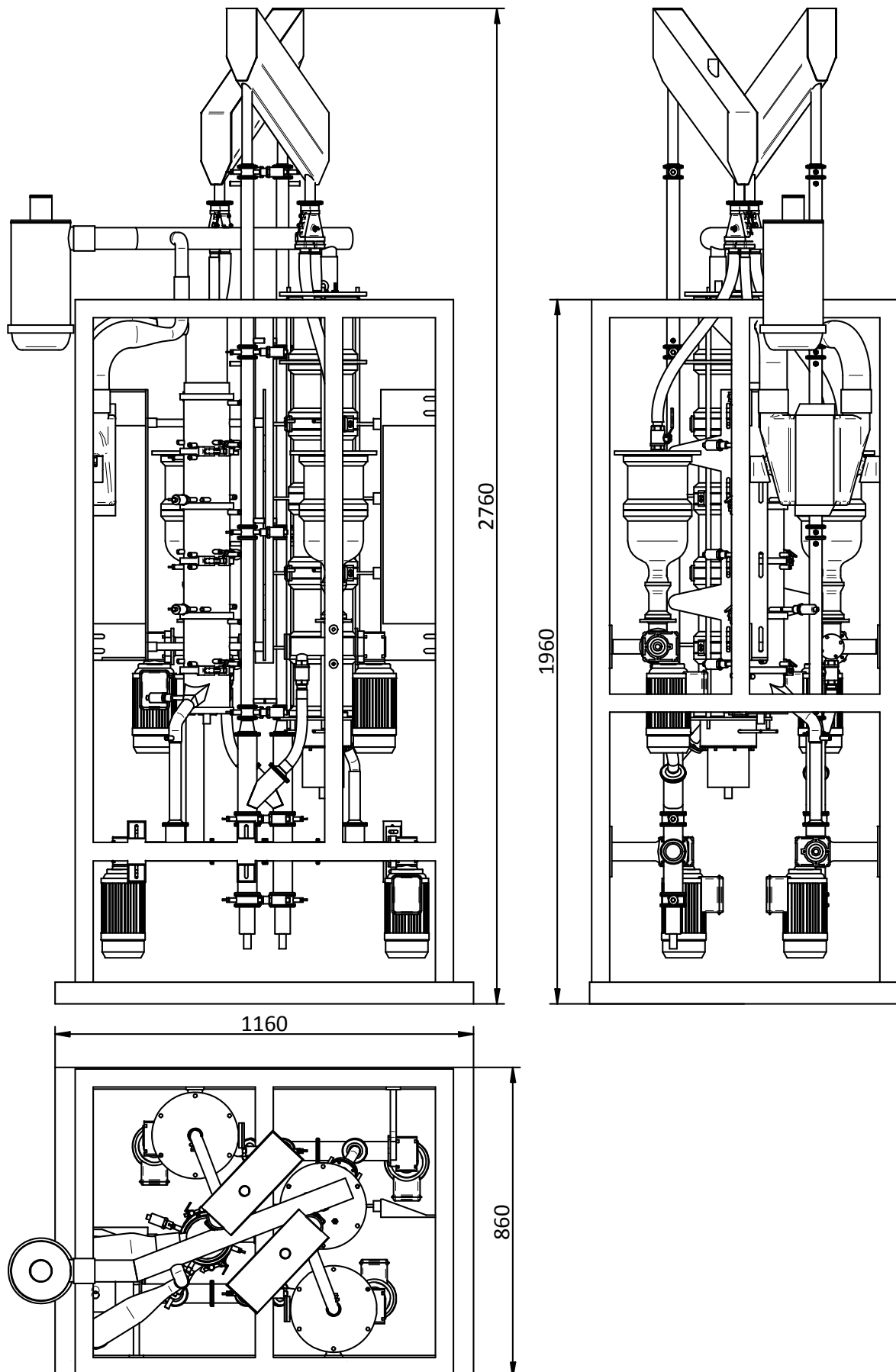
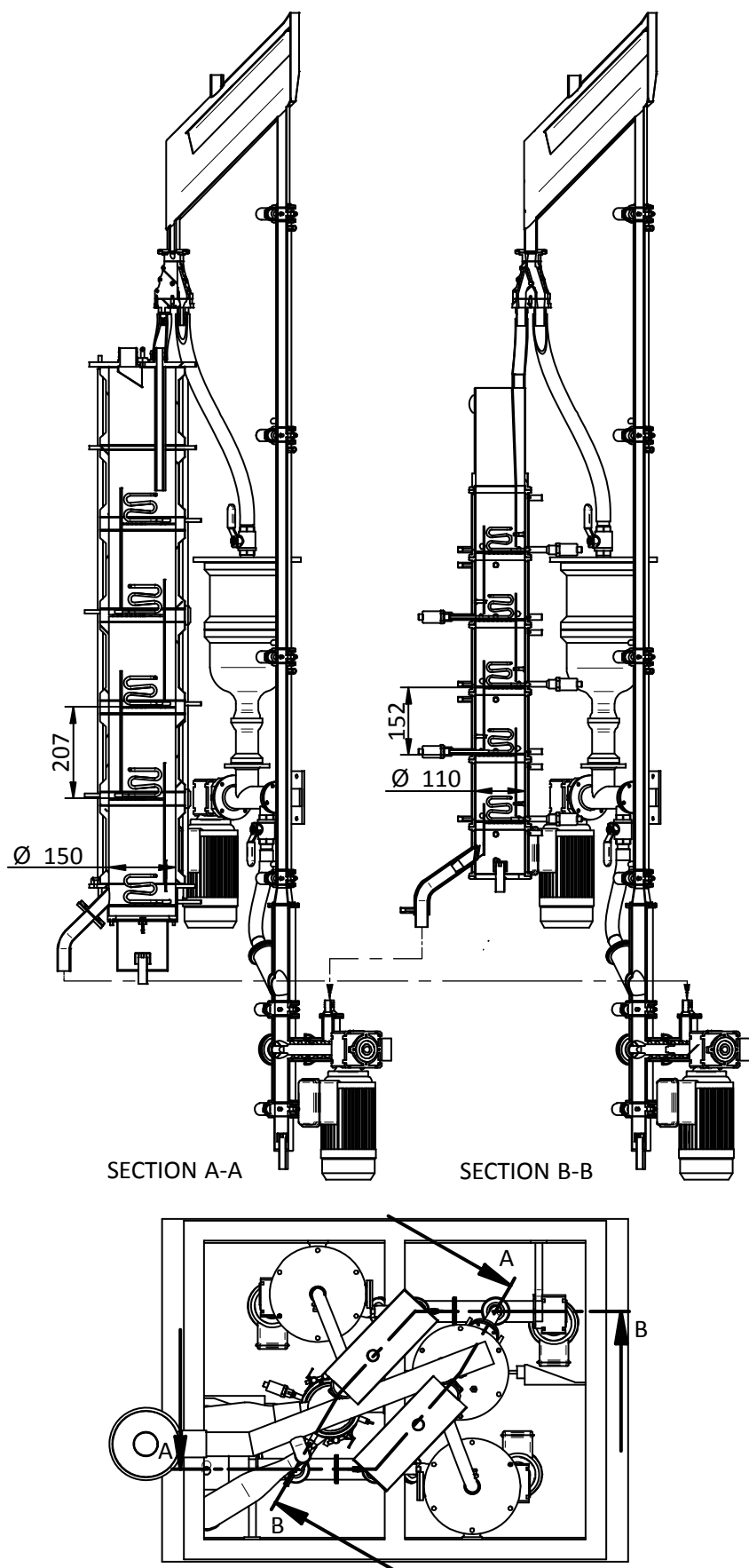


Figure A 3: Sectional view of TSA BSU design.



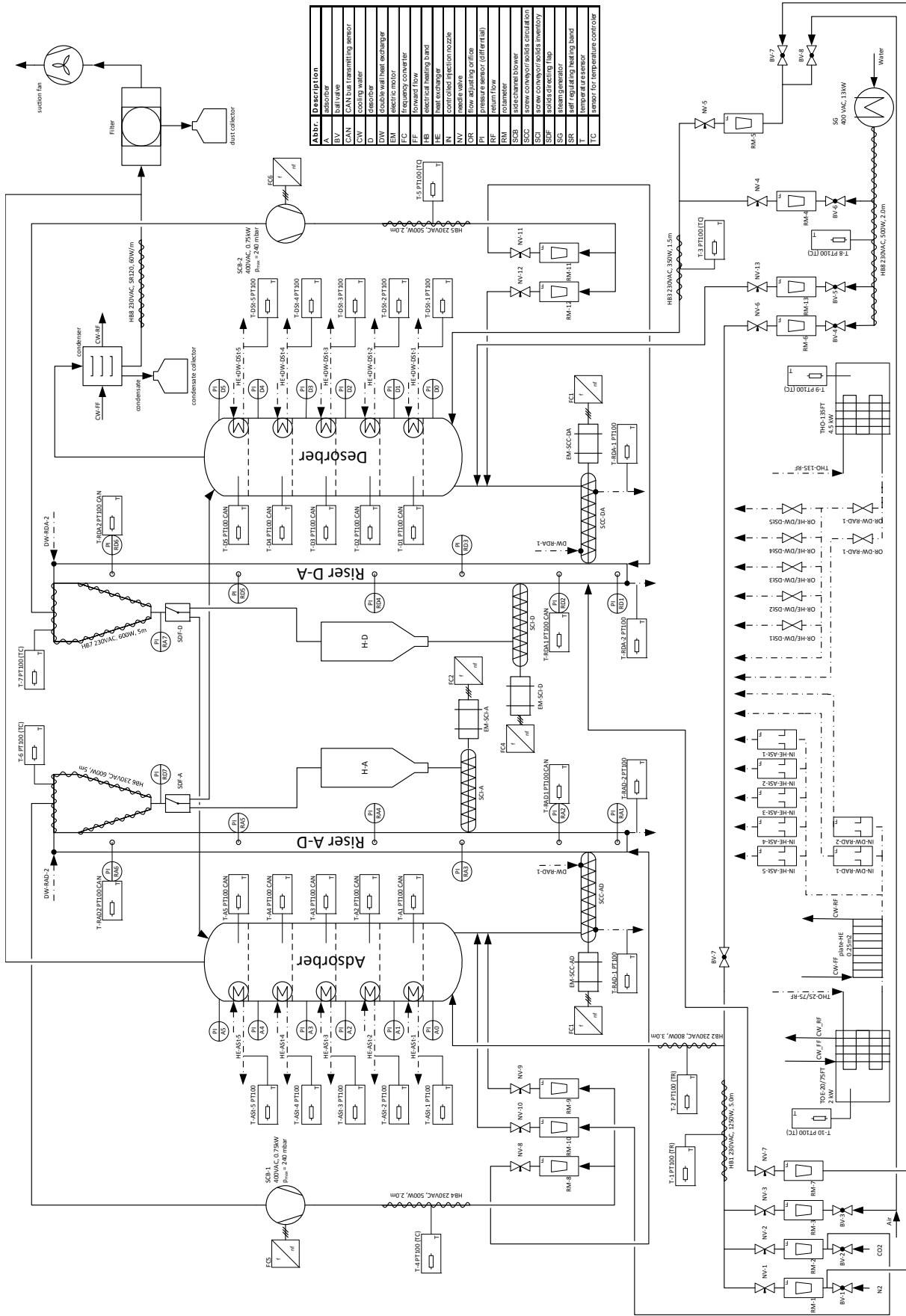
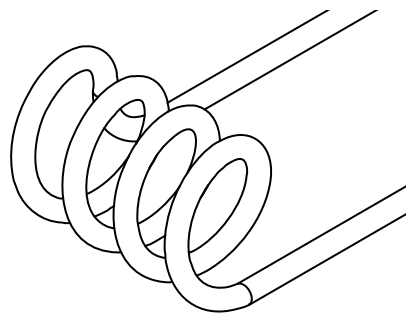
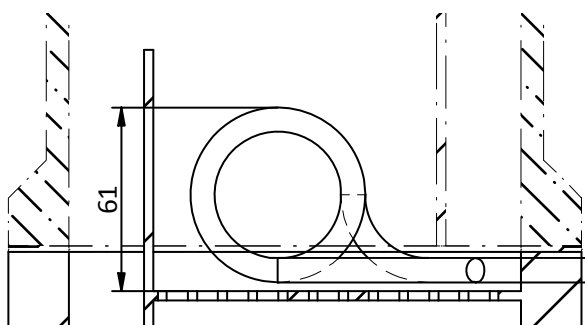
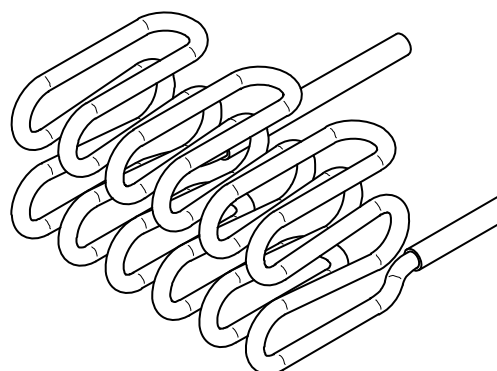
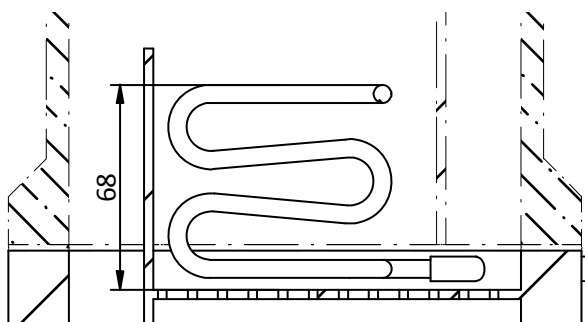


Figure A 5: Design update of stage heat exchangers.

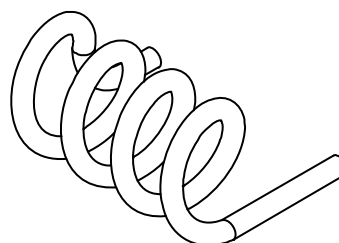
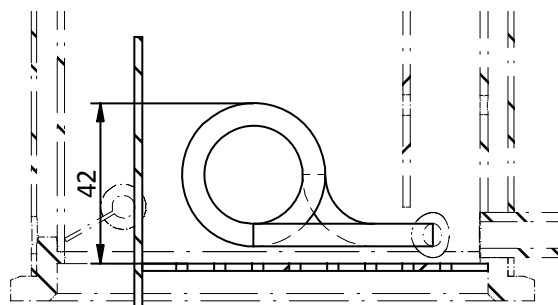
HEX Adsorber: old design
 $A=17990\text{mm}^2$



HEX Adsorber: new design
 $A=37840\text{mm}^2$



HEX Desorber: old design
 $A=8870\text{mm}^2$



HEX Desorber: new design
 $A=25260\text{mm}^2$

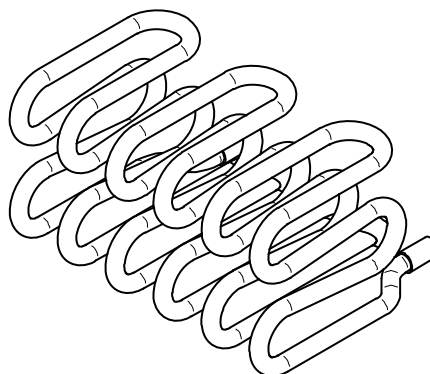
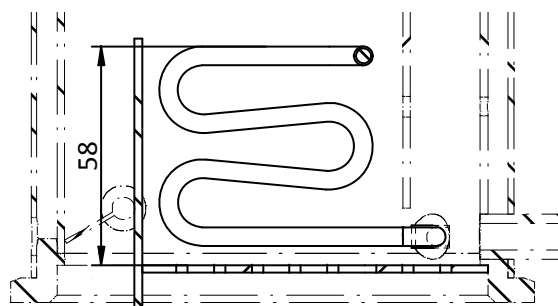
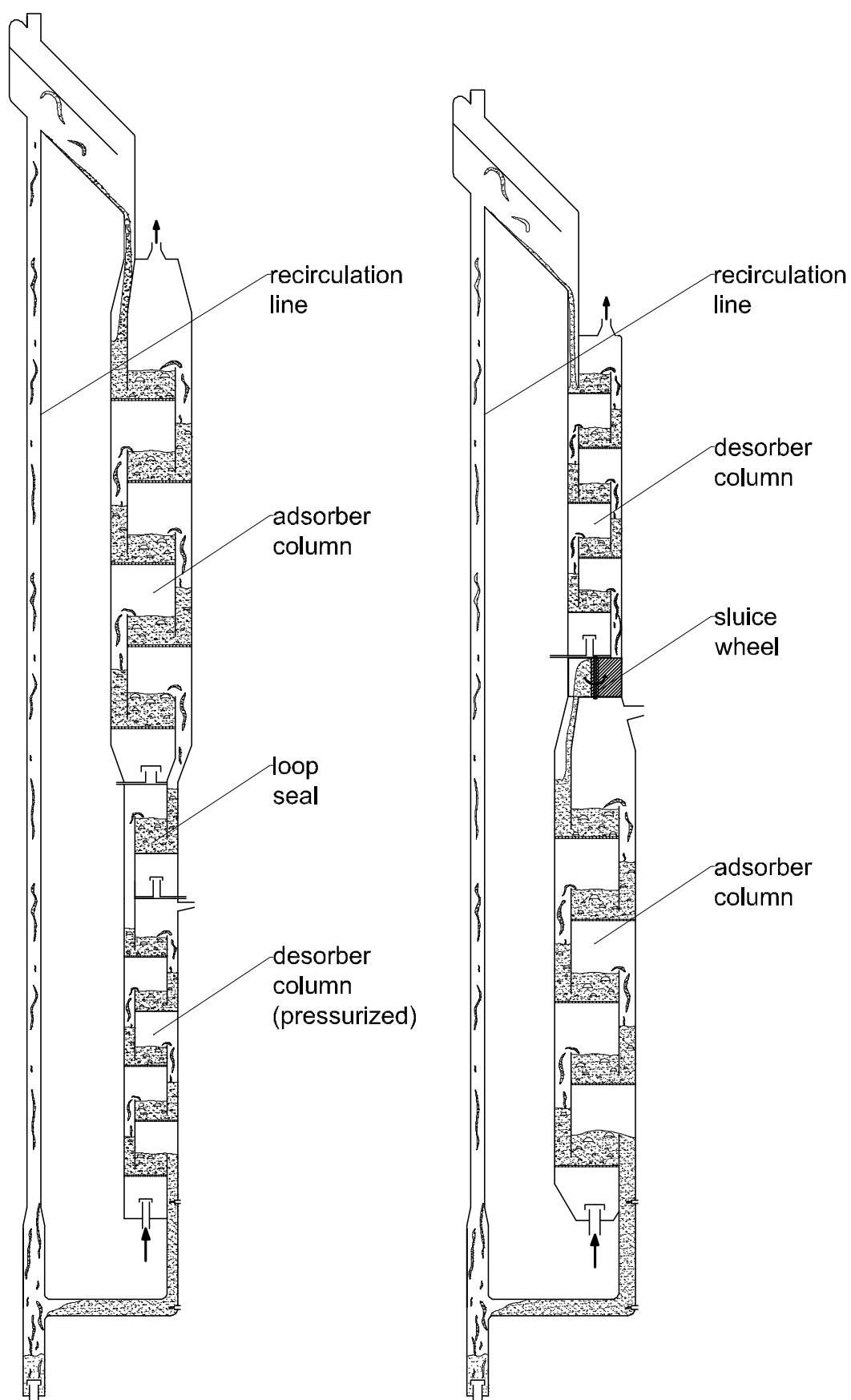


Figure A 6: Continuous TSA bench scale unit (at BOKU laboratories, status March 2014).



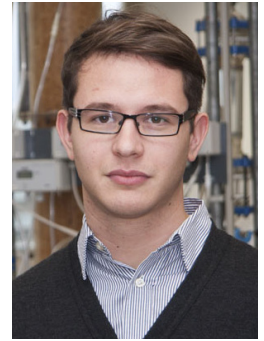
Figure A 7: Alternative TSA process designs - stacked multi-stage fluidized bed column design.



Contact:

Tel: +43 (1) 58801 166371

Mail: gerhard.schoeny@tuwien.ac.at



Personal Information

Date of birth	28.06.1985
Nationality	Austrian
Home address	Costagasse 5/16 A-1150 Wien Austria

Education

since November 2011

Vienna University of Technology

PhD student at the Institute of Chemical Engineering

PhD thesis: Post Combustion CO₂ Capture based on Temperature Swing Adsorption – from Process Evaluation to Continuous Bench Scale Operation

Supervisor: Univ. Prof Dipl.-Ing. Dr. Tobias Pröll
Univ. Prof Dipl.-Ing. Dr. Hermann Hofbauer

October 2011

Vienna University of Technology

Graduation as mechanical engineer, Dipl.-Ing. (equivalent to MSc)

Graduation Institute: Institute of Chemical Engineering

Master thesis- Assessment of the Scale-Up and Operational Design of the Fuel Reactor in Chemical Looping Combustion.

November 2010 – April 2011

Chalmers University of Technology

Department of Energy and Environment

Elaboration of Master thesis project

Supervisor: Dr. David Pallarès
Dr. Henrik Leion

October 2005 – October 2011

Vienna University of Technology

Student majoring in mechanical engineering

Special focus on Energy Technology

September 1999 – June 2004

HTL Mödling

Secondary College for Mechanical Engineering

Division Mechatronics

Final thesis: Automatic Tuning Device for Membranes of Condenser Microphones (in cooperation with AKG Acoustics GmbH))

Work Experience

October 2009 – November 2010

RUAG Space GmbH, Vienna

Department of Mechanisms & Mechanical Equipment

Assistant Engineer

July 2009, 2008	Austrian Aerospace GmbH , Vienna Dep. Mechanisms & Mechanical Equipment Assistant Engineer
August 2009	Andritz AG , Vienna Division Pulp&Paper, Department Service Assistant Engineer
September 2008 – June 2009	Andritz AG , Vienna Division Pulp&Paper, Department Service Assistant Engineer
August, 2008	ATEC Powerplant Systems , Vienna
September 2006 – September 2007	71media , TV broadcasting, Austria leadership of marketing and technical information tour
July 2004	AKG Prof. Group , Vienna Department for Measurement & Control Systems

Languages and skills

Languages	German (native) English (fluent written and spoken)
Software	AutoCAD, AutoCAD Inventor, CATIA Matlab, IPSE Pro, Office

Achievements

- Winner of the **1st place at the 'EU-Contest for Young Scientists'** in Dublin- August 2004
- Winner of the **1st place, category engineering 'Jugend Innovativ'** in Vienna- May 2004
- 'Award for Special Achievement' from the Austrian Ministry of Education- January 2005

Vienna, February 5th, 2015

Dipl.-Ing. Gerhard Schöny